

**Anion Recognition: From the Perspectives
of Fluorescent Probes and Transmembrane
Ion Transporters**

A Thesis

Submitted in Partial Fulfillment of the Requirements

for the Degree of

Doctor of Philosophy

by

Arundhati Roy

ID: 20113136



Indian Institute of Science Education and Research (IISER), Pune

2017

Dedicated to

Baba, Ma and Bhai



भारतीय विज्ञान शिक्षा एवं अनुसंधान संस्थान, पुणे

INDIAN INSTITUTE OF SCIENCE EDUCATION AND RESEARCH (IISER), PUNE

(An Autonomous Institution, Ministry of Human Resource Development, Govt. of India)

900 NCL Innovation Park, Dr. Homi Bhabha Road, Pune 411008

Dr. Pinaki Talukdar

Associate Professor
Department of Chemistry,
IISER Pune

CERTIFICATE

Certified that the work incorporated in the thesis entitled *“Anion Recognition: From the Perspectives of Fluorescent Probes and Transmembrane Ion Transporters”* submitted by *Arundhati Roy* was carried out by the candidate, under my supervision. The work presented here or any part of it has not been included in any other thesis submitted previously for the award of any degree or diploma from any other university or institution.

Date: 23rd December 2016

Dr. Pinaki Talukdar
(Research Supervisor)



भारतीय विज्ञान शिक्षा एवं अनुसंधान संस्थान, पुणे

INDIAN INSTITUTE OF SCIENCE EDUCATION AND RESEARCH (IISER), PUNE

(An Autonomous Institution, Ministry of Human Resource Development, Govt. of India)

900 NCL Innovation Park, Dr. Homi Bhabha Road, Pune 411008

Declaration

I declare that this written submission represents my ideas in my own words and wherever other's ideas have been included; I have adequately cited and referenced the original sources. I also declare that I have adhered to all principles of academic honesty and integrity and have not misrepresented or fabricated or falsified any idea/data/fact/source in my submission. I understand that violation of the above will cause for disciplinary action by the Institute and can also evoke penal action from the sources which have thus not been properly cited or from whom proper permission has not been taken when needed.

Date: 23rd December 2016

Arundhati Roy

ID: 20113136

Acknowledgment

First and foremost, I would like to express my sincere gratitude to my mentor and research advisor Dr. Pinaki Talukdar for his constant support, guidance and encouragement in my five years research career. Moreover his patience, immense enthusiasm, suggestion and motivation helped me to learn all the time of my research period. Words cannot possibly be enough for the level of indebtedness I have for him. I also convey my sincere thanks to him for trusting and supporting me in my initial days of PhD tenure, when I was struggling to synthesize first target compound. I am very much fortunate to work in his group and without his guidance and persistent help, this thesis would not have been possible.

I am also grateful to my Research Advisory Committee (RAC) members Dr. Sayam Sen Gupta (CSIR-National Chemical Laboratory) and Dr. Nirmalya Ballav (IISER Pune) for their valuable and helpful suggestions during research advisory committee meetings.

I would like to acknowledge Indian Institute of Science Education and Research (IISER), Pune and its director Prof. K. N. Ganesh for providing high quality research atmosphere and excellent research facilities. I am also extremely thankful to all faculty members of our Chemistry department and especially Prof. M. Jayakanan (Chair, Chemistry department) for being extremely helpful during my research period. I would like to acknowledge Dr. Arnab Mukherjee and Dr. Anirban Hazra for theoretical calculation.

Besides my supervisor, I sincerely thank to all of my labmates Dr. Dnyaneshwar Kand, Dr. Sharad Deshmukh, Dinesh, Tanmoy, Sopan, Javed, Debashis, Rashmi, Avisikta, and Manzoor for their constant support and help regarding problems of research at various stages of my projects and maintaining healthy atmosphere in lab. Special thanks goes to Dr. Sharad Deshmukh with whom I started learning synthesis after joining IISER, Pune and Dr. Dnyaneshwar Kand for supporting and encouraging me during hard times, regarding any problem of research. Also I want to thank Prashant, Sanjit, Aditi, Konoya, Oindrila, Nihar, Manjeet, Pratyush, Sreejit, Gourab, Shahid, Sharique, Anjana, Aashish, Komal, Aakash, Saptashwa and many more alumni members for being

helpful and making my journey truly joyful. It was indeed a pleasure to work in such a superb group. I also want to thank Avdhoot, Debasis and Amitosh for theoretical calculation and Tanmoy Saha for live cell imaging experiments.

I convey my sincere thanks to IISER, Pune and University Grand Commission (UGC) for providing funding and research fellowship respectively. I thank Dr. Umeshreddy Kacherki (deputy librarian) and Anuradha for library support and all instrument operators (Deepali, Chinmay, Archana, Swati, Nayana). I would like to thank all IISER Pune non-teaching staff members, especially Mr. Mayuresh, Mr. Tushar, Mr. Mahesh, Mr. Sandeep, Mr. Ganesh, Mr. Prabhas for their help at a number of times.

I sincerely thank many of my school and college teachers for motivating me in learning so many things and they encouraged me for higher studies. Among all teachers, particularly, I am thankful to Dr. Gautam Chattopadhyay (former Presidency College), Dr. Gandhi Kumar Kar (former Presidency College), Dr. Achintya Sarkar (former Presidency College), Dr. Dipak K. Mandal (former Presidency College), Dr. Amita Kar (former Presidency College), Balai Chand Kundu (former Presidency College), Dr. Sujoy Chakroborty (Teacher, Physical chemistry), Dr. Chandan Saha (Teacher, Organic chemistry), Dr. Sanjib Ganguly (St. Xavier's College, Calcutta), Dr. Rana Sen (Scottish Church College), Prof. Manas Chakroborty (Bose Institute), Dr. Dinabandhu Kundu (Scottish Church College). I was fortunate to come across as a student of all of them.

I am thankful to all my friends specially Sohini, Sudeshna, Kajari, Sneha, Sagar, Partha, Abhigyan da, Biplab da, Manna da, Koushik da, Sunil, Arindam da, Barun, Abhik, Avishek, Maidul, Rahi, Bijoy da, Anindita, Madhuri, Trimbak, Tanpreet Di in IISER. Special thanks to Sohini who always stood beside me whether I am right or wrong and moreover being foodie like me. Also, I would like to thank friends outside IISER specially Arpita, Karuna, Arpan, Suman, Turbasu, Sayantani, Deepika, Soma, Sudipta, Debasish, and Arindam.

I sincerely thank American Chemical Society (ACS), Royal Society of Chemistry (RSC), John Wiley & Sons (Wiley-VCH) and Elsevier for publishing a number of my research articles during my PhD tenure at IISER Pune.

Finally, I am indebted for my father (Sudhanya Kumar Roy), mother (Arati Roy) and brother (Surdeep Roy) for their endless love, care and constant encouragement. They paved the path before me and they are the ones upon whose shoulders, I could stand. Their optimism and strong believe in me has given me strength to overcome all difficulties, I have come across and reach towards goal. Also I express my deepest gratitude to my grandpa Late Pran nath Roy, grandma Late Kamala Roy and maternal grandpa Late Gurudas Sarkar, maternal grandma Late Lakshmi Sarkar for their boundless love. Apart from them, I am thankful to my best friend Soumya, who is the sole saviour during my tough times and stood beside me irrespective of situations. The simple phrase 'thank you' would be pale and diminish in the sheer enormity of the gratitude I owe for him.

Arundhati Roy

Contents

A. Detection of Fluoride Ion Sensing by Cascade Based Reactions

1. Fluorescent Turn-On NBD Probe for Fluoride Sensing: Theoretical Validation and Experimental Studies

1.1.	Introduction	1.1-1.3
1.2.	Results and Discussions	1.3-1.16
1.2.1.	Theoretical Calculations	1.3-1.9
1.2.2.	Synthesis	1.9-1.10
1.2.3.	Photophysical Properties	1.10-1.13
1.2.4.	Fluoride Sensing	1.13-1.15
1.2.5.	Cell imaging	1.15-1.16
1.3.	Conclusion	1.16
1.4.	Experimental Section	1.16-1.20
1.5.	Appendix Section	1.20-1.21
1.6.	References	1.22-1.23

2. Development of Probes for Rapid Detection of Fluoride Ion: Improvement of Sensitivity and Application in Aqueous Media

2.1.	Introduction	2.1-2.2
2.2.	Results and Discussions for Probe 1	2.2-2.9
2.2.1.	Synthesis	2.2-2.3
2.2.2.	Evidence of Cascade Reaction Mechanism	2.3-2.4
2.2.3.	Photophysical Properties and Fluoride Sensing	2.4-2.9
2.2.4.	Cell imaging	2.9
2.3.	Conclusion for Probe 1	2.9-2.10
2.4.	Improvement of Sensitivity	2.10
2.5.	Results and Discussions for Probe 2	2.10-2.17
2.5.1.	Synthesis	2.10-2.11
2.5.2.	Evidence of Cascade Reaction Mechanism	2.11-2.12
2.5.3.	Photophysical Properties and Fluoride Sensing	2.12-2.16
2.5.4.	Cell imaging	2.16-2.17
2.6.	Conclusion for Probe 2	2.17
2.7.	Improvement of Aqueous Solubility	2.17
2.8.	Results and Discussions for Probe 3	2.18-2.25
2.8.1.	Addressing Water Solubility and Membrane Permeability	2.18-2.19
2.8.2.	Synthesis	2.19
2.8.3.	Evidence of Mechanism	2.20-2.21
2.8.4.	Photophysical Properties and Fluoride Sensing	2.21-2.25

2.8.5.	Cell imaging	2.25
2.9.	Summary of All Probes	2.25-2.26
2.10.	Experimental Section	2.26-2.32
2.11.	Appendix Section	2.33-2.39
2.12.	References	2.39

B. Chloride Ion Recognition by Transmembrane Ion Transporters

3. Design and Synthesis of Triazine-Based Tripodal Receptors for Chloride Transport

Section 3A: Design, Synthesis and Ion Transport Activity of Tripodal Receptors for Chloride Transport

3A.1.	Introduction	3A.1-3A.2
3A.2.	Results and Discussions	3A.3-3A.15
3A.2.1.	Synthesis	3A.3
3A.2.2.	Crystal Structure	3A.4-3A.5
3A.2.3.	Ion Transport Activity	3A.5-3A.13
3A.2.4.	Mass Spectrometric Studies for Anion Recognition	3A.13
3A.2.5.	Molecular Dynamics Simulation	3A.14-3A.15
3A.3.	Conclusion	3A.15
3A.4.	Experimental Section	3A.16-3A.31
3A.5.	Appendix Section	3A.31-3A.40
3A.6.	References	3A.40-3A.42

Section 3B: One-pot Synthesis and Transmembrane Chloride Transport Properties of C_3 -Symmetric Benzoxazine Urea

3B.1.	Introduction	3B.1-3B.2
3B.2.	Results and Discussions	3B.2-3B.10
3B.2.1.	Synthesis	3B.2-3B.3
3B.2.2.	Binding Study	3B.3-3B.5
3B.2.3.	Ion Transport Activity	3B.5-3B.8
3B.2.4.	Mass Spectrometric Studies for Anion Recognition	3B.8-3B.9
3B.2.5.	Molecular Dynamics Simulation	3B.9-3B.10
3B.3.	Conclusion	3B.10
3B.4.	Experimental Section	3B.10-3B.17
3B.5.	Appendix Section	3B.18-3B.22
3B.6.	References	3B.22-3B.24

4. Synthesis of Malemide and Fumaramide Derivatives and Evaluation of Their Ion Transport Activity

4.1.	Introduction	4.1-4.3
4.2.	Results and Discussions	4.3-4.11
4.2.1.	Synthesis	4.3-4.4
4.2.2.	Ion Transport Activity	4.4-4.8
4.2.3.	Light-induced Transport Activity	4.8-4.9
4.2.4.	Bilayer Lipid Membrane	4.9-4.10
4.2.5.	Molecular Modelling of Ion Channel	4.10-4.11
4.3.	Conclusion	4.11-4.12
4.4.	Experimental Section	4.12-4.19
4.6.	Appendix Section	4.19-4.31
4.7.	References	4.31-4.32
5.	Trimodal Control of Ion Transport Activity of Cyclo-Oligo-(1→6)-β-D-Glucosamine Based Artificial Ion Transport Systems	
5.1.	Introduction	5.1-5.4
5.2.	Results and Discussions	5.4-5.7
5.2.1.	Synthesis	5.4
5.2.2.	Ion Transport Activity	5.4-5.6
5.2.3.	Ion Selectivity Assay	5.6-5.7
5.3.	Conclusion	5.7
5.4.	Experimental Section	5.8
5.5.	References	5.8-5.9

Synopsis

The thesis is primarily focused upon anion recognition which is a key event based on several fundamental chemical and biological phenomena such as sensing and transport. The presence of diverse anions in living organisms is a ubiquitous reality and these anions play crucial roles for the maintenance of essential life processes. Typically, halide ions such as fluoride and chloride ions have vital roles in a number of biological systems.

Among biologically relevant halides, fluoride (F^-) ion is one of the most exciting target of research owing to its well-recognized importance behind miscellaneous health and environmental issues. The United States Environmental Protection Agency (USEPA) affirmed the drinking water standard for F^- 4 ppm to prevent osteofluorosis, dental fluorosis etc. Considering the widespread use of the ion in daily life and its implication in biological effects, it is very interesting to develop highly sensitive and selective molecular probes for detection of F^- ion in chemical as well as in biological systems. Albeit several analytical techniques are available to recognize F^- , the development of colorimetric fluorescent probes scores a distinct advantage over other methods. Furthermore, cascade reactions offer a couple of advantages such as atom economy, economy of time and waste generation aspects, all of which were together exploited to design relevant fluorescent probes. Later on, cascade reaction strategy encouraged us to develop *off-on* probes based on NBD-amine fluorophore for selective detection of F^- . The limitation of high response time associated with this probe was overcome by employing another strategy of cascade reaction. Very fast response time and improvement of sensitivity was achieved with this strategy for selective detection of F^- using fluorescein as a fluorophore. Further, fluorophore was varied aimed at the improvement of reaction time, sensitivity and aqueous solubility facets. The mechanism of cascade reaction involved in detection of F^- was proved by 1H -NMR and HPLC titration and cell-permeability and ability to detect F^- inside cell was also evaluated.

In cells, the transport of anions across phospholipid bilayers is an essential phenomenon for maintaining the concentration gradient, imperative for signaling and cellular regulation. Chloride, one of the most important anions, regulates the flux of metabolites into and out of the cell during maintenance of the osmotic pressure, which causes cystic fibrosis, myotonia and epilepsy. Hence, it is important to develop artificial transport systems which can mimic natural

ion transport systems to prevent health issues related to imbalance transport of ions. A new class of pre-organized tripodal receptors based on triazine core and bispidine arms were developed to facilitate preorganized cavity formation which was further functionalized to result into controlled anion binding along with facile transport through liposomal membranes. Tripodal tris-amide and tris-urea compounds based on benzoxazine-core were synthesized which led to better Cl⁻ binding ability. Transmembrane anionophoric behavior of the tris-urea receptor along with its theoretical binding model were also demonstrated. To obtain controlled ion transport activity, light gated ion transport activity and chloride selectivity were comprehensively evaluated by designing very small molecules attached with a photo-active alkene core. Also, ion transport activity of cyclo-oligo-(1→6)-β-D-glucosamine based artificial ion transport systems were assessed.

Chapter 1. Fluorescent Turn-On NBD Probe for Fluoride Sensing: Theoretical Validation and Experimental Studies

Design, synthesis and fluoride sensing ability of a 7-nitro-2,1,3-benzoxadiazole (NBD) based chemodosimeter is reported. Theoretical calculations were used to design more applicable *off-on* response, by choosing NBD as the accurate fluorophore. Reaction of the NBD-probe with 300 equivalent of tetrabutyl ammonium fluoride (TBAF) exhibited a response time of 80 minutes and

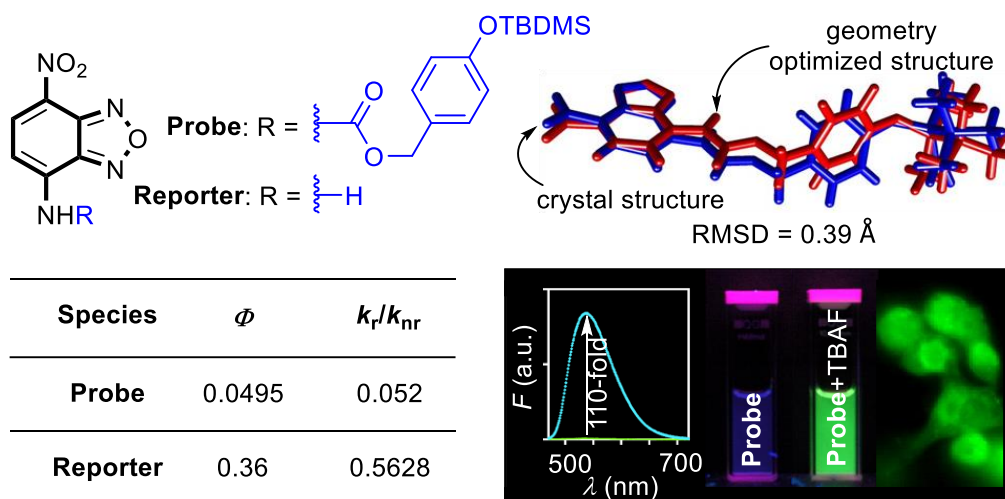


Figure 1: Schematic representation of cascade reaction based fluorescent probe, matching of their crystal structure and geometry optimized structure and photophysical property.

the reaction was selective to F^- and sensing of the ion was marked by a 110-fold enhancement of green fluorescence. The *off-on* fluorescence characteristics of the probe enabled its application in live-cell imaging of intracellular F^- ions.

Publications from this chapter:

1. *A Fluorescent Off-On NBD Probe for Fluoride Sensing: Theoretical Validation and Experimental Studies.*

Arundhati Roy, Avdhoot Datar, Dnyaneshwar Kand, Tanmoy Saha, Pinaki Talukdar.*

Org. Biomol. Chem. **2014**, *12*, 2143-2149.

Chapter 2. Development of Probes for Rapid Detection of Fluoride Ion: Improvement of Sensitivity and Application in Aqueous Media

A series of cascade reaction-based colorimetric and fluorescent probe for selective fluoride ion detection is reported based on fluorescein, resorufin and NBD-amine. The fluorescein based probe displays fast response ($t_{1/2} = 2.41$ min) and 550-fold fluorescence enhancement during sensing of fluoride ion. Application of the probe in live cell imaging is demonstrated. A resorufin based colorimetric and fluorescence *off-on* probe for selective fluoride ion detection is reported. 1H -NMR and HPLC experiments confirm the formation of phthalide and resorufin in the deprotection-cyclization based sensing mechanism. The cascade reaction strategy ensures the rapid release ($t_{1/2} = 1.96$ min) of pink fluorescent resorufin dye. Selective sensing of fluoride ion results in the 1820-fold fluorescence enhancement. The probe also displays a detection limit of 60 nM (*i.e.* 1.15 ppb) during the sensing of the ion from water. Permeability of the probe and sensing of intracellular fluoride ion is demonstrated by live cell imaging. Another probe based on NBD-Amine fluorophore for selective detection of fluoride ion in aqueous media is reported. The probe was designed by applying rules for water solubility and membrane permeability. The probe functions through the fluoride mediated cascade reaction which was studied by 1H -NMR, HPLC analysis, UV-vis and fluorescence spectroscopy. The sensing process was marked by the by a color change from colorless to yellow, and an intriguing 120-fold turn-on green fluorescence. Application of the probe for selective detection of fluoride was demonstrated by live-cell imaging.

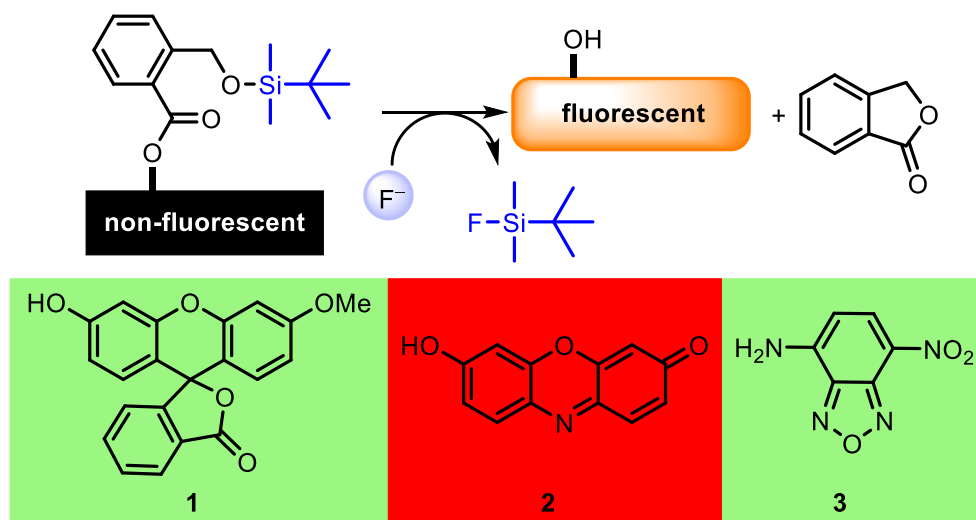


Figure 2: Schematic representation of cascade reaction based three fluorescent probes based on fluorescein, resorufin and NBD-amine for fluoride sensing.

Publications from this chapter:

1. *A Cascade Reactions Based Fluorescent Probe for Rapid and Selective Fluoride Ion Detection.*
Arundhati Roy, Dnyaneshwar Kand, Tanmoy Saha, Pinaki Talukdar.*
Chem. Commun. **2014**, 50, 5510-5513.
2. *Pink Fluorescence Emitting Fluoride Ion Sensor: Investigation of the Cascade Sensing Mechanism and Bioimaging Applications.*
Arundhati Roy, Dnyaneshwar Kand, Tanmoy Saha, Pinaki Talukdar.*
RSC Adv. **2014**, 4, 33890-33896.
3. *Turn-On Fluorescent Probe Designed for Fluoride Ion Sensing in Aqueous Media.*
Arundhati Roy, Tanmoy Saha, Pinaki Talukdar.*
Tetrahedron Lett. **2015**, 56, 4975-4979.

Chapter 3. Design, Synthesis and Ion Transport Activity of Tripodal Receptors for Chloride Transport

A new class of pre-organized triazine based tripodal receptors is reported as efficient transmembrane Cl^- carrier. These receptors were designed based on triazine core and 3,7-diazabicyclo[3.3.1]nonane arms to facilitate preorganized cavity formation. Each bicyclic arm

was further functionalized to control protonation and lipophilicity which are crucial for their efficient anion binding and facile transport through liposomal membranes. The benzyl substituted receptor was superior as the most efficient ion transporter compared to the pentafluorobenzyl substituted one. The non-substituted receptor was least active due to its high polarity. Two active transporters were found to function as mobile carriers for Cl^- via an antiport mechanism. Molecular dynamic simulation with the most active receptor established strong Cl^- binding within the cavity by multiple hydrogen bonds involving $\text{N-H}\cdots\text{Cl}^-$, water bridged $\text{O-H}\cdots\text{Cl}^-$ interactions.

One-pot synthesis of a C_3 -symmetric benzoxazine-based tris-urea compound was discussed in next part. $^1\text{H-NMR}$ titrations indicate a stronger Cl^- binding compared to Br^- and I^- by the receptor. Effective Cl^- transport across liposomal membranes via Cl^-/X^- antiport mechanism is confirmed. The theoretical calculation suggests that a few water molecules along with N-H, C=O, and the aromatic ring of the receptor create a H-bonded polar cavity where a Cl^- is recognized by $\text{O-H}\cdots\text{Cl}^-$ interactions from five bridged water molecules.

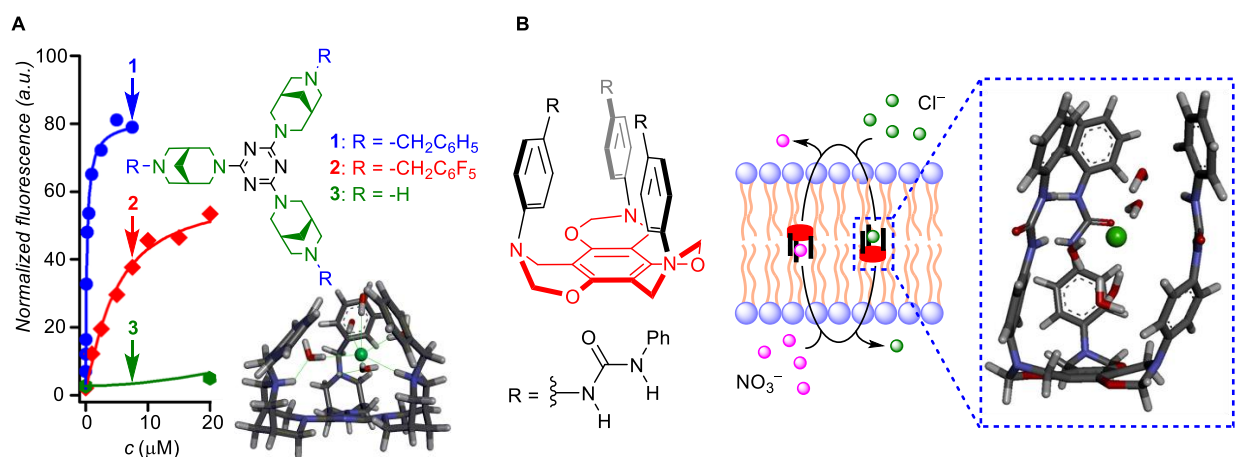


Figure 3: A) The design strategy of triazine based receptor, its ion transport activity and binding motif. B) benzoxazine-based tris-urea receptor, its ion transport activity and binding motif.

Publications from this chapter:

1. *pH-Gated Chloride Transport by Triazine-based Tripodal Semicage.*

Arundhati Roy, Debasis Saha, Prashant Sahebrao Mandal, Arnab Mukherjee, Pinaki Talukdar.*

Chem. Eur. J. (selected as Very Important Paper) **2017**, 23, 1241 – 1247.

2. One-Pot Synthesis and Transmembrane Chloride Transport Properties of C₃-Symmetric Benzoxazine Urea.

Arundhati Roy, Debasis Saha, Arnab Mukherjee, Pinaki Talukdar.*

Org. Lett. **2016**, 18, 5864–5867.

Chapter 4. Synthesis of Maleimide and Fumaramide Derivatives and Evaluation of Their Ion Transport Activity

A new series of *cis*-isomers based on light sensitive double bond core were designed. We postulated that upon irradiation of light, these *cis*-isomers convert into *trans*-isomers which can self-assemble to form a ion channel. Therefore, five pairs of maleimide (*cis*-isomer) derivatives and fumaramide (*trans*-isomer) derivatives were synthesized and their ion transport ability was evaluated by fluorescence based vesicle leakage assay with EYPC liposomes. As expected higher activity was observed for *trans*-isomer in comparison with *cis*-isomer and highest activity was observed in case of *trans*-isomer with cyclohexyl side arm ($EC_{50} = 3.5 \mu\text{M}$) and this compound is almost 77 fold more active as compared to its *cis*-isomer. Further experiment based on chloride sensitive lucigenin dye showed that compound can transport anions particularly chloride across EYPC liposome which was proved by EYPC and Lucigenin assay. Light-gated

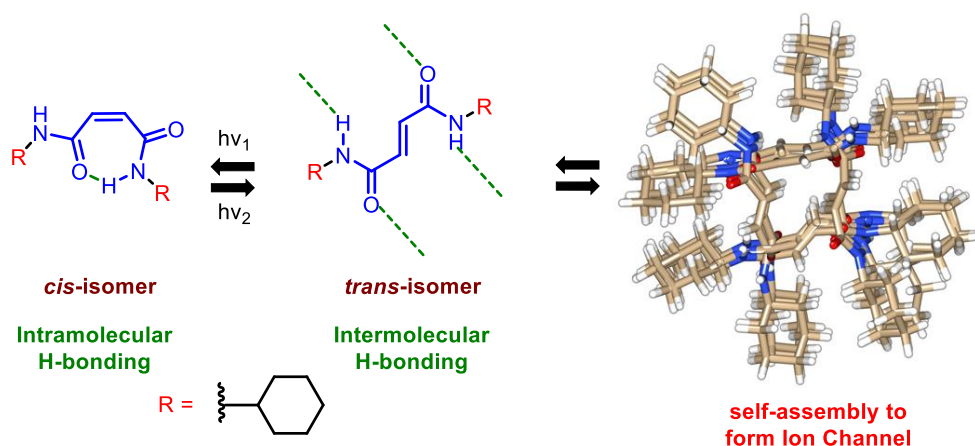


Figure 4: Schematic representation of probable mode of self-assembly for the channel formation with fumaramide (*trans*) derivatives.

ion transport activity was assessed with EYPC liposomes and observed data suggested nearly 95% activity retained after three consecutive cycles. Additionally, formation of ion channel was demonstrated by bilayer lipid membrane experiment and from single-channel conductance measurements, diameter of channel was found to be 3.84 Å which is close to diameter of unsolvated chloride ion.

Publication from this chapter:

1. Self-assembled Synthetic Light-Gated Ion Channel for Potential Transmembrane Chloride Ion Transport.

Arundhati Roy, Amitosh Gautam, Pinaki Talukdar.*

Manuscript Under Preparation.

Chapter 5. Trimodal Control of Ion Transport Activity of Cyclo-Oligo-(1→6)-β-D-Glucosamine Based Artificial Ion Transport Systems

Artificial ion channels were designed on the basis of a new type of functionalized cyclic oligosaccharide scaffolds, namely cyclo-oligo-(1→6)-β-D-glucosamines. They were rationally designed for Cl⁻ selectivity due to presence of smaller and hydrophilic cavity in comparison with cyclodextrins. Additionally, Amenability of ring-size alteration and its associated correlation with the ring rigidity made it possible to control the ion transporting activity. Importance of number of membrane spanning tails were established by varying tail length and number of tails. Half-channel dimers as the active structures were formed with a medium sized tail. Short tail

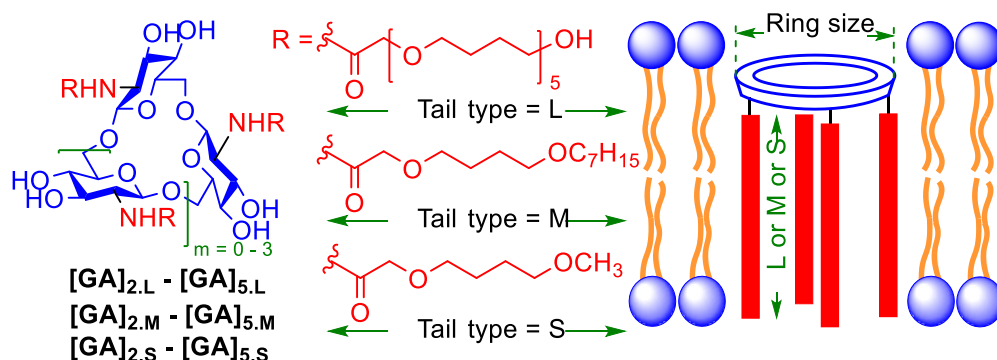


Figure 5: The design strategy for glucosamine based ion channel and variation of ion transport activity by modulating ring size, tail length and number of tail.

connected derivatives that displayed poor ion transport activity worked as negative controls for ion transport studies. All molecules displayed a uniform $\text{Cl}^- > \text{Br}^- > \text{I}^-$ selectivity sequence.

Publication from this chapter:

1. *Cyclo-Oligo-(1->6)- β -D-Glucosamine Based Artificial Channels for Tunable Transmembrane Ion Transport.*
Tanmoy Saha, **Arundhati Roy**, Marina L. Gening, Denis V. Titov, Alexey G. Gerbst, Yury E. Tsvetkov, Nikolay E. Nifantiev,* Pinaki Talukdar.*
Chem. Commun. **2014**, 50, 5514-5516.
2. *Trimodal Control of Ion-Transport Activity on Cyclo-Oligo-(1->6)- β -D-Glucosamine-Based Artificial Ion-Transport Systems.*
Arundhati Roy,[‡] Tanmoy Saha,[‡] Marina L. Gening, Denis V. Titov, Alexey G. Gerbst, Yury E. Tsvetkov, Nikolay E. Nifantiev,* Pinaki Talukdar.*
([‡] **Equal author contribution declared**)
Chem. Eur. J. **2015**, 21, 17445–17452.

Glossary of Acronyms

A

α	Alpha
Å	Angstrom
A	Absorbance
Ar	Aromatic
Ac	Acetyl
ATP	Adenosine Tri-Phosphate

B

β	Beta
br	Broad singlet
BLM	Bilayer lipid membrane or Black lipid membrane
Boc	<i>tert</i> -Butoxycarbonyl

C

<i>c</i>	Concentration
Calc	Calculated
CCDC	Cambridge Crystallographic Data Centre
CD	Cyclodextrin
CF	Carboxyfluorescein
CHCl ₃	Chloroform
CH ₂ Cl ₂	Dichloromethane
CDCl ₃	Deuterated chloroform
CH ₃ CN	Acetonitrile
CLCA	Calcium-activated chloride channel
cm	Centimeter
CsCl	Cesium chloride
CsOH	Cesium hydroxide
CTAB	Cetyl trimethylammonium bromide

D

δ	Delta (Chemical shift)
----------	------------------------

°C	Degree Celsius
<i>d</i>	Diameter
d	Doublet
dd	Doublet of doublet
DFT	Density functional theory
DPhPC	2-diphytanoyl- <i>sn</i> -glycero-3-phosphocholine
DMSO	Dimethylsulfoxide
DMF	Dimethylformamide
DCM	Dichloromethane
DMEM	Dulbecco's Modified Eagle's Medium
DMAP	4-Dimethylaminopyrine

E

EYPC	L- α -phosphatidylcholine from egg-yolk
EC_{50}	Effective concentration at half maximal activity
EtOAc	Ethylacetate
EtOH	Ethanol
Et ₃ N	Triethylamine
ESI	Electrospray ionization

F

F_t	Fluorescence intensity at time <i>t</i>
FCCP	Carbonyl cyanide- <i>p</i> -trifluoromethoxyphenylhydrazone

G

g	Gram
<i>g</i>	corrected conductance
GA	Glucosamine
G	Free energy
G_{hyd}	Free energy of hydration

H

Hz	Hertz
h	Hour

HPTS	8-Hydroxypyrene-1,3,6-trisulfonate trisodium salt
HEPES	4-(2-hydroxyethyl)-1-piperazineethanesulfonic acid
HCl	Hydrochloric acid
HPLC	High performance liquid chromatography
HRMS	High Resolution Mass Spectrometry

I

I_F	Normalized Fluorescence Intensity
IR	Infrared spectroscopy
ISE	Ion selective electrode

J

J	Coupling constant
-----	-------------------

K

k	Kilo
k	Rate constant
K	Equilibrium constant
KBr	Potassium bromide
KCl	Potassium chloride
KOH	Potassium hydroxide

L

λ	Lambda
LAH	Lithium aluminium hydride
LiCl	Lithium chloride
LiOH	Lithium hydroxide
LUV	Large unilamellar vesicle
logP	Partition Coefficient
logS	Logarithm of the solubility

M

m	Multiplet
M	Molar

μM	Micromolar
μL	Microliter
M.P.	Melting Point
MHz	Mega hertz
min	Minute(s)
max	Maximum
mg	Milligram(s)
MD	Molecular Dynamics
mol	Mole(s)
mmol	Millimole(s)
mM	Millimolar
mL	Milliliter
MALDI	Matrix Assisted Laser Desorption Ionization
MeOH	Methanol
Me	Methyl

N

n	Hill coefficient
nm	Nanometer
NMR	Nuclear magnetic resonance
Na_2SO_4	Sodium sulfate
NaBr	Sodium bromide
NaCl	Sodium chloride
NaClO_4	Sodium perchlorate
NaF	Sodium fluoride
NaNO_3	Sodium nitrate
NaOAc	Sodium acetate
NaOH	Sodium hydroxide
NaSCN	Sodium thiocyanate
NaI	Sodium iodide
NBD-Cl	7-Chloro-4-nitrobenz-2-oxa-1,3-diazole

O

obs	Observed
-----	----------

ORTEP Oak ridge thermal ellipsoid plot

P

pA Pico ampere

Ph Phenyl

PBS Phosphate-Buffered Saline

ppm Parts per million

pS Pico ampere

R

R Ideal gas constant

ρ Resistivity

RT Room temperature

RbCl Rubidium chloride

RbOH Rubidium hydroxide

S

s Second

SCXRD Single Crystal X-ray diffraction

T

t Triplet

t Time

T_x Triton X-100

TBA Tetrabutyl ammonium

TLC Thin Layer Chromatography

*t*_{1/2} Half-life

THF Tetrahydrofuran

TFA Trifluoroacetic acid

TOF Time of flight

V

V_m Membrane Potential

Val Valinomycin

Research Publications

Included in Thesis

1. *A Fluorescent Off-On NBD Probe for Fluoride Sensing: Theoretical Validation and Experimental Studies.*
Arundhati Roy, Avdhoot Datar, Dnyaneshwar Kand, Tanmoy Saha, Pinaki Talukdar.*
Org. Biomol. Chem. **2014**, *12*, 2143-2149.
2. *A Cascade Reactions Based Fluorescent Probe for Rapid and Selective Fluoride Ion Detection.*
Arundhati Roy, Dnyaneshwar Kand, Tanmoy Saha, Pinaki Talukdar.*
Chem. Commun. **2014**, *50*, 5510-5513.
3. *Pink Fluorescence Emitting Fluoride Ion Sensor: Investigation of the Cascade Sensing Mechanism and Bioimaging Applications.*
Arundhati Roy, Dnyaneshwar Kand, Tanmoy Saha, Pinaki Talukdar.*
RSC Adv. **2014**, *4*, 33890-33896.
4. *Turn-On Fluorescent Probe Designed for Fluoride Ion Sensing in Aqueous Media.*
Arundhati Roy, Tanmoy Saha, Pinaki Talukdar.*
Tetrahedron Lett. **2015**, *56*, 4975-4979.
5. *pH-Gated Chloride Transport by Triazine-based Tripodal Semicage.*
Arundhati Roy, Debasis Saha, Prashant Sahebrao Mandal, Arnab Mukherjee, Pinaki Talukdar.*
Chem. Eur. J. (selected as Very Important Paper) **2017**, *23*, 1241-1247.
6. *One-Pot Synthesis and Transmembrane Chloride Transport Properties of C₃-Symmetric Benzoxazine Urea.*
Arundhati Roy, Debasis Saha, Arnab Mukherjee, Pinaki Talukdar.*
Org. Lett. **2016**, *18*, 5864-5867.
7. *Self-assembled Synthetic Light-Gated Ion Channel for Potential Transmembrane Chloride Ion Transport.*

Arundhati Roy, Amitosh Gautam, Pinaki Talukdar.*
Manuscript Under Preparation.

8. *Cyclo-Oligo-(1->6)- β -D-Glucosamine Based Artificial Channels for Tunable Transmembrane Ion Transport.*
Tanmoy Saha, **Arundhati Roy**, Marina L. Gening, Denis V. Titov, Alexey G. Gerbst, Yury E. Tsvetkov, Nikolay E. Nifantiev,* Pinaki Talukdar.*
Chem. Commun. **2014**, 50, 5514-5516.
9. *Trimodal Control of Ion-Transport Activity on Cyclo-Oligo-(1->6)- β -D-Glucosamine-Based Artificial Ion-Transport Systems.*
Arundhati Roy,[†] Tanmoy Saha,[†] Marina L. Gening, Denis V. Titov, Alexey G. Gerbst, Yury E. Tsvetkov, Nikolay E. Nifantiev,* Pinaki Talukdar.*
([†] Equal author contribution declared)
Chem. Eur. J. **2015**, 21, 17445-17452.

Not Included in Thesis

10. *Diastereoselective Construction of syn- α -Oxyamines via Three-Component α -Oxyaldehyde-Dibenzylamine-Alkynes Coupling Reaction: Application in the Synthesis of (+)- β -Conhydrine and Its Analogues.*
Sharad Chandrakant Deshmukh, **Arundhati Roy**, Pinaki Talukdar.*
Org. Biomol. Chem. **2012**, 10, 7536-7544.
11. *Bis(sulfonamide) Transmembrane Carrier Allows pH Gated Inversion of Ion Selectivity*
Arundhati Roy, Oindrila Biswas, Pinaki Talukdar.*
Chem. Commun. **2017**, DOI: 10.1039/C7CC00165G.

Section 1

Detection of Fluoride Ion Sensing by Cascade Based
Reactions

Introduction

Anion recognition and sensing via artificial receptor has become an area of great interest in supramolecular chemistry in recent years because of the significance of anions in biological and chemical processes.¹ Among biologically relevant anions, fluoride ion is of particular interest owing to its importance in health and environmental issues.² Among all anions, fluoride (F^-) is a quite peculiar anion due to its smallest size and highest charge density, and its ionic radius is comparable with K^+ . Also, being most electronegative anion, F^- behaves as a strong Brønsted base. Solvation of F^- is also interesting. The water molecules make a highly structured first solvation sphere around it and thus makes the detection process less favored³. It is known that the enthalpy of hydration is in the order of $100 \text{ Kcal mol}^{-1}$, which is highest for any singly charged species. Fluoride ions are widely used as an essential ingredient in toothpaste, many pharmaceutical agents, and in the treatment of osteoporosis. It is also associated with nerve gases and the refinement of uranium used in nuclear manufacture. But a large intake of fluoride ion can cause both acute and chronic toxicity in human body as it inhibits the biosynthesis of neurotransmitters in fetuses, and it can cause diseases such as osteoporosis, fluorosis, urolithiasis or even cancer.^{2d, 4} Fluoride toxicity in the body can also cause increment in bone density. In addition, NaF can function as a potent G-protein activator and Ser/Thr phosphatase inhibitor, and affects plenty of essential cell signaling elements. Novel importance of fluoride has been discovered in the field of ion batteries, for enhancement of photocurrent in supramolecular solar cells and in F-PET imaging. In near future, it might have a role in constructing superconductor and hydrogen gas storage. Presence of fluoride in low concentration in drinking water prevents dental caries and enamel demineralization resulting from wearing orthodontic appliances. The United States Environmental Protection Agency (USEPA) affirmed the drinking water standard for F^- 4 ppm to prevent osteofluorosis, and a secondary fluoride standard 2 ppm to protect against dental fluorosis. Considering the widespread use of the ion in daily life and its implication in biological effects, it is very interesting to develop highly sensitive and selective molecular probes for detection of F^- ion in chemical as well as in biological systems.

The ion selective electrode, ion chromatography, HPLC, and standard Willard and Winter methods are used for quantitative measurement of F^- . However all these methods are complicated and cost-effective. For these reasons, considerable efforts have been made to develop highly

Section 1

selective and sensitive systems capable of recognition, binding/or sensing the ion in competitive environment. The fluorescent analysis method has gained considerable attention due to its high sensitivity, operational simplicity, and *in vivo* imaging analysis both qualitatively as well as quantitatively.^{2a, 5} Depending on the fluorescence outcome after detection of fluoride, probes can be categorised into mainly three classes such as ratiometric, turn-*on* and turn-*off* probes. On the other hand, fluorescent probes can be classified into two categories i.e. chemosensors and chemodosimeters depending on the mode of sensing. Two subunits are mainly required to make a chemosensors (Figure 1A) *i.e.* receptor (recognition site) and a signaling source (chromophore or fluorophore)⁶. The former resides a coordination site for reversible binding of a particular anion (by hydrogen bonding, Lewis acid coordination etc.) whereas the latter translate the recognition event by changing some spectroscopic characteristics such as color or fluorescence change associated with absorbance and or emission intensity.⁶ In past decade, a large number of fluorescent probes for F⁻ sensing have been developed exploiting anion- π interaction,⁷ hydrogen bonding,⁸ and Lewis acid-base interaction^{2d, 9} and fluoride induced chemical reaction.¹⁰ Hydrogen bonding approach is not effective in aqueous solution owing to the strong tendency of hydration of fluoride ions. The boron-fluoride complexation approach is also not suitable for biological applications because of its instability and cytotoxicity. Moreover, Lewis acidic boron based receptors bind with fluoride ions covalently and cause fluorescence quenching due to intramolecular charge transfer between the boron p π orbital and electrons from F⁻ ions. Bhosale *et al.* reported naphthalene diimide sensor bearing a bis-sulfonamide group where fluoride binds with two sulfonamide N-H binds with F⁻ ion through hydrogen bonding (Figure 1B).¹¹ Chemosensors can be turn *on* (or turn *off*) where the probe is nonfluorescent (or fluorescent) and produces fluorescent (or nonfluorescent) product after reacting with anion. Another class is ratiometric

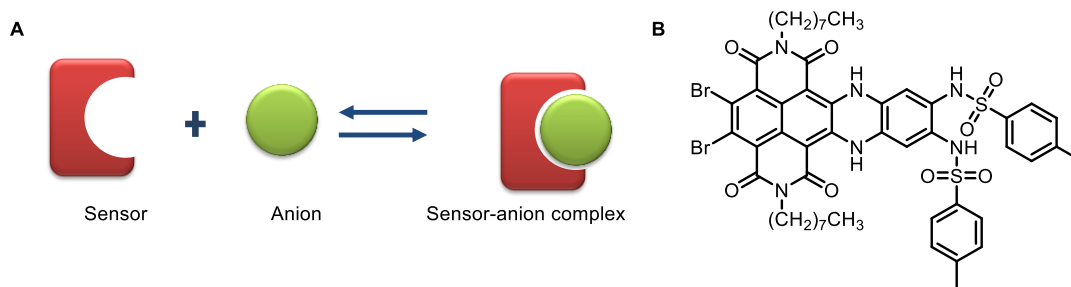


Figure 1: A) Schematic representation of chemosensor, and B) one of the reported examples of chemosensor for F⁻.

Section 1

chemosensor where probe emits light at a certain wavelength which shifted to another wavelength after reacting with anion. However, the limitation associated with these chemosensors that in some cases, selective recognition of F^- is difficult in presence of other oxygen-containing anions (AcO^- , $H_2PO_4^-$ etc.).

On the other hand, the selectivity issue during F^- sensing can be addressed by irreversible chemical reaction of the probe to form either single product or multiple products in the presence of target anion.⁶ As the chemical reaction is irreversible, the term chemosensor cannot be used strictly rather these systems can be referred as chemodosimeter or chemoreactant (Figure 2A). This approach is highly advantageous in terms of selectivity and sensitivity as compared to traditional chemosensor methods used for detection of anions. Similar to chemosensors, chemodosimeters can be turned *on* (or turned *off*) or ratiometric depending on the mode of detection.

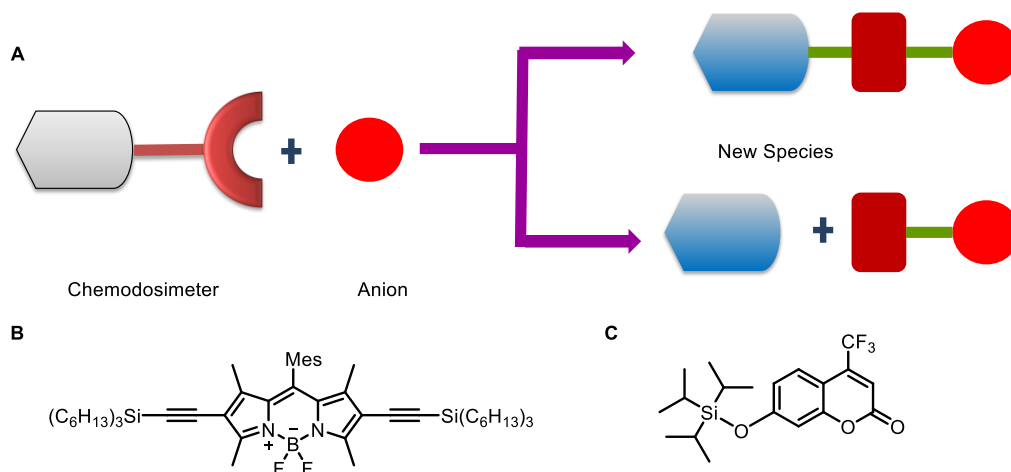


Figure 2: A) Schematic representation of chemodosimeter, B) reported examples of F^- triggered Si–C cleavage based chemodosimeters and C) reported examples of Si–O cleavage based chemodosimeters.

Fluoride ion also has very high affinity towards silicon *e.g.* Si–F is one of the strongest bonds which makes it significant in synthetic organic chemistry, and this property has been exploited in the development of numerous fluorescent probes for selective detection of F^- . Some F^- triggered Si–C bond cleavage based ratiometric chemodosimeters also reported (Figure 2B). Jiang *et. al.* connected trihexylsilylacetylene group with BODIPY at 2,6 position where extended π conjugation causes absorption at 555 nm and fluorescence emission at 571 nm.¹² In case of Si–O bond cleavage based probes, F^- mediated desilylation of silyl ethers are reported to provide ratiometric,^{10d, 13} *on-off*¹⁴ and *off-on*¹⁵ fluorescence responses. Thus, *tert-*

Section 1

butyldimethylsilylchloride (TBDMS), *tert*-butyldiphenylsilylchloride (TBDPS), *tri*-isopropylsilylchloride (TIPS) can be used as reacting sites for F^- in chemodosimeters. Sokkalingam *et. al.* reported a fluorescent turn-*on* probe for fluoride detection based on desilylation of TIPS group (Figure 2C).¹⁶ However, the detection time for these probes are very high.

On the other hand, cascade reactions offer advantages such as atom economy as well as economies of time and waste generation. These reactions save labor, waste and resources. As such, cascade reactions can be considered to fall under the category of “green chemistry”.¹⁷ Subsequently, silyl ether deprotection strategies were also applied for developing probes that release fluorophore via cascade reaction mechanisms.^{10a, 10d, 18} The advantages of these reactions are associated with mainly two factors, either reaction site can be modulated to achieve different sensing property or fluorophore can be altered to obtain different photophysical properties (Figure 3A). In 2011, Kim and coworkers reported a novel cascade reaction based ratiometric fluorescent probe which is based on fluoride-triggered Si-O bond cleavage that resulted in the formation of green fluorescent 4-amino-1,8-naphthlimide and 4- methylenecyclohexa-2,5-dione.^{10d} Song and coworkers reported a novel pink emitting another cascade reaction based probe and application of the probe in live cell imaging was also established.^{18b} In 2012, Ahn and coworkers reported another probe which undergoes fluoride specific desilylation followed by cyclisation to form an

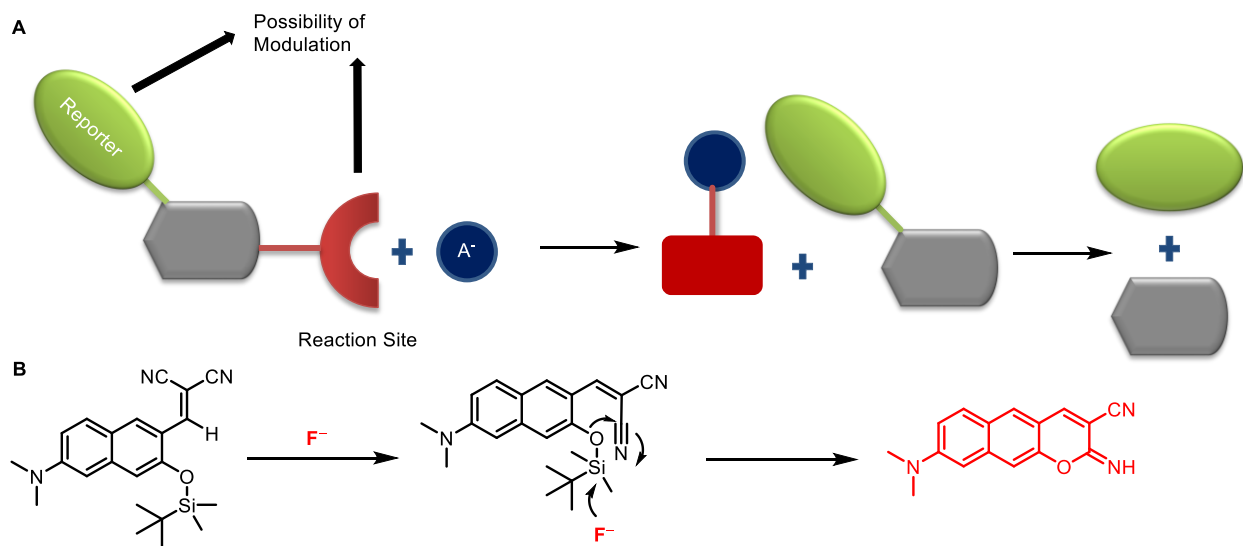


Figure 3: A) Schematic representation of cascade reaction and B) reported example of F^- triggered cascade reaction based probe.

iminocoumarin derivative and the probe was used for detecting the F⁻ ion in living cells as well as in zebrafish (Figure 3B).^{10a} However, these probes suffer from general limitations such as low sensitivity and longer response time. Sensing activity either in pure organic solvent or in combined aqueous/organic media is a general concern of most desilylation based probes. Therefore, development of new fluorescent turn-*on* probes have been reinvigorated for detecting fluoride ion in aqueous medium so that these can be more suitable for biological application.

References

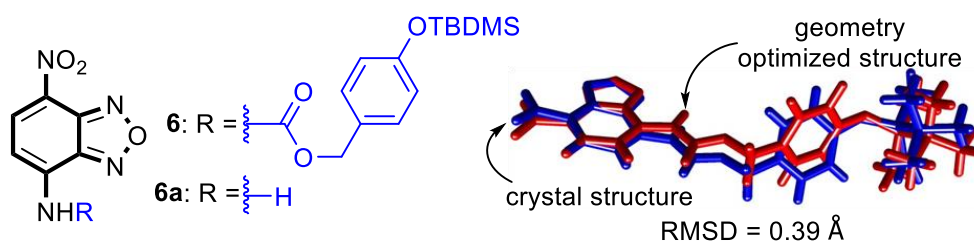
- (a) Caltagirone, C.; Gale, P. A. *Chem. Soc. Rev.* **2009**, *38*, 520-563; (b) de Silva, A. P.; Gunaratne, H. Q. N.; Gunnlaugsson, T.; Huxley, A. J. M.; McCoy, C. P.; Rademacher, J. T.; Rice, T. E. *Chem. Rev.* **1997**, *97*, 1515-1566; (c) Beer, P. D.; Gale, P. A. *Angew. Chem., Int. Ed.* **2001**, *40*, 486-516; (d) Martínez-Mañez, R.; Sancenón, F. *Chem. Rev.* **2003**, *103*, 4419-4476.
- (a) Krishnamachari, K. A. *Prog. food nutr. Sci.* **1986**, *10*, 279-314; (b) Barbier, O.; Arreola-Mendoza, L.; Del Razo, L. M. *Chem. Biol. Interac.* **2010**, *188*, 319-333; (c) Kleerekoper, M. *Endocrinol. Metab. Clin. North Am.* **1998**, *27*, 441-452; (d) Wade, C. R.; Broomsgrove, A. E. J.; Aldridge, S.; Gabbai, F. P. *Chem. Rev.* **2010**, *110*, 3958-3984; (e) Lam, S.-T.; Zhu, N.; Yam, V. W.-W. *Inorg. Chem.* **2009**, *48*, 9664-9670; (f) Broomsgrove, A. E. J.; Addy, D. A.; Bresner, C.; Fallis, I. A.; Thompson, A. L.; Aldridge, S., *Chem. Eur. J.* **2008**, *14*, 7525-7529.
- Cametti, M.; Rissanen, K. *Chem. Soc. Rev.* **2013**, *42*, 2016-2038.
- (a) Ayoob, S.; Gupta, A. K. *Crit. Rev. Env. Sci. Tec.* **2006**, *36*, 433-487; (b) Cametti, M.; Rissanen, K. *Chem. Commun.* **2009**, 2809-2829; (c) Zhou, Y.; Zhang, J. F.; Yoon, J. *Chem. Rev.* **2014**, *114*, 5511-5571.
- (a) Schäferling, M.; Wolfbeis, O. S. *Chem. Eur. J.* **2007**, *13*, 4342-4349; (b) Maity, D.; Manna, A. K.; Karthigeyan, D.; Kundu, T. K.; Pati, S. K.; Govindaraju, T. *Chem. Eur. J.* **2011**, *17*, 11152-11161.
- Du, J.; Hu, M.; Fan, J.; Peng, X. *Chem. Soc. Rev.* **2012**, *41*, 4511-4535.
- (a) Guha, S.; Saha, S. *J. Am. Chem. Soc.* **2010**, *132*, 17674-17677; (b) Guha, S.; Goodson, F. S.; Corson, L. J.; Saha, S. *J. Am. Chem. Soc.* **2012**, *134*, 13679-13691.
- (a) Swinburne, A. N.; Paterson, M. J.; Beeby, A.; Steed, J. W. *Chem. Eur. J.* **2010**, *16*, 2714-2718; (b) Veale, E. B.; Tocci, G. M.; Pfeffer, F. M.; Kruger, P. E.; Gunnlaugsson, T. *Org. Biomol. Chem.* **2009**, *7*, 3447-3454.
- Keymeulen, F.; De Bernardin, P.; Giannicchi, I.; Galantini, L.; Bartik, K.; Dalla Cort, A. *Org. Biomol. Chem.* **2015**, *13*, 2437-2443.
- (a) Kim, D.; Singha, S.; Wang, T.; Seo, E.; Lee, J. H.; Lee, S.-J.; Kim, K. H.; Ahn, K. H. *Chem. Commun.* **2012**, *48*, 10243-10245; (b) Zheng, F.; Zeng, F.; Yu, C.; Hou, X.; Wu, S. *Chem. Eur. J.* **2013**, *19*, 936-942; (c) Zhu, B.; Yuan, F.; Li, R.; Li, Y.; Wei, Q.; Ma, Z.; Du, B.; Zhang, X. *Chem. Commun.* **2011**, *47*, 7098-7100; (d) Zhang, J. F.; Lim, C. S.; Bhuniya, S.; Cho, B. R.; Kim, J. S. *Org. Lett.* **2011**, *13*, 1190-1193; (e) Kim, S. Y.; Park, J.; Koh, M.; Park, S. B.; Hong, J.-I. *Chem. Commun.* **2009**, 4735-4737; (f) Buckland, D.; Bhosale, S. V.; Langford, S. J. *Tetrahedron Lett.* **2011**, *52*, 1990-1992; (g) Kim, S. Y.; Hong, J.-I. *Org. Lett.* **2007**, *9*, 3109-3112.
- Bhosale, S. V.; Bhosale, S. V.; Kalyankar, M. B.; Langford, S. J. *Org. Lett.* **2009**, *11*, 5418-5421.

Section 1

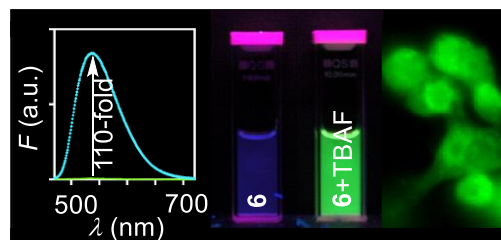
12. Jo, M.; Lim, J.; Miljanić, O. Š. *Org. Lett.* **2013**, *15*, 3518-3521.
13. (a) Fu, L.; Jiang, F.-L.; Fortin, D.; Harvey, P. D.; Liu, Y. *Chem. Commun.* **2011**, *47*, 5503-5505; (b) Cao, J.; Zhao, C.; Feng, P.; Zhang, Y.; Zhu, W. *RSC Adv.* **2012**, *2*, 418-420.
14. Bozdemir, O. A.; Sozmen, F.; Buyukcakil, O.; Guliyev, R.; Cakmak, Y.; Akkaya, E. U. *Org. Lett.* **2010**, *12*, 1400-1403.
15. Bao, Y.; Liu, B.; Wang, H.; Tian, J.; Bai, R. *Chem. Commun.* **2011**, *47*, 3957-3959.
16. Sokkalingam, P.; Lee, C.-H. *J. Org. Chem.* **2011**, *76*, 3820-3828.
17. Nicolaou, K. C.; Edmonds, D. J.; Bulger, P. G. *Angew. Chem., Int. Ed.* **2006**, *45*, 7134-7186.
18. (a) Dong, M.; Peng, Y.; Dong, Y.-M.; Tang, N.; Wang, Y.-W. *Org. Lett.* **2011**, *14*, 130-133; (b) Hou, P.; Chen, S.; Wang, H.; Wang, J.; Voitchovsky, K.; Song, X. *Chem. Commun.* **2014**, *50*, 320-322; (c) Roy, A.; Kand, D.; Saha, T.; Talukdar, P. *Chem. Commun.* **2014**, *50*, 5510-5513; (d) Roy, A.; Datar, A.; Kand, D.; Saha, T.; Talukdar, P. *Org. Biomol. Chem.* **2014**, *12*, 2143-2149; (e) Roy, A.; Kand, D.; Saha, T.; Talukdar, P. *RSC Adv.* **2014**, *4*, 33890-33896.

Chapter 1

Fluorescent Turn-On NBD Probe for Fluoride Sensing: Theoretical Validation and Experimental Studies



Species	Φ	k_r/k_{nr}
6	0.0495	0.052
6a	0.36	0.5628



1.1. Introduction

Sensing and recognition of anions by artificial receptors have become field of great interest in supramolecular chemistry in recent years because of their importance in regulatory roles in cellular pathology and chemical processes.¹ Several analytical methods such as HPLC,² UV,³ fluorescence,⁴ gas chromatography,⁵ ion selective electrode,⁶ etc. are available to detect anions. Among these, fluorescence-based techniques have gained more interest in recent years because of their high selectivity, sensitivity and straightforward measurement protocol.^{4b, 7} Moreover, fluorescent probes can exhibit high specificity in terms of excitation and emission wavelengths, and intensity changes by using simple and straightforward fluorescent measurement protocol⁸ and they could be used in live-cell imaging which allow real time analysis of different analytes and various biological events.⁹ On the other hand, anion recognition with colorimetric probe has advantages over others, such as colorimetric probes which can detect ion by color change as a naked eye detection tool and offer qualitative and quantitative information by using inexpensive methods.

Biological importance of fluoride ion in preventing enamel demineralization, dental and skeletal fluorosis, osteoporosis treatment, etc. encouraged us to design new fluorescent probe for selective detection of the ion.¹⁰ Even though a number of F⁻ sensing ratiometric,¹¹ *on-off* probes,¹² and *off-on* probes¹³ are reported which are highly sensitive, selective and easy to handle, still their application is restricted for detection of F⁻ in aqueous medium. Due to affinity of F⁻ towards silicon and boron, several probes have been developed for detection of F⁻. Hong *et. al.* reported the first example^{13a} of fluorescent turn on chemodosimeter **1** (Figure 1.1) using same desilylation strategy based on resorufin fluorophore where silyl ether bond is easily cleaved by F⁻ and shows drastic change in UV-Vis absorption and emission intensity.

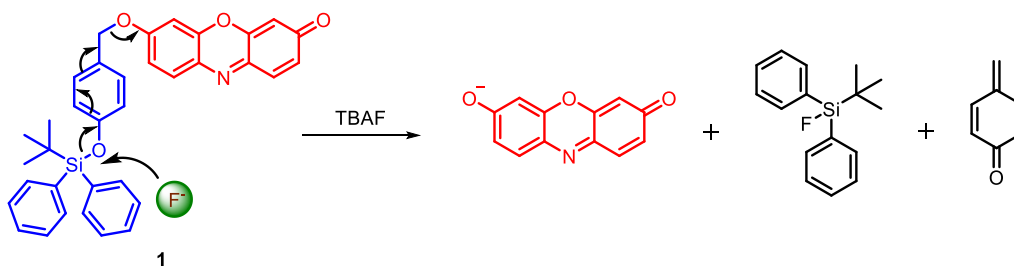


Figure 1.1: Reaction mechanism of spectroscopic changes of **1** in presence of TBAF.

However, F^- mediated deprotection of an aryl silyl ethers frequently resulted either in ratiometric or *on-off* or *off-on* response due to the choice of the aryl fluorophores. For example, the probe **2** (Figure 1.2) consisting of triisopropylsilyl (TIPS) group connected to dipyrrometheneboron difluoride (BODIPY) fluorophore,¹² provided the *on-off* response. On the other hand, the fluorophore alteration to coumarin resulted in the *off-on* response by probe **3**.^{13b} A similar *tert*-butyldiphenylsilyl (TBDPS) group when connected to benzoimidazole fluorophore in the design of probe **4**, F^- sensing resulted in the ratiometric response.¹⁴

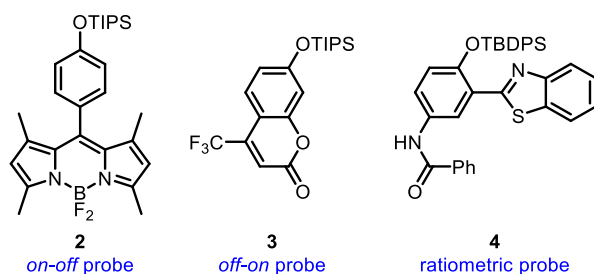


Figure 1.2: Structures of fluoride selective fluorescent probes **2-4**.

As discussed earlier, cascade reactions offer advantages such as atom economy as well as economies of time and waste generation. As such, cascade reactions can be considered to fall under the category of “green chemistry”.¹⁵ Recently, literature showed cascade reaction based chemodosimeter consisting of 4-(hydroxymethyl) phenol linker between the fluorophore and the silyl group are also reported for sensing of F^- ion (Figure 1.3A). For example, the probe **5**, reported by Kim and co-workers exhibited a ratiometric response upon treatment with F^- (Figure 1.3B).¹⁶ Although, a novel feature was implicated which involve F^- promoted silyl deprotection followed by decarboxylation strategy was incorporated in the design of probe **5**. However, F^- mediated push-pull deprotection chemistry of the probe encouraged us to develop the fluorophore having *off-on* characteristics. Herein, we propose the probe **6** for providing *off-on* response during F^- ion sensing based on same cascade reaction based strategy (Figure 1.3C).

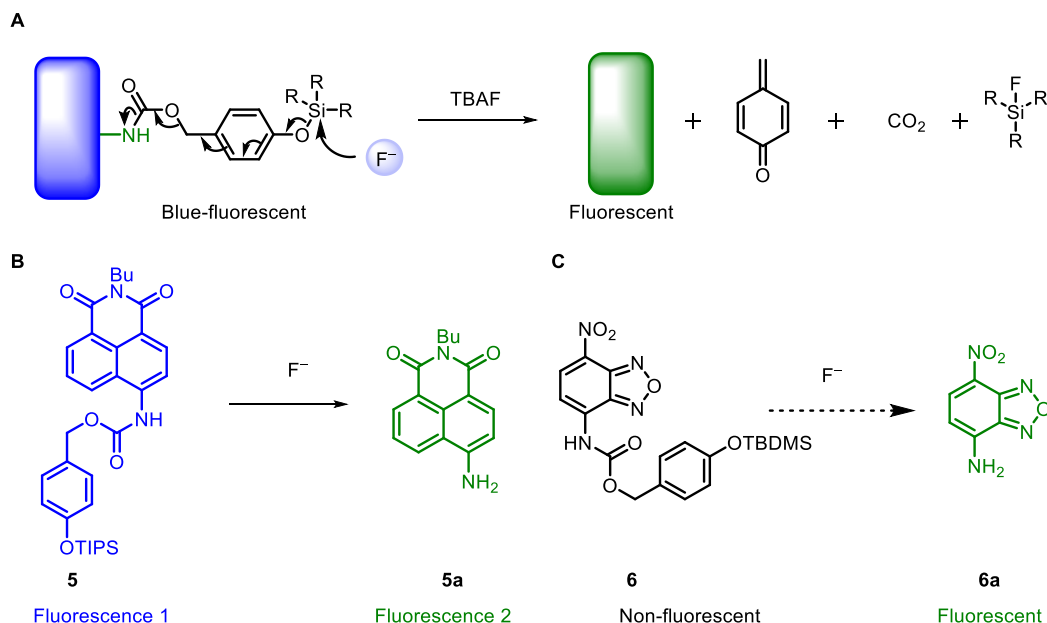


Figure 1.3: A) Schematic presentation of cascade reaction based F^- sensing, B) Structures of ratiometric probe **5** and released fluorophore **5a** and C) Structures of proposed *off-on* probe **6** and released fluorophore **6a**.

1.2. Results and Discussions

1.2.1. Theoretical Calculations

We used TDDFT method to rationalize the ratiometric response of the probe **5** and use of the computational tool to design new probe **6** for providing *off-on* response during F^- ion sensing (Figure 1.3C). Lin *et. al.* reported BODIPY-coumarin hybrid probe for detection of the F^- ion also supports the use of theoretical calculations to validate *off-on* response. Recently, theoretical calculations have been used in the development of fluorescent *off-on* probes.¹⁷ Interestingly, in case of probes for F^- detection, occasionally theoretical calculations were used to validate the experimental outcome of the photophysical properties. Wang *et. al.* used DFT and TDDFT to rationalize the photophysical properties of the probe^{11c}. In recent times, we realized that theoretical calculations¹⁸ can be used in a better way to predict the photophysical properties and also the fluorescence *Off-On* mechanism, if any. We have carried out theoretical calculation for a number of fluorophore-quencher pairs to get the best pair for *Off-On* response. We have found out that NBD-amine fluorophore can be used for getting *Off-On* response.

All calculations were carried out by Avdhoot from the group of Anirban Hazra. Computational methods were used to rationalize the ratiometric outcome of the reported probe **5** and predict the response of the proposed probe **6** towards F^- ion. At first, ground state geometry optimization of species **5**, **5a**, **6** and **6a** were carried out in the water medium with CAM-B3LYP/6-311G(d,p) basis sets¹⁹ using the Gaussian 09 program.²⁰ The polarizable continuum model (PCM) was used in calculation of the absorption and emission spectra in water.²¹ Then, geometry optimized structures were further used for TDDFT calculations with same level of theory. Although the vibrational effects lay an important role in determining the structural details of absorption and emission spectrum,²² they do not affect the qualitative position of the spectral bands and also have no bearing on the calculation of oscillator strengths. Since, computing the oscillator strengths at the absorption and emission geometries are sufficient to predict fluorescence outcomes, calculation of fine structure of the spectrum by including vibrational effects were not considered. Some selected parameters for the vertical excitation (UV–Vis absorption) and the fluorescence emission are shown in Table 1.1 and Table 1.2 respectively. According to TDDFT calculation based on the optimized ground state (S_0) geometry, main allowed electronic transition observed for **5** was $S_0 \rightarrow S_1$ (HOMO \rightarrow LUMO, $f = 0.4323$) and for **5a** was $S_0 \rightarrow S_1$ (HOMO \rightarrow LUMO) with oscillator strength, $f = 0.2690$ (Table 1.1). From the HOMO and LUMO contours electronic transitions for **5**, **5a**, **6** and **6a** were assigned as n, π^* or π, π^* transitions. $S_0 \rightarrow S_1$ transitions for **5** and **5a** were characterized as $\pi \rightarrow \pi^*$ transitions (Figure 1.4). In order to investigate the emission of **5** and **5a**, the geometry of the singlet excited state (S_1) was optimized and the excitation based on the S_1 geometry was calculated. The TDDFT calculations indicate an emissive S_1 state and allowed $S_1 \rightarrow S_0$ transition with $f = 0.3820$ and 0.2029 for **5** and **5a** respectively was observed and thus the radiative $S_1 \rightarrow S_0$ decay is possible (Table 1.2). $S_1 \rightarrow S_0$ transitions for **5** and **5a** were characterized as $\pi^* \rightarrow \pi$ transitions (Figure 1.5).

Following steps were followed for excitation calculations in solvent:

- 1) Optimize ground state using keyword SCRF. This gives ground state optimized geometry with solvent equilibrated.
- 2) A TDDFT calculation is performed to find excited states at ground state equilibrium geometry. Solvent is not equilibrated with respect to excited states. This step assumes linear response of

the solvent to excited state. Solvent effects are not accurately accounted in this step. State specific solvation method is followed after this step for describing solvent effects.

- 3) Self-consistent calculation is done to consider interaction of solvent and excited state electron density of the molecule. These calculations are called as state specific calculation since; it assumes interaction of particular excited state with the solvent.

Emission calculations were done using following procedure:

- 1) Excited state is optimized, with linear response from solvent. This optimization is carried out using TDDFT method, since, excited state calculation is involved. Minimum energy geometry on the excited state (under consideration) is found.
- 2) State specific equilibrium solvation of excited state at corresponding equilibrium geometry is carried out. Then solvation data at this step is written in PCM inputs for next step. This step is necessary to achieve equilibrium of solvent-molecule system for fast and slow degrees of freedom. Usually, electron density is treated as fast degree of freedom which adjusts instantaneously on excitation of molecule. Slow degree often refers to nuclear motion.

Ground state energy calculation at excited state geometry is done. Static solvation at excited state is read from PCM inputs written in last step.

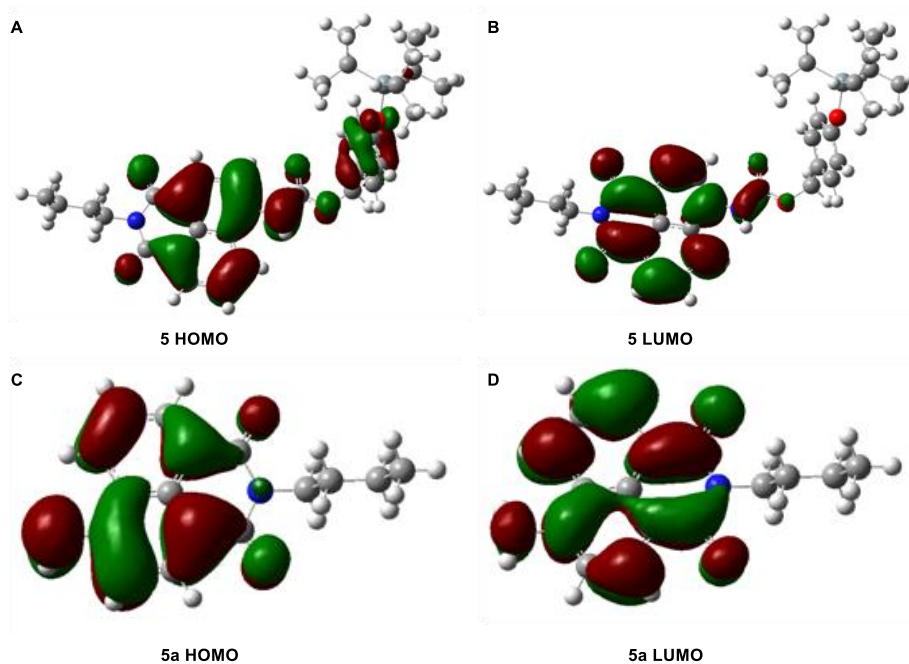


Figure 1.4: View of the ground state frontier molecular orbitals (MOs), **A)** HOMO, **B)** LUMO of **5** and **C)** HOMO and **D)** LUMO of **5a** generated from TDDFT/CAM-B3LYP/6-311G (d,p) geometry optimization.

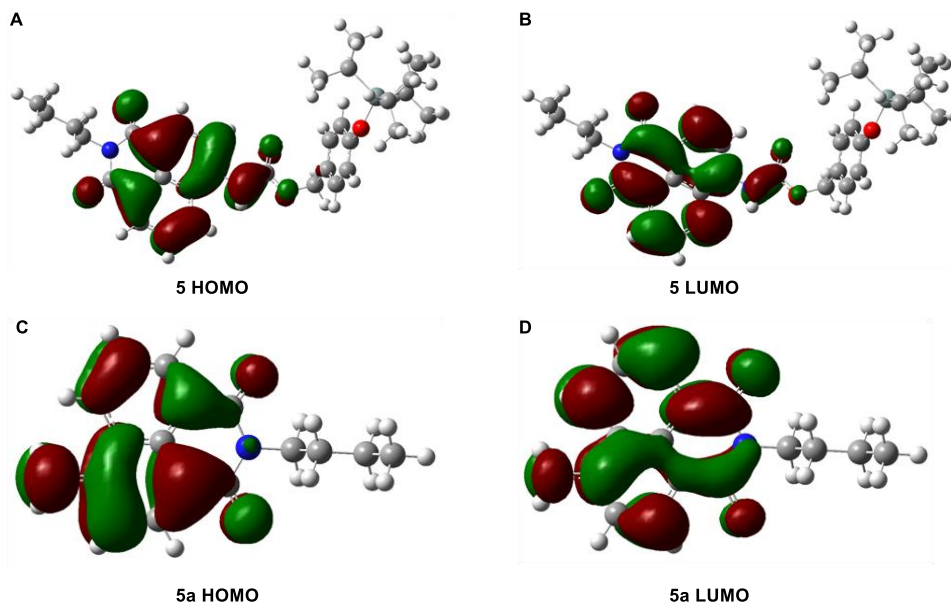


Figure 1.5: View of the excited state frontier molecular orbitals (MOs), A) HOMO, B) LUMO of **5** and C) HOMO and D) LUMO of **5a** generated from TDDFT/CAM-B3LYP/6-311G (d,p) geometry optimization.

Similarly, TDDFT calculation based on the optimized ground state (S_0) geometry, electronic transition for **6** $S_0 \rightarrow S_1$ transition was not allowed (HOMO \rightarrow LUMO, $f = 0.0000$). $S_0 \rightarrow S_1$ transition was characterized as $\pi \rightarrow \pi^*$ and $\pi \rightarrow n$ transition (Figure 1.6). Similarly, $S_0 \rightarrow S_2$ transition with $f = 0.0000$ was not allowed. First allowed transition is $S_0 \rightarrow S_3$ with $f = 0.4471$. As shown in Figure 1.6, it is clear from the distributions of the MOs, that the HOMO and LUMO are localized at different locations for **6**. The HOMO is located on the phenyl moiety, whereas, the LUMO is mainly localized on the NBD fluorophore. Consequently, the excitation from the S_0 to S_1 state involves an intramolecular charge transfer to the NBD unit. To investigate the emission of **5** the geometry of the singlet excited state (S_1) was optimized and the excitation based on the S_1 geometry was calculated. Absence of an emissive S_1 state ($S_1 \rightarrow S_0$ transition with $f = 0.0000$) suggests that the radiative $S_1 \rightarrow S_0$ decay is not possible. $S_0 \rightarrow S_1$ transition was characterized as $\pi^* \rightarrow \pi$ and $n \rightarrow \pi$ transition (Figure 1.7). $S_2 \rightarrow S_0$ transition with $f = 0.0000$ was not allowed. First allowed transition is $S_3 \rightarrow S_0$ with $f = 0.3807$. As shown in Figure 1.7, the distributions of the MOs for **6**, the HOMO is located on the phenyl moiety, whereas, the LUMO is mainly localized on the NBD fluorophore. Consequently, the emission from the S_1 to S_0 state involves an intramolecular charge transfer from the NBD unit. For **6a**, allowed electronic transition was $S_0 \rightarrow S_1$ (HOMO \rightarrow LUMO, $f = 0.2590$). $S_0 \rightarrow S_1$ transition was characterized as $\pi \rightarrow \pi^*$ and $\pi \rightarrow n$ transition.

To investigate the emission of **6a** the geometry of the singlet excited state (S_1) was optimized and the excitation based on the S_1 geometry was calculated. For **6a** presence of an emissive S_1 state (an allowed $S_0 \rightarrow S_1$ transition with $f = 0.1611$) suggesting that the radiative $S_1 \rightarrow S_0$ decay is possible. $S_0 \rightarrow S_1$ transition was characterized as $\pi^* \rightarrow \pi$ and $n \rightarrow \pi$ transition. Therefore, all these calculation is matching with ratiometric outcome of probe **5** and also indicated that compound **6** can behave as *off-on* probe.

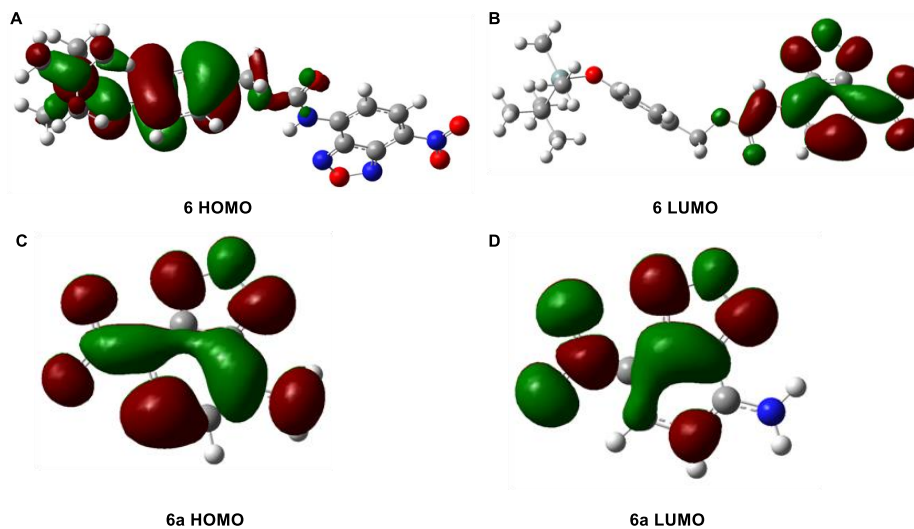


Figure 1.6: View of the ground state frontier molecular orbitals (MOs), **A**) HOMO, **B**) LUMO of **6**, **C**) HOMO and **D**) LUMO of **6a** generated from TDDFT/CAM-B3LYP/6-311G (d,p) geometry optimization.

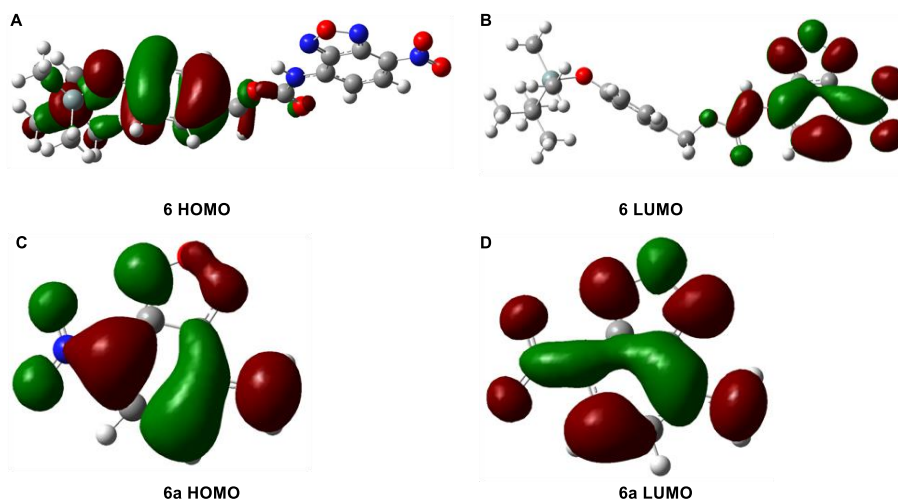


Figure 1.7: View of the excited state frontier molecular orbitals (MOs), **A**) HOMO, **B**) LUMO of **6**, **C**) HOMO and **D**) LUMO of **6a** generated from TDDFT/CAM-B3LYP/6-311G (d,p) geometry optimization.

Table 1.1: Selected parameters for the vertical excitation (UV–vis Absorptions) of probe **5**, **5a**, **6** and **6a** obtained by the TDDFT/CAM-B3LYP/6-311G (d, p), based on the optimized ground state geometries (water was employed as solvent in all the calculations).

Compound	Electronic transitions ^a	Energy (eV)	λ (nm)	f^b	Main configurations	CI coefficients ^c
5	$S_0 \rightarrow S_1$	3.69	335.82	0.4323	HOMO→LUMO	0.669590
					HOMO-1→LUMO	0.192950
5a	$S_0 \rightarrow S_1$	3.39	365.52	0.2690	HOMO→LUMO	0.697590
6	$S_0 \rightarrow S_1$	2.40	516.33	0.0000	HOMO→LUMO	0.699830
					HOMO-7→LUMO	0.183510
					HOMO-7→LUMO+1	0.158180
					HOMO-5→LUMO	0.501130
					HOMO-5→LUMO+5	0.396020
	$S_0 \rightarrow S_3$	3.45	359.92	0.4471	HOMO-1→LUMO	0.698210
6a	$S_0 \rightarrow S_1$	3.24	382.39	0.2590	HOMO→LUMO	0.695880
					HOMO→LUMO+1	0.102610

^a Only the main configurations are presented, ^b Oscillator strength, ^c The CI coefficients are in absolute values.

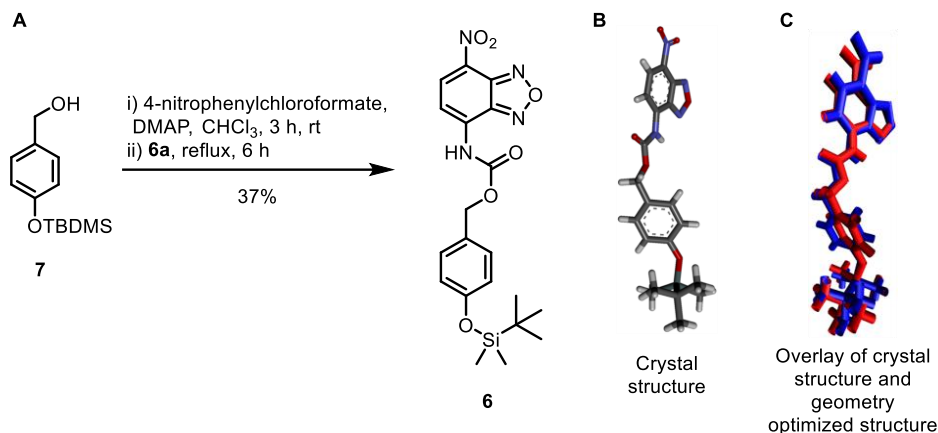
Table 1.2: Selected parameters for the fluorescence emission of probe **5**, **5a**, **6** and **6a** obtained by the TDDFT/CAM-B3LYP/6-311G (d, p), based on the optimized ground state geometries (water was employed as solvent in all the calculations).

Compound	Electronic transitions ^a	Energy (eV)	λ (nm)	f^b	Main configurations	CI coefficients ^c
5	S ₁ →S ₀	3.05	406.31	0.3820	HOMO→LUMO	0.698850
5a	S ₁ →S ₀	2.69	460.61	0.2029	HOMO→LUMO	0.700760
6	S ₁ →S ₀	0.80	1543.28	0.0000	HOMO→LUMO	0.702350
	S ₂ →S ₀	3.99	310.97	0.0000	HOMO-4→LUMO	0.536010
					HOMO-4→LUMO+1	0.422640
					HOMO-4→LUMO+5	0.138810
	S ₃ →S ₀	3.00	413.63	0.3807	HOMO-1→LUMO	0.700580
6a	S ₁ →S ₀	2.62	473.75	0.1611	HOMO→LUMO	0.700210

^a Only the main configurations are presented, ^b Oscillator strength, ^c The CI coefficients are in absolute values.

1.2.2. Synthesis

Synthesis of the probe **6** was carried out from NBD-amine **6a**.²³ 4-(*tert*-Butyldimethylsilyloxy)benzylalcohol **7** was synthesized first according to the reported protocol from 4-hydroxybenzaldehyde.²⁴ Alcohol **7** was then treated with 4-nitrophenylchloroformate in presence of DMAP in CHCl₃ at room temperature to generate corresponding active carbonate intermediate which was reacted subsequently with **6a** to provide probe **6** with overall 37% yield (Scheme 1.1A). The structure of probe **6** was confirmed by ¹H-NMR, ¹³C-NMR spectroscopy, high resolution mass spectrometry and single crystal X-ray diffraction studies (Scheme 1.1B). Superimposition of crystal structure (blue) and geometry optimized structure (red) of **6** based on Si-atom and all N-atom alignment provided a RMSD = 0.39 Å (Scheme 1.1C). Excellent superimposition of two structures indicates correct atom coordinates were used for the TDDFT calculation.



Scheme 1.1: A) Synthesis of the probe **6**, B) crystal structure and C) overlay of crystal structure and geometry optimized structure.

1.2.3. Photophysical Properties

Absorption spectra and fluorescence spectra of probe **6** (10 μM) were recorded in 9:1 EtOH/HEPES (10 mM, pH = 7.4) solution. Molar absorption coefficients were calculated from absorption spectra using Lambert-Beer Law. Photophysical studies of the probe **6** displayed a strong absorption band centered at $\lambda_{\text{max}} = 399$ nm with molar extinction coefficient value, $\epsilon = 12190 \text{ M}^{-1} \text{ cm}^{-1}$ in 9:1 EtOH /HEPES buffer (10 mM, pH = 7.4) solution. However, the probe **6** exhibited negligible fluorescence intensity and low quantum yield, $\Phi_{\text{F}} = 0.0495$ (standard: NBD-NHMe in acetonitrile $\Phi_{\text{F}} = 0.38$).²⁵ NBD-amine **6a** displayed a strong absorption band centered at $\lambda_{\text{max}} = 460$ nm ($\epsilon = 13113 \text{ M}^{-1} \text{ cm}^{-1}$), intense fluorescence with $\lambda_{\text{em}} = 535$ nm ($\lambda_{\text{ex}} = 460$ nm) and $\Phi_{\text{F}} = 0.36$. These data confirm the predicted *off-on* characteristics, if probe **6** is subjected to chemical conversion to **6a** (Figure 1.8).

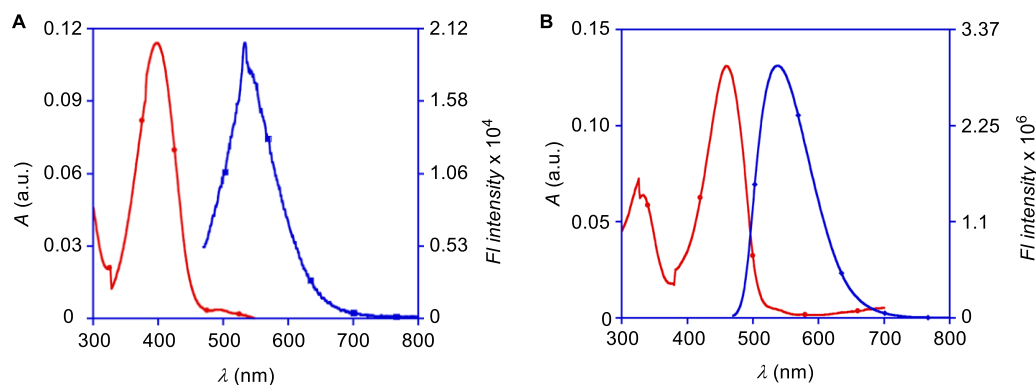


Figure 1.8: Normalized UV-vis absorption and emission spectra of **A)** probe **6** and **B)** **6a** in 9:1 EtOH/HEPES buffer (10 mM, pH = 7.4) solution at room temperature.

Determination of quantum yields

The quantum yield of probe was determined according to the following equation:

$$\Phi_1 = \Phi_B \times \frac{I_1 \times A_B \times \lambda_{exB} \times (\eta_1)^2}{I_B \times A_1 \times \lambda_{ex1} \times (\eta_B)^2}$$

where, Φ is quantum yield; I is integrated area under the corrected emission spectra; A is absorbance at the excitation wavelength; λ_{ex} is the excitation wavelength; η is the refractive index of the solution; the subscripts 1 and B refer to the unknown and the standard, respectively.

N-methyl NBD was used as standard ($\Phi=0.38$) in acetonitrile.

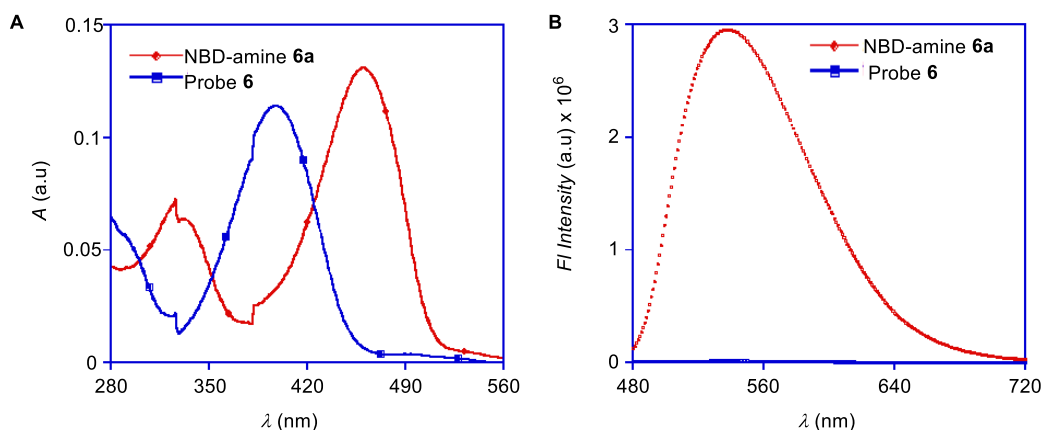


Figure 1.9: **A)** UV-vis absorption spectra and **B)** emission spectra of **6a** (10 μ M) and probe **6** (10 μ M) in 9:1 EtOH/HEPES buffer (10 mM, pH = 7.4) solution at room temperature.

Table 1.3. Photophysical Properties of **6** and **6a**.

Compound	λ_{max} (nm)	ϵ ($M^{-1} cm^{-1}$)	λ_{em} (nm)	Φ^a
6	399	12190	535	0.0495
6a	459	13113	535	0.36

^a Standard: NBD-NHMe in acetonitrile $\Phi_F = 0.38$.

The observed photophysical properties of molecules **6** and **6a** encouraged us to investigate further into the quenching mechanism operative in these systems. The life-time experiment for both compounds showed the fluorescence decay profile of probes **6** and **6a** recorded in 9:1 ethanol/HEPES buffer (10 mM, pH = 7.4) with excitation at 460 nm (Figure 1.10). Emission at 535 nm for the probe **6** showed mono-exponential decay profile with $\tau = 1.303$ ns. On the other hand, amine **6a** exhibited a mono-exponential decay profile with $\tau = 5.465$ ns. From these data, radiative decay rate constant (k_r) and non-radiative decay rate constant (k_{nr}) for species **6** and **6a** were determined using following equations.²⁶

$$k_r = \Phi/\tau \quad (1)$$

$$k_{nr} = (1/\tau) - k_r \quad (2)$$

The probe **6** displayed k_r value of 0.0379 ns^{-1} and a corresponding $k_{nr} = 0.727 \text{ ns}^{-1}$. For amine **6a**, calculated k_r and k_{nr} values were 0.0658 and 0.1169 ns^{-1} , respectively. For probe **6**, the $k_r / k_{nr} = 0.052$ confirmed a predominant non-radiative pathway, responsible for its quenched fluorescence state. On the other hand, $k_r / k_{nr} = 0.5628$ calculated for **6a** corroborate with its strong fluorescence due to radiative pathway as the main channel.

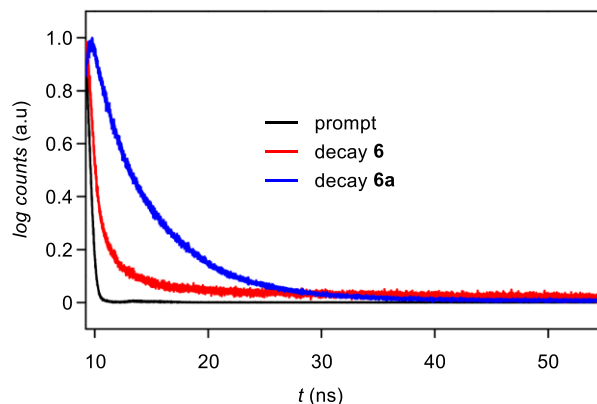


Figure 1.10: Fluorescence lifetime decay profiles ($\lambda_{ex} = 460$ nm) of probe **6** (—) and **6a** (—) in 9:1 EtOH/HEPES buffer (10 mM, pH = 7.4) monitored at 535 nm. Prompt represents the laser profile (—).

Table 1.4: Time resolved fluorescence data for **6** and **6a**.

Probe	τ (ns)	k_r (ns^{-1})	k_{nr} (ns^{-1})	k_r / k_{nr}
6	1.303	0.0379	0.727	0.052

1.2.4. Fluoride Sensing

It is expected that because of the high affinity of F^- ion towards silicon, it would lead to the cleavage of Si-O bond which will release the green fluorescent molecule **6a**. The response of probe **6** for F^- was assayed by UV-Visible spectroscopy upon addition of F^- to solution of probe. Absorption band shifted 61 nm red shift from $\lambda_{max} = 399$ nm to 460 nm (Figure 1.9).

To evaluate the response time, the reaction of probe **6** and F^- was evaluated by fluorescence kinetics (Figure 1.11). In this experiment, 300 equivalent of tetrabutylammonium fluoride (TBAF) was added to probe **6** (10 μ M) in 9:1 EtOH/HEPES buffer (10 mM, pH = 7.4) solution at 30 s and enhancement of fluorescence intensity at $\lambda_{em} = 535$ nm ($\lambda_{ex} = 460$ nm) was recorded in time (Figure 1.11). Sharp enhancement of fluorescence intensity was observed up to 60 minutes followed by flattening of the enhancement and 110 fold of intensity enhancement was observed. Therefore, a reaction time of 60 minutes was used for further studies with $\sim 80\%$ completion of reaction.

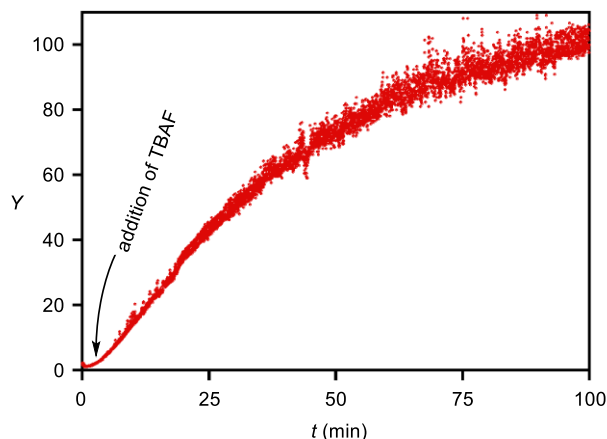


Figure 1.11: Emission kinetics profile of probe **6** (10 μ M) in 9:1 EtOH/HEPES buffer (10 mM, pH = 7.4) solution at room temperature at $\lambda_{em} = 535$ nm upon excitation of $\lambda_{ex} = 460$ nm.

In the next stage the selectivity of probe **6** towards F^- was examined in presence of various competitive anions (Figure 1.12). When probe **6** (10 μ M) in EtOH/HEPES buffer (10 mM, pH 7.4) solution (9:1) was treated with the 200 equivalent of F^- , 110 fold enhancement in the fluorescence intensity was observed after 1 h stirring at rt. The fluorescence measurements were carried out

under comparable condition in presence of various possibly interfering ions *e.g.* Br^- , I^- , Cl^- , ClO_4^- , PF_6^- , NO_3^- , HSO_4^- , OAc^- , SO_4^{2-} (2 mM) which showed no change in emission intensity (Figure 1.12A, front row). The probe **6** showed intensity enhancement only after addition of F^- which showed the sensitivity of the probe **6** towards F^- in presence of other ions (Figure 1.12A, back row). All data were taken after 1 h of addition of anions at room temperature at $\lambda_{\text{em}} = 535$ nm. Naked eye monitoring of the detection process was associated with the color change from colorless to yellow in presence of F^- ion and other anions did not provide any color change (Figure 1.12B).

Quantitative *off-on* response of **6** towards F^- was done by fluorometric titrations (Figure 1.13A). Titration of probe **6** (10 μM) with increasing concentration of F^- resulted in the enhancement of fluorescence intensity at $\lambda_{\text{em}} = 535$ nm ($\lambda_{\text{ex}} = 460$ nm) in a concentration dependent manner and with a saturation of fluorescence intensity after 300 equivalent of F^- added. Each spectrum was taken after 1h after addition of F^- . The fluorescence intensity reaches to saturation

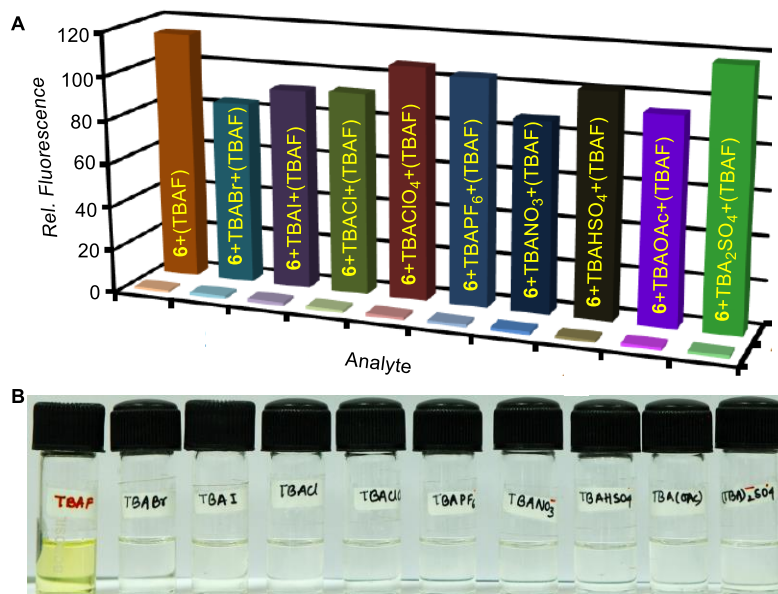


Figure 1.12: **A)** Relative fluorescent intensity of the probe **6** (10 μM) in 9:1 EtOH/ HEPES buffer (10 mM, pH = 7.4) solution towards ranges of anions (2 mM) followed by addition of TBAF (2 mM). **B)** Photograph was taken under ambient light upon treating probe **6** with respective analytes in 9:1 EtOH HEPES buffer (10 mM, pH = 7.4) solution.

when 300 equivalent of F^- was added to probe **6**. When images were taken under the hand-held UV lamp, the cuvette containing probe **6** exhibited negligible blue fluorescence (Figure 1.13B). On the other hand, the reaction mixture containing probe **6** and TBAF displayed strong green fluorescence.

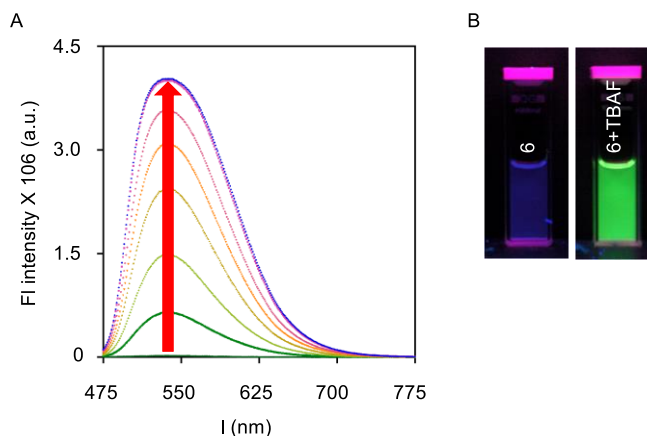


Figure 1.13: **A)** Fluorescence enhancement of the probe **6** (10 μ M) in EtOH/ HEPES buffer (10 mM, pH 7.4) solution (9:1) with increasing concentration of by 50 equivalents and **B)** Cuvette image of probe **6** and after addition of TBAF under handheld 365 nm UV light.

1.2.5. Cell imaging

Further to demonstrate the practical application of **6**, we have carried out *in vitro* live cell imaging using fluorescence microscopic technique with A549 human lung carcinoma cell line^{13f} (Figure 1.14). No significant fluorescence was observed when A549 cell were incubated with only Probe **6** (50 μ M in 1:100 DMSO-DMEM v/v, pH = 7.4) at 37 °C for 7 h (Figure 1.14E). But when A549 cells were pre-treated with 50 mM NaF (50 mM in 1:100 H₂O-DMEM, pH=7.4) at 37 °C for 3 h followed by incubation of **6** (50 μ M in 1:100 DMSO-DMEM v/v, pH = 7.4) at 37 °C for 7 h, showed strong fluorescence inside the cell (Figure 1.14B). This data indicates the cell permeability of **6** and its ability to detect F^- in intracellular environment of living organism.

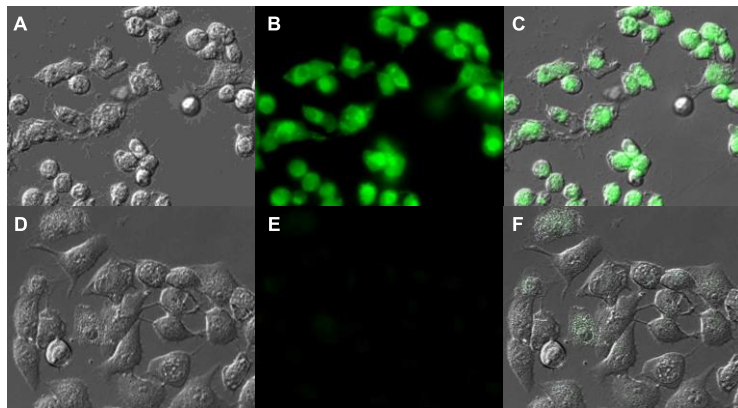


Figure 1.14 Cell image of A549 (human epithelial lung carcinoma cell): **A)** DIC, **B)** fluorescence, and **C)** overlay, image of A-549 cell first incubated with NaF (50 mM) for 3 h followed by incubation with **6** (50 μ M) for 7h (**D-F**) are the respective DIC, fluorescence and overlay image of A-549 cell incubated with **6** (50 μ M) for 7h.

1.3. Conclusion

In conclusion, we have successfully designed, synthesized and investigated the properties of a NBD-based *off-on* probe for sensing of F^- ion using theoretical calculations. Based on TDDFT calculations of excitation and emission for the probe and for the NBD-amine fluorophore rationalized the predicted *off-on* response. Steady state and time resolved fluorescence properties of these species further validated the design. The NBD-probe exhibited a response time of 80 min in presence of 300 equivalent of TBAF and the reaction was selective to only F^- , even in the presence of various interfering analytes. F^- ion sensing ability of the probe was associated with 110-fold enhancement in fluorescence at $\lambda_{em} = 535$ nm and selectivity was achieved even in the presence of competing anions. The sensing of F^- ion were marked by visible color change from colorless to yellow and green turn-on fluorescence under UV-light. Cell permeability of the probe and its ability of detecting intracellular F^- ion was confirmed by live cell imaging.

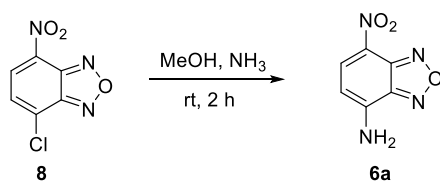
1.4. Experimental Section

General Methods: All reactions were carried under the nitrogen atmosphere. All the chemicals were purchased from commercial sources and used as received unless stated otherwise. Solvents: petroleum ether and ethyl acetate (EtOAc) were distilled prior to thin layer and column

chromatography. Column chromatography was performed on Merck silica gel (100-200 mesh). TLC was carried out with E. Merck silica gel 60-F-254 plates.

Instrumentation and Software: The ^1H and ^{13}C spectra were recorded on 400 MHz Jeol ECS-400 (or 100 MHz for ^{13}C) spectrometers using either residual solvent signals as an internal reference or from internal tetramethylsilane on the δ scale (CDCl_3 δ_{H} , 7.26 ppm, δ_{C} 77.0 ppm). The chemical shifts (δ) are reported in ppm and coupling constants (J) in Hz. The following abbreviations are used: s (singlet), d (doublet). High-resolution mass spectra were obtained from MicroMass ESI-TOF MS spectrometer. All MALDI-MS measurements were recorded on an Applied Biosystems 4800 Plus MALDI TOF/TOF analyzer. Absorption spectra were recorded on a PerkinElmer, Lambda 45 UV-Vis spectrophotometer. Steady State fluorescence experiments were carried out in a micro fluorescence cuvette (Hellma, path length 1.0 cm) on a Fluoromax 4 instrument (Horiba Jobin Yvon). Time-resolved fluorescence measurements were carried on a TCSPC instrument (Horiba Jobin Yvon, Fluoro 3PS). (FT-IR) spectra were obtained using NICOLET 6700 FT-IR spectrophotometer as KBr disc and reported in cm^{-1} . Melting points were measured using a VEEGO Melting point apparatus. All melting points were measured in open glass capillary and values are uncorrected. Crystal structures were recorded on a Bruker single crystal X-Ray diffractometer. Geometry optimizations and emission characteristics were carried out using the Gaussian 09 software package.²⁰ Superimposition of crystal structure and geometry optimized structure of **5** were obtained using VMD 1.9.1 software.

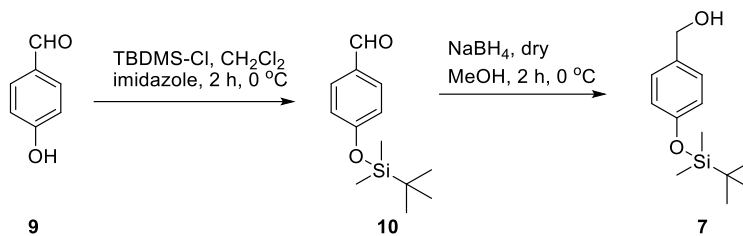
Synthesis Procedure:



Scheme 1.2: Synthesis of NBD-amine **6a**.

Synthesis of NBD-amine 6a: Compound NBD-Cl **8** (1 g, 5.025 mmol) was dissolved in MeOH (100 mL). To this solution was added 25% aqueous ammonia solution (20 mL) was added dropwise and kept at room temperature for 2 hours. At the completion of the reaction, solvent was evaporated from the reaction mixture under reduced pressure and the residue was subjected to column chromatography to afford 60% **6a** as brown powder. ^1H NMR (400 MHz, 1:1

$\text{CDCl}_3/\text{CD}_3\text{OD}$): δ 8.23 (d, $J = 8.6$ Hz, 1H), 6.14 (d, $J = 8.7$ Hz, 1H). The obtained data were matched with the literature data.²³



Scheme 1.3: Synthesis of alcohol **7**.

Synthesis of 4-((tert-butyldimethylsilyl)oxy)benzaldehyde 10: 4-hydroxybenzaldehyde **9** (2 g, 16.39 mmol) was dissolved in CH_2Cl_2 (30 mL) and subsequently imidazole (1.67 g, 24.58 mmol) was added to it. Then, *tert*-butyldimethylsilylchloride (TBDMS-Cl) (0.53 g, 32.70 mmol) solution in CH_2Cl_2 was added dropwisely to the solution at 0 °C. This temperature was maintained for 2 h. After completion of reaction, organic layer was washed with water, brine (10 mL) and dried over Na_2SO_4 . The solvent was removed under reduced pressure and the obtained residue was purified by column chromatography (*Eluent*: 3% EtOAc in petroleum ether) to get pure product **10**. $^1\text{H NMR}$ (400 MHz, CDCl_3): δ 7.77 (d, $J = 8.6$ Hz, 1H), 6.93 (d, $J = 8.6$ Hz, 1H). Obtained data were matched with literature data.²⁴

Synthesis of (4-((tert-butyldimethylsilyl)oxy)phenyl)methanol 7: Compound **10** (1.25 g, 5.08 mmol) was dissolved in dry MeOH (20 mL) and stirred for 15 min at 0 °C. Then NaBH_4 (0.23 g, 6.1 mmol) was added to the reaction mixture and kept for 2 h at this temperature. The solvent was evaporated under reduced pressure and the crude was extracted with EtOAc (15 mL x 2), water (15 mL x 2), brine (20 mL) and dried over Na_2SO_4 . The organic layer was evaporated under reduced pressure and the residue was purified through column chromatography over silica gel to get pure **7** (*Eluent*: 15% EtOAc in petroleum ether) as colorless liquid (1.1 g, 87%). $^1\text{H NMR}$ (400 MHz, CDCl_3): δ 7.21 (d, $J = 8.4$ Hz, 1H), 6.81 (d, $J = 8.5$ Hz, 1H). Obtained data were matched with literature data.²⁴

Synthesis of 4-((tert-butyldimethylsilyl)oxy)benzyl (7-nitrobenzo[*c*][1,2,5]oxadiazol-4-yl)carbamate 6: Alcohol **7** (264 mg, 1.1 mmol) was dissolved in chloroform (15 mL) and then 4-dimethylaminopyridine (DMAP) (0.16 gm, 1.32 mmol) and 4-nitrophenylchloroformate were added to it and stirred at room temperature for 3 h. TLC showed the consumption of both starting materials at this stage. NBD-amine **6a** (0.18 gm, 0.99 mmol), DMAP (0.16 gm, 1.32 mmol)

dissolved in CHCl_3 (5 mL) was added dropwisely to the reaction mixture and refluxed for overnight. After the completion of reaction, the solvent was evaporated under reduced pressure and the yellow residue was subjected to column chromatography over silica gel (*Eluent*: 5% EtOAc in petroleum ether) to furnish pale yellow compound **6** (175 mg, 37%). **M.p.**: 134.5 – 135.5 °C; **IR (KBr)**: $\nu_{\text{max}}/\text{cm}^{-1}$: 3415, 2940, 2857, 1740, 1565, 1514, 1454, 1365, 1326, 1258; **^1H NMR (400 MHz, CDCl_3)**: δ 8.57 (d, $J = 8.24$ Hz, 1H), 8.17 (d, $J = 8.7$ Hz, 1H), 7.32 (d, $J = 8.7$ Hz, 2H), 6.87 (d, $J = 8.6$ Hz, 2H), 5.25 (s, 2H), 0.99 (s, 9H), 0.21 (s, 6H); **^{13}C NMR (100 MHz, CDCl_3)**: δ 156.5, 151.9, 144.7, 143.0, 134.3, 133.9, 130.3, 126.9, 120.2, 110.4, 68.0, 25.2, 18.2, -4.4; **HRMS (ESI)**: Calc. for $\text{C}_{20}\text{H}_{24}\text{N}_4\text{O}_6\text{Si}$ $[\text{M}-\text{H}]^-$: 443.1392; Found: 443.1387.

X-Ray single crystal determination: Single crystal of **6** suitable for X-ray diffraction study was grown as mentioned below. These data can be obtained free of charge via www.ccdc.cam.ac.uk/data_request/cif, by emailing data_request@ccdc.cam.ac.uk, or by contacting The Cambridge Crystallographic Data Centre, 12, Union Road, Cambridge CB2 1EZ, U.K. (fax +44 1223 336033).

Crystal structure of probe 6 (CCDC 955810): $\text{C}_{20}\text{H}_{24}\text{N}_4\text{O}_6\text{Si}$; Compound **6** was crystallized from ethyl acetate at room temperature. A yellow needle shaped crystal with approximate dimensions 0.16 x 0.14 x 0.10 mm³ gave a Triclinic lattice with space group P-1; $a = 6.2718(19)$ Å $b = 18.621(6)$ Å $c = 19.391(6)$ Å, $\alpha = 82.717(6)^\circ$ $\beta = 84.770(6)^\circ$ $\gamma = 86.359(6)^\circ$; $V = 2233.9(12)$ Å³; $T = 200(2)$ K; $Z = 4$; $\rho_{\text{calc}} = 1.322$ g cm⁻³; $2\theta_{\text{max}} = 55.98^\circ$; $\text{MoK}\alpha\lambda = 0.71073$ Å. Fine-focus sealed tube source with graphite monochromator. $R = 0.0793$ (for 5031 reflection $I > 2\sigma(I)$), $wR = 0.2393$ which was refined against $|F_2|$ and $S = 0.947$ for 569 parameters and 10720 unique reflections. The structure was obtained by direct methods using SHELXS-97. All non-hydrogen atoms were refined isotropically. The hydrogen atoms were fixed geometrically in the idealized position and refined in the final cycle of refinement as riding over the atoms to which they are bonded. $\mu = 0.148$ mm⁻¹.

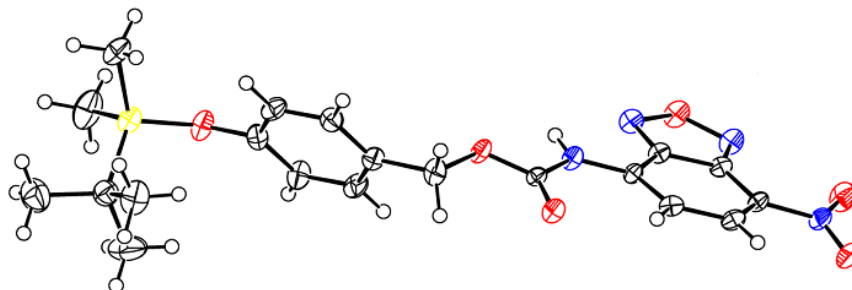
Preparation of Solvent System: HEPES (10 mM, pH = 7.4) buffer was prepared by using deionized water. Solvent system was prepared by mixing 90% EtOH and 10% HEPES buffer (10 mM, pH = 7.4).

Preparation of the sample Solutions: A stock solution of probe (3777 μM) was prepared in THF. The final concentration during assay is 10 μM . Stock solution of TBAF was prepared by diluting 1 M TBAF in THF.

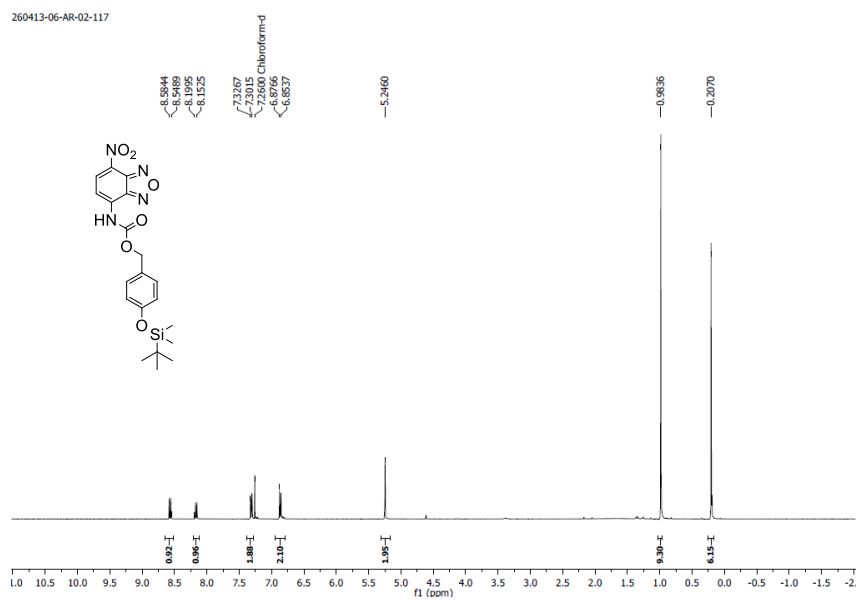
General Methods for UV-Vis and Fluorescence titration: For absorbance and emission studies 1 cm path length was used for cells. All UV and Fluorescence measurements were performed with 10 μM of probe. Fluorescence measurements were done using 2 nm x 5 nm slit. Fluorescence titrations were performed after 1 h of mixing of probe and TBAF.

Live Cell Imaging: The A549 cells were purchased from National Centre for Cell Science, Pune (India). A549 cells were grown in DMEM supplemented with 10% heat inactivated fetal bovine serum (FBS), 100 IU/mL penicillin, 100 mg/mL streptomycin and 2 mM L-glutamine. Cultures were maintained in a humidified atmosphere with 5% CO_2 at 37 $^\circ\text{C}$. The cultured cells were subcultured twice in each week, seeding at a density of about 15×10^4 cells/mL. Typan blue dye exclusion method was used to determine Cell viability. The fluorescence images were taken using Olympus Inverted IX81 equipped with Hamamatsu Orca R2 microscope by exciting at $\lambda_{\text{ex}} = 460\text{-}480$ nm (by using GFP filter). The A549 cells were incubated with solution of the probe **6** (50 μM in 1:100 DMSO-DMEM v/v, pH = 7.4) at 37 $^\circ\text{C}$ for 7 h. After washing with PBS the fluorescence images were acquired. In this case no significant fluorescence was observed. Another set of A549 cells were treated with NaF (50 mM in 1:100 DMSO-DMEM v/v, pH = 7.4) at 37 $^\circ\text{C}$ for 3 h and then the cells were washed thoroughly with PBS and incubated with solution of the probe (50 μM in 1:100 DMSO-DMEM v/v, pH = 7.4) at 37 $^\circ\text{C}$ for 7 h. After washing with PBS the fluorescence images showed strong green fluorescence.

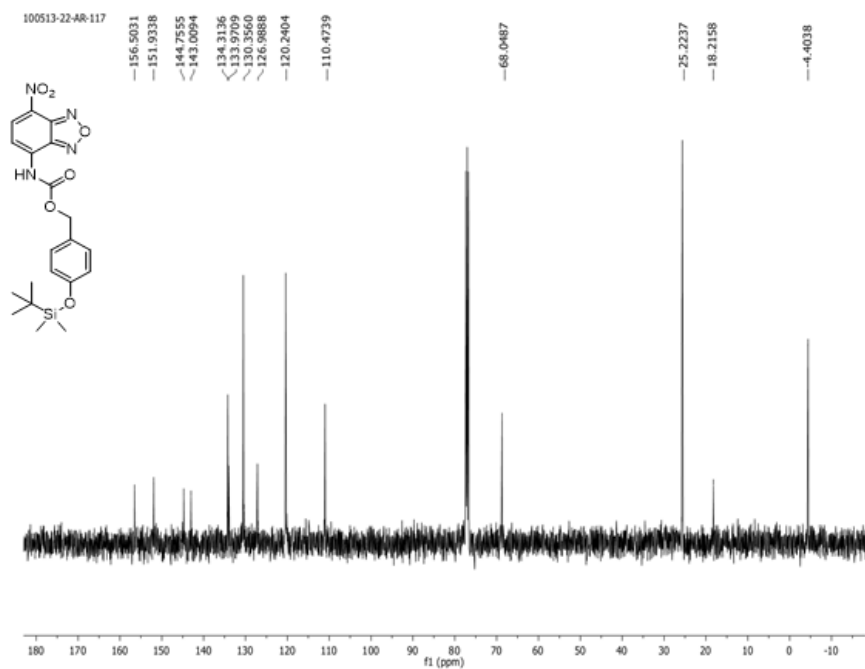
1.5 Appendix Section



Appendix 1.1: ^{13}C NMR data of probe **6** in CDCl_3 .



Appendix 1.2: ^1H NMR data of probe 6 in CDCl_3 .



Appendix 1.3: ^{13}C NMR data of probe 6 in CDCl_3 .

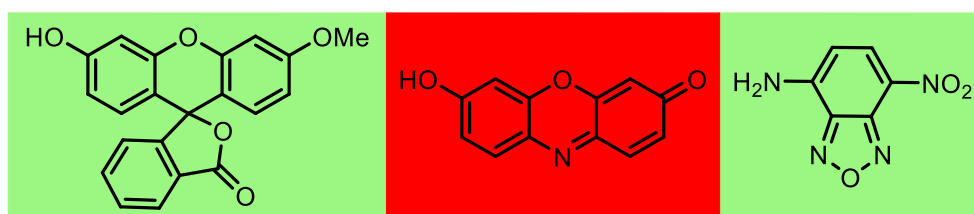
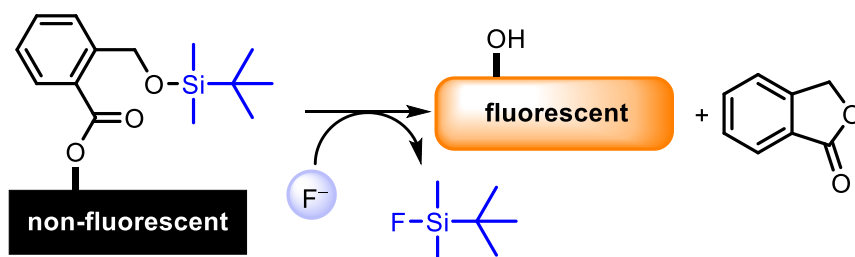
1.6. References

1. Wenzel, M.; Hiscock, J. R.; Gale, P. A. *Chem. Soc. Rev.* **2012**, *41*, 480-520.
2. (a) Rendl, J.; Seybold, S.; Börner, W. *Clin. Chem.* **1994**, *40*, 908-13; (b) Kibbey, C. E.; Meyerhoff, M. E. *Anal. Chem.* **1993**, *65*, 2189-2196.
3. Vázquez, M.; Fabbrizzi, L.; Taglietti, A.; Pedrido, R. M.; González-Noya, A. M.; Bermejo, M. R. *Angew. Chem., Int. Ed.* **2004**, *43*, 1962-1965.
4. (a) Duke, R. M.; Veale, E. B.; Pfeffer, F. M.; Kruger, P. E.; Gunnlaugsson, T. *Chem. Soc. Rev.* **2010**, *39*, 3936-3953; (b) Gunnlaugsson, T.; Glynn, M.; Tocci, G. M.; Kruger, P. E.; Pfeffer, F. M., *Coord. Chem. Rev.* **2006**, *250*, 3094-3117.
5. (a) Bérubé, P. R.; Parkinson, P. D.; Hall, E. R. *J. Chromatogr. A* **1999**, *830*, 485-489; (b) Butts, W. C.; Rainey, W. T. *Anal. Chem.* **1971**, *43*, 538-542.
6. Harwood, J. E. *Water Res.* **1969**, *3*, 273-280.
7. Martínez-Mañez, R.; Sancenón, F. *Chem. Rev.* **2003**, *103*, 4419-4476.
8. Moragues, M. E.; Martinez-Manez, R.; Sancenon, F. *Chem. Soc. Rev.* **2011**, *40*, 2593-2643.
9. Cametti, M.; Rissanen, K. *Chem. Commun.* **2009**, 2809-2829.
10. (a) Cametti, M.; Rissanen, K. *Chem. Soc. Rev.* **2013**, *42*, 2016-2038; (b) Gale, P. A. *Chem. Soc. Rev.* **2010**, *39*, 3746-3771; (c) Gale, P. A.; Garcia-Garrido, S. E.; Garric, J. *Chem. Soc. Rev.* **2008**, *37*, 151-190.
11. (a) Yang, X.-F.; Qi, H.; Wang, L.; Su, Z.; Wang, G. *Talanta* **2009**, *80*, 92-97; (b) Zhu, B.; Yuan, F.; Li, R.; Li, Y.; Wei, Q.; Ma, Z.; Du, B.; Zhang, X. *Chem. Commun.* **2011**, *47*, 7098-7100; (c) Cao, X.; Lin, W.; Yu, Q.; Wang, J. *Org. Lett.* **2011**, *13*, 6098-6101; (d) Dong, M.; Peng, Y.; Dong, Y.-M.; Tang, N.; Wang, Y.-W. *Org. Lett.* **2011**, *14*, 130-133; (e) Rao, M. R.; Mobin, S. M.; Ravikanth, M. *Tetrahedron* **2010**, *66*, 1728-1734; (f) Bao, Y.; Liu, B.; Wang, H.; Tian, J.; Bai, R. *Chem. Commun.* **2011**, *47*, 3957-3959.
12. Bozdemir, O. A.; Sozmen, F.; Buyukcikir, O.; Guliyev, R.; Cakmak, Y.; Akkaya, E. U. *Org. Lett.* **2010**, *12*, 1400-1403.
13. (a) Kim, S. Y.; Hong, J.-I. *Org. Lett.* **2007**, *9*, 3109-3112; (b) Sakkalingam, P.; Lee, C.-H. *J. Org. Chem.* **2011**, *76*, 3820-3828; (c) Kim, D.; Singha, S.; Wang, T.; Seo, E.; Lee, J. H.; Lee, S.-J.; Kim, K. H.; Ahn, K. H. *Chem. Commun.* **2012**, *48*, 10243-10245; (d) Ke, B.; Chen, W.; Ni, N.; Cheng, Y.; Dai, C.; Dinh, H.; Wang, B. *Chem. Commun.* **2013**, *49*, 2494-2496; (e) Yang, X.-F. *Spectrochim. Acta Mol. Biomol. Spectrosc.* **2007**, *67*, 321-326; (f) Kim, S. Y.; Park, J.; Koh, M.; Park, S. B.; Hong, J.-I. *Chem. Commun.* **2009**, 4735-4737.
14. Hu, R.; Feng, J.; Hu, D.; Wang, S.; Li, S.; Li, Y.; Yang, G. *Angew. Chem., Int. Ed.* **2010**, *49*, 4915-4918.
15. Nicolaou, K. C.; Edmonds, D. J.; Bulger, P. G. *Angew. Chem., Int. Ed.* **2006**, *45*, 7134-7186.
16. Zhang, J. F.; Lim, C. S.; Bhuniya, S.; Cho, B. R.; Kim, J. S. *Org. Lett.* **2011**, *13*, 1190-1193.
17. (a) Ji, S.; Guo, H.; Yuan, X.; Li, X.; Ding, H.; Gao, P.; Zhao, C.; Wu, W.; Wu, W.; Zhao, J. *Org. Lett.* **2010**, *12*, 2876-2879; (b) Long, L.; Li, X.; Zhang, D.; Meng, S.; Zhang, J.; Sun, X.; Zhang, C.; Zhou, L.; Wang, L. *RSC Adv.* **2013**, *3*, 12204-12209; (c) Caballero, A.; Espinosa, A.; Tárraga, A.; Molina, P. *J. Org. Chem.* **2008**, *73*, 5489-5497; (d) Otón, F.; Ratera, I.; Espinosa, A.; Wurtz, K.; Parella, T.; Tárraga, A.; Veciana, J.; Molina, P. *Chem. Eur. J.* **2010**, *16*, 1532-1542.

18. (a) Kand, D.; Kalle, A. M.; Varma, S. J.; Talukdar, P. *Chem. Commun.* **2012**, *48*, 2722-2724; (b) Kand, D.; Mishra, P. K.; Saha, T.; Lahiri, M.; Talukdar, P. *Analyst* **2012**, *137*, 3921-3924.
19. (a) Chiba, M.; Tsuneda, T.; Hirao, K. *J. Chem. Phys.* **2007**, *126*, 034504; (b) Wiggins, P.; Williams, J. A. G.; Tozer, D. J. *J. Chem. Phys.* **2009**, *131*, 091101; (c) Guido, C. A.; Mennucci, B.; Jacquemin, D.; Adamo, C. *Phys. Chem. Chem. Phys.* **2010**, *12*, 8016-8023.
20. Frisch, M. J.; Trucks, G. W.; Schlegel, H. B.; Scuseria, G. E.; Robb, M. A.; Cheeseman, J. R.; Scalmani, G.; Barone, V.; Mennucci, B.; Petersson, G. A.; Nakatsuji, H.; Caricato, M.; Li, X.; Hratchian, H. P.; Izmaylov, A. F.; Bloino, J.; Zheng, G.; Sonnenberg, J. L.; Hada, M.; Ehara, M.; Toyota, K.; Fukuda, R.; Hasegawa, J.; Ishida, M.; Nakajima, T.; Honda, Y.; Kitao, O.; Nakai, H.; Vreven, T.; Montgomery Jr., J. A.; Peralta, J. E.; Ogliaro, F.; Bearpark, M. J.; Heyd, J.; Brothers, E. N.; Kudin, K. N.; Staroverov, V. N.; Kobayashi, R.; Normand, J.; Raghavachari, K.; Rendell, A. P.; Burant, J. C.; Iyengar, S. S.; Tomasi, J.; Cossi, M.; Rega, N.; Millam, N. J.; Klene, M.; Knox, J. E.; Cross, J. B.; Bakken, V.; Adamo, C.; Jaramillo, J.; Gomperts, R.; Stratmann, R. E.; Yazyev, O.; Austin, A. J.; Cammi, R.; Pomelli, C.; Ochterski, J. W.; Martin, R. L.; Morokuma, K.; Zakrzewski, V. G.; Voth, G. A.; Salvador, P.; Dannenberg, J. J.; Dapprich, S.; Daniels, A. D.; Farkas, Ö.; Foresman, J. B.; Ortiz, J. V.; Cioslowski, J.; Fox, D. J. *Gaussian 09*, Gaussian, Inc.: Wallingford, CT, USA, **2009**.21. (a) Mennucci, B. *Phys. Chem. Chem. Phys.* **2013**, *15*, 6583-6594; (b) Jacquemin, D.; Mennucci, B.; Adamo, C. *Phys. Chem. Chem. Phys.* **2011**, *13*, 16987-16998; (c) Pedone, A.; Barone, V. *Phys. Chem. Chem. Phys.* **2010**, *12*, 2722-2729; (d) Jacquemin, D.; Planchat, A.; Adamo, C.; Mennucci, B. *J. Chem. Theory Comput.* **2012**, *8*, 2359-2372; (e) Improta, R.; Scalmani, G.; Frisch, M. J.; Barone, V. *J. Chem. Phys.* **2007**, *127*, 074504; (f) Pedone, *J. Chem. Theory Comput.* **2013**, *9*, 4087-4096.
22. (a) Bloino, J.; Biczysko, M.; Santoro, F.; Barone, V. *J. Chem. Theory Comput.* **2010**, *6*, 1256-1274; (b) Pedone, A.; Bloino, J.; Barone, V. *J. Phys. Chem. C* **2012**, *116*, 17807-17818; (c) Adamo, C.; Jacquemin, D. *Chem. Soc. Rev.* **2013**, *42*, 845-856; (d) Biczysko, M.; Bloino, J.; Brancato, G.; Cacelli, I.; Cappelli, C.; Ferretti, A.; Lami, A.; Monti, S.; Pedone, A.; Prampolini, G.; Puzzarini, C.; Santoro, F.; Trani, F.; Villani, G. *Theor. Chem. Acc.* **2012**, *131*, 1-19; (e) Barone, V.; Bloino, J.; Monti, S.; Pedone, A.; Prampolini, G. *Phys. Chem. Chem. Phys.* **2010**, *12*, 10550-10561; (f) Improta, R.; Barone, V.; Santoro, F. *Angew. Chem., Int. Ed.* **2007**, *46*, 405-408.
23. Boiocchi, M.; Del Boca, L.; Esteban-Gomez, D.; Fabbrizzi, L.; Licchelli, M.; Monzani, E. *Chem. Eur. J.* **2005**, *11*, 3097-3104.
24. Weiss, K. L.; Alshafie, G.; Chapman, J. S.; Mershon, S. M.; Abou-Issa, H.; Clagett-Dame, M.; Curley, R. W. *Bioorg. Med. Chem. Lett.* **2001**, *11*, 1583-1586.
25. Qian, F.; Zhang, C.; Zhang, Y.; He, W.; Gao, X.; Hu, P.; Guo, Z. *J. Am. Chem. Soc.* **2009**, *131*, 1460-1468.
26. Kand, D.; Kalle, A. M.; Talukdar, P. *Org. Biomol. Chem.* **2013**, *11*, 1691-1701.

Chapter 2

Development of Probes for Rapid Detection of Fluoride Ion: Improvement of Sensitivity and Application in Aqueous Media



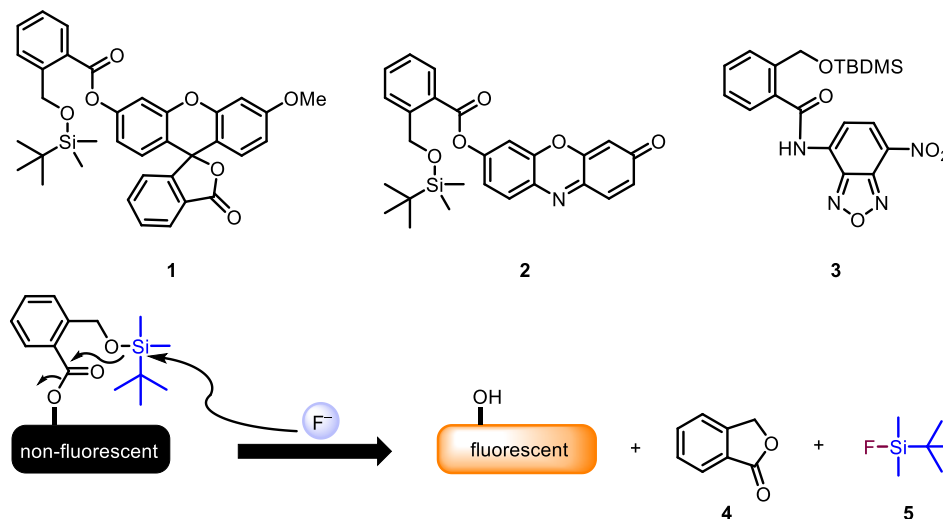
2.1. Introduction

Development of artificial molecular systems for sensing of anions have received great research interests as anions play pivotal role in a wide range of biological, metabolic processes and participate in various enzymatic reactions.¹ Among biologically relevant anions, fluoride is one of the most attractive target due to its significance in diverse health and environmental issues.² Presence of fluoride in low level has proven to be critical for the prevention of dental and skeletal fluorosis, enamel demineralization while wearing orthodontic appliances and osteoporosis treatment. The optimal level of the ion is routinely maintained from toothpaste, drinking water, foods and other fluoride supplements. However, excess intake of fluoride can result in metabolic disorders, skeletal disease, mottled teeth, inhibition of neuro-transmitter biosynthesis in fetuses, nephrolithiasis. For these reasons, controlled consumption of fluoride in human body is a serious concern throughout the world.³ Therefore, it is of great necessity to develop techniques for selective detection of fluoride ion in biological samples as well as inside human live cells in terms of human health and environmental protection. Fluorescent probes offer promising approach owing to its simplicity, high selectivity, sensitivity and bioimaging analysis *in vivo*, even in single living cells.⁴

For these reasons considerable efforts have been made to develop highly selective and sensitive systems capable of recognition, binding/or sensing in competitive environment rapidly. A large number of fluorescent probes have been developed for detection of F^- .^{3a} Compared to other silyl halides, the Si-F linkage is one of the strongest single bond. This chemistry has been widely used in synthesizing many chemodosimeters for fluoride sensing. Facile cleavage of either C-Si or O-Si bond by F^- has been the key to design the reaction sites in these probes. These deprotection strategies were further develop new probes via cascade reaction process.

As discussed earlier, cascade reactions offer advantages, such as atom economy as well as economies of time and waste generation. We expected that introduction of cascade reaction into sensing domain could lead to shorter response time. Herein, we report the design, synthesis, photophysical characterization of a new cascade reaction based on highly selective and sensitive colorimetric and fluorescent *off-on* three different probes **1**, **2** and **3** for the detection of F^- (Scheme 2.1). Non-fluorescent species upon treatment with fluoride was expected to undergo a cleavage of

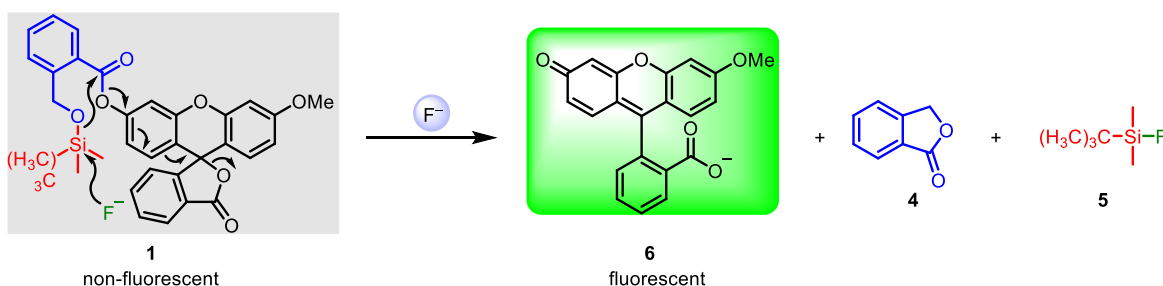
the Si–O bond to release *tert*-butyldimethylsilyl fluoride **5**. A subsequent cyclisation was proposed to form phthalide **4** with the release of fluorophore.



Scheme 2.1: Structures of proposed compounds (**1-3**) and schematic representation of fluoride ion sensing mechanism using cascade reaction.

2.2. Results and Discussions for Probe 1

Carboxyfluorescein fluorophore was chosen to design probe **1** which was expected to be non-fluorescent. Therefore, this non-fluorescent species **1** upon treatment with fluoride was anticipated to undergo cleavage of the Si–O bond to release *tert*-butyldimethylsilyl fluoride **5** and subsequent cyclisation could be possible to form phthalide **4** with the release of fluorophore **6** (Scheme 2.2).⁵

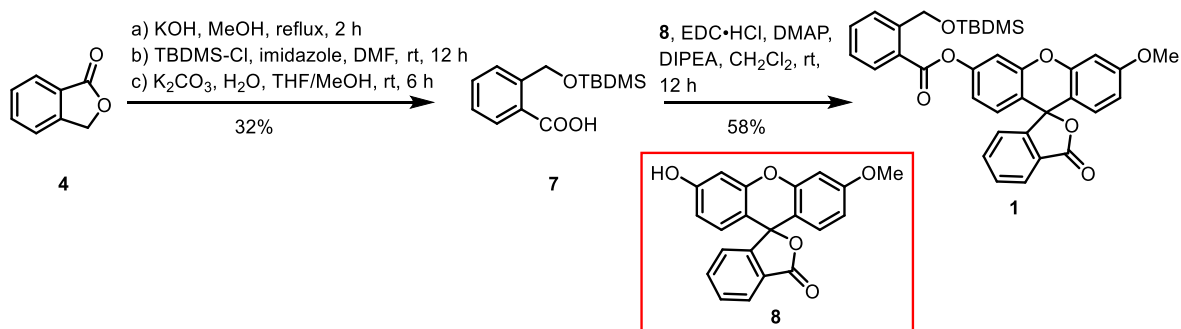


Scheme 2.2: Structure and fluoride ion sensing mechanism of probe **1**.

2.2.1. Synthesis of probe 1

Synthesis of probe **1** was carried out in two steps (Scheme 2.3). At first, **4** was converted to free acid in one-pot three-step strategy via opening of the lactone using methanolic KOH followed by silyl protection of both benzylic alcohol and –COOH group. Subsequent selective

deprotection of silyl ester provided acid **7** with overall 32% yield. Acid **7** was then coupled with fluorescein derivative **8** using EDC•HCl and DMAP/DIPEA in presence of CH₂Cl₂ to form probe **1** in 58% yield.



Scheme 2.3: Synthesis of probe **1**.

2.2.2. Evidence of Cascade Reaction Mechanism

The proposed mechanism of F⁻ sensing by probe **1** was confirmed by ¹H-NMR titration (Figure 2.1) and MALDI data (Figure 2.2).

¹H-NMR titration: To a solution of probe **1** in DMSO-*d*₆ (4.3 mg in 0.7 mL) increasing concentration of F⁻ (0-300 equivalent) were added and spectra were recorded after 7 min. The characteristic singlet at $\delta = 5.10$ ppm (H_a protons) for probe **1** disappeared gradually and new

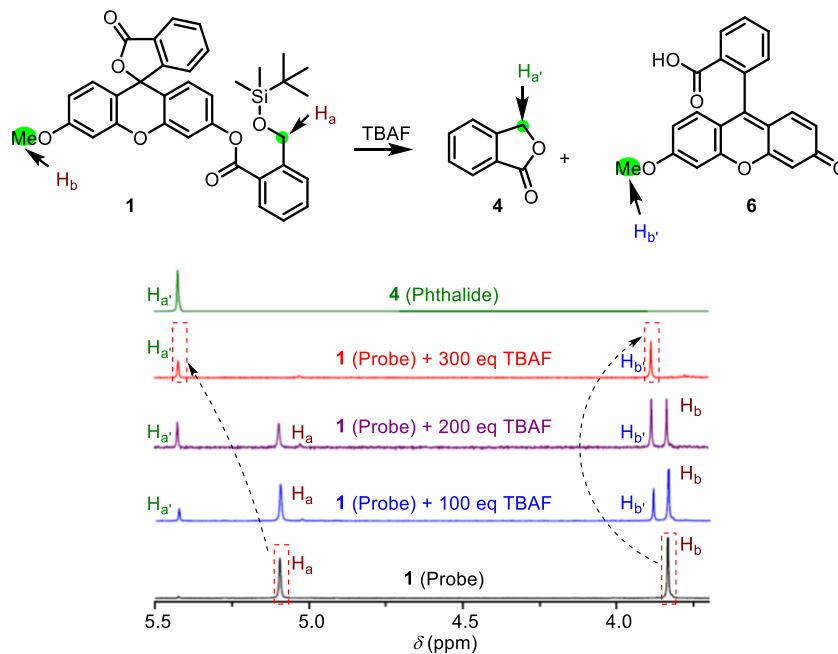


Figure 2.1: ¹H-NMR spectral changes for probe **1** in DMSO-*d*₆ with increasing concentration of TBAF (0-300 equivalents).

singlet at $\delta = 5.43$ ppm, corresponding to H_a protons of phthalide **4** appeared. Similarly, another singlet at $\delta = 3.83$ ppm (H_b protons) for the $-OMe$ group of probe **1** disappeared and a new singlet at $\delta = 3.89$ ppm (H_b protons) corresponding to the $-OMe$ group of compound **6** appeared (Figure 2.1).

Mass (MALDI-TOF) Analysis: Probe **1** was reacted with TBAF in THF at room temperature for 7 min and mass analysis of reaction mixture was carried out (Figure 2.2). In mass spectrum, peaks corresponding to $[M+H]^+$, $[M+Na]^+$ and $[M+K]^+$ *i.e.* $m/z = 347, 369, 385$ were observed which confirms the formation of fluorescent compound **6**.

These two data confirmed the mechanism of fluoride detection using cascade reaction.

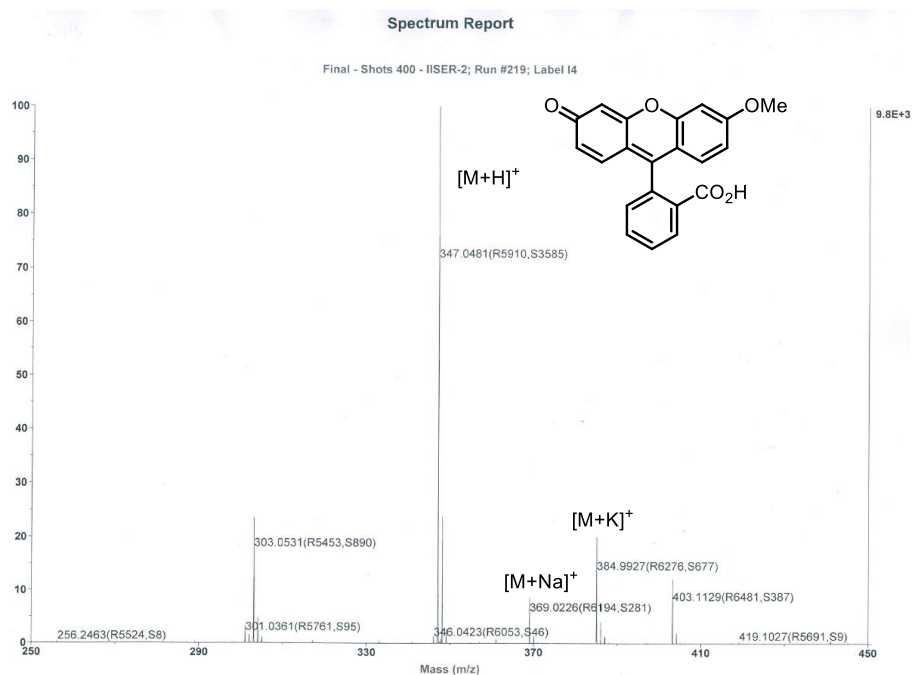


Figure 2.2: MALDI-TOF spectrum of probe **1** after reaction with TBAF in THF.

2.2.3. Photophysical Properties and Fluoride Sensing

All photophysical properties of probe **1** were investigated in DMSO. Probe **1** did not show any characteristic UV-Visible absorption band between 300-700 nm and was non-fluorescent. Upon addition of tetrabutylammonium fluoride, TBAF (300 equivalents) to the solution of probe **1** (10 μ M), a fluorescence band centered at $\lambda_{em} = 523$ nm ($\lambda_{ex} = 460$ nm) was observed (Figure 2.3). A pseudo first order reaction kinetics was observed with rate constant $k = 0.28$ min⁻¹ and $t_{1/2}$

= 2.41 min (Figure 2.3A) and sensing process was completed within ~ 7 min. As probe **1** was not capable of F^- detection in pure aqueous conditions, to overcome this limitation we prepared the stock of F^- in water and assay was carried out in DMSO solvent. The sensitivity of probe towards F^- was comparable irrespective of the medium of F^- source (water or THF). When the response of **1** ($10 \mu\text{M}$) towards increasing concentrations of TBAF (0-350 equivalent) were monitored, a stepwise increase in fluorescence was observed upto 300 equivalent of the salt (Figure 2.3B).

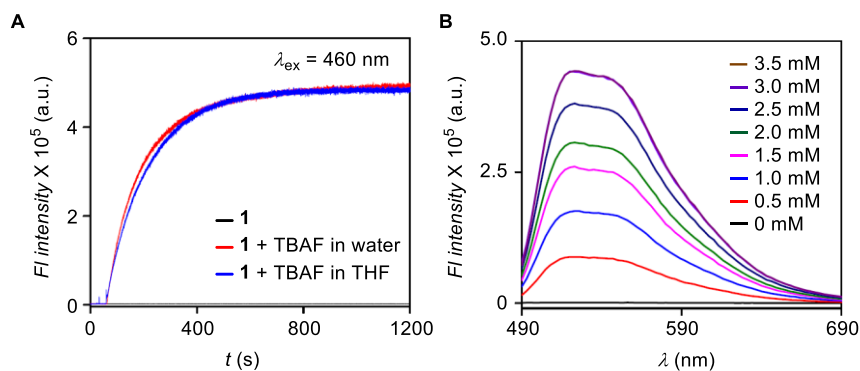


Figure 2.3: A) Fluorescence kinetics of **1** ($10 \mu\text{M}$) in presence of TBAF (3 mM in either THF or H_2O) in DMSO at $\lambda = 523 \text{ nm}$ and B) fluorescence spectra of **1** with increasing concentration of TBAF (0-3.5 mM) in DMSO.

When fluorescence intensity measured at $\lambda = 523 \text{ nm}$ was plotted against the concentration, a linear increase was observed within 0-200 equivalents of F^- (Figure 2.4A). Each spectrum was recorded 7 min after addition of F^- to the solution of probe **1**. From this plot detection limit was calculated to be $1.03 \mu\text{M}$ (19.6 ppb). Fluorescence intensity was measured with increasing time which showed increment in fluorescence intensity with time (Figure 2.4B) and saturation in fluorescence intensity was observed after ~ 10 min. Detection limit of probe **1** toward F^- was found to be $1.03 \mu\text{M}$ (19.6 ppb) which was well below 4 ppm, the allowed concentration level of F^- in drinking water specified by USEPA. Low detection limit of **1** shows its potential application in the detection of F^- in biological and environmental system as higher F^- concentration is toxic (0.1 mM for drinking water standard and $> 3 \text{ mM}$ in biological systems). Detection limit and response time for probe **1** was either comparable or better than reported probes (Table 2.1).

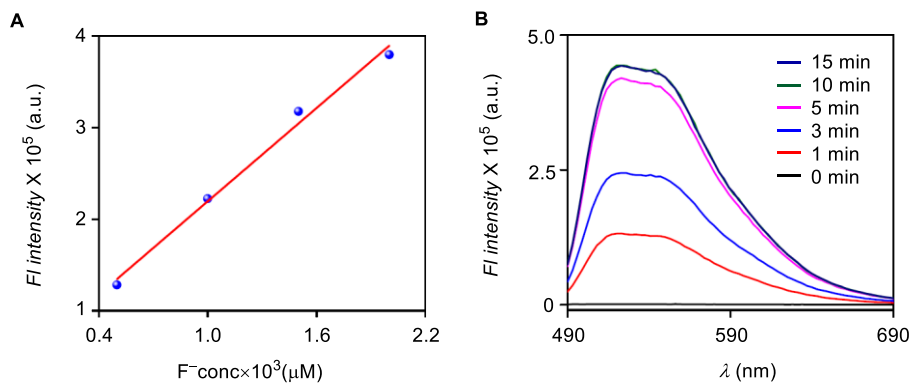
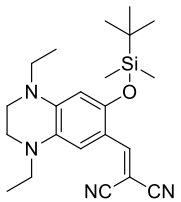
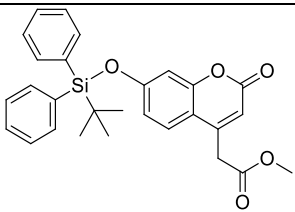
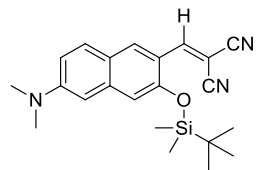
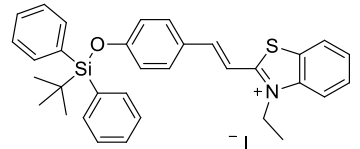


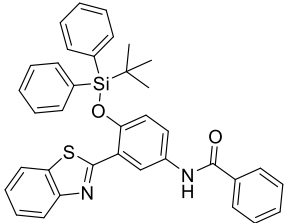
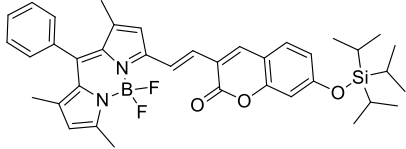
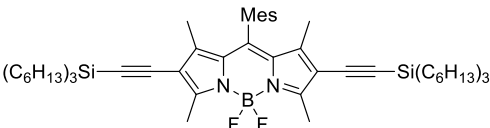
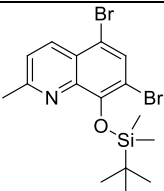
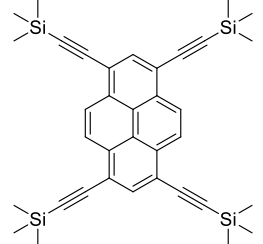
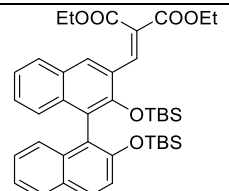
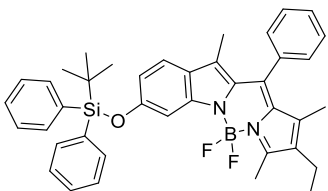
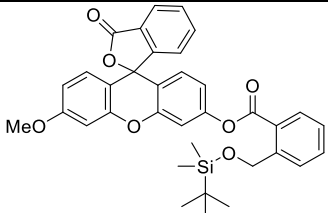
Figure 2.4: A) Linear relationship of probe **1** (10 μM) at 523 nm between the fluorescence emission intensity of probe **1** and concentration (0.5 mM – 2 mM) of F^- (in water) in DMSO (upon $\lambda_{\text{ex}} = 460 \text{ nm}$) and B) fluorescence spectra of probe **1** (10 μM) with increasing time in the presence of F^- (300 equivalent).

Comparison of detection limit with reported probes:

Table 2.1. Comparison of detection limit and response time of probe **1** with reported probes:

Probes	Detection limit	Solvent	Time	Reference
	5.4 μM	HEPES: ACN (7:3)	10 min	6
	380 μM	HEPES	4h	7
	210 μM Below 4 ppm	HEPES:ACN (8:2)	60 min	8
	80 μM	EtOH:H ₂ O (3:7)	50 min	9

Chapter 2

	5.2 μM 100 ppb	2 mM CTAB in H_2O	4 min	10
	0.12 μM	DMSO	ND	11
	0.067 μM	Acetone	ND	12
	1 μM	THF	10s	13
	52 μM 1 ppm	THF	20s	14
	1.86 μM	THF	ND	15
	0.1 μM	CH_2Cl_2	30s	16
	1 μM	DMSO	7 min	Present work

To evaluate selectivity of probe **1** towards F^- over other possibly competitive analytes, the fluorescence intensity at $\lambda_{em} = 523 \text{ nm}$ ($\lambda_{ex} = 460 \text{ nm}$) was measured in presence of various interfering ions (Br^- , I^- , Cl^- , ClO_4^- , PF_6^- , NO_3^- , HSO_4^- , OAc^- and SO_4^{2-}) and analytes (H_2O_2 , Cys and GSH). When probe **1** ($10 \mu\text{M}$) in DMSO was treated with the 300 equivalent of TBAF, a 550-fold enhancement in the fluorescence intensity was observed within 7 min of stirring at room temperature (Figure 2.5A, blue bar) but other analytes (3 mM) did not show any change in emission intensity (Figure 2.5A, front row). The probe **1** showed fluorescence intensity enhancement only after addition of F^- into these solutions, confirming that the selectivity of the probe towards F^- ion, even in the presence of competitive analytes (Figure 2.5A, back row). The resulting solution also provided quantum yield $\Phi = 0.06$ (standard: fluorescein, $\Phi = 0.85$ in 0.1 N NaOH). Response of **1** towards F^- ion under ambient light was associated with the colour change from colourless to

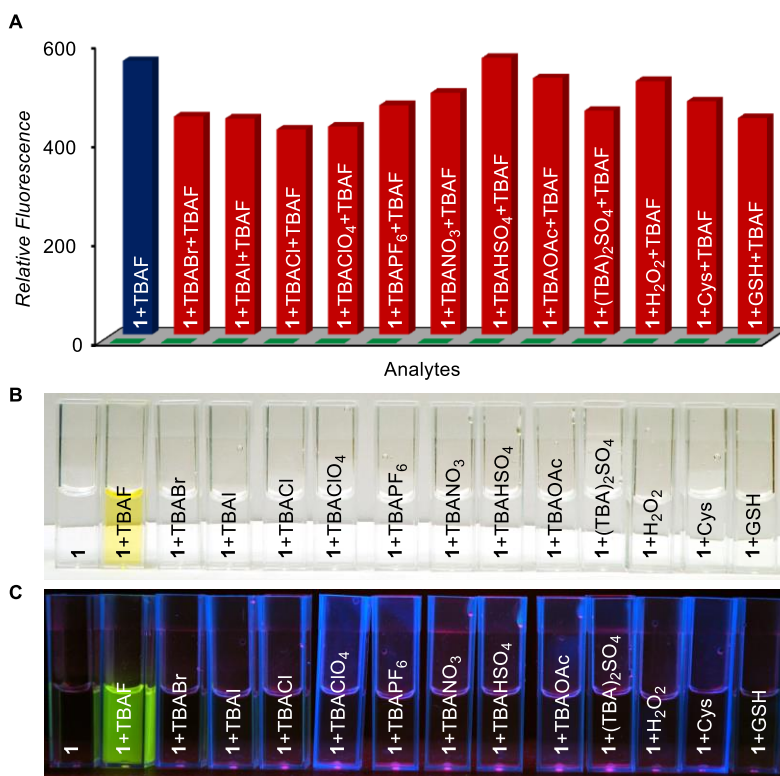


Figure 2.5: **A**) Relative fluorescence of **1** ($10 \mu\text{M}$) in presence of either F^- (3 mM) or various analytes (front row) and subsequent addition of F^- (back row) to the same sample, **B**) colour change for **1** in presence of various analytes under visible light and **C**) emission colour change for **1** in presence of various analytes. Image of cuvettes under hand-held UV-lamp with $\lambda_{ex} = 365 \text{ nm}$.

yellow and inertness towards other analytes were supported by no change in visible color (Figure 2.5B). The fluorescence turn-*on* response upon sensing of F^- was also confirmed by the appearance of green fluorescence of the reaction mixture when cuvette images were taken under hand-held UV-lamp ($\lambda_{ex} = 365$ nm) (Figure 2.5C). These results confirmed that probe **1** is highly selective towards fluoride ions.

2.2.4. Cell Imaging

Practical application of the probe **1** was demonstrated by live cell imaging experiment with Human cervical cancer cell line (HeLa cells). No significant fluorescence was observed when HeLa cells were incubated with only probe **1** ($10 \mu\text{M}$ in 1:100 DMSO-DMEM v/v, pH = 7.4) at 37°C for 2 h (Figure 2.6A-C). When same cells were again incubated with 20 mM NaF (1:100 H_2O -DMEM, pH = 7.4) at 37°C for 30 min, strong fluorescence was observed inside the cell (Figure 2.6D-F). This data indicates that probe **1** can be applied for selective detection of intracellular F^- ion.

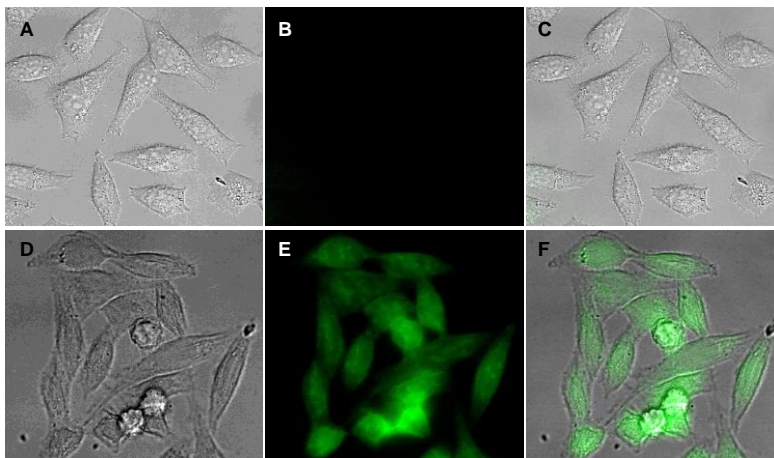


Figure 2.6: Live cell image of HeLa cell: **A)** differential interference contrast, **B)** fluorescence, and **C)** overlay image of HeLa cell incubated with Probe **1** ($10 \mu\text{M}$) for 2 h. **(D – F)** are the respective differential interference contrast, fluorescence and overlay image of HeLa cell first incubated with **1** ($10 \mu\text{M}$) for 2 h followed by incubation with NaF (20 mM) for 30 min.

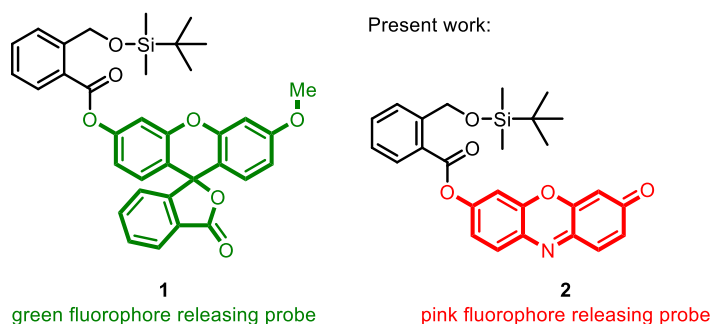
2.3. Conclusion

In conclusion, we have successfully designed, synthesized and investigated the selective detection of F^- of probe **1**. The non-fluorescent probe undergoes a cascade reaction in presence of

the F^- to release the lactone phthalide and a fluorescein derivative as fluorophore. The fast response of the probe towards the F^- provided $t_{1/2} = 2.41$ min and 550-fold fluorescence enhancement with detection limit of 19.6 ppb. The F^- detection ability of the probe in living cells was demonstrated.

2.4. Improvement of Sensitivity

Outcome of the previous fluoride mediated rapid cascade reaction strategy encouraged us to investigate further to develop *off-on* probe with excitation and emission properties in the bathochromic region. Cascade reaction based approach for fluoride sensing can lead to shorter response time as these reactions are entropically highly favoured. Herein, we report the design, synthesis and photophysical studies of a new cascade reaction based colorimetric and pink fluorescent *off-on* probe **2** for highly selective and sensitive detection of fluoride ion.¹⁷ In the design, resorufin was selected as the fluorophore because of its attractive pink color and pink fluorescence. Recently, a Michael addition of thiolate anion on the dye was reported by Yasuhiro Shiraishi and coworkers due to local softness at its electrophilic sites.¹⁸ However, we believed that fluoride ion being hard nucleophile, such addition reaction is not feasible.

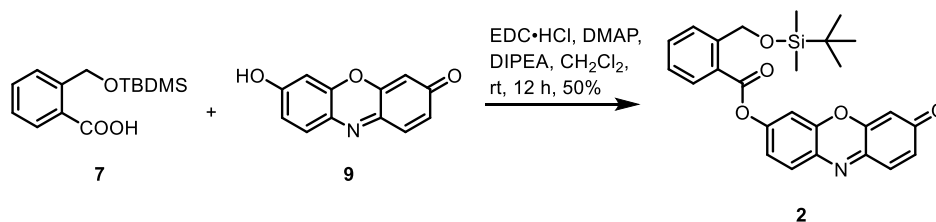


Scheme 2.4: Structure of probe **1** and proposed probe **2**.

2.5. Results and Discussions for Probe 2

2.5.1. Synthesis

Synthesis of the probe **2** was carried out started from acid **7** which was prepared from phthalide **4**. Synthesis of acid **7** was discussed earlier. Treatment of acid **7** with resorufin **9** using EDC•HCl and DMAP/DIPEA conditions provided probe **2** in 50% yield (Scheme 2.5). Probe **2** was well characterized by 1H , ^{13}C , COSY, NOESY NMR spectra and mass analysis. Purity of the probe **2** was further checked by HPLC analysis.

Scheme 2.5: Synthesis of probe **2**.

2.5.2. Evidence of Mechanism

¹H-NMR experiments: To establish the mechanism of the cascade reaction and to exclude the possibility of undesired Michael addition on resorufin, ¹H-NMR experiment was carried out. The probe **2** (4 mg) was dissolved in CD₃CN (0.75 mL) and titration was performed upon addition of TBAF with increasing concentration. The ¹H-NMR spectrum of pure probe **2** was marked by its characteristic signals at $\delta = 6.25$, 6.80 and 7.47 ppm corresponding to H_a, H_b and H_c, respectively (Figure 2.7A). Resorufin **9** was obtained from the commercial source which provided signals at $\delta = 6.01$, 6.40 and 7.25 ppm characteristics signal of H_{a'}, H_{b'}, and H_{c'}, respectively (Figure 2.7A).

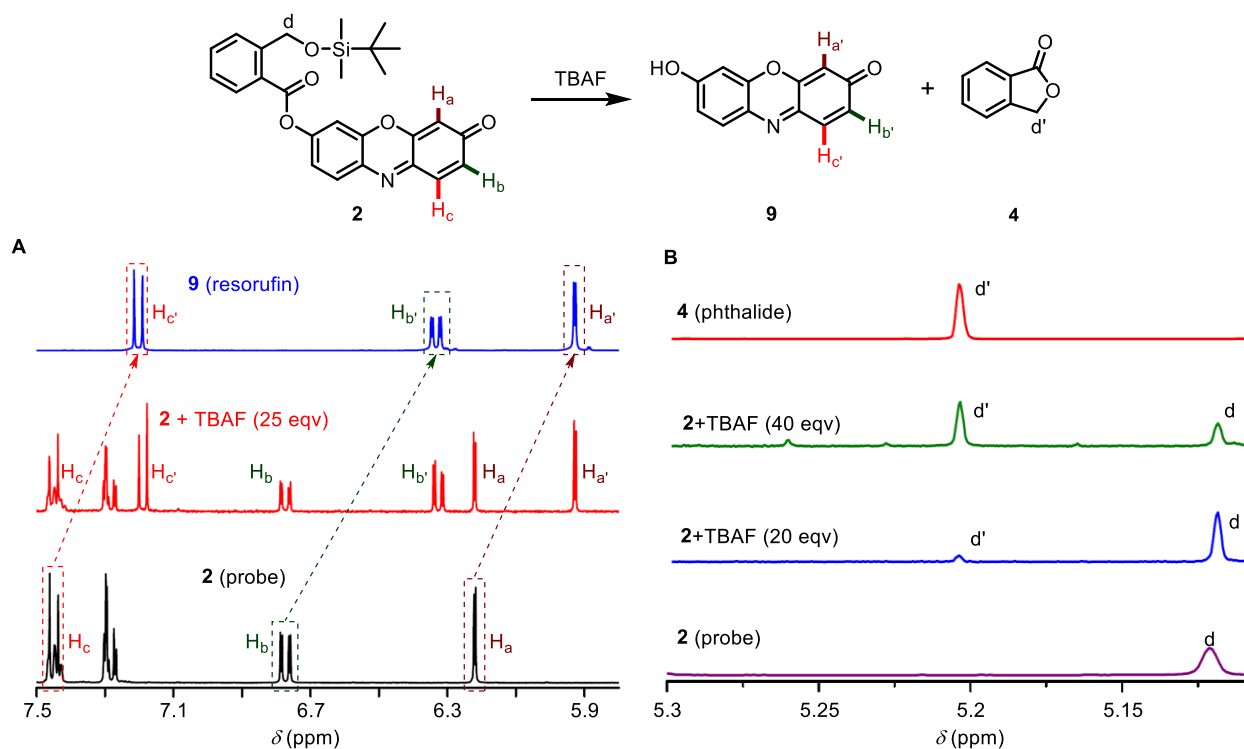


Figure 2.7: ¹H-NMR titration of probe **2** upon addition of TBAF (25 eqv) in CD₃CN at room temperature after 10 min to monitor **A**) resorufin **9** formation and **B**) phthalide **4** formation upon addition of TBAF.

When TBAF (25 eqv) was added to a solution of probe **2** in CD₃CN and spectrum was recorded at room temperature after 10 minutes, signals corresponding to **2** partially disappeared with the appearance of new set of signals corresponding to resorufin **9** (Figure 2.7A). Formation of phthalide **4** in the cascade reaction process was confirmed by ¹H-NMR experiment (Figure 2.7B). Therefore, ¹H-NMR experiments also ruled out possibility of any undesired product formation via the Michael addition of F⁻ on the resorufin dye.

HPLC analysis: Cascade reaction based F⁻ sensing mechanism was reconfirmed by HPLC analysis. HPLC chromatograms were recorded in the gradient method using acetonitrile and H₂O eluent and obtained data showed that the reaction of probe **2** ($t_R = 15.2$ min) with F⁻ resulted in desilylation based cascade reaction to release resorufin **9** (Figure 2.8). Addition of fluoride resulted in the formation of a new peak appearing at $t_R = 6.8$ min corresponds to resorufin **9**.

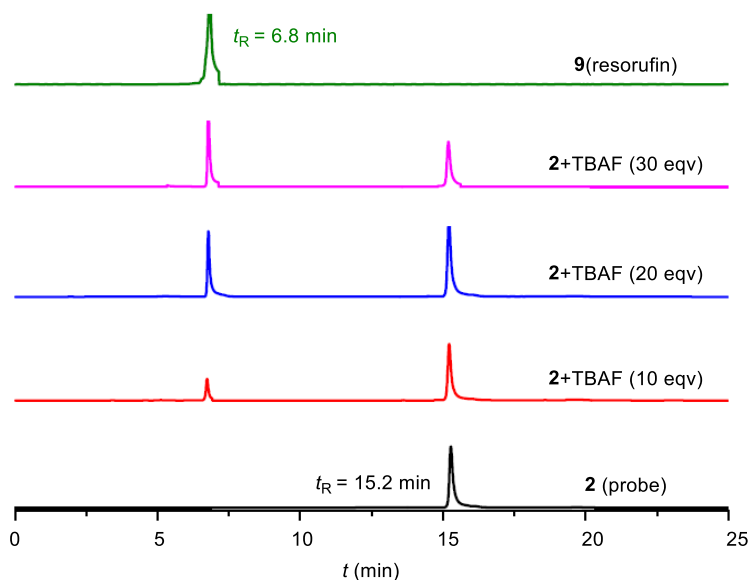


Figure 2.8: HPLC chromatograms of probe **2** (10 μ M) upon reaction with F⁻ (10-30 eqv) recorded in a gradient solvent system of acetonitrile and H₂O.

2.5.3. Photophysical Properties and Fluoride Sensing

After establishing the mechanism by ¹H-NMR titration and HPLC analysis, UV-Visible spectroscopic studies of the probe **2** and its F⁻ sensing ability was determined. The probe **2** displayed a strong absorption bands centered at $\lambda = 347$ nm ($\epsilon = 10415$ M⁻¹ cm⁻¹) and 437 nm ($\epsilon = 11411$ M⁻¹ cm⁻¹) and was completely non-fluorescent in THF. When response of the probe **2** (10

μM) was monitored in THF upon treating with 0.5 mM tetrabutylammonium fluoride (TBAF), absorption peaks at $\lambda = 347$ and 437 nm decreased gradually along with appearance of new absorption peaks at $\lambda = 550$ nm, 573 nm and 591 nm (Figure 2.9A). Emergence of these new peaks is characteristic of the free resorufin **9** and complete release of the fluorophore was observed within 9 min of addition. Based on the outcome, the probe **2** (10 μM) was then titrated with TBAF (0-0.6 mM) and absorption spectra were recorded after 10 min of addition (Figure 2.9B). In this experiment, disappearance of signals (at $\lambda = 347$ nm and 437 nm) corresponding to the probe **2** and appearance corresponding signals of resorufin (at $\lambda = 550$ nm, 573 nm and 591 nm) were observed.

To evaluate response time of **2** (10 μM) towards F^- (0.5 mM) ion by fluorescence method, a solution of TBAF in THF was added to the probe and fluorescence spectra ($\lambda_{\text{ex}} = 550$ nm) were recorded in THF at 0-12 min (Figure 2.10A). A saturation of fluorescence, comparable to the UV-Visible method was observed. Time dependent change of fluorescence with probe **2** in presence of TBAF was also monitored which indicates completion of sensing process within 10 min (Figure 2.10A). Further, to analyze the solvent dependencies of the F^- source, fluorescence kinetics experiments were done by adding TBAF (in either THF or H_2O) to the probe **2**. In these experiments, fluorescence intensities at $\lambda = 595$ nm ($\lambda_{\text{ex}} = 550$ nm) with time and TBAF from different sources were added at 1 min of monitoring. When TBAF was added from THF, saturation

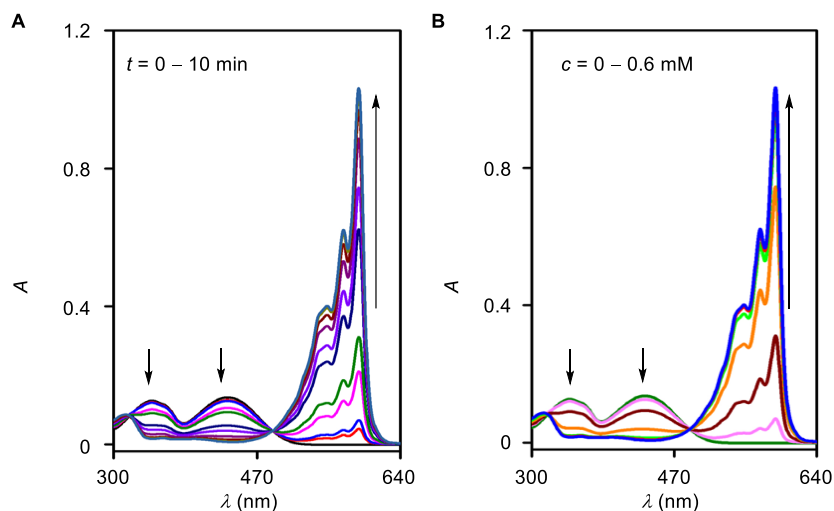


Figure 2.9: A) UV-visible spectra of probe **2** (10 μM) at 0 – 10 min upon addition of 0.5 mM TBAF and B) UV-visible spectra of probe **2** (10 μM) after 10 min upon addition of 0 – 0.6 mM TBAF.

of fluorescence was observed within 9 min of addition (Figure 2.10B). The pseudo first order kinetics afforded rate constant $k = 0.00589 \text{ s}^{-1}$ and half-life $t_{1/2} = 1.96 \text{ min}$. With H_2O as the source of TBAF, the reaction was comparatively slower with pseudo first order rate constant $k = 0.00589 \text{ s}^{-1}$ and $t_{1/2} = 4.56 \text{ min}$ (Figure 2.10B). In this experiment, complete reaction was recorded within 20 min of addition.

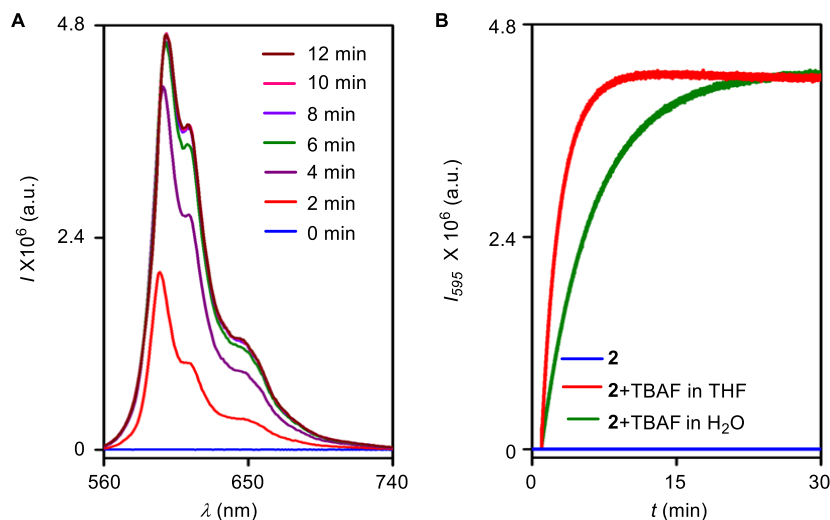


Figure 2.10: **A)** Fluorescence spectra ($\lambda_{\text{ex}} = 550 \text{ nm}$) of probe **2** ($10 \mu\text{M}$) at 0 – 12 min upon addition of 0.5 mM TBAF and **B)** fluorescence kinetics profile at $\lambda = 595 \text{ nm}$ ($\lambda_{\text{ex}} = 550 \text{ nm}$) of probe **2** ($10 \mu\text{M}$) towards 0.5 mM TBAF (prepared in either THF or in H_2O). Final concentration for assay in water was 5.5%.

In the next stage, response of the probe **2** was examined in presence of different bio-relevant analytes and fluorescence intensity was monitored at $\lambda = 595 \text{ nm}$ ($\lambda_{\text{ex}} = 550 \text{ nm}$). When **2** was treated separately with possibly interfering analytes (0.5 mM of Br^- , I^- , Cl^- , ClO_4^- , PF_6^- , NO_3^- , HSO_4^- , OAc^- , SO_4^{2-} , H_2O_2 , Na_2S , Cys and GSH) for 10 min at room temperature and all spectra were recorded, no significant enhancement in fluorescence intensity was observed (Figure 2.11A, front row). Treatment of F^- (0.5 mM) under same condition resulted in an excellent 1820-fold enhancement (Figure 2.11A, blue bar of back row). When F^- (0.5 mM) was added to the cuvettes containing probe **2** pretreated with other analytes (Br^- , I^- , Cl^- , ClO_4^- , PF_6^- , NO_3^- , HSO_4^- , OAc^- , SO_4^{2-} , H_2O_2 , Na_2S , Cys and GSH), *off-on* fluorescence enhancements similar to **2** with TBAF were observed (Figure 2.11A, red bars of back row). Thus, probe **2** is highly selective towards fluoride and even it can selectively sense fluoride with equal efficiency in presence of other competitive anions. The light yellow solution of **2** upon reaction with TBAF turned to pink

(Figure 2.11B). For other analytes, no change in color was observed. Fluorescence *off-on* response of **2** towards F^- , when monitored under the hand-held UV-lamp ($\lambda_{ex} = 365$ nm), appearance of strong pink fluorescence was observed and for other analytes no fluorescence was observed (Figure 2.11C).

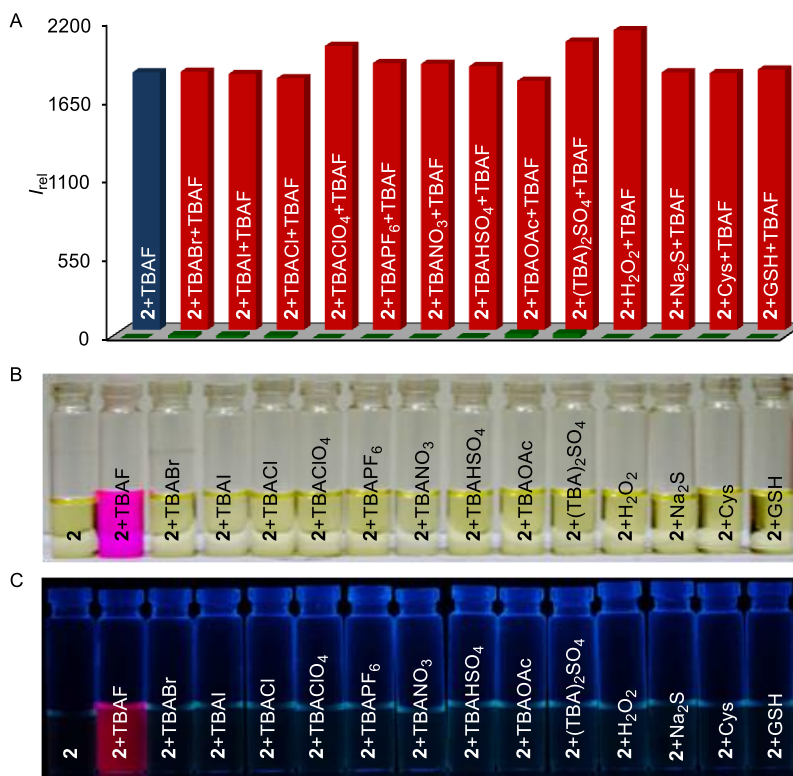


Figure 2.11: A) Relative fluorescence intensity enhancement of probe **2** (10 μ M) towards various anions (0.5 mM). All data were recorded after 10 min addition of analyte(s) at room temperature at $\lambda = 595$ nm ($\lambda_{ex} = 550$ nm) in THF, B) photograph of visible color changes of probe **2** in presence of different analytes, recorded under ambient light and C) photograph of fluorescence color changes of probe **2** in presence of different analytes, recorded under hand-held UV-lamp ($\lambda_{ex} = 365$ nm).

Fluorometric titration of **2** (10 μ M) in THF with increasing concentration of TBAF (0 – 0.7 mM) in water resulted to the increment of fluorescence intensity upto 0.5 mM (Figure 2.12A). Further increase in concentration of TBAF did not show any increase in fluorescence intensity. All data were recorded 10 min after addition TBAF. From the linear region of the plot (Figure 2.12B), a limit of detection (LOD) = 60 nM (*i.e.* 1.15 ppb) was calculated which is well below of 4 ppm, the allowed concentration level in drinking water set by USEPA. The detection limit of the probe **2** is comparable or superior to the F^- sensors, reported till date (Table 2.1).

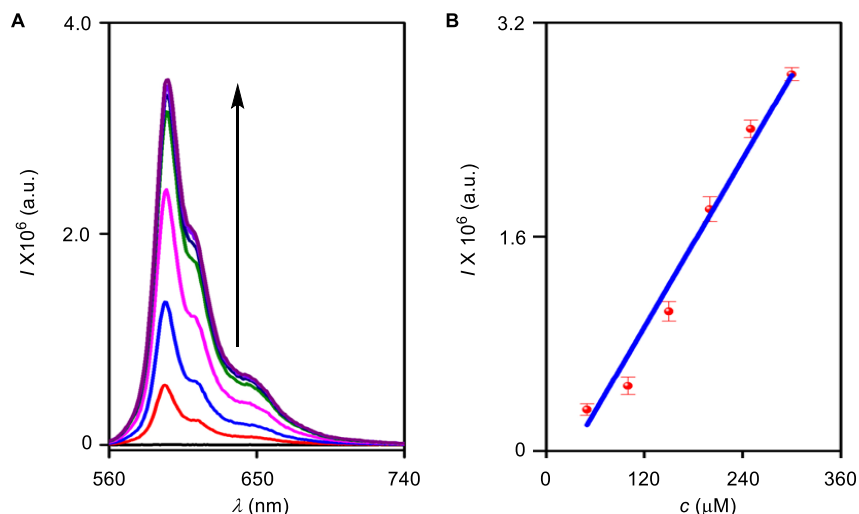


Figure 2.12: **A)** Fluorescence intensity of probe **2** (10 μM) in THF with increasing concentration of TBAF (0-0.7 mM) in water ($\lambda_{\text{ex}} = 550$ nm) and **B)** linear region of the I_{595} versus c_{TBAF} plot for calculation of LOD .

2.5.4. Cell Imaging

Further cell permeability and fluoride sensing ability of probe **2** in intracellular system was done by HeLa cell line. No significant fluorescence was observed when HeLa cell was incubated with only probe **2** (10 μM in 1:100 DMSO-DMEM v/v, pH = 7.4) at 37 $^{\circ}\text{C}$ for 1 h (Figure 2.13A-C). Interestingly, when same cells were incubated further with 2 mM NaF (1:100 H₂O-DMEM, pH = 7.4) at 37 $^{\circ}\text{C}$ for 30 min, strong fluorescence was observed inside cells (Figure 2.13D-F).

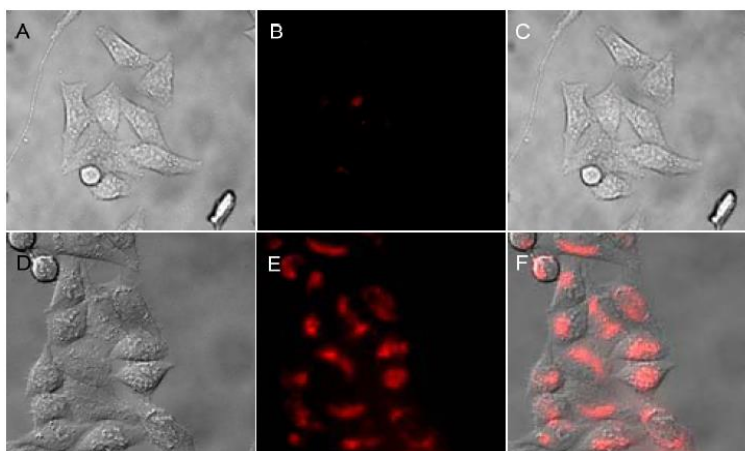


Figure 2.13: Cell images of HeLa cell: **A)** differential interference contrast, **B)** fluorescence, and **C)** overlay image of HeLa cell incubated with probe **2** (10 μM) for 1 h. **(D – F)** are the respective brightfield, fluorescence and overlay image of HeLa cell first incubated with probe **2** (10 μM) for 1 h followed by incubation with NaF (2 mM) for 30 min.

These differential interference contrast and fluorescence images demonstrate the permeation of probe **2** through the living cell membranes and its ability of sensing F^- inside cell.

2.6. Conclusion

Another cascade reaction based highly sensitive and selective fluorescent fluoride probe was developed. The cascade reaction mechanism of sensing fluoride was monitored by 1H NMR titration and HPLC analysis. The probe exhibited rapid release ($t_{1/2} = 1.96$ min) of pink fluorescent resorufin dye which resulted in an excellent 1820-fold turn-*on* response during sensing of the ion. Fluoride sensing ability of the probe was successfully evaluated in the presence of other interfering anions. The probe also offered detection limit of 60 nM (*i.e.* 1.15 ppb) which is comparable to the lowest fluorescent probes reported so far. Application of the probe in live cell imaging was also demonstrated.

2.7. Improvement of Aqueous Solubility

Sensing activity either in pure organic solvent or in combined H_2O /organic media is a general concern of most desilylation based probes and probes functioning in aqueous media are rare. Till date, a coumarin based probe **10** by Kim *et. al.*⁷ and a 2-aryl benzothiazole based probe **11** by Rui Hu *et. al.*¹⁰ were reported for sensing fluoride ion in aqueous media (Figure 2.14). Therefore a new endeavour was initiated to address the issue and to design a new probe working under aqueous conditions using same cascade reaction strategy. Our recent studies on cascade reaction based fluorescent F^- probe suggest faster response during sensing when compared with many reported probes. In the present study, we present the first desilylation mediated cascade reaction based probe **3**, rationally designed to sense F^- in the aqueous media.

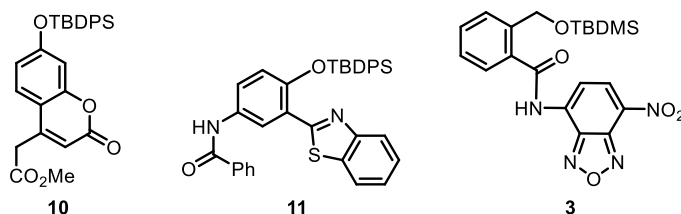


Figure 2.14: Structures of reported fluorescent F^- probes **10** and **11** working in aqueous media and proposed cascade reaction based probe **3** for sensing F^- in aqueous media.

2.8. Results and Discussions for Probe 3

2.8.1. Addressing Water Solubility and Membrane Permeability

In drug discovery and development, solubility and membrane permeability¹⁹ are two crucial parameters routinely addressed during the design of new molecules. A theoretical analysis of various drug molecules using *OSIRIS Property Explorer* suggests that more than 80% of the drugs on the market have a (estimated) clogS value greater than -4 (solubility measured in mol L⁻¹). Lipinski rule of five²⁰ is another important guideline to predict solubility and membrane permeability of a molecule. According to the rule, clogP (the logarithm of the partition coefficient between water and 1-octanol) value of a molecule determines its lipophilicity and a value around 5 is crucial for the better membrane permeability. It is believed that the ineffectiveness of major fluoride probe in aqueous media is due to the solubility. The aqueous solubility of a probe is essential for its ability to react with a water soluble analyte.

Therefore theoretical analysis was done for eleven desilylation based fluorescent F⁻ probes **10-11, 3** (Figure 2.14) and **12-17, 1, 2** (Figure 2.15) to correlate their clogS and clogP values to the use of F⁻ sensing media. For these molecules clogS and clogP values were determined from the *OSIRIS Property Explorer* program (Table 2.2) and presented in the increasing order of clogS values. Surprisingly, for probe **9** which was reported to function in H₂O (2 mM CTAB) media, provided clogS and clogP values of -7.85 and 8.63, respectively. But for other molecules, the estimated order of clogS was **1 < 12 < 13 < 14 < 15 < 16 < 10 < 17 < 2 < 3**. For these molecules,

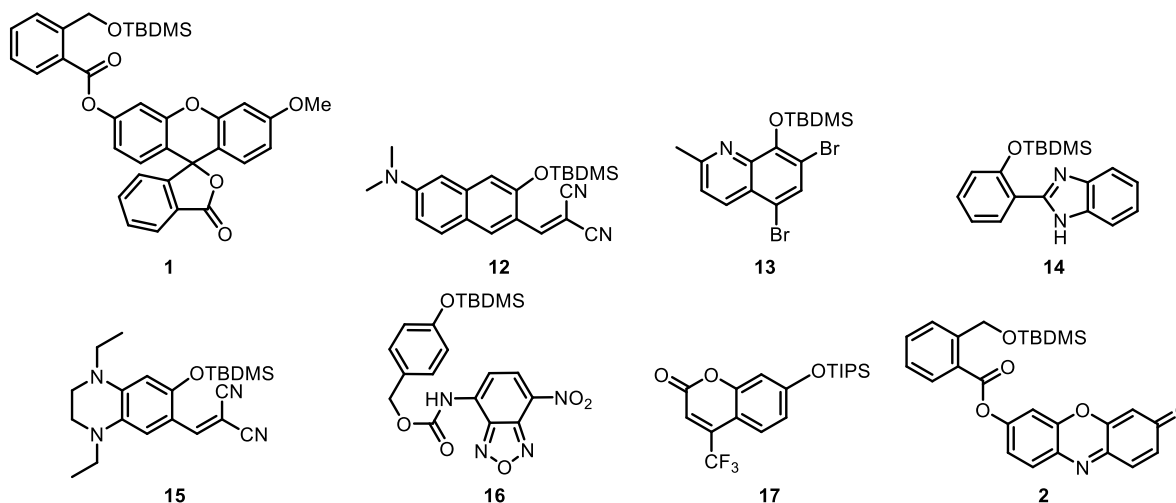


Figure 2.15: Structures of reported fluorescent F⁻ probes.

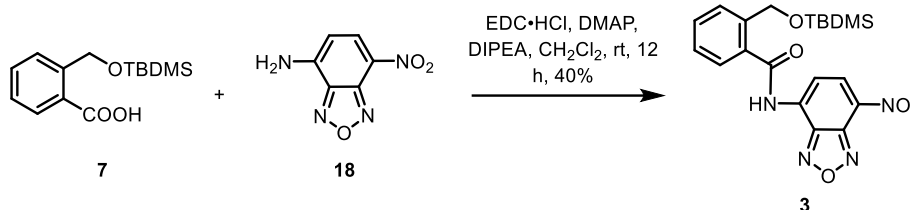
= -5.13 and $\text{clogP} = 5.17$ values were good enough to correlate to HEPES buffer (10 mM in H_2O , pH 7.4) as the sensing media. For the new probe **3**, $\text{clogS} = -3.84$ and $\text{clogP} = 4.17$ were estimated. These values predict good water solubility and membrane permeability of the probe and therefore prophecy its activity in the aqueous media.

Table 2.2 Comparison of clogS and clogP of probe **3** with reported probes.

Probe	clogS	clogP	Sensing media
11	-7.85	8.63	H_2O (2 mM CTAB)
1	-6.96	8.12	DMSO
12	-6.32	5.56	HEPES buffer (10 mM in H_2O , pH 7.4) / CH_3CN (8:2)
13	-6.09	6.44	THF
14	-5.70	5.52	DMF / H_2O (8:2)
15	-5.49	4.87	HEPES buffer (10 mM in H_2O , pH 7.4) / CH_3CN (7:3)
16	-5.42	4.63	EtOH/ H_2O (9:1)
10	-5.13	5.17	HEPES buffer (10 mM in H_2O , pH 7.4)
17	-4.87	4.75	CH_3CN
2	-4.60	5.15	THF/ H_2O (95:5)
3	-3.84	4.17	Current work

2.8.2. Synthesis

Encouraged by the noticeable prediction of clogS and clogP value for probe **3**, synthesis of the probe was carried out from acid **7** which was prepared by using protocol discussed earlier. Reaction of acid **7** with 4-amino-7-nitrobenzofurazan (NBD- NH_2) **18** under EDC•HCl/DMAP coupling conditions in the presence of DIPEA provided probe **3** with 40% yield (Scheme 2.6).



Scheme 2.6: Synthesis of probe **3**.

2.8.3. Evidence of Mechanism

¹H-NMR experiments: ¹H-NMR titration spectroscopic experiments were carried out in order to prove the fluoride mediated cascade reaction mechanism. In these experiments, varied proportions (0, 200 and 400 eqv) of tetra-n-butylammonium fluoride (TBAF) were added to solutions of probe **3** in CD₃OD (4 mg in 0.7 mL). For pure probe **3**, characteristic aromatic proton signals at $\delta = 7.4$, 7.5, 7.7, 8.6 and 8.7 ppm were observed in the ¹H-NMR spectrum (Figure 2.16, red trace). ¹H-NMR spectra of pure NBD-NH₂ **18** (Figure 2.16, pink trace) and phthalide **4** (Figure 2.16, brown trace) were also recorded. ¹H-NMR spectrum recorded after treating **3** with TBAF (200 eqv) in CD₃OD at room temperature for 10 min, indicated partial disappearance of signals corresponding to **3** and appearance of new signals corresponding to NBD-NH₂ **18** at $\delta = 6.4$ and 8.4 ppm (Figure 2.16, green trace). Formation of phthalide **4** was also confirmed by appearance of signal at $\delta = 7.4$, 7.6 and 7.8 ppm. ¹H-NMR spectrum recorded for the reaction mixture of **3** and TBAF (400 eqv) in CD₃OD indicated complete disappearance of signals corresponding to probe **3** and new sets of signals corresponding to **4** and **18** were present (Figure 2.16, blue trace).

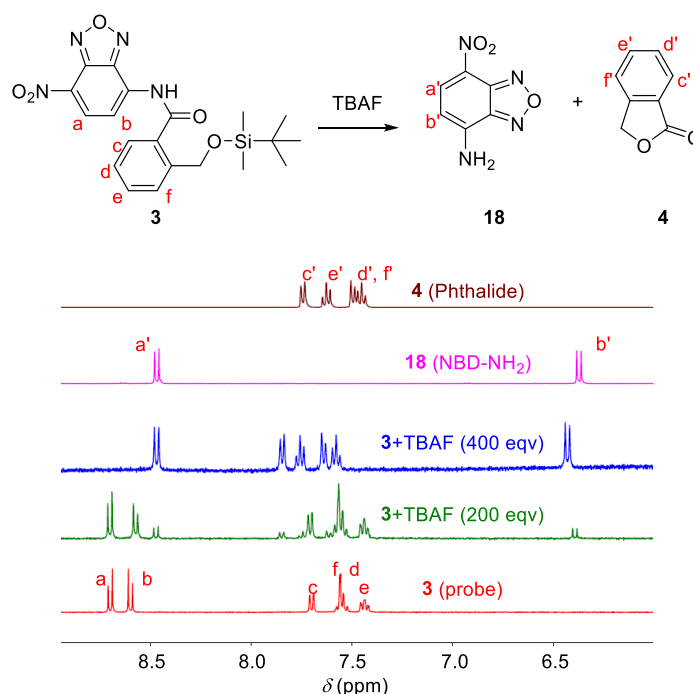


Figure 2.16: ¹H-NMR spectra of **3** (4.0 mg) upon addition of TBAF (0 – 400 eqv) in CD₃OD (0.7 mL) at room temperature after 10 min. ¹H-NMR spectra of pure **18** and **4** are also presented.

HPLC analysis: A further proof of the mechanism was provided from HPLC analysis. HPLC chromatograms recorded in the gradient method using acetonitrile and H₂O eluent displayed signal at $t_R = 14.5$, 13.5 and 37.0 min for pure NBD-NH₂ **18** (Figure 2.17, green trace), Phthalide **4** (Figure 2.17, pink trace) and **3** (Figure 2.17, black trace), respectively. Probe **3** (10 μ M) was separately treated with 100 and 300 eqv of TBAF in MeOH at room temperature for 5 min. HPLC analysis of these samples confirmed consumption of **3** and formation of amine **18** and phthalide **4** (Figure 2.17, red and blue traces for 100 and 300 eqv, respectively).

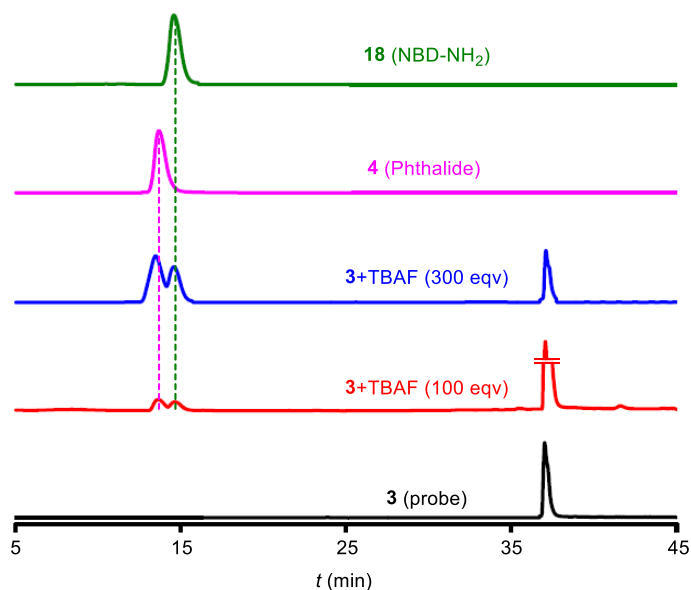


Figure 2.17 HPLC chromatograms of probe **3** (10 μ M) upon reaction with TBAF (100 and 300 eqv) recorded in a gradient solvent system of CH₃CN and H₂O. Chromatograms of pure **3**, Phthalide **4** and NBD-NH₂ **18** are also presented.

2.8.4. Photophysical Properties and Fluoride Sensing

The photophysical properties of probe **3** were studied in the aqueous media (0.5 mM CTAB *i.e.* Cetrimonium bromide). Probe **3** displayed an absorption maxima centered at $\lambda_{\max} = 400$ nm (Figure 2.18, black trace) with molar extinction coefficient, $\epsilon = 10120 \text{ M}^{-1} \text{ cm}^{-1}$. On the other hand, NBD-NH₂ **18** displayed an absorption band with $\lambda_{\max} = 460$ nm with $\epsilon = 18840 \text{ M}^{-1} \text{ cm}^{-1}$. When F⁻ (15 mM) was added to the solution of the **3** (10 μ M) and the reaction was monitored with time upto 60 min, decrease in absorbance at $\lambda = 278$ nm, 400 nm and a subsequent enhancement in absorbance at 460 nm were observed with an isosbestic point at $\lambda = 430$ nm. Therefore, solubility and F⁻ sensing data of **3** in water corroborates to its estimated log*S* and Clog*P* values.

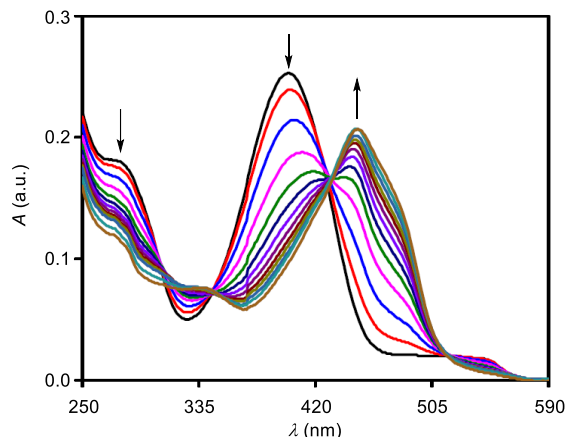


Figure 2.18 Changes of absorbance of probe **3** (10 μM) with time (0-60 min) towards F^- (15 mM) in water (0.5 mM CTAB)

Fluorescence spectroscopic experiments were carried out to demonstrate the fluoride sensing properties of **3** in aqueous media. Upon addition of F^- (15 mM) to the **3** (10 μM) in water (containing 0.5 mM CTAB), the fluorescence emission band centered at $\lambda = 553 \text{ nm}$ ($\lambda_{\text{ex}} = 460 \text{ nm}$) displayed gradual enhancement in intensity and saturation complete reaction carried out to determine the rate (k) of the reaction under pseudo first order conditions (Figure 2.19B). Monitoring of fluorescence intensity at $\lambda = 553 \text{ nm}$ ($\lambda_{\text{ex}} = 460 \text{ nm}$), provided pseudo first order rate constant $k = 0.0008268 \text{ s}^{-1}$ and $t_{1/2} = 13.97 \text{ min}$. The response of the probe **3** (10 μM) towards F^- (15 mM) was also determined in organic solvent, e.g. THF at room temperature and a faster saturation (within 30 min) of fluorescence intensity was observed under these conditions.

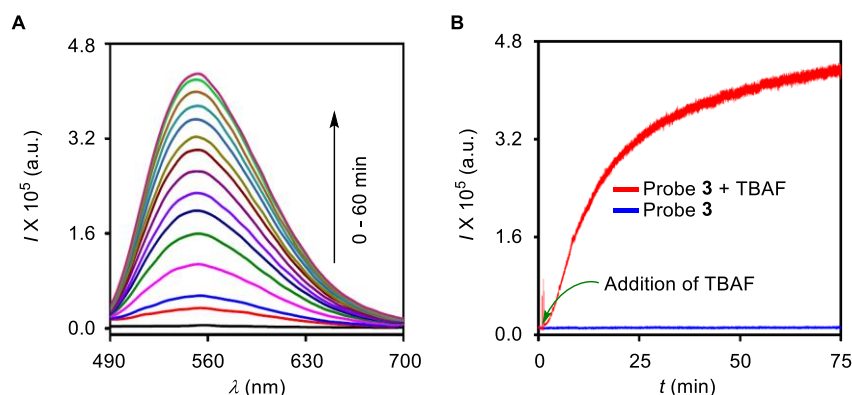


Figure 2.19 **A**) Fluorescence spectra ($\lambda_{\text{ex}} = 460 \text{ nm}$) of **3** (10 μM) at 0-60 min upon addition of 0.5 mM F^- and **B**) fluorescence kinetics profile of **3** (10 μM) at $\lambda = 553 \text{ nm}$ ($\lambda_{\text{ex}} = 460 \text{ nm}$) towards 15 mM F^- .

Quantitative *off-on* response of the probe **3** (10 μM) towards fluoride was then evaluated by

fluorometric titration with increasing concentration of the F^- (0-16 mM) in water (Figure 2.20A). Probe **3** was non fluorescent when excited at $\lambda = 460$ nm and showed very low quantum yield, $\Phi_F = 0.016$ (standard: N-methyl NBD (nitrobenzofurazan) amine in acetonitrile, $\Phi_F = 0.38$). The variation of fluoride ion concentration (0-16 mM) provided a stepwise enhancement of fluorescence intensity up to 14 mM concentration of F^- . The addition of F^- (14 mM) to the probe **3** resulted strong fluorescence centered at $\lambda_{em} = 553$ nm with $\Phi_F = 0.89$. These data ensured 120- and 56-fold enhancements in fluorescence intensity and quantum yield, respectively, during the sensing of fluoride ion by probe **3**. When fluorescence intensities at $\lambda = 553$ nm were plotted against respective F^- concentration, a linear relationship (Figure 2.20B) was observed up to 5 mM of F^- (regression factor, $R = 0.9759$). From the linear region of the plot, a limit of detection (LOD) = 24.5 μM (*i.e.* 0.46 ppm) which is well below of 4 ppm, the allowed concentration level in drinking water set by USEPA. Thus, the probe **3** is a promising indicator for detection of F^- . Therefore, selectivity of the probe **3** was evaluated in the next stage because; the specificity of the probe towards fluoride ion even under competing environment of other analytes is desired for its applications in environmental and biological systems.

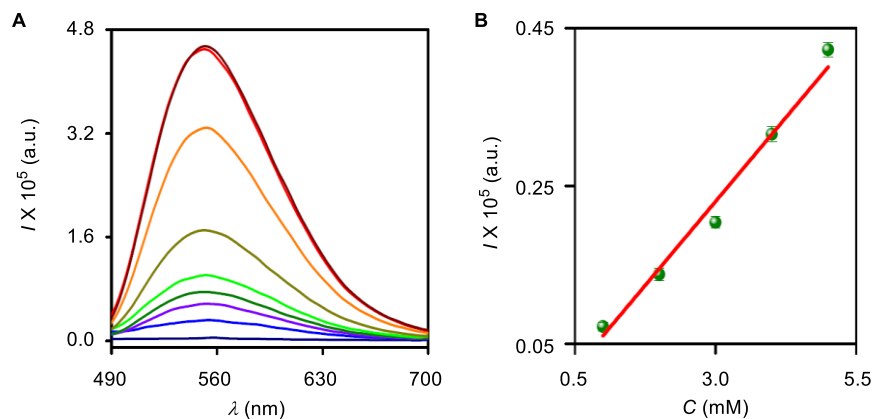


Figure 2.20 A) Fluorescence spectra of the probe **3** (10 μM in water containing 0.5 mM CTAB) in the presence of increasing concentration of F^- (0, 2, 4, 6, 8, 10, 12, 14, 16 mM) with $\lambda_{ex} = 460$ nm and B) linear relationship between the I_{553} and C_{TBAF} of **3** (1-5 mM).

The selectivity of the probe **3** towards F^- and its inertness towards ranges of analytes were examined. Selectivity of the probe towards fluoride in the competing environment of these potentially interfering analytes was also evaluated under similar conditions. In each case, probe **3** (10 μM) was treated with 15 mM of other possibly interfering analytes (Br^- , I^- , Cl^- , ClO_4^- , PF_6^- ,

NO_3^- , HSO_4^- , OAc^- , SO_4^{2-} , H_2O_2 , Na_2S , Cys and GSH) in water (0.5 mM CTAB) at room temperature for 60 min and fluorescence intensity was monitored at $\lambda = 553$ nm ($\lambda_{\text{ex}} = 460$ nm). No significant fluorescent intensity was observed in the presence of applied analytes indicating the inertness of the probe towards these species (Figure 2.21A, front row, violet bars). However the treatment of TBAF (15 mM) resulted about 120-fold fluorescent intensity enhancement (Figure 2.21A, back row, blue bar). The addition of TBAF (15 mM) to cuvettes containing probe **3** and a competing analyte provided fluorescence jumps (Figure 2.21A, back row, red bars) similar to the addition of the anion to pure **3** in water (0.5 mM CTAB). Each data was recorded after 1 h of the addition of an analyte. Thus, **3** possess high selectivity towards fluoride with equal efficiency in the presence of other competing anions. Response of **3** towards F^- under ambient light was marked by the visible change from colorless to yellow demonstrating the expediency of the probe as a "naked eye" indicator for F^- in water (Figure 2.21B). The probe was inert to other analytes and no

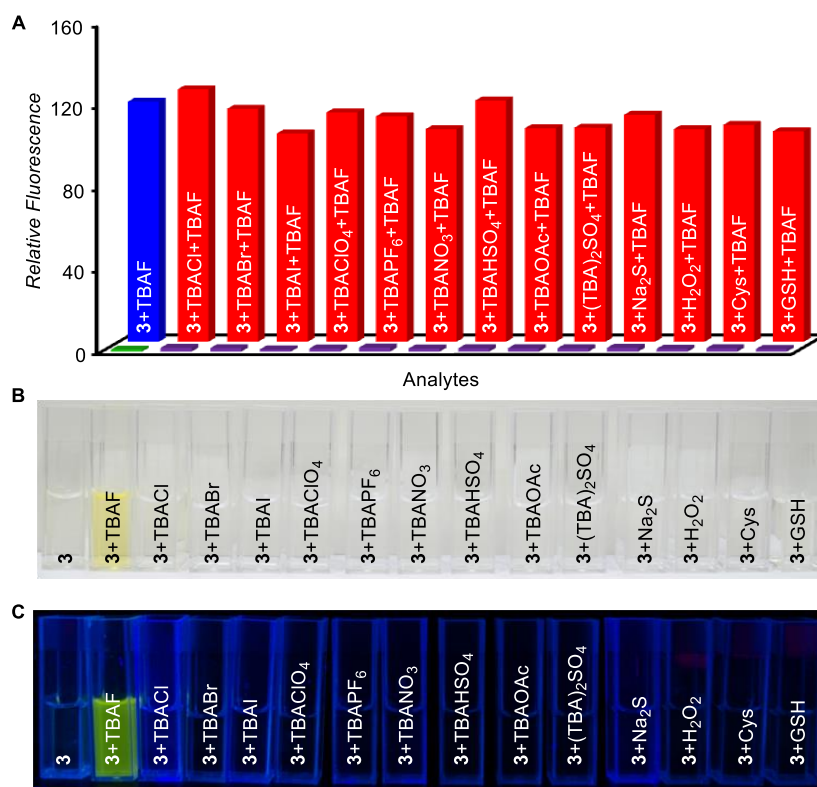


Figure 2.21 A) Relative fluorescence intensity at $\lambda = 553$ nm ($\lambda_{\text{ex}} = 460$ nm) for **3** (10 μM) in water (0.5 mM CTAB) toward F^- (15 mM) and in the absence and presence of various analytes (15 mM each). Color codes: ■ = **3**, ■ = **3**+TBAF, ■ = **3**+analyte and ■ = **3**+analyte+TBAF. Photographs taken under B) ambient light and C) handheld UV-lamp in the absence and presence of various analytes.

change in color was observed for any of these analytes. The fluorescence turn-*on* response upon sensing of F^- was also confirmed by the appearance of green fluorescence of the reaction mixture when Cuvette images were taken under handheld UV-lamp ($\lambda_{ex} = 365 \text{ nm}$) (Figure 2.21C). These results confirmed that the probe **3** is highly selective towards F^- .

2.8.5. Cell Imaging

Application of probe **3** was demonstrated by live cell fluorescence microscopic technique using HeLa cells. When cells were incubated with only probe **3** ($10 \mu\text{M}$ in 1:100 DMSO-DMEM v/v, pH = 7.4) at $37 \text{ }^\circ\text{C}$ for 1h, no significant fluorescence was observed (Figure 2.22A-C). On the other hand, when cells pre-treated with $2 \text{ mM } F^-$ (1:1000 DMSO-DMEM v/v, pH = 7.4) for 30 min and then incubated with the probe **3** ($10 \mu\text{M}$ in 1:100 DMSO-DMEM v/v, pH = 7.4) for 30 min showed strong fluorescence inside these cells (Figure 2.22D-F). These differential interference contrast and fluorescence images demonstrate the permeation of probe **3** through the living cell membranes and its ability of sensing intracellular F^- .

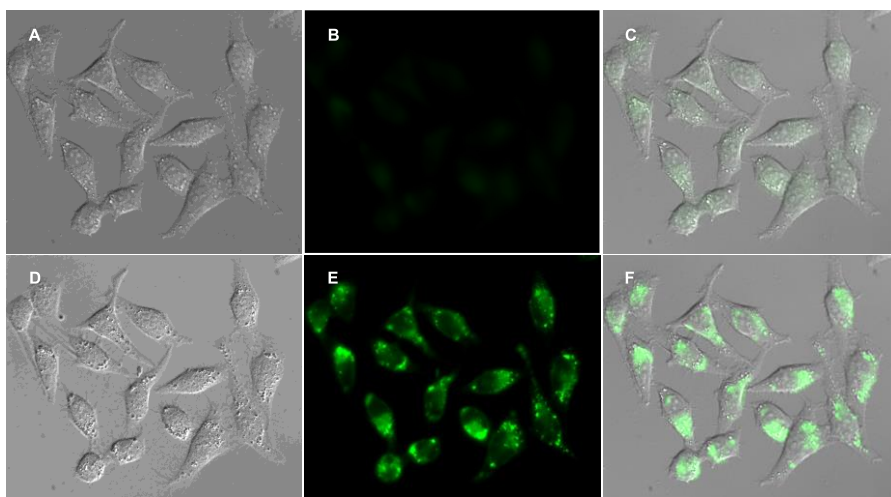


Figure 2.22. Cell images of HeLa cell: **A)** differential interference contrast, **B)** fluorescence, and **C)** overlay, image of HeLa cell incubated with probe **3** ($10 \mu\text{M}$) for 1 h. **(D – F)** are the respective differential interference contrast, fluorescence and overlay image of HeLa cell first incubated with incubation with NaF (2 mM) for 30 min followed by probe **3** ($10 \mu\text{M}$) for 30 min.

2.9. Summary of All Probes

In summary, we have presented the design, synthesis, and properties of a colorimetric and fluorometric probes for detection of fluoride. These probe exhibits high sensitivity and selectivity

toward fluoride over other interfering anions. The detection limit of all probes were found to be less than 4 ppm, the allowed concentration level of F^- in drinking water specified by USEPA. Low detection limit of probes show their potential application in the detection of F^- in biological and environmental systems as higher F^- concentration is toxic (0.1 mM for drinking water standard and > 3 mM in biological systems). A change in color from colorless to yellow (in case of carboxyfluorescein and NBD-amine) or pink (in case of resorufin dye) and non-fluorescent to fluorescence prove the significance of the probe in “naked-eye” detection of F^- . The cell permeability and ability of all the probes to detect F^- in live cell was also confirmed by live cell imaging. Finally fluoride detection was achieved in 100% aqueous media.

2.10. Experimental Section

General Methods: All reactions were performed under the nitrogen atmosphere. All the chemicals were purchased from commercial sources and used as received unless stated otherwise. Solvents were dried by standard methods prior to use. TLC was carried out with E. Merck silica gel 60-F₂₅₄ plates and column chromatography was performed over silica gel (100-200 mesh) obtained from commercial suppliers.

Instrumentation and Software: The 1H and ^{13}C NMR spectra were recorded on 400 MHz Jeol ECS-400 (or 100 MHz for ^{13}C) spectrometers using either residual solvent signals as an internal reference or from internal tetramethylsilane on the δ scale ($CDCl_3$ δ_H 7.26 ppm, CD_3OD δ_H 3.3 ppm, $CDCl_3$ δ_C 77.0 ppm). The chemical shifts (δ) are reported in ppm and coupling constants (J) in Hz. The following abbreviations are used: s (singlet), d (doublet), dd (doublet of doublet), dt (doublet of triplet) and m (multiplet). All MALDI-MS measurements were recorded on an Applied Biosystems 4800 Plus MALDI TOF/TOF analyzer. HPLC analysis was performed on an Agilent model with Zorbax SB C-18 reversed phase column (250 nm \times 4.6 nm, 5 μ m). Absorption spectra were recorded on a PerkinElmer, Lambda 45 UV-Vis spectrophotometer. Steady State fluorescence experiments were carried out in a micro fluorescence cuvette (Hellma, path length 1.0 cm) on a Fluoromax 4 instrument (Horiba Jobin Yvon). Time-resolved fluorescence measurements were carried on a TCSPC instrument (Horiba Jobin Yvon, Fluoro 3PS). (FT-IR) spectra were obtained using NICOLET 6700 FT-IR spectrophotometer as KBr disc and reported

in cm^{-1} . Melting points were measured using a VEEGO Melting point apparatus. All melting points were measured in open glass capillary and values are uncorrected.

Synthesis of 2-(((*tert*-butyldimethylsilyl)oxy)methyl)benzoic acid 7: Acid **7** was synthesized by three steps.

Step I: In a 50 mL round bottom flask Phthalide **4** (1.00 g, 7.40 mmol) and KOH (0.49 g, 8.88 mmol) were dissolved in MeOH (24 mL). Reaction mixture was refluxed for 2 h until all starting material got consumed which was monitored by TLC analysis. The resulting reaction mixture was allowed to cool to room temperature and solvent was evaporated under reduced pressure to obtain white residue. This crude solid was used directly for the next step.

Step II: In same round bottom flask crude white solid was dissolved in dimethylformamide (DMF) (6.0 mL) and then imidazole (1.50 g, 22.20 mmol) was added to it. *tert*-butyldimethylsilylchloride (2.22 g, 14.80 mmol) dissolved in DMF (9.0 mL) was added dropwise to the reaction mixture at room temperature and resultant reaction mixture was stirred at room temperature for overnight. After completion of reaction, reaction mixture was diluted with water (15 mL) and diethyl ether (15 mL). Organic layer was separated. And aqueous layer was extracted with diethyl ether (3×10 mL). The combined organic layer was washed with brine and dried over Na_2SO_4 and concentrated in vacuo and directly used for next step.

Step III: In a 25 mL round bottom flask, the crude residue was dissolved in MeOH (2.5 mL) and THF (2.5 mL). Potassium carbonate (2.04 g, 14.80 mmol) in water (7 mL) was added to it and stirred at room temperature for 6 h. Solvent was removed under reduced pressure and residue was acidified to pH 5-6 by dropwise addition of 1(N) HCl. Reaction mixture was diluted with water (10 mL) and diethyl ether (10 mL). Organic layer was separated and aqueous layer was extracted with diethyl ether (3×10 mL). The combined organic layer was dried over Na_2SO_4 , and solvent was evaporated under reduced pressure to obtain residue which was subjected to column chromatography over silica gel to afford 32% compound **7** (0.30 g) as white solid (*Eluent*: 10% EtOAc in petroleum ether). **M.p.:** 90 – 91 °C; **IR (KBr):** ν/cm^{-1} : 1699, 1602, 1576, 1466, 1442, 1404, 1306, 1262, 1197, 1145; **^1H NMR(400 MHz, CDCl_3):** δ 8.08 (dd, $J = 1.2, 8.0$ Hz, 1H), 7.70 (d, $J = 7.6$ Hz, 1H), 7.59 (td, $J = 1.2, 8.7$ Hz, 1H), 7.36 (td, $J = 1.2, 7.6$ Hz, 1H), 5.06 (s, 2H), 0.96 (s, 9H), 0.15 (s, 6H); **^{13}C NMR (100 MHz, CDCl_3):** δ 172.5, 143.8, 132.9, 131.1, 126.4, 126.3,

126.0, 63.1, 25.5, 17.9, 5.7; **HRMS (ESI)**: Calc. for $C_{14}H_{22}O_3Si$ $[M-H]^-$: 265.1252; Found: 265.1252.

Synthesis of probe 1: Compound **8** was prepared using reported procedure.²¹ In a 25 mL round bottom flask, a mixture of compound **8** (0.15 g, 0.43 mmol) and compound **7** (0.12 g, 0.43 mmol) was dissolved in CH_2Cl_2 (7 mL) and then EDC.HCl (99.87 mg, 0.52 mmol), DIPEA (0.29 μ L, 1.73 mmol) and DMAP (0.01 g, 0.08 mmol) were added simultaneously at room temperature and stirred for 12 h at room temperature. Solvent was removed from reaction mixture under reduced pressure and the crude residue was directly subjected to column chromatography over silica gel to afford probe **1** (0.15 g, 58%) as white solid (*Eluent*: 15% EtOAc in petroleum ether). **M.p.**: 150 – 151 °C; **HPLC Purity**: 99.3%; **IR (KBr)**: ν/cm^{-1} : 1755, 1613, 1507, 1421, 1256, 1027, 847; **1H NMR (400 MHz, DMSO- d_6)**: δ 8.14 (d, $J = 7.6$ Hz, 1H), 8.05 (d, $J = 7.2$ Hz, 1H), 7.84-7.72 (m, 4H), 7.49 (t, $J = 6.8$ Hz, 1H), 7.43 (d, $J = 2.4$ Hz, 1H), 7.34 (d, $J = 7.6$ Hz, 1H), 7.08 (dd, $J = 2.4$, 8.6 Hz, 1H), 6.98 (d, $J = 2.4$ Hz, 1H), 6.91 (d, $J = 8.8$ Hz, 1H), 6.78-6.72 (m, 2H), 5.09 (s, 2H), 3.81 (s, 3H), 0.98 (s, 9H), 0.08 (s, 6H); **^{13}C NMR (100 MHz, $CDCl_3$)**: δ 169.4, 164.7, 161.5, 153.1, 152.3, 152.1, 152.0, 145.9, 138.5, 135.2, 133.7, 131.0, 129.9, 129.2, 129.1, 126.7, 126.6, 125.2, 125.1, 124.1, 117.7, 116.9, 112.1, 110.9, 110.7, 100.9, 82.4, 63.3, 55.7, 26.1, 18.5, 5.3; **HRMS (ESI)**: Calc. for $C_{35}H_{34}O_7Si$ $[M+H]^+$: 595.2148; Found: 595.2156.

Synthesis of probe 2: In a 25 mL round bottom flask, acid **7** (150 mg, 0.70 mmol) and resorufin **9** (187 mg, 0.70 mmol) was dissolved in DCM (8 mL) and then EDC.HCl (161.90 mg, 0.84 mmol), DIPEA (0.478 μ L, 2.812 mmol) and DMAP (17 mg, 0.141 mmol) were added to the reaction flask at room temperature simultaneously and stirred for overnight at this temperature. Solvent was removed from reaction mixture under reduced pressure and the crude residue was directly subjected to column chromatography over silica gel to afford probe **2** (110 mg, 50%) as yellow solid (*Eluent*: 15% EtOAc in petroleum ether). **M.p.**: 120 – 121 °C; **HPLC Purity**: 99.93%; **IR (KBr)**: ν/cm^{-1} : 1729, 1620, 1509, 1243, 1125, 1030, 857, 724; **1H NMR (400 MHz, $CDCl_3$)**: δ 8.22 (dd, $J = 1.2$, 8.0 Hz, 1H), 7.92 (d, $J = 7.6$ Hz, 1H), 7.86 (d, $J = 8.4$ Hz, 1H), 7.68 (dt, $J = 1.2$, 7.4 Hz, 1H), 7.40-7.47 (m, 2H), 7.26 (m, 1H), 7.23 (m, 1H), 6.88 (dd, $J = 2.0$, 10.0 Hz, 1H), 6.35 (d, $J = 2$ Hz, 1H), 5.16 (s, 2H), 0.97 (s, 9H), 0.13 (s, 6H); **^{13}C NMR (100 MHz, $CDCl_3$)**: δ 186.4, 164.3, 153.8, 149.3, 148.4, 146.1, 144.5, 135.2, 134.9, 134.1, 131.4, 131.1, 126.8, 126.7, 124.7,

119.7, 109.9, 107.2, 63.21, 25.9, 18.4, -5.39; **MALDI**: Calculated for $C_{26}H_{27}NO_5Si$ $[M+H]^+$: 462.17; Found: 462.15.

Synthesis of probe 3: Acid **7** was prepared by using same protocol discussed earlier. In a 25 mL round bottom flask, a mixture of NBD-amine **18** (75 mg, 0.41 mmol) and acid **7** (111 mg, 0.41 mmol) were dissolved in CH_2Cl_2 (8 mL). EDC·HCl (94 mg, 0.49 mmol), DIPEA (0.28 μ L, 1.62 mmol) and DMAP (0.01 g, 0.08 mmol) were simultaneously added to the round bottom flask at room temperature and stirred for 12 h at room temperature. After completion of reaction solvent was removed under reduced pressure and column chromatography was performed over silica gel to afford probe **3** (71 mg, 40%) as yellow solid (*Eluent*: 12% EtOAc in petroleum ether). **M.p.**: 180 – 181 °C; **IR (KBr)**: ν/cm^{-1} : 1692, 1547, 1444, 1370, 1315, 1251, 1091; **1H NMR (400 MHz, MeOH-*d*₄)**: δ 8.7 (dd, $J = 8.4$ Hz, 1H), 8.6 (dd, $J = 8.4$ Hz, 1H), 7.7 (d, $J = 8.0$ Hz, 1H), 7.5-7.6 (m, 2H), 7.3-7.4 (m, 1H), 5.0 (s, 2H), 0.85 (s, 9H), 0.08 (s, 6H); **^{13}C NMR (100 MHz, $CDCl_3$)**: δ 168.0, 145.7, 143.5, 138.6, 134.7, 134.6, 134.0, 132.9, 131.4, 130.9, 130.5, 129.2, 114.4, 65.1, 26.5, 19.1, 4.1; **HRMS (ESI)**: Calc. for $C_{20}H_{24}N_4O_5Si$ $[M+H]^+$: 429.1588; Found: 429.1614.

Procedures:

Preparation of the sample solution: Stock solution of all probes (2 mM) was prepared in Acetonitrile. The final concentration during assay is 10 μ M. Stock solution of TBAF was prepared by diluting 1M TBAF in THF.

Preparation of the solution of analytes: Stock solutions of TBABr, TBAI, TBACl, TBAClO₄, TBAPF₆, TBANO₃, TBAHSO₄, TBAOAc, (TBA)₂SO₄, were prepared in THF and stock solutions of H₂O₂, Cysteine (Cys), Glutathione (GSH) were prepared in deionized water. Calculated volumes of analytes were added from respective stock solutions to each fluorescence cuvette to provide required concentration. Stock solution of TBAF was made in water for determining detection limit and for all assay to detect fluoride in aqueous media.

General method for UV-Vis and Fluorescence titration: For absorbance and emission studies 1 cm path length was used for cells. The excitation and emission slit width were 2 nm and 3 nm, respectively. All spectral data were recorded after the addition of analyte(s) to the solution of probes and TBAF.

Determination of quantum yields:

The quantum yield of probes was determined according to the Equation 1:

$$\Phi_1 = \Phi_B \times \frac{I_1 \times A_B \times \lambda_{exB} \times (\eta_1)^2}{I_B \times A_1 \times \lambda_{ex1} \times (\eta_B)^2} \quad (\text{Equation 1})$$

where, Φ is quantum yield; I is integrated area under the corrected emission spectra; A is absorbance at the excitation wavelength; λ_{ex} is the excitation wavelength; η is the refractive index of the solution; the subscripts 1 and B refer to the unknown and the standard, respectively.

Determination of reaction rate (k) and half-life ($t_{1/2}$) for all probes:

Reaction rate (k), half-life ($t_{1/2}$) and response time (t_R) for probes **1**, **2** and **3** were determined by fluorescence kinetics experiments. In fluorescence kinetics experiment, Fluoride (3 mM) (either in THF or in H₂O) was added to the solution of probe (10 μ M) in DMSO in a cuvette at room temperature at $t = 60$ s and fluorescence intensity at $\lambda = 523$ nm (upon $\lambda_{ex} = 460$ nm) was recorded. Rate constant, k and response time (t_R) for all probes was determined according to the following equation (Equation 2):

$$Y = a \times [1 - e^{(-kt)}] \quad (\text{Equation 2})$$

Where, Y = fractional fluorescence intensity, a = arbitrary constant, k = pseudo first order rate constant, t = time.

Half-life of the reaction ($t_{1/2}$) was calculated using Equation (3)

$$t_{1/2} = 0.693/k \quad (\text{Equation 3})$$

Where k = pseudo first order rate constant.

Determination of relative fluorescence: determined according to the following equation 4:

$$\text{Relative Fluorescence} = I_s/I_0 \quad (\text{Equation 4})$$

where, I_0 = fluorescence intensity of free probe at fixed wavelength and I_s = fluorescence intensity at fixed wavelength after addition of analyte to probe.

Detection Limit Calculation: ²² Limit of Detection for F⁻ was calculated using fluorometric titrations using equation 5,

$$LOD = 3\sigma/m \quad (\text{Equation 5})$$

where σ = standard deviation of 6 blank measurements and m = slope obtained from the graph of fluorescence intensity vs. concentration of F^- added.

Cell Imaging: All cell imaging experiment was carried out by Tanmoy saha from our group. The HeLa cells were purchased from National Centre for Cell Science, Pune (India). HeLa cells were grown in DMEM supplemented with 10% heat inactivated fetal bovine serum (FBS), 100 IU/ml penicillin, 100 mg/ml streptomycin and 2 mM L-glutamine. Cultures were maintained in a humidified atmosphere with 5% CO_2 at 37 °C. The cultured cells were subcultured twice in each week, seeding at a density of about 15×10^3 cells/ml. Typan blue dye exclusion method was used to determine Cell viability. The fluorescence images were taken using Olympus Inverted IX81 equipped with Hamamatsu Orca R2 microscope by exciting at $\lambda_{ex} = 460-480$ nm (by using GFP filter). The HeLa cells were incubated with solution of the probe (10 μ M in 1:100 DMSO-DMEM v/v, pH = 7.4) at 37 °C for 2 h. After washing with PBS the fluorescence images were acquired. In this case no significant fluorescence was observed. Another set of HeLa cells were treated with all Probes (10 μ M in 1:100 DMSO-DMEM v/v, pH = 7.4) at 37 °C for 2 h and then after washing the cells thoroughly by PBS, cells were incubated with solution of NaF (20 mM in 1:100 DMSO-DMEM v/v, pH = 7.4) at 37 °C for 30 min. After washing with PBS the fluorescence images were recorded.

HPLC Data: Reverse Phase HPLC analysis was performed to confirm that the reaction of probe **2** with fluoride which results in the fluoride mediated desilylation followed by cascade reaction and formation of resorufin **9**. HPLC chromatograms were obtained by treating probe **2** (10 μ M) with increasing concentration of fluoride (10 eqv - 30 eqv) in mixture of acetonitrile/water. HPLC gradient used for the analysis was as follows:

Column: Phenomenex (4.6 mm \times 250 mm)

Flow: 1.0 mL/min

Method: Gradient

50 % Acetonitrile/water	0 min
50 % Acetonitrile/water	0 to 15 min
100 % Acetonitrile	15 to 18 min
50 % Acetonitrile/water	18 to 25 min

Chapter 2

50 % Acetonitrile/water 25 to 30 min

Wavelength: 250 nm

Reverse phase HPLC analysis was performed to confirm the mechanism of probe **3** during reaction with fluoride. The reaction resulted in the formation of NBD-amine **18** and Phthalide **4**. HPLC chromatograms were obtained for probe **3** (10 μ M), NBD-amine **18**, Phthalide **4** and by treating it with increasing concentration of TBAF (100 – 300 equiv) in mixture of acetonitrile/water. HPLC gradient used for the analysis was as follows:

Column: Reversed phase column (4.6 mm \times 250 mm, 5 μ m)

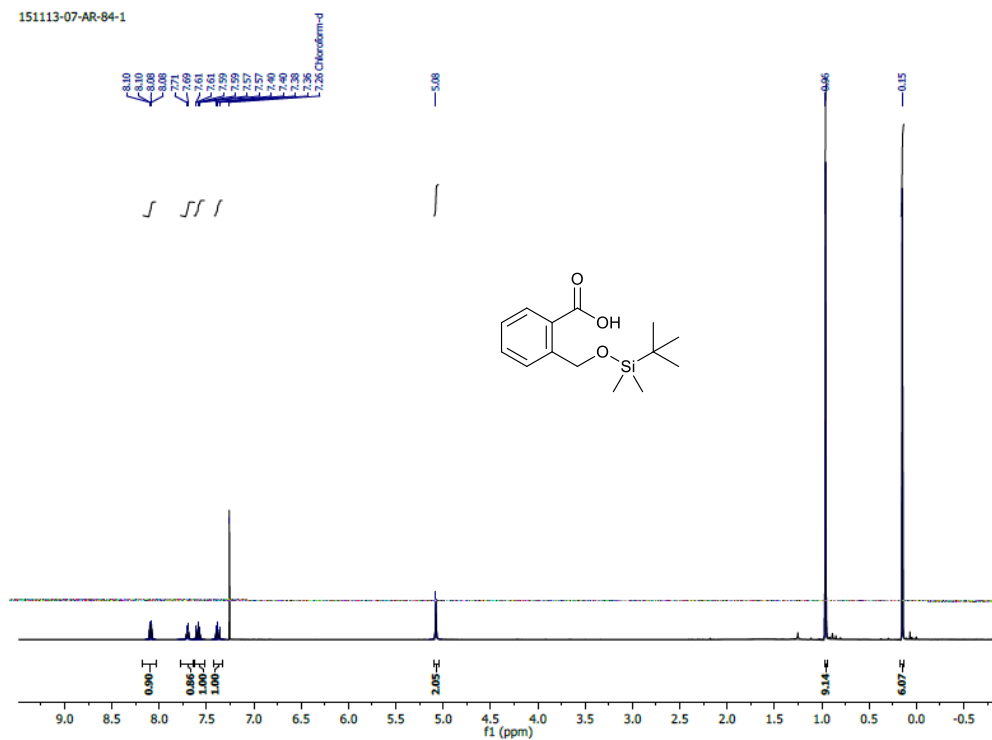
Flow: 1.0 mL/min

Method: Gradient

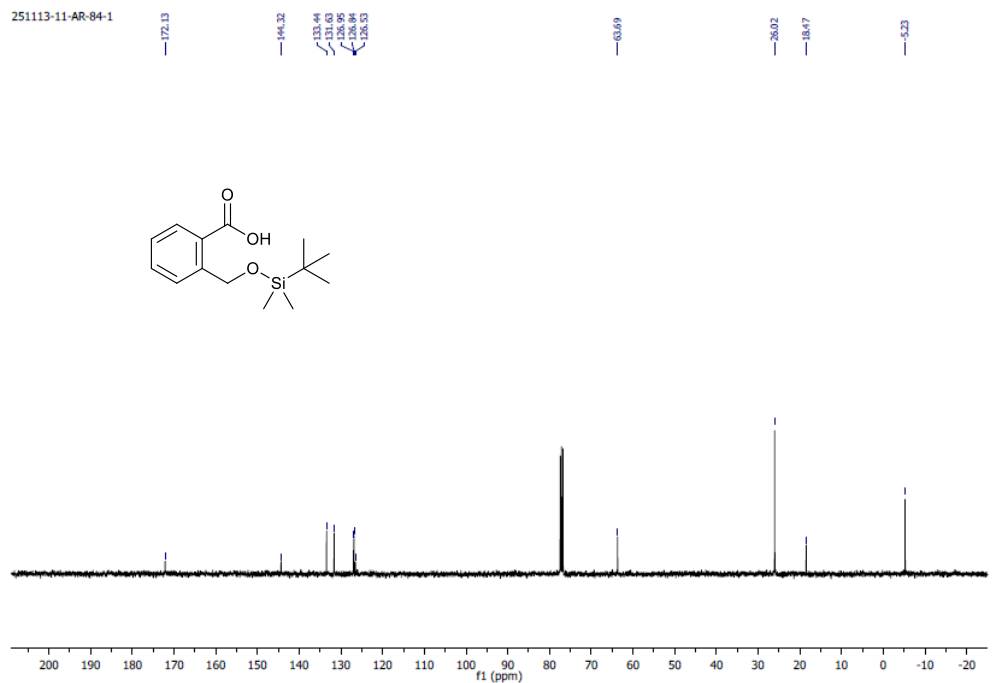
10 % Acetonitrile/water	:	0 min
20 % Acetonitrile/water	:	10 min
30 % Acetonitrile/water	:	15 min
40 % Acetonitrile/water	:	20 min
50 % Acetonitrile/water	:	25 min
75 % Acetonitrile/water	:	30 min
100 % Acetonitrile	:	35 min
100 % Acetonitrile	:	40 min
60 % Acetonitrile/water	:	45 min
40 % Acetonitrile/water	:	50 min
10 % Acetonitrile/water	:	55 min

Wavelength: 280 nm.

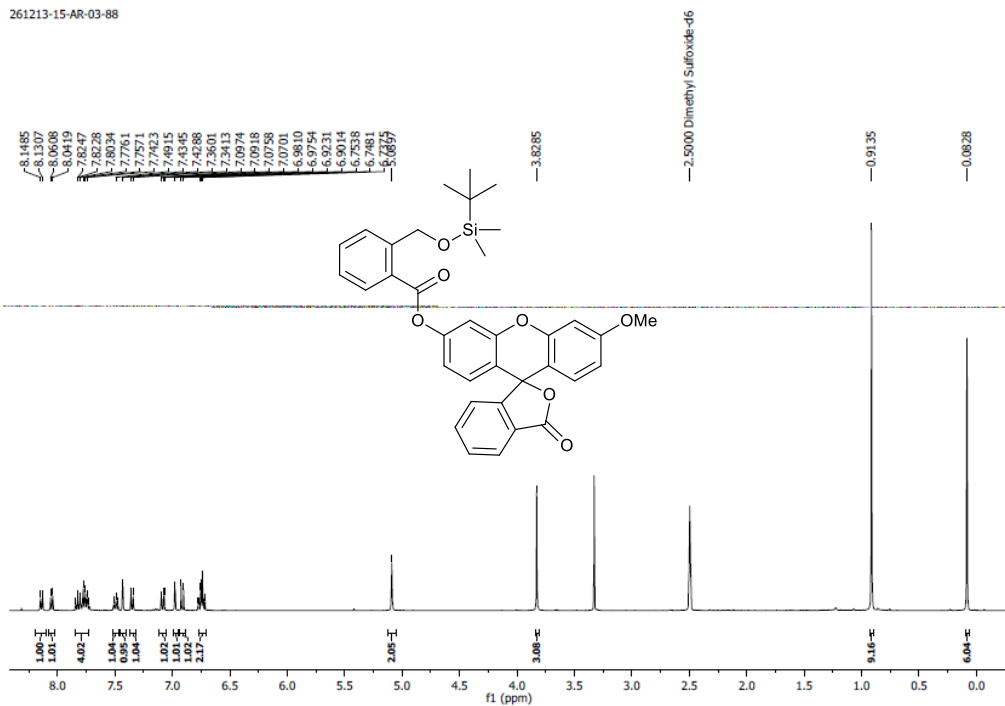
2.11. Appendix Section



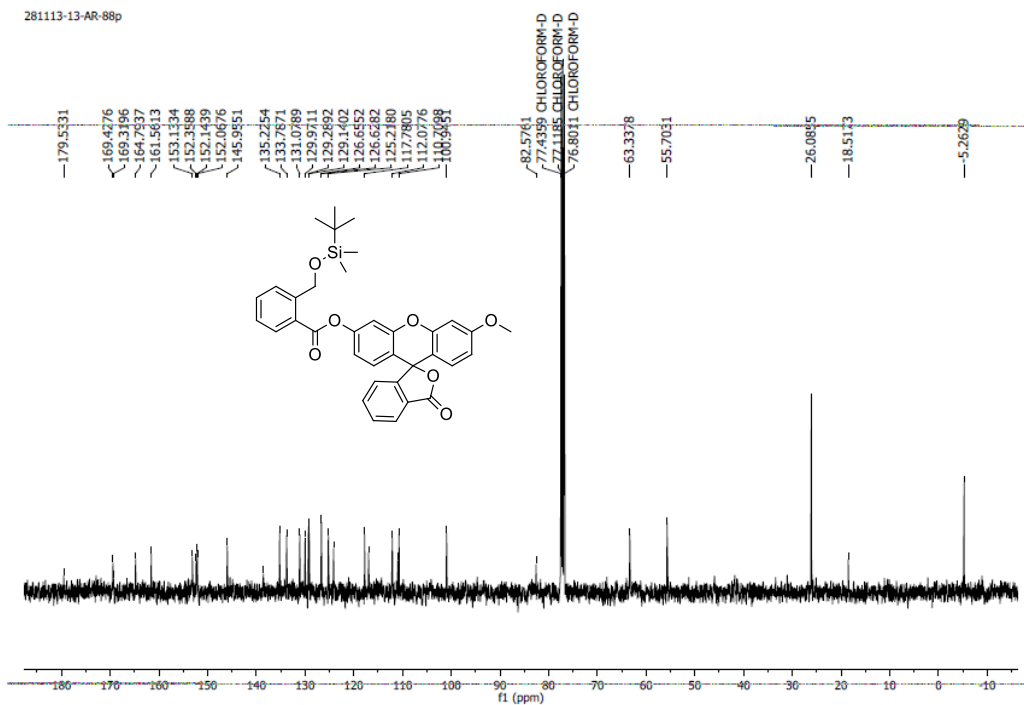
Appendix 2.1: ^1H NMR spectra of 7 in CDCl_3 .



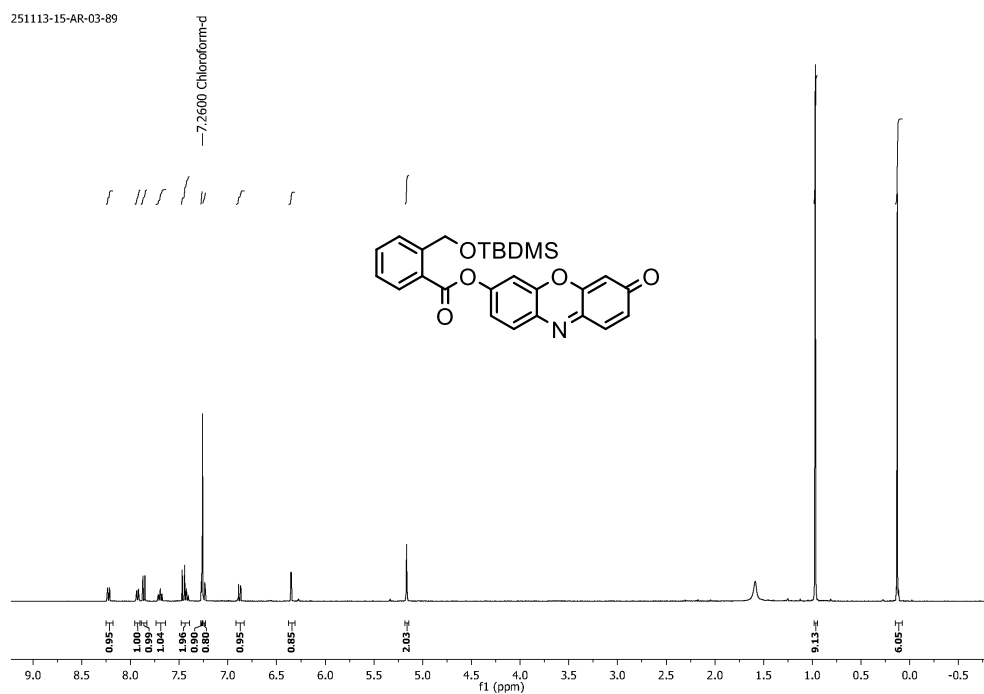
Appendix 2.2: ^{13}C NMR spectra of 7 in CDCl_3 .



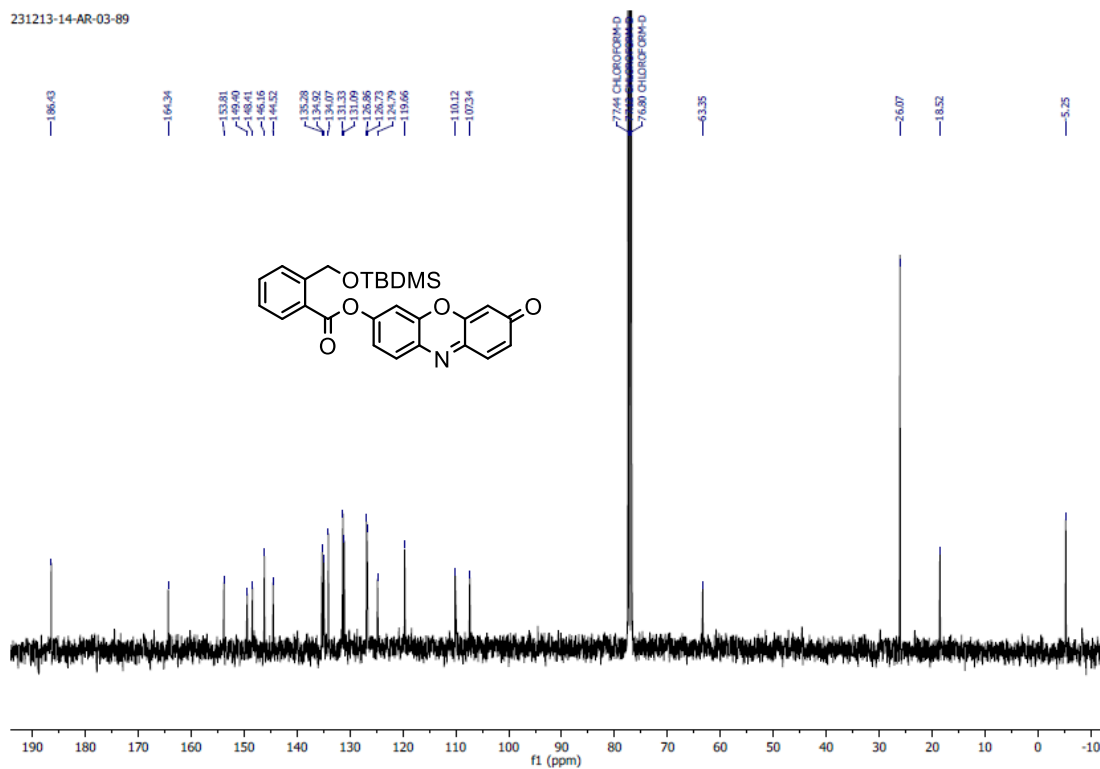
Appendix 2.3: ^1H NMR spectra of probe 1 in $\text{DMSO-}d_6$.



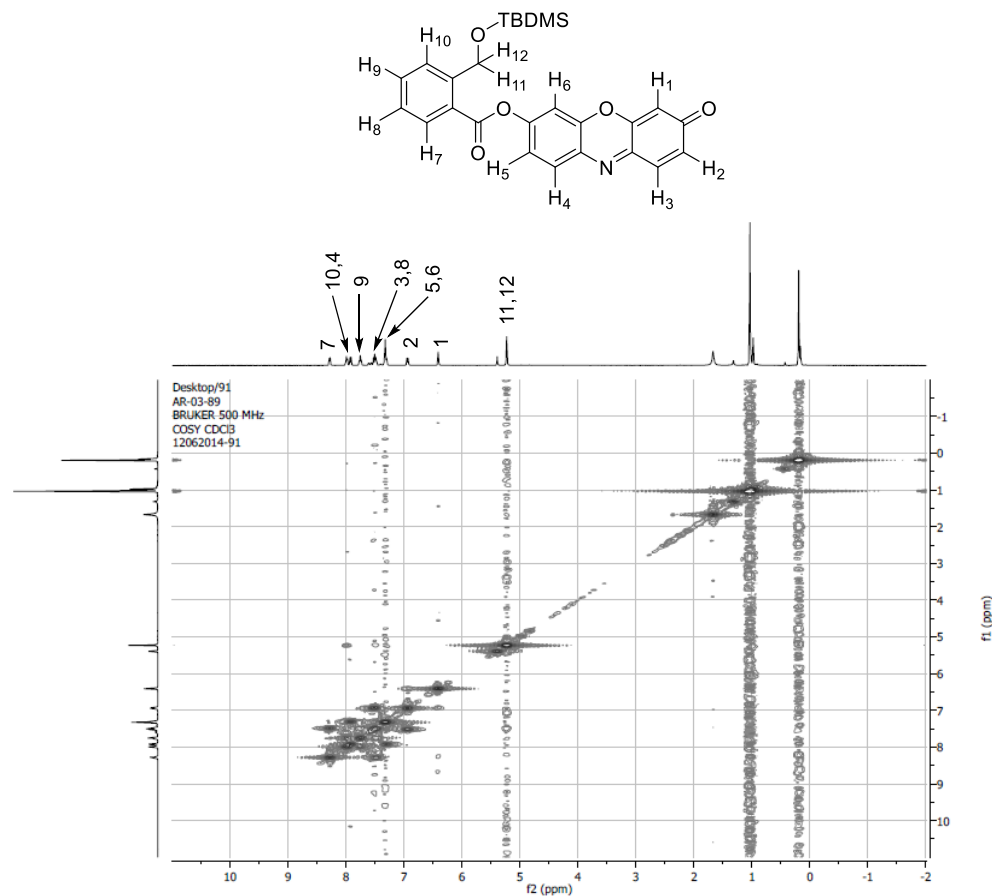
Appendix 2.4: ^{13}C NMR spectra of probe 1 in CDCl_3 .



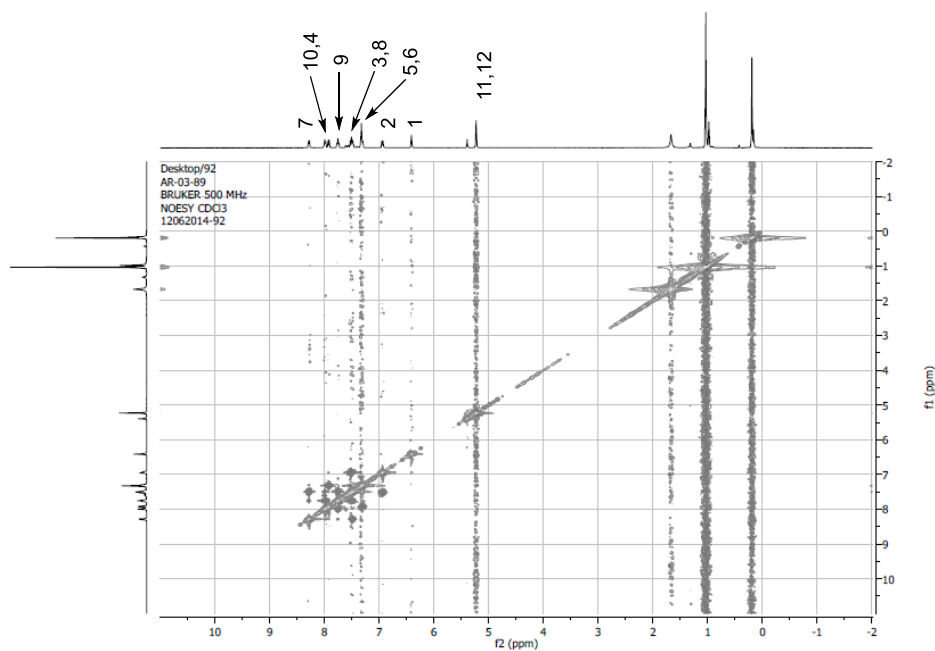
Appendix 2.5: ^1H NMR spectra of **2** in CDCl_3 .



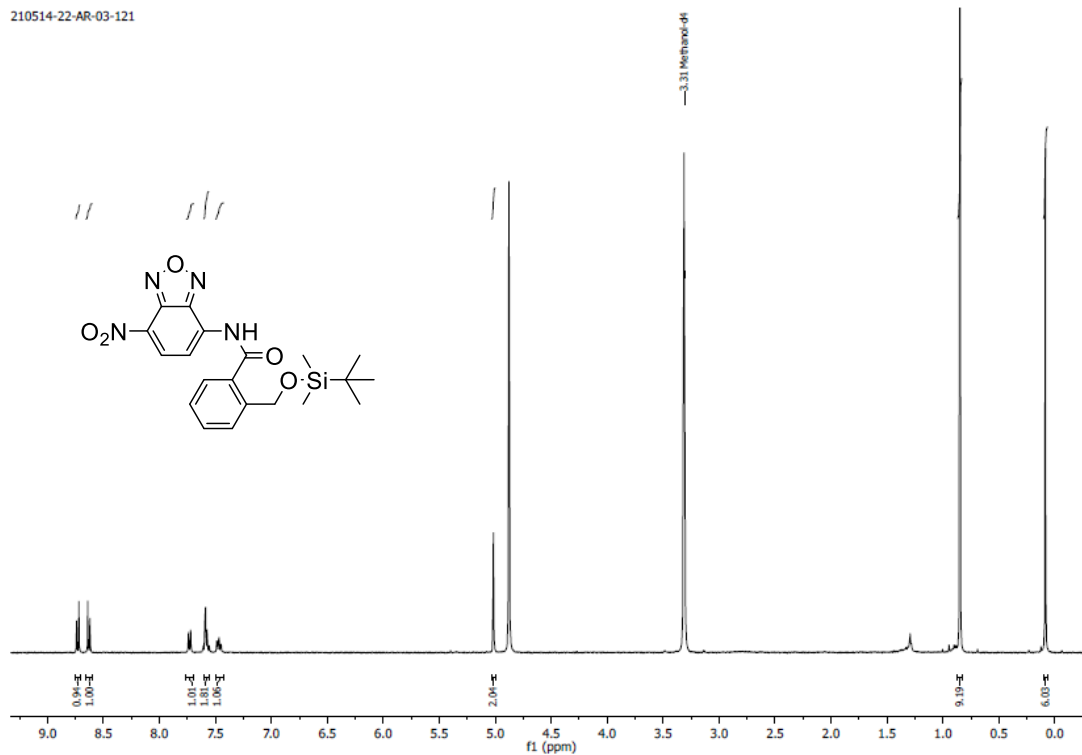
Appendix 2.6: ^{13}C NMR spectra of **2** in CDCl_3 .



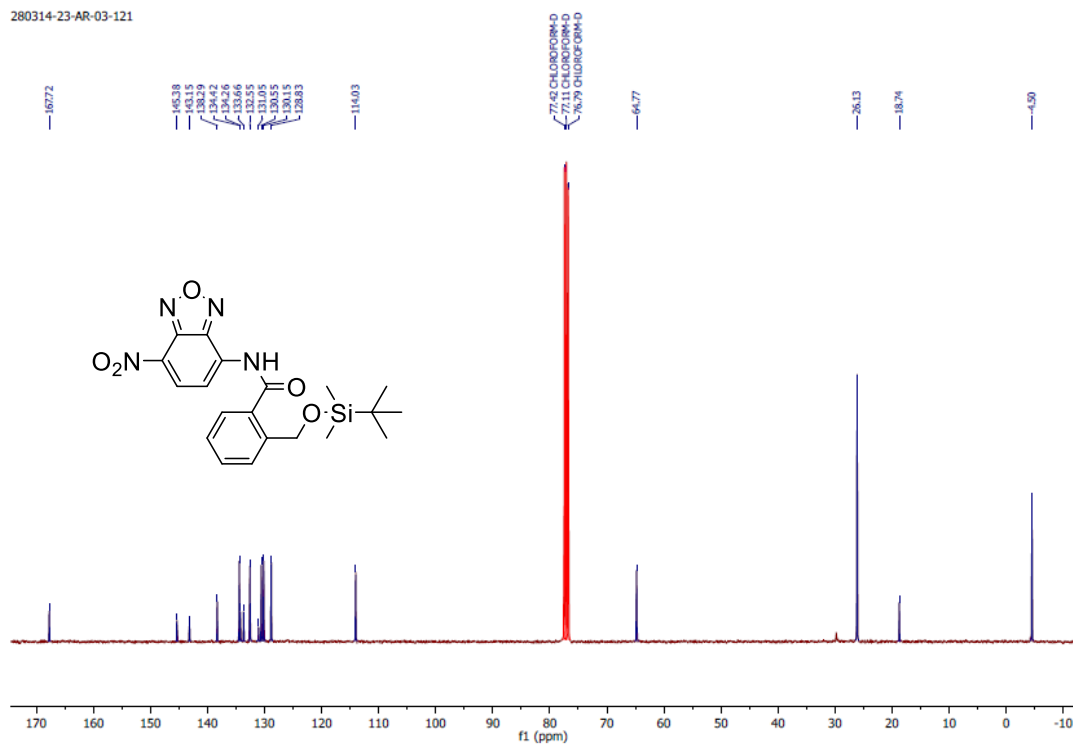
Appendix 2.7: COSY spectra of **2** in CDCl₃.



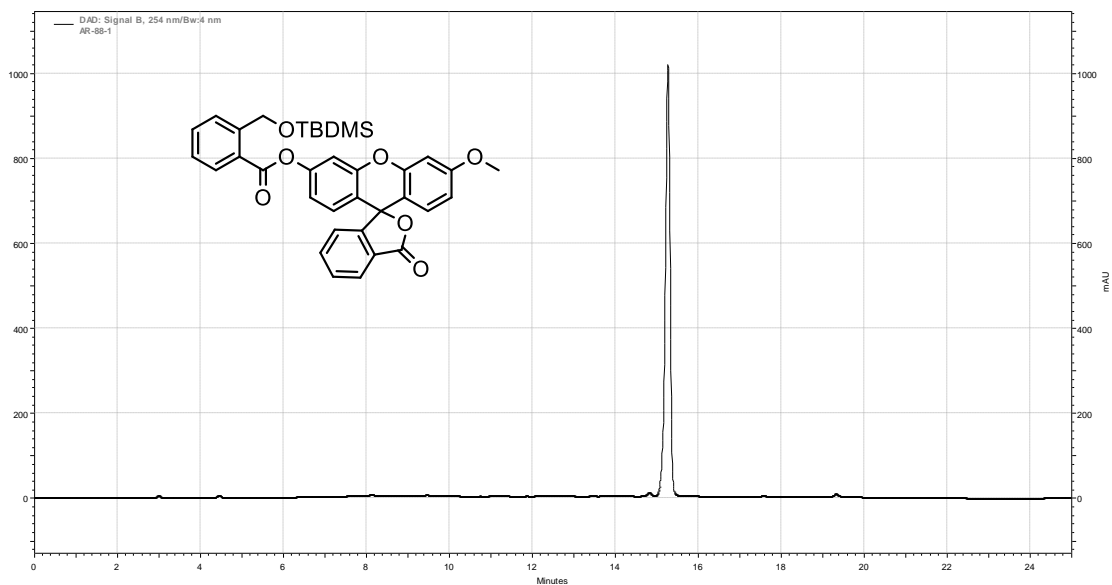
Appendix 2.8: NOESY spectra of **2** in CDCl₃.



Appendix 2.9: $^1\text{H NMR}$ of probe 3 in $\text{MeOH-}d_4$.



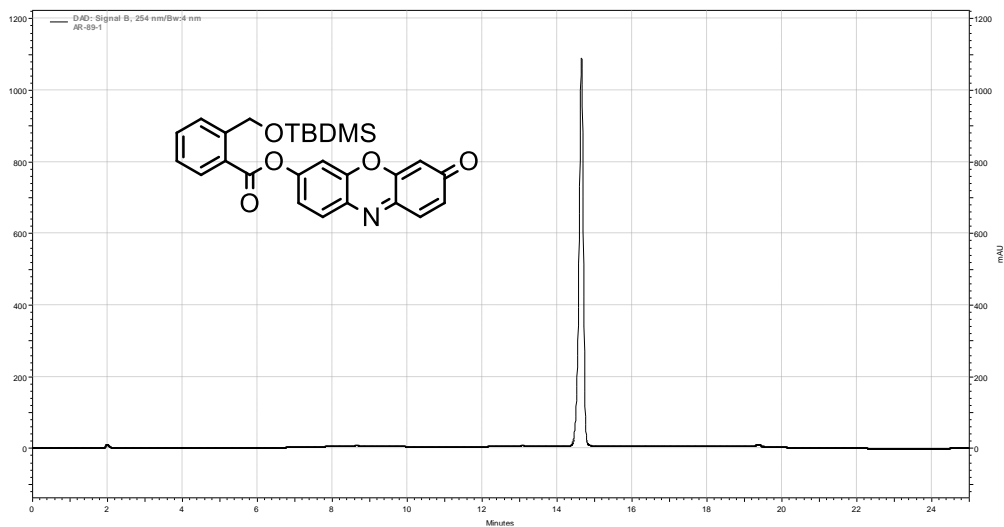
Appendix 2.10: $^{13}\text{C NMR}$ of probe 3 in CDCl_3 .



**DAD: Signal B,
254 nm/Bw:4 nm
Results**

Retention Time	Area	Area %	Height	Height %
14.827	127045	0.74	17525	0.82
15.280	16987928	99.26	2126869	99.18
Totals		17114973	2144394	100.00

Appendix 2.11: HPLC Data of Probe 1.



DAD: Signal B,
254 nm/Bw:4 nm
Results

Retention Time	Area	Area %	Height	Height %
0.100	106	0.00	20	0.00
14.660	18505888	99.93	2271571	99.92
15.267	13639	0.07	1729	0.08
Totals	18519633	100.00	2273320	100.00

Appendix 2.12: HPLC Data of probe 2.

2.12. References

- (a) Hudson, Z. M.; Wang, S. *Acc. Chem. Res.* **2009**, *42*, 1584-1596; (b) Duke, R. M.; Veale, E. B.; Pfeffer, F. M.; Kruger, P. E.; Gunnlaugsson, T. *Chem. Soc. Rev.* **2010**, *39*, 3936-3953.
- Wade, C. R.; Broomsgrrove, A. E. J.; Aldridge, S.; Gabbai, F. P. *Chem. Rev.* **2010**, *110*, 3958-3984.
- (a) Cametti, M.; Rissanen, K. *Chem. Commun.* **2009**, 2809-2829; (b) Li, Y.; Zhang, X.; Zhu, B.; Yan, J.; Xu, W. *Anal. Sci.* **2010**, *26*, 1077-1080.
- Maity, D.; Manna, A. K.; Karthigeyan, D.; Kundu, T. K.; Pati, S. K.; Govindaraju, T. *Chem. Eur. J.* **2011**, *17*, 11152-11161.
- Roy, A.; Kand, D.; Saha, T.; Talukdar, P. *Chem. Commun.* **2014**, *50*, 5510-5513.
- Hou, P.; Chen, S.; Wang, H.; Wang, J.; Voitchovsky, K.; Song, X. *Chem. Commun.* **2014**, *50*, 320-322.
- Kim, S. Y.; Park, J.; Koh, M.; Park, S. B.; Hong, J.-I. *Chem. Commun.* **2009**, 4735-4737.
- Kim, D.; Singha, S.; Wang, T.; Seo, E.; Lee, J. H.; Lee, S.-J.; Kim, K. H.; Ahn, K. H. *Chem. Commun.* **2012**, *48*, 10243-10245.
- Zhu, B.; Yuan, F.; Li, R.; Li, Y.; Wei, Q.; Ma, Z.; Du, B.; Zhang, X. *Chem. Commun.* **2011**, *47*, 7098-7100.
- Hu, R.; Feng, J.; Hu, D.; Wang, S.; Li, S.; Li, Y.; Yang, G., *Angew. Chem., Int. Ed.* **2010**, *49*, 4915-4918.
- Cao, X.; Lin, W.; Yu, Q.; Wang, J. *Org. Lett.* **2011**, *13*, 6098-6101.
- Fu, L.; Jiang, F.-L.; Fortin, D.; Harvey, P. D.; Liu, Y., *Chem. Commun.* **2011**, *47*, 5503-5505.
- Bao, Y.; Liu, B.; Wang, H.; Tian, J.; Bai, R. *Chem. Commun.* **2011**, *47*, 3957-3959.
- Lu, H.; Wang, Q.; Li, Z.; Lai, G.; Jiang, J.; Shen, Z. *Org. Biomol. Chem.* **2011**, *9*, 4558-4562.
- Dong, M.; Peng, Y.; Dong, Y.-M.; Tang, N.; Wang, Y.-W. *Org. Lett.* **2011**, *14*, 130-133.
- Cao, J.; Zhao, C.; Feng, P.; Zhang, Y.; Zhu, W. *RSC Adv.* **2012**, *2*, 418-420.
- Roy, A.; Kand, D.; Saha, T.; Talukdar, P. *RSC Adv.* **2014**, *4*, 33890-33896.
- Shiraishi, Y.; Yamamoto, K.; Sumiya, S.; Hirai, T. *Chem. Commun.* **2013**, *49*, 11680-11682.
- Lipinski, C. A.; Lombardo, F.; Dominy, B. W.; Feeney, P. J. *Adv. Drug Deliv. Rev.* **2001**, *46*, 3-26.
- Lipinski, C. A.; Lombardo, F.; Dominy, B. W.; Feeney, P. J. *Adv. Drug Deliv. Rev.* **1997**, *23*, 3-25.
- Mugherli, L.; Burchak, O. N.; Chatelain, F.; Balakirev, M. Y. *Bioorg. Med. Chem. Lett.* **2006**, *16*, 4488-4491.
- Zheng, F.; Zeng, F.; Yu, C.; Hou, X.; Wu, S. *Chem. Eur. J.* **2013**, *19*, 936-942.

Section 2

Chloride Ion Recognition by Transmembrane Ion Transporters

Introduction

Molecular recognition is an event based on many fundamental chemical and biological phenomena such as catalysis, sensing and transport which constitutes a foremost important topic in supramolecular chemistry. Recently, anion recognition chemistry has been developed significantly.¹ Anions regulate the flux of metabolites into and out of the cell for maintenance of osmotic pressure and cell volume, they help in regulating pH and cellular signalling pathways. Hence, movement of anions across the phospholipid-bilayer is essential.² In biological system, the plasma membrane of a cell is a hydrophobic lipid bilayer which separates the interior of the cells from the outside environment and it is selectively permeable and poses a barrier for passage of solutes into and out of the cell. It allows small neutral molecules such as CO₂, H₂O to easily pass through the hydrophobic bilayer but exchange of charged solutes across the biological membrane cannot occur as easily as seen for neutral molecules and they require assistance from natural complex proteins *i.e* ion transport systems. Additionally, the spatial distribution of anions is not even in tissues and cells, thus leading to a concentration gradient which is created and maintained by a coordinated action of transport proteins that are present within the impermeable bilayer. In recent years, several genetic diseases have been associated with anion channels (also called as channelopathies).³ Channelopathies include vision loss caused by a malfunction of the Ca²⁺-activated Cl⁻ channel bestrophin in the retinal pigment epithelium. The neurological disorders such as Startle disease and Angelman syndrome are associated with the malfunction of glycine and GABA receptors due to ligand-gated Cl channels.^{1b, 4} Abnormalities in transport activity causes myotonia (muscle stiffness), nephrolithiasis (kidney stones), Bartter's syndrome type III (severe renal salt loss), osteopetrosis (bone disease) and a rare form of deafness. In addition, few reports

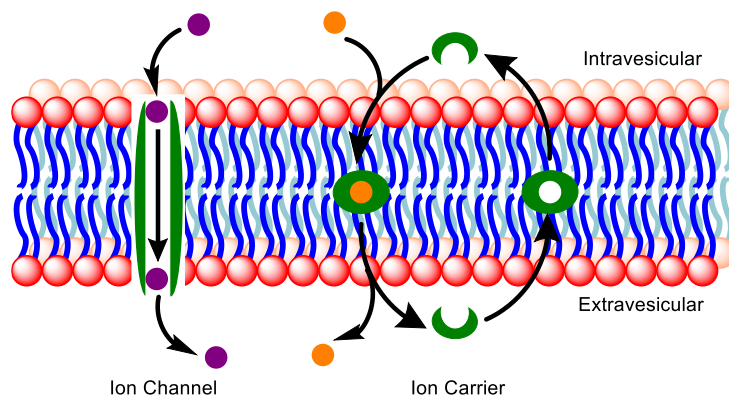


Figure 1: The two major mechanisms of ion transport involving Ion channel and Ion channels.

Section 2

have come recently about anionophores which can trigger cancer cells.⁵ As the malfunction pathways for anion transport have significant effects on biological systems, it is very necessary to know about the activity and mode of action of biological ion channels.⁶ But, as most of the naturally occurring ion channels are made up of complex protein structure, is very difficult to modulate the activity and they are also pretty much unstable for handling. So development of new synthetic ion transporters as a mimic of their natural congeners is an important area of research. Anion transport can be achieved by two ways: the provision of relatively static pathways for anion across membranes (synthetic channels) or development of small molecule which can carry anion across the membrane (anion carriers) and they should be lipophilic enough to be able to diffuse across the hydrophobic bilayer. The peptide gramicidin is an example of ion channel which forms a head-to-head helical dimer to give a tubular channel within a bilayer membrane. Additionally a naturally occurring antibiotic, Amphotericin aggregates to form a channel and it is mostly selective towards cation (Figure 2B). Valinomycin is one example of naturally occurring non-protein based carrier for potassium (Figure 2A). Prodigiosin is another naturally occurring ion carrier which transport chloride ion (Figure 2C).

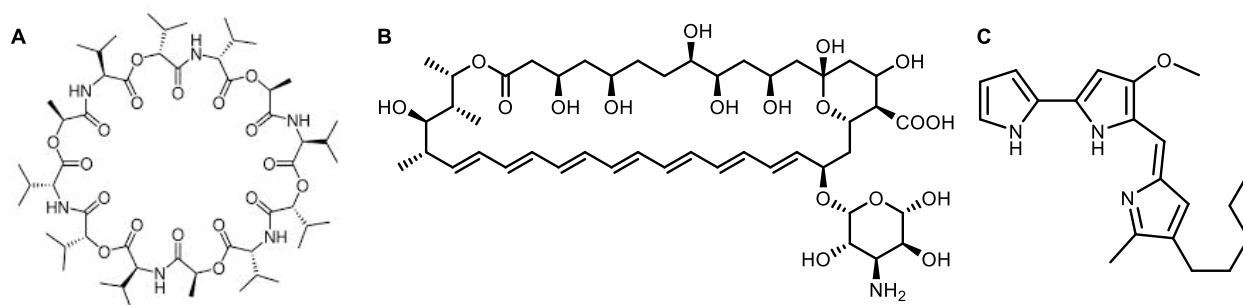


Figure 2: Examples of naturally occurring non-protein based ion transporters **A)** valinomycin, **B)** Amphotericin and **C)** Prodigiosin.

Ion transport across the membrane can either be active or passive. Passive transport occurs by diffusion of ions down an electrochemical gradient, whereas active transport is a process of ion transport involving energy derived from hydrolysis of ATP. Ion transporters can be classified based on direction of transport of ions. Uniport transport involves transport of only one ion at a time whereas Co-transporters function by carrying two different ions at a time. Co-transporters are further classified as symporters which transport two different solutes in the same direction and antiporters which transport two different solutes in the opposite direction (Figure 3).

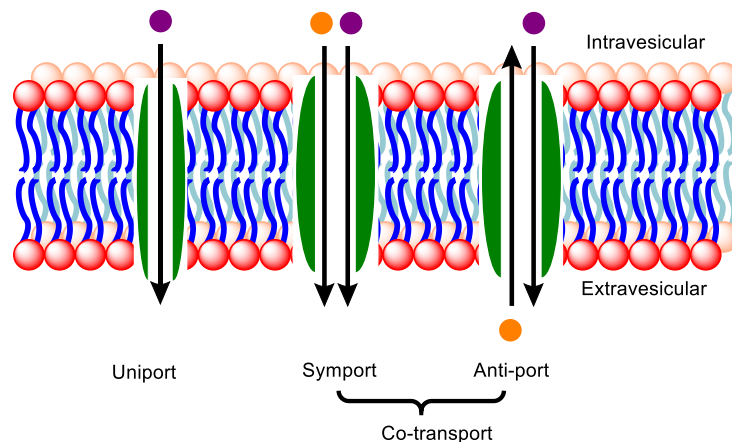


Figure 3: Classification of transport based on direction of ion transport.

Synthetic ion channels⁷ are mainly composed by self-aggregation of small molecules by non-covalent interaction such as, hydrogen bonding, π - π stacking, hydrophobic and dipolar interaction⁸ and most of them are based on several scaffold such as peptide, calixarenes, crown-ether etc.⁹ Depending on the mode of aggregation synthetic ion channels are classified in several classes such as unimolecular, barrel-stave, barrel-rosette, barrel-hoop, β -barrel and micellar. Ion channels can be classified also depending on their mode of action; (a) Ligand gated, (b) Voltage gated, (c) Mechanically gated according to their gating activity. Most of the synthetic chloride transporters reported so far are based on a variety of molecular scaffolds such as polyamides (or urea/thiourea),¹⁰ calixarenes,¹¹ pyrroles,¹² Cholapod,¹³ *trans*-decalin,¹⁴ cyclohexane,¹⁵ peptide fragments¹⁶ and some other scaffolds.¹⁷ They mainly exploit some non-covalent interactions such as anion – π and hydrogen bonding to bind with chloride. A commonly observed hydrogen bonding is between anion and hydrogen bond donor ($-\text{NH}$, $-\text{OH}$). Recently an alternate promising hydrogen bonding based on $\text{C}-\text{H}\cdots\text{anion}$ has been used for transmembrane anion transport.^{11b, 17d, 18} In addition to that pre-organization of the receptor molecule is a crucial for obtaining high binding affinity with anions.¹⁹ A receptor has to undergo conformational change to adapt its shape and binding sites disposition to the potential guest anion in order to bonding to take place. A pre-organized receptor has well defined binding sites and complementary well defined geometry which is required to form stable complex. Thus a pre-organized receptor is advantageous in terms of forming thermodynamically stable complexes with anion by lowering the ΔG of the binding process.²⁰

Section 2

Mainly two techniques are available to study the activity and properties of synthetic ion transporters (a) Vesicle based method and (b) Planar Bilayer study. in aqueous medium.^{1b, 21}

Vesicle Based Methods: Vesicles (or liposomes) are prepared from lipids in an aqueous buffer solution to form spherical closed-shell structures and they are bounded by one or more layers of bilayer membrane. The inner volume of vesicles are in order of femto to attoliters and therefore, highly sensitive detection technique is required to monitor small number of transported ion. The ion selective (Lucigenin), pH-sensitive (HPTS, 8-hydroxypyrene-1,3,6-trisulfonic acid), membrane potential sensitive (Safranin O) fluorescent dye can be trapped interior of vesicle and ion transport can be monitored by change in fluorescence intensity (Figure 4A). On the other hand NMR spectroscopy (Sodium, Chloride, carbon etc.) have been extensively used to determine transport activity. The difference in chemical shift of intravesicular and extravesicular salt can be observed after addition of suitable paramagnetic agent (Figure 4B). Addition of transporter molecule allows exchange of ions which leads to change in the line width or peak shape of the signal. The efflux of ions from vesicles such as sodium, potassium, chloride etc. can be observed by ion selective electrode (ISE) which is very much sensitive and specific as they give direct measurement of concentration of ions (Figure 4C).

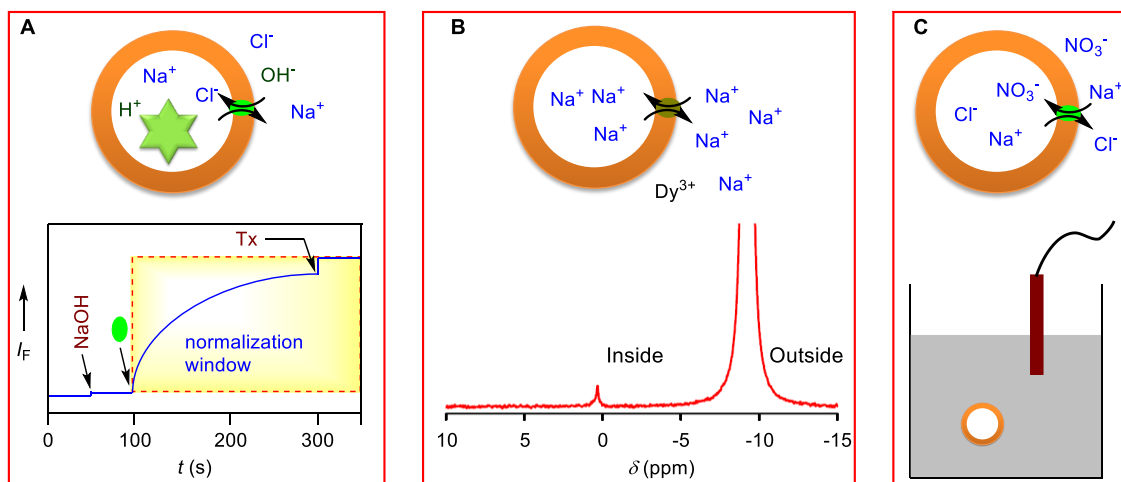


Figure 4: **A)** Representation of ion transport activity assay using EYPC vesicles and representation of ion transport experiment using fluorescence. **B)** Representation of ion transport activity assay using ^{23}Na -NMR technique and **C)** Representation of ion transport study using ion selective electrode.

Planar Bilayer studies: In these experiments, two compartments (*cis*-chamber and *trans*-chamber) filled with electrolyte, are separated by a small hole (with diameter of 150 – 250 μm) where lipid

Section 2

bilayer can be formed by painting a small amount of lipid (Figure 5). Salt bridge is used to connect the chamber with electrode. In general protocol, lipids are dissolved in decane which can be used for bilayer painting and formed bilayer behaves as an insulator by not allowing any ions to pass through it. Addition of channel forming molecule can open up ionic flux in response to applied potential and generate electrical communication between two compartments by allowing ions to flow by producing current in the range of Pico ampere (pA). Therefore, the change in conductance of electrolyte solution provide the confirmation about ion channel formation and ion selectivity of channel. This technique is remarkably reliable to study the ionic conductance (resistivity, capacitance) and ion channel formation.

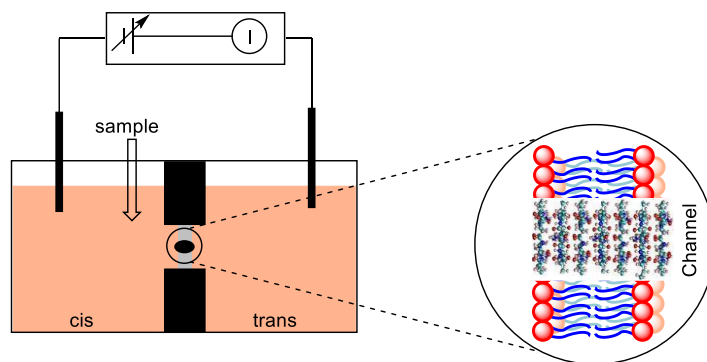


Figure 5: Schematic representation of planar bilayer conductance measurement technique.

References

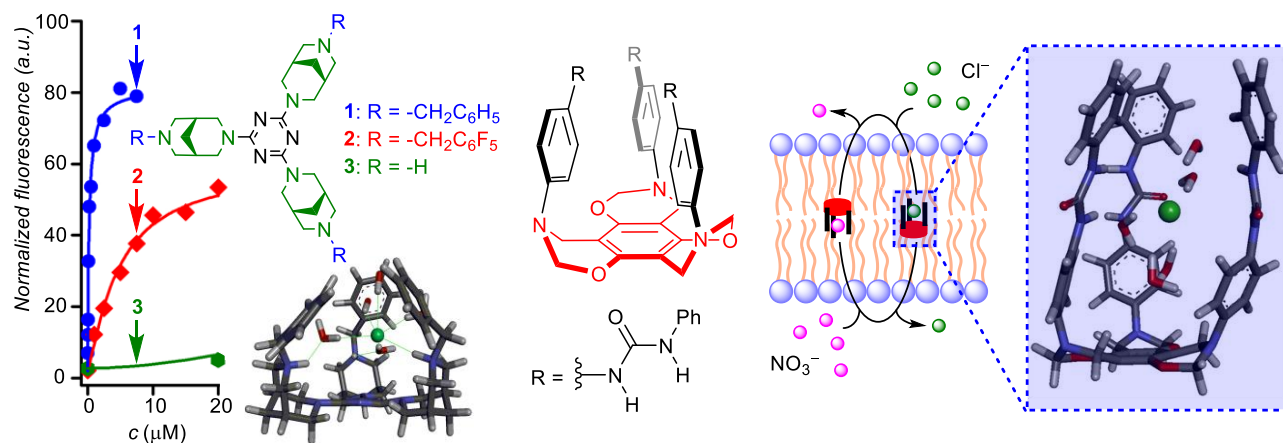
1. (a) Martínez-Mañez, R.; Sancenón, F. *Chem. Rev.* **2003**, *103*, 4419-4476; (b) Davis, A. P.; Sheppard, D. N.; Smith, B. D. *Chem. Soc. Rev.* **2007**, *36*, 348-357; (c) Gale, P. A. *Acc. Chem. Res.* **2006**, *39*, 465-475; (d) Busschaert, N.; Caltagirone, C.; Van Rossom, W.; Gale, P. A. *Chem. Rev.* **2015**, *115*, 8038-8155.
2. Gale, P. A. *Acc. Chem. Res.* **2011**, *44*, 216-226.
3. Jentsch, T. J.; Stein, V.; Weinreich, F.; Zdebik, A. A. *Molecular Structure and Physiological Function of Chloride Channels.* **2002**, *82*, 503-568.
4. (a) Ko, S.-K.; Kim, S. K.; Share, A.; Lynch, V. M.; Park, J.; Namkung, W.; Van Rossom, W.; Busschaert, N.; Gale, P. A.; Sessler, J. L.; Shin, I. *Nat. Chem.* **2014**, *6*, 885-892; (b) Gale, P. A.; Pérez-Tomás, R.; Quesada, R. *Acc. Chem. Res.* **2013**, *46*, 2801-2813.
5. (a) Sessler, J. L.; Eller, L. R.; Cho, W.-S.; Nicolaou, S.; Aguilar, A.; Lee, J. T.; Lynch, V. M.; Magda, D. J. *Angew. Chem., Int. Ed.* **2005**, *44*, 5989-5992; (b) Sato, T.; Konno, H.; Tanaka, Y.; Kataoka, T.; Nagai, K.; Wasserman, H. H.; Ohkuma, S. *J. Biol. Chem.* **1998**, *273*, 21455-21462; (c) Ohkuma, S.; Sato, T.; Okamoto, M.; Matsuya, H.; Arai, K.; Kataoka, T.; Nagai, K.; Wasserman, H. H. *Biochem. J.* **1998**, *334*, 731-741; (d) Matsuyama, S.; Llopis, J.; Deveraux, Q. L.; Tsien, R. Y.; Reed, J. C. *Nat. Cell. Biol.* **2000**, *2*, 318-325; (e) Seganish, J. L.; Davis, J. T. *Chem. Commun.* **2005**, 5781-5783.
6. Alfonso, I.; Quesada, R. *Chem. Sci.* **2013**, *4*, 3009-3019.

Section 2

7. Kano, K.; Fendler, J. H. *Biochim. Biophys. Acta* **1978**, *509*, 289-299.
8. Matile, S.; Vargas Jentzsch, A.; Montenegro, J.; Fin, A. *Chem. Soc. Rev.* **2011**, *40*, 2453-2474.
9. (a) Fyles, T. M. *Chem. Soc. Rev.* **2007**, *36*, 335-347; (b) Kim, D. S.; Sessler, J. L. *Chem. Soc. Rev.* **2015**, *44*, 532-546.
10. (a) Busschaert, N.; Wenzel, M.; Light, M. E.; Iglesias-Hernández, P.; Pérez-Tomás, R.; Gale, P. A. *J. Am. Chem. Soc.* **2011**, *133*, 14136-14148; (b) Davis, J. T.; Gale, P. A.; Okunola, O. A.; Prados, P.; Iglesias-Sánchez, J. C.; Torroba, T.; Quesada, R. *Nat. Chem.* **2009**, *1*, 138-144; (c) Busschaert, N.; Elmes, R. B. P.; Czech, D. D.; Wu, X.; Kirby, I. L.; Peck, E. M.; Hendzel, K. D.; Shaw, S. K.; Chan, B.; Smith, B. D.; Jolliffe, K. A.; Gale, P. A. *Chem. Sci.* **2014**, *5*, 3617-3626.
11. (a) Sidorov, V.; Kotch, F. W.; Abdrakhmanova, G.; Mizani, R.; Fetting, J. C.; Davis, J. T. *J. Am. Chem. Soc.* **2002**, *124*, 2267-2278; (b) Vargas Jentzsch, A.; Emery, D.; Mareda, J.; Metrangolo, P.; Resnati, G.; Matile, S. *Angew. Chem., Int. Ed.* **2011**, *50*, 11675-11678; (c) Izzo, I.; Licen, S.; Maulucci, N.; Autore, G.; Marzocco, S.; Tecilla, P.; De Riccardis, F. *Chem. Commun.* **2008**, 2986-2988.
12. (a) Tong, C. C.; Quesada, R.; Sessler, J. L.; Gale, P. A. *Chem. Commun.* **2008**, 6321-6323; (b) Moore, S. J.; Fisher, M. G.; Yano, M.; Tong, C. C.; Gale, P. A. *Chem. Commun.* **2011**, *47*, 689-691; (c) Gale, P. A.; Tong, C. C.; Haynes, C. J. E.; Adeosun, O.; Gross, D. E.; Karnas, E.; Sedenberg, E. M.; Quesada, R.; Sessler, J. L. *J. Am. Chem. Soc.* **2010**, *132*, 3240-3241.
13. (a) McNally, B. A.; Koulov, A. V.; Smith, B. D.; Joos, J.-B.; Davis, A. P. *Chem. Commun.* **2005**, 1087-1089; (b) McNally, B. A.; Koulov, A. V.; Lambert, T. N.; Smith, B. D.; Joos, J.-B.; Sisson, A. L.; Clare, J. P.; Sgarlata, V.; Judd, L. W.; Magro, G.; Davis, A. P. *Chem. Eur. J.* **2008**, *14*, 9599-9606; (c) Edwards, S. J.; Valkenier, H.; Busschaert, N.; Gale, P. A.; Davis, A. P. *Angew. Chem., Int. Ed.* **2015**, *54*, 4592-4596.
14. Hussain, S.; Brotherhood, P. R.; Judd, L. W.; Davis, A. P. *J. Am. Chem. Soc.* **2011**, *133* (6), 1614-1617.
15. Cooper, J. A.; Street, S. T. G.; Davis, A. P. *Angew. Chem., Int. Ed.* **2014**, *53*, 5609-5613.
16. (a) Schlesinger, P. H.; Ferdani, R.; Liu, J.; Pajewska, J.; Pajewski, R.; Saito, M.; Shabany, H.; Gokel, G. W. *J. Am. Chem. Soc.* **2002**, *124*, 1848-1849; (b) You, L.; Ferdani, R.; Li, R.; Kramer, J. P.; Winter, R. E. K.; Gokel, G. W. *Chem. Eur. J.* **2008**, *14*, 382-396; (c) Shank, L. P.; Broughman, J. R.; Takeguchi, W.; Cook, G.; Robbins, A. S.; Hahn, L.; Radke, G.; Iwamoto, T.; Schultz, B. D.; Tomich, J. M. *Biophys. J.* **2006**, *90*, 2138-2150.
17. (a) Mareda, J.; Matile, S. *Chem. Eur. J.* **2009**, *15*, 28-37; (b) Li, X.; Shen, B.; Yao, X.-Q.; Yang, D. *J. Am. Chem. Soc.* **2009**, *131*, 13676-13680; (c) Elie, C.-R.; Hebert, A.; Charbonneau, M.; Haiun, A.; Schmitzer, A. R. *Org. Biomol. Chem.* **2013**, *11*, 923-928; (d) Lisbjerg, M.; Valkenier, H.; Jessen, B. M.; Al-Kerdi, H.; Davis, A. P.; Pittelkow, M. *J. Am. Chem. Soc.* **2015**, *137*, 4948-4951; (e) Cranwell, P. B.; Hiscock, J. R.; Haynes, C. J. E.; Light, M. E.; Wells, N. J.; Gale, P. A. *Chem. Commun.* **2013**, *49*, 874-876.
18. Cai, J.; Sessler, J. L. *Chem. Soc. Rev.* **2014**, *43*, 6198-6213.
19. Caltagirone, C.; Mulas, A.; Isaia, F.; Lippolis, V.; Gale, P. A.; Light, M. E. *Chem. Commun.* **2009**, 6279-6281.
20. Lee, S.; Hua, Y.; Park, H.; Flood, A. H. *Org. Lett.* **2010**, *12*, 2100-2102.
21. (a) Robertson, J. W. F.; Kasianowicz, J. J.; Banerjee, S. *Chem. Rev.* **2012**, *112*, 6227-6249; (b) Gokel, G. W.; Carasel, I. A. *Chem. Soc. Rev.* **2007**, *36*, 378-389; (c) Davis, J. T.; Okunola, O.; Quesada, R. *Chem. Soc. Rev.* **2010**, *39*, 3843-3862.

Chapter 3

Design, Synthesis and Ion Transport Activity of Tripodal Receptors for Chloride Transport



Chapter 3A

Design, Synthesis and Ion Transport Activity of
Tripodal Receptors for Chloride Transport

3A.1. Introduction

Development of synthetic molecular receptors capable of functioning as ion transporters is a rapidly expanding area of supramolecular chemistry.¹ Anion transporters could be an important research topic like cation transporters in therapeutic applications.² In biological system, transport of ions across cell membranes is facilitated by complex transmembrane proteins, and the process has wide significances in human body. For example, selective transport of chloride ion (Cl^-) is associated with the regulation of different neurons' excitability, *viz.* skeletal, cardiac, smooth muscle, etc. Other important biological processes, such as transepithelial salt transport, acidification of internal and extracellular compartments, cell volume regulation, cell cycle and apoptosis,³ etc. are also controlled by the selective transport of the ion. Dysfunction of the anion selective ion channels cause several life-threatening diseases *e.g.* cystic fibrosis, Bartter's syndrome, myotonia, etc. Recently, a novel treatment modality tackling multiple ion channel diseases was introduced, based on synthetic channels and carriers, is recognized as channel replacement therapy.⁴ Moreover, there are promising reports of cancer cell death, upon treatment of synthetic anion carriers.⁵ Therefore, the design of small molecule-based artificial receptors capable of transporting anions across lipid bilayer has emerged as an attractive area of supramolecular chemistry and therapeutic development.¹ The contributions of noncovalent interactions such as electrostatic, H-bonds ($\text{N-H}\cdots\text{anion}$, $\text{C-H}\cdots\text{anion}$, etc.), $\text{anion}\cdots\pi$ and halogen–anion interactions are now well-established in supramolecular chemistry, and designs of anion transporters exploiting these non-covalent interactions were also reported.⁶

Tripodal receptors are acyclic ionophores consisting of multi-armed ligands and each arm bears a functional group which can coordinate to the target analyte (ion).⁷ The tripodal molecular platform has three arms to which ligating or binding groups are attached. Their design is such that it allows control of binding properties such as complex stability and selectivity. The selectivity arises due to the rigidity of its arms and cavity size. Receptors that have tripodal shape have several advantages over monopodal or bipodal receptors (i) enhanced chelating effects to bind strongly to ions and (ii) their bulkiness can be tuned for controlled reactivity thus due to these features design and synthesis of tripodal receptors is an important area of research.

It is well-known that the preorganization of a host is also imperative to its high binding affinity signatures with ions.⁸ Occasionally, a host undergoes a conformational change to adapt the size and shape of the binding site for accommodating a potential guest. A preorganized receptor possesses a distinct binding site and a complementary geometry to form a stable complex by lowering the ΔG value of the binding process.⁹ Following the rationale mentioned above for infusing both the vital aspects, herein, we report new triazine-based tripodal receptors **1–3** (Figure 3A.1A), anticipated to exhibit anion selective response. The 3,7-diazabicyclo[3.3.1]nonane (or bispidine) moiety was introduced as a rigid and conformationally restricted hydrophobic arm to maximize the preorganization of the receptor system. The moiety also has a distinct hydrophobic outer surface to favour interactions with the lipid membranes. Either a benzyl or a pentafluorobenzyl moiety was tethered at the other end of each bispidine to allow tactical manipulation of anion binding ability. Therefore the contributions for anion recognition could be restricted to the C-H \cdots anion interactions for **1** (from benzyl group), and only anion $\cdots\pi$ ¹⁰ (from pentafluorobenzyl group) interactions for **2** (Figure 3A.1B). Predictions by the calculator plugins of MarvinSketch program¹¹ also indicates better membrane permeability of **1** ($\log P = 7.44$) compared to **2** ($\log P = 9.58$). In addition to this, the attachment of electron deficient pentafluorobenzyl moiety was believed to contribute in lowering the pK_a values of the neighboring amino groups, and therefore, the anion transport activity. The molecule **3** with no substituent at one end of each bispidine was designed as a negative control due to its low $\log P = 1.12$.

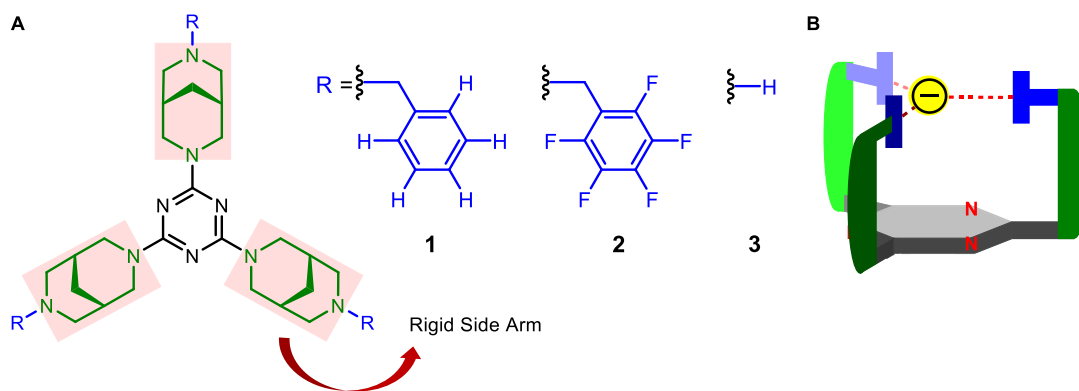
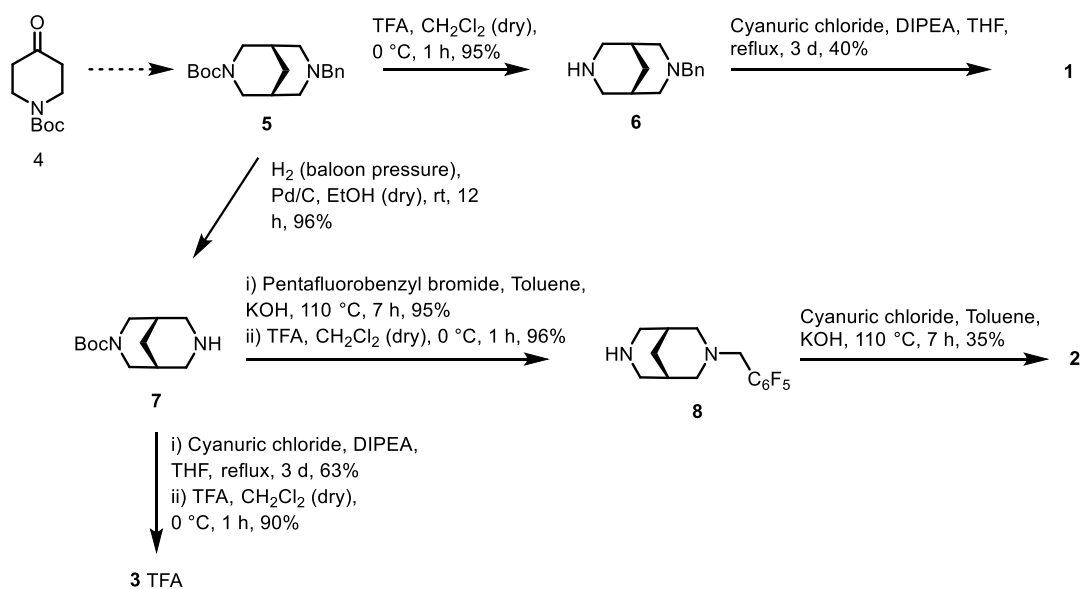


Figure 3A.1: A) Structures of the tripodal receptors **1–3** and B) General schematic representation of the anion binding model for tripodal receptors **1–3**.

3A.2. Results and Discussions

3A.2.1. Synthesis

Syntheses of tripodal compounds **1–3** were accomplished from bicyclic compound **5**, which was prepared from 1-Boc-4-piperidone **4** according to the reported protocol.¹² The *tert*-butyloxycarbonyl group of compound **5** was deprotected with trifluoroacetic acid (TFA) and isolated as free amine **6** in 95% yield (Scheme 3A.1). Amine **6** was subsequently coupled with cyanuric chloride in the presence of DIPEA in THF solvent to form tripodal compound **1** in 40% yield. For the synthesis of tripodal compound **2** and **3**, compound **5** was converted to amine **7** by debenzoylation reaction in presence of hydrogen and Pd/C, following the reported procedure.¹³ Free amine **7** was first reacted with pentafluorobenzyl bromide to give the corresponding pentafluorobenzyl derivative (yield = 95%) in presence of KOH in toluene solvent, which upon treatment with TFA followed by neutralization gave free amine **8** (yield = 96%). In the final step, coupling of amine **8** with cyanuric chloride in the presence of KOH in toluene furnished tripodal compound **2** (yield = 35%). Reaction of compound **7** with cyanuric chloride in presence of DIPEA and THF as a solvent provided the corresponding *tri*(*tert*-butyloxycarbonyl) protected compound (yield = 63%) which upon treatment with TFA in CH₂Cl₂ solvent provided tripodal compound **3** as TFA salt (yield = 90%).

Scheme 3A.1: Synthesis of tripodal receptors **1–3**.

3A.2.2. Crystal Structure

All three tripodal compounds were crystallized from MeOH/CHCl₃ (1:1) solvent system. Crystal structure of compound **1** (CCDC number: 1494040) confirmed similar orientations for all three bicyclic moieties bent identically toward the inner core (a pre-organisation requisite), and hence commensurate binding with the anion would be facilitated by stronger N–H···anion electrostatic interaction (Figure 3A.2A and 3A.2B). Since compound **2** (CCDC number: 1494041) possesses electron deficient pentafluorinated benzylic moiety attached to each bispidine, its analogous crystal structure shows distinct signs as compared to its congener specie **1**. Notably, precise analysis of the crystal structure for molecule **2** reveals that it comprises of two crystallographically and structurally unique C₄₅ units. The distinctness between these arises from the dissimilar spatial orientation adapted by one of the pentafluorobenzyl tail (linked with C52 centre) with respect to the central triazine core (Figure 3A.2C and 3A.2D). For each of the C₄₅ units, two bicyclic moieties similarly face the inner triazine core, while the third one lies on the reverse side, opposing any proximity with the said triazine moiety. Such asymmetric architecture observed in the crystal structure adds on to the less degree of preorganization which further can cause weaker binding and lowering anion transporting activity (Figure 3A.2C and 3A.2D). Compound **3** (CCDC number: 1494042) was isolated and crystallized as trifluoroacetate salt. Analysis of its crystal structure indicates the presence of one trifluoroacetate moiety within the cavity of compound **3** while two others residing outside the cavity for overall charge neutralization. The central trifluoroacetate is

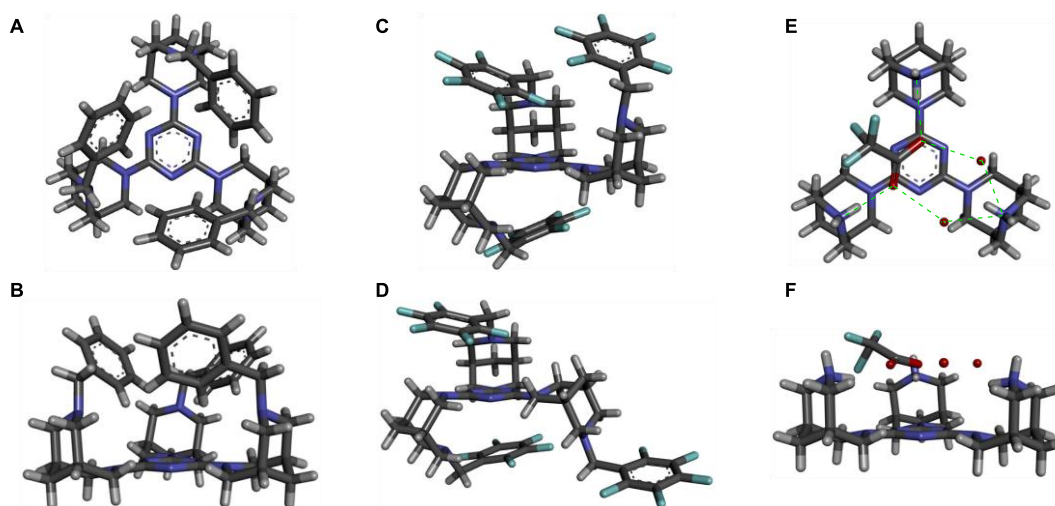


Figure 3A.2: Crystal structures of the tripodal compounds **1–3**. Representation of **A)** top view, and **B)** side view for **1**. **C, D)** Two different orientations of **2**. Representation of **E)** top view, and **F)** side view for **3**.

bonded through multiple intermolecular H-bonding arrays; each of the two oxygens of having a two-fold H-bonding, one directly with NH_2^+ group and the other to an adjacent NH_2^+ group via a bridging water molecule (Figure 3A.2E and 3A.2F). The presence of the trifluoroacetate within the cavity was sufficient to assure the anion binding ability of the protonated tripodal system.

3A.2.3. Ion Transport Activity

Ion transport activities of all tripodal compounds **1–3** across large unilamellar vesicles (LUVs) composed of egg yolk phosphatidylcholine (EYPC) and entrapped 8-hydroxypyrene-1,3,6-trisulfonate (HPTS, $pK_a = 7.2$) dye (*i.e.* EYPC-LUVs \supset HPTS) were evaluated by fluorescence (at $\lambda_{em} = 510$ nm with $\lambda_{ex} = 450$ nm) kinetics (Figure 3A.3A).¹⁴ The destruction of the pre-applied pH gradient, $\Delta\text{pH} \sim 0.8$ ($\text{pH}_{in} = 7.0$ and $\text{pH}_{out} = 7.8$) upon addition of each compound (via H^+ ion efflux or OH^- ion influx), was monitored with time. All tripodal compounds displayed an increase in HPTS fluorescence intensity. Concentration profiles for all compounds indicated compound **1** as the most efficient ion transporter in comparison to other two derivatives (Figure 3A.3B). Concentration profile of compound **1** provided $EC_{50} = 0.25$ μM (Figure 3A.4A). The Hill coefficient $n = 1.09$ for compound **1** suggests that one molecule is sufficient to form the active transporter structure. Compound **2**, on the other hand, was quite less active with $EC_{50} = 7.14$ μM , and $n = 1.36$ also indicates that only one molecule is involved in the formation of an active

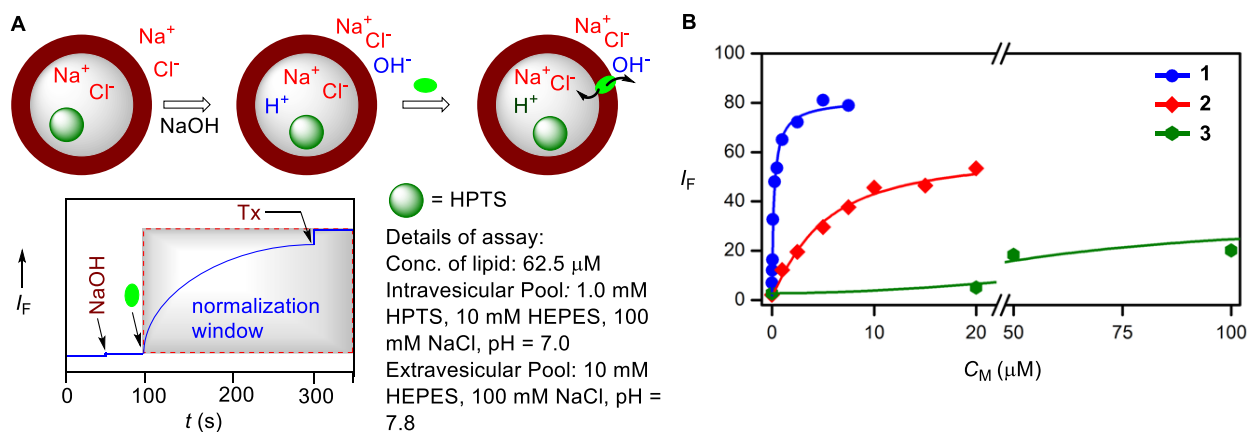


Figure 3A.3: A) Representation of ion transport activity assay using EYPC vesicles, ion transport experiment based on fluorescence and assay detail and B) comparison of concentration profiles for all tripodal molecules **1–3**, with increasing concentration, presented as a function of their normalized emission intensities (I_F).

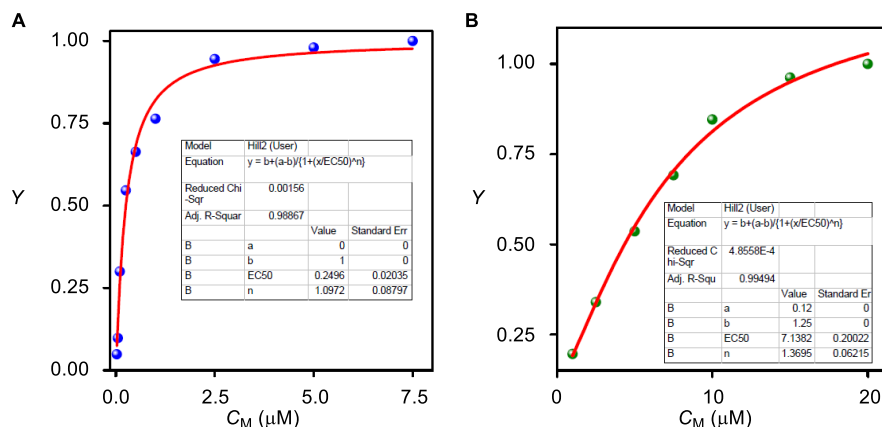


Figure 3A.4: Representation of Hill plot for tripodal **A**) compound **1** and **B**) compound **2** from HPTS assay.

transporter (Figure 3A.4B). Therefore the higher degree of preorganization and predicted electrostatic interactions with anion for compound **1**, aided in much higher ion transport activity as compared to compound **2** under assay condition (pH = 7.0 – 7.8). The activity of compound **3** was very low for calculating corresponding EC_{50} and n values. This results evince the importance of either benzyl or pentafluorobenzyl moiety in the ion recognition process. However, an additional limitation of poor membrane permeability for compound **3**, compared to **1** and **2** cannot be ignored (calculated $\log P = 7.44, 9.58$ and 1.12 for tripodal compounds **1**, **2** and **3**, respectively).¹¹ Further studies were done with active transporters **1** and **2**.

Depending on the ion selectivity of a transporter there are four plausible ion transport mechanisms involving OH^-/X^- antiport, H^+/M^+ antiport, H^+/X^- symport and M^+/OH^- symport. Therefore to identify the correct mechanism operative in the transport process, ion transport studies were done for **1-2**, two different assays were carried out. In one of the experiments, vesicles were prepared with HPTS with only buffer (without any intravesicular and extravesicular salt) and during assay, MOH pulses ($\text{M}^+ = \text{Li}^+, \text{Na}^+, \text{K}^+, \text{Rb}^+, \text{and Cs}^+$) were added at $t = 20$ s, followed by addition of **1** at $t = 100$ s (Figure 3A.5A). In this assay, fluorescence increment could be associated with either M^+/OH^- symport or H^+/M^+ antiport. Obtained data indicated unaltered enhancement of HPTS fluorescence after addition of compound **1** ruling out both transport possibilities (Figure 3A.5B). Therefore, either OH^-/X^- antiport or H^+/X^- symport could be possible. In another experiment, external buffers were varied by keeping internal NaCl buffer constant. Cation selectivity was checked in varied isoosmolar buffer containing different salts MCl ($\text{M}^+ = \text{Li}^+, \text{Na}^+,$

K^+ , Rb^+ , and Cs^+). Fluorescence intensity was monitored after addition of compound **1** ($0.25 \mu M$) which provided a very little change in the rate of ion-transporting activity (Figure 3A.6A). The

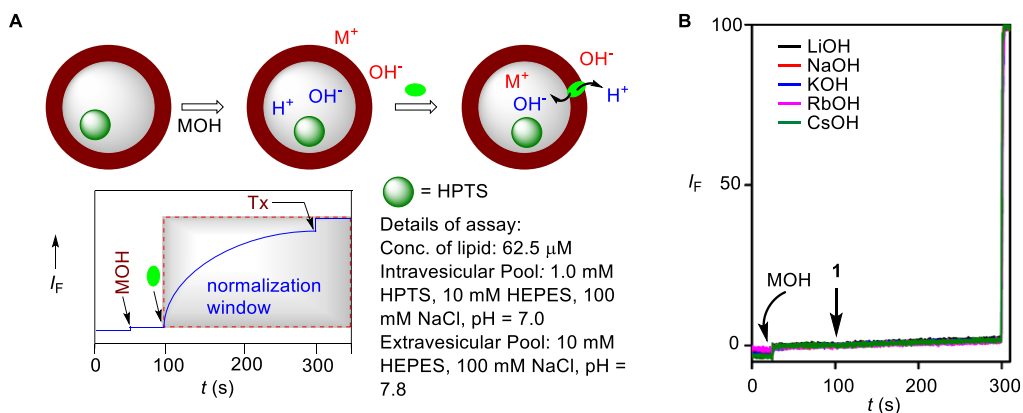


Figure 3A.5: A) Representation of direct cation selectivity assay using EYPC vesicles, ion transport experiment based on fluorescence and assay detail and B) HPTS assay for transporter **1** in presence of MOH ($M^+ = Li^+, Na^+, K^+, Rb^+, \text{ and } Cs^+$). Compound **1** was added at $t = 100$ s and Triton-X at $t = 300$ s.

observation was very similar for the fluorinated compound **2** (Figure 3A.6C). Therefore, the involvement of metal ions is absent in the pH equilibration process which rules out H^+/M^+ antiport and M^+/OH^- symport, reconfirming data obtained from earlier experiment. To investigate further, the anions in the external NaX solution were varied ($X^- = F^-, Cl^-, Br^-, I^-, SCN^-, OAc^-, \text{ and } NO_3^-$, ClO_4^-). For compound **1**, the collapse of the pH gradient was steady with most of the anions except, external I^- . The observed selectivity topology, $Cl^- \gg SCN^- > Br^- > F^- > OAc^- > NO_3^- > ClO_4^-$ clearly indicated the involvement of anions in the transport process (Figure 3A.6B). In this assay, the Cl^-/X^- antiport is expected to be faster than Cl^-/OH^- antiport due to a much higher

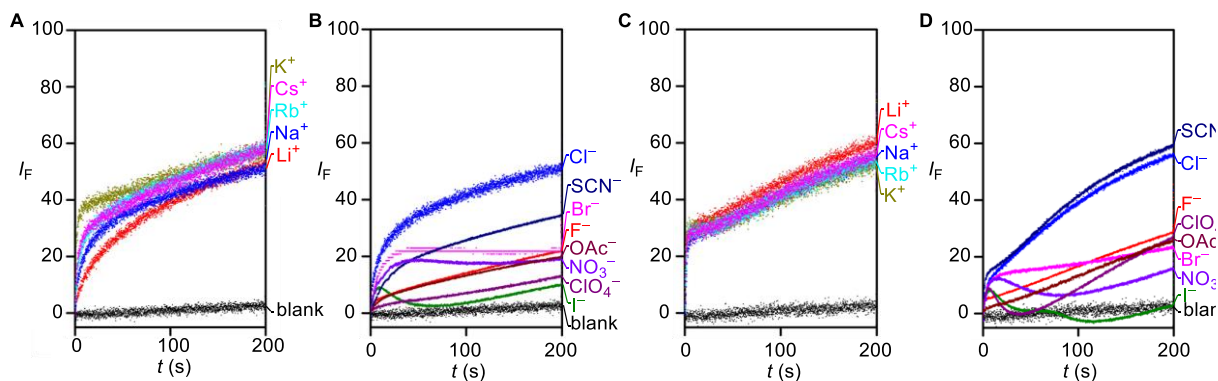


Figure 3A.6: Cation selectivity of A) **1** ($0.25 \mu M$) and C) **2** ($7 \mu M$) determined with varied extravascular cations M^+ . Anion selectivity of B) **1** ($0.25 \mu M$) and D) **2** ($7 \mu M$) determined with varied extravascular anions X^- with intravesicular Cl^- ion.

concentration gradient of X^- (100 mM) as compared to that of OH^- (pH = 7.8). The addition of compound **1** leads to quick equilibration of Cl^-/X^- exchange and rise in fluorescence intensity of HPTS dye indicates the X^-/OH^- antiport. Similar pH equilibration experiments for compound **2** (7 μ M) was found to be unaffected by varying different extravascular cations (Figure 3A.6C). For this compound, the variation of external anion showed clear differences in the ion pH equilibration rates. In this case too, unusual features were observed for I^- , NO_3^- and ClO_4^- (Figure 3A.6D). The observed selectivity topology, $SCN^- \geq Cl^- > SCN^- > F^- > OAc^- > Br^-$ clearly indicated the involvement of anions in the transport process (Figure 3A.6B). The abnormality in pH equilibration (for I^- , in case of compound **1**, and for I^- , NO_3^- and ClO_4^- , in case of compound **2**) is suggest a competitive H^+/X^- influx (*i.e.* symport) which is responsible for the lowering internal HPTS fluorescence.

Ion transport activity of compound **1** was further evaluated in the presence of the proton transporter, carbonyl cyanide 4-(trifluoromethoxy)phenylhydrazone (FCCP), to check which antiport mechanism H^+/M^+ (M^+ = alkali metal cation) or OH^-/X^- (X^- = monovalent anion) is predominating (Figure 3A.7A) during transport mechanism.¹⁵ In this method, after applying a pH gradient, FCCP allows selective efflux of H^+ ions across the membrane to equilibrate the pH. FCCP (2.5 μ M) alone induced a negligible increase in the internal fluorescence intensity of HPTS, while compound **1** (0.25 μ M) exhibited fluorescence amplification by 6.7-fold. When the ion

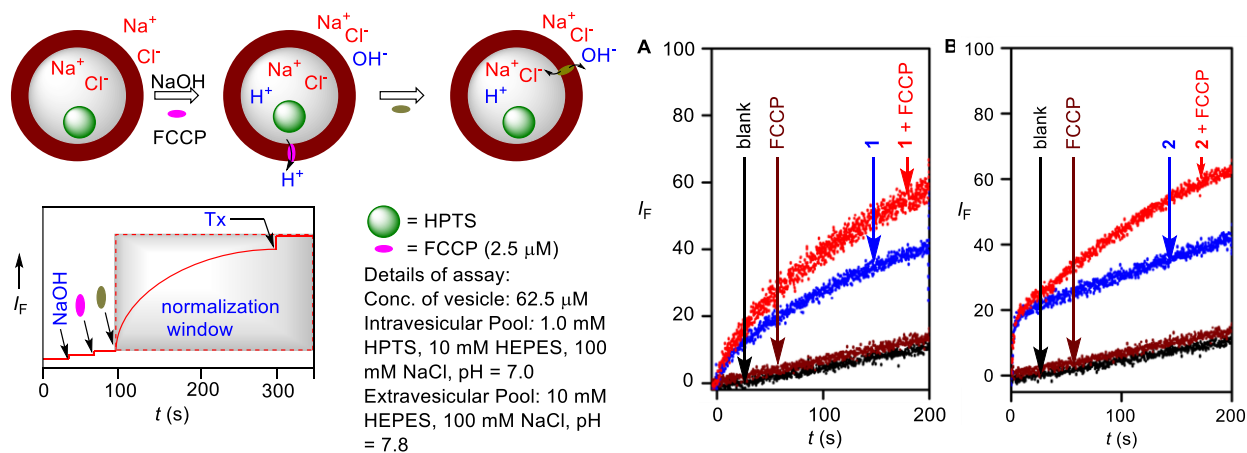


Figure 3A.7: A) Representations of fluorescence based FCCP assay using EYPC vesicle and ion transport kinetics showing normalization window. Ion transport activity of B) compound **1** (0.25 μ M) and C) compound **2** (7 μ M) determined in the absence and in the presence of FCCP.

transport by compound **1** was studied in the presence of FCCP, an 11-fold increase of HPTS fluorescence was observed (Figure 3A.7B) indicating a cooperative effect of compound **1** and FCCP. This data excluded the H^+ transport by compound **1** thus, corroborating to the X^-/OH^- antiport as the operating mechanism. A similar trend was observed in the case of compound **2**. While compound **2** ($7\ \mu\text{M}$) came up with 8-fold emission enhancement, the presence of FCCP in the system induced 12-fold enhancement (Figure 3A.7C). Therefore, both the tripodal receptors **1**, **2** registered preferential selectivity for anion over cation.

To compare the preferential transport rate between OH^- and Cl^- ; valinomycin, a K^+ ion-selective carrier was used in HPTS assay (Figure 3A.8A).¹⁶ In this assay, the interior of the vesicle has Na^+ , and extravesicular water pool contains K^+ . During influx of K^+ by valinomycin, simultaneous OH^- and/or Cl^- influx is expected to maintain the charge equality. Valinomycin ($2.5\ \mu\text{M}$) exhibited negligible ion transport. The ion influx rates were nearly similar when compound **1** ($0.25\ \mu\text{M}$) was tested in the absence and presence of valinomycin (Figure 3A.8B). The observed data confirmed preferential transport of Cl^- ion over OH^- ion (*i.e.* $\text{Cl}^- > \text{OH}^-$). Similarly, ion transport activity of **2** ($7\ \mu\text{M}$) in the presence of valinomycin was negligibly different than that studied in the absence of valinomycin (Figure 3A.8C).

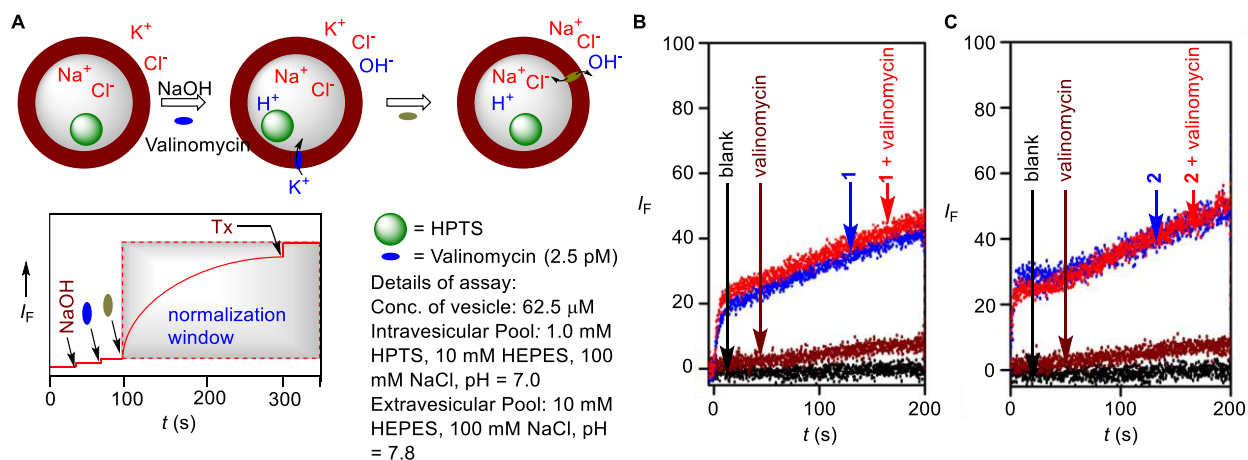


Figure 3A.8: A) Representations of fluorescence based Valinomycin assay using EYPC vesicle and ion transport kinetics showing normalization window. Ion transport activity of B) compound **1** ($0.25\ \mu\text{M}$) and C) compound **2** ($7\ \mu\text{M}$) determined in the absence and in the presence of Valinomycin.

Transport of Cl^- ion by compound **1** and **2** was further investigated by monitoring the flow of the ion (either influx or efflux) across LUVs (EYPC-LUVs \supset Lucigenin) with an average

diameter of 200 nm entrapped with chloride sensitive lucigenin dye ($\lambda_{\text{ex}} = 455 \text{ nm}$, $\lambda_{\text{em}} = 535 \text{ nm}$).¹⁷ The vesicles were encapsulated with NaNO_3 (225 mM) and lucigenin (1 mM) and they were suspended in NaNO_3 (225 mM) solution. After this, NaCl (25 mM) was added to the extravesicular water pool, and fluorescence decay was observed after addition of transporters. Finally, Triton X-100 was added to lyse all the vesicles (Figure 3A.9A). Both compound **1** (Figure 3A.9B) and compound **2** (Figure 3A.9C) showed quenching of lucigenin fluorescence emission by promoting transport of Cl^- into the vesicle and NO_3^- out of the vesicle in a concentration-dependent manner which directly proves that tripodal compounds can transport Cl^- . Further, to quantify transport efficiency, half-life ($t_{1/2}$) and initial rate (I_R) of compound **1** (20 μM) was calculated and $t_{1/2} = 34 \text{ s}$ and $I_R = 0.69 \text{ s}^{-1}$ was obtained. Same calculation for compound **2** (20 μM) showed $t_{1/2} = 54 \text{ s}$ and initial rate $I_R = 1.10 \text{ s}^{-1}$.

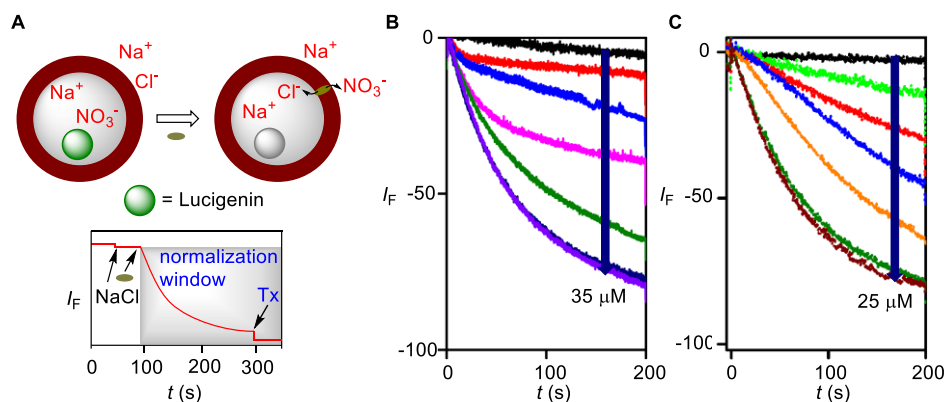


Figure 3A.9: A) Representation of Cl^- transport activity assay by monitoring Lucigenin fluorescence using EYPC and representation of ion transport experiment using fluorescence. Cl^- transport by tripodal transporter **B**) **1** (0 – 35 μM) and **C**) **2** (0 – 25 μM) by $\text{NO}_3^-/\text{Cl}^-$ exchange by Lucigenin Assay.

Extravesicular cations were then varied to determine their effect on Cl^- ion influx by compound **1** (30 μM). In the presence of different alkali metal cations ($\text{M}^+ = \text{Li}^+, \text{Na}^+, \text{K}^+, \text{Rb}^+, \text{and } \text{Cs}^+$), comparable lucigenin fluorescence quenching kinetics was observed (Figure 3A.10A), making M^+/Cl^- symport an unlikely event. In the case of antiport assay, EYPC vesicles (intravesicular solution: 225 mM NaCl , 1 mM lucigenin) were added to the extravesicular buffer of isoosmolar varied anions ($\text{X}^- = \text{F}^-, \text{HCO}_3^-, \text{NO}_3^-, \text{ClO}_4^- \text{ and } \text{SO}_4^{2-}$). After addition of compound **1** (20 μM), an increase in fluorescence was observed in the case of ClO_4^- , F^- , NO_3^- and HCO_3^- . As expected, hydrophilic nature SO_4^{2-} anion led to a slow exchange of the anion with Cl^- .

Therefore, the observed differences in the Cl^- ion efflux rates established Cl^-/X^- antiport as the dominant ion transport mechanism (Figure 3A.10B). Unfortunately, compound **2** could not be evaluated under similar experimental conditions due to its solubility problem.

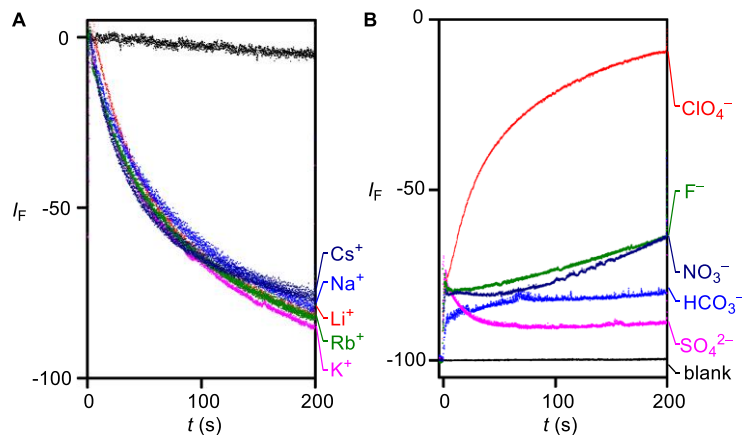


Figure 3A.10: **A)** Symport assay for **1** ($30\ \mu\text{M}$) by applying different cation pulses and **B)** antiport assay for **1** ($20\ \mu\text{M}$) by varying extravesicular anions.

In order to elucidate the mechanism for anion transport via mobile carrier mechanism transport activities of **1** ($20\ \mu\text{M}$) and **2** ($20\ \mu\text{M}$) were tested with LUVs having different lipid composition. It is known that cholesterol can increase viscosity of lipid bilayer thereby hampers the movement of carriers to diffuse through membrane. For that purpose, two different set of LUVs were prepared with only POPC (1-palmitoyl-2-oleoyl-*sn*-glycero-3-phosphocholine) and POPC: cholesterol (4:1). Within both LUVs lucigenin dye (1 mM) and NaNO_3 (225 mM) were trapped, and then placed in external buffer containing NaCl (25 mM). Chloride influx as a result of compound addition was monitored through the quenching of lucigenin fluorescence. As expected, rate of chloride transport ability of both compound **1** (Figure 3A.11A) and compound **2** (Figure 3A.11B) slowed down noticeably under the comparable assay conditions in cholesterol loaded POPC vesicle. Thus, these data confirmed that tripodal transporters can function as a mobile carrier but not as ion channel. Moreover, compounds **1-2** didn't cause any defection of membrane which was proved by carboxyfluorescein-leakage assay (Figure 3A.11C).

To investigate the origin of transport activity, pH dependence activity of both the tripodal transporters **1** and **2** were assessed by vesicle leakage assay with the chloride ion selective electrode (ISE) at different pH solutions (i.e. 5.3, 6.0, 7.0, 8.0, and 8.8 respectively). We have prepared five different vesicles with pH mentioned above, and chloride efflux was monitored

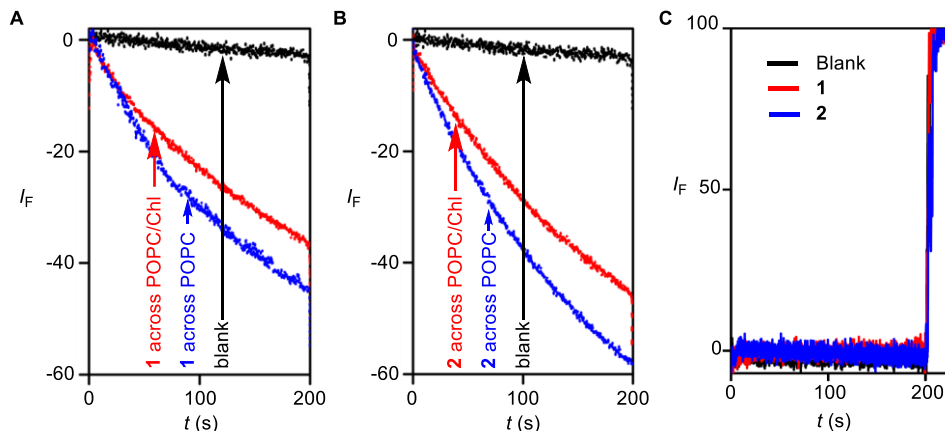


Figure 3A.11: Chloride efflux promoted by tripodal molecules **A**) **1** and **B**) **2** from unilamellar POPC vesicles or unilamellar 8:2 POPC: cholesterol vesicles **C**) Carboxyfluorescein assay for both **1-2**.

for both compounds (**1** and **2**). We observed a significant increment in chloride transport activity from pH 8.8 to pH 7.0 for compound **1**. However, a considerable decrease of chloride transport activity was realized at pH = 6.0 and even lower at pH = 5.3 (Figure 3A.12A). On the contrary, compound **2** showed the highest chloride efflux activity only at pH = 5.3 (Figure 3A.12B). Obtained data validated the effect of pK_a in transport activity. Significantly lower activity of compound **2** compared to compound **1** at pH = 7 from the ISE measurement correlates to the ion transport data obtained from the HPTS based studies. For the **1**, the highest activity at pH = 7.0 suggest predominant protonation of N-atoms linked to benzyl groups. The decrease in activity at higher pH correlates to the deprotonation of these N-atoms. The drop of activity at lower pHs indicates further protonation of the triazine core leading to an increase in the polarity at the exterior

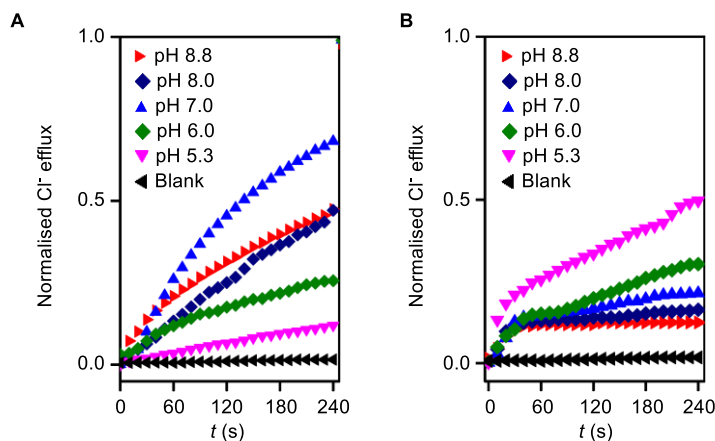


Figure 3A.12: Chloride efflux by **A**) compound **1** (50 μ M) and **B**) compound **2** (35 μ M) at different pH by nitrate/chloride exchange with chloride ion selective electrode.

of the receptor, and thus influencing the permeation of the Cl^- bound receptor. However, for compound **2**, the cooperativity effect due to Cl^- within its cavity is expected to give higher basicity of the N-atoms linked to pentafluorobenzyl moieties compared to the N-atoms of the triazine core. In such case, the lower activity of compound **2** compared to compound **1** at $\text{pH} \sim 7$ corroborates to the lesser probability of protonation within its cavity, and improvement of transport activity at lower pH suggests the protonation components within the cavity.

3A.2.4. Mass Spectrometric Studies for Anion Recognition

Direct experimental evidence for protonation of **1** and affinity of chloride ion was established by Electrospray Ionization Mass Spectrometric (ESI-MS) studies. In this experiment, **1** and tetramethylammonium chloride (TMACl) were prepared in acetonitrile and were mixed in 1:1 molar ratios and then electrosprayed under as mild as possible ionization conditions in the positive mode. Obtained data clearly showed the presence of $[\text{M}+\text{HCl}+\text{H}]^+$ and $[2\text{M}+\text{HCl}+\text{H}]^+$ adduct which supports the chloride ion recognition upon protonation of the molecule (Figure 3A.13) (where, M = exact molecular weight of **1**).

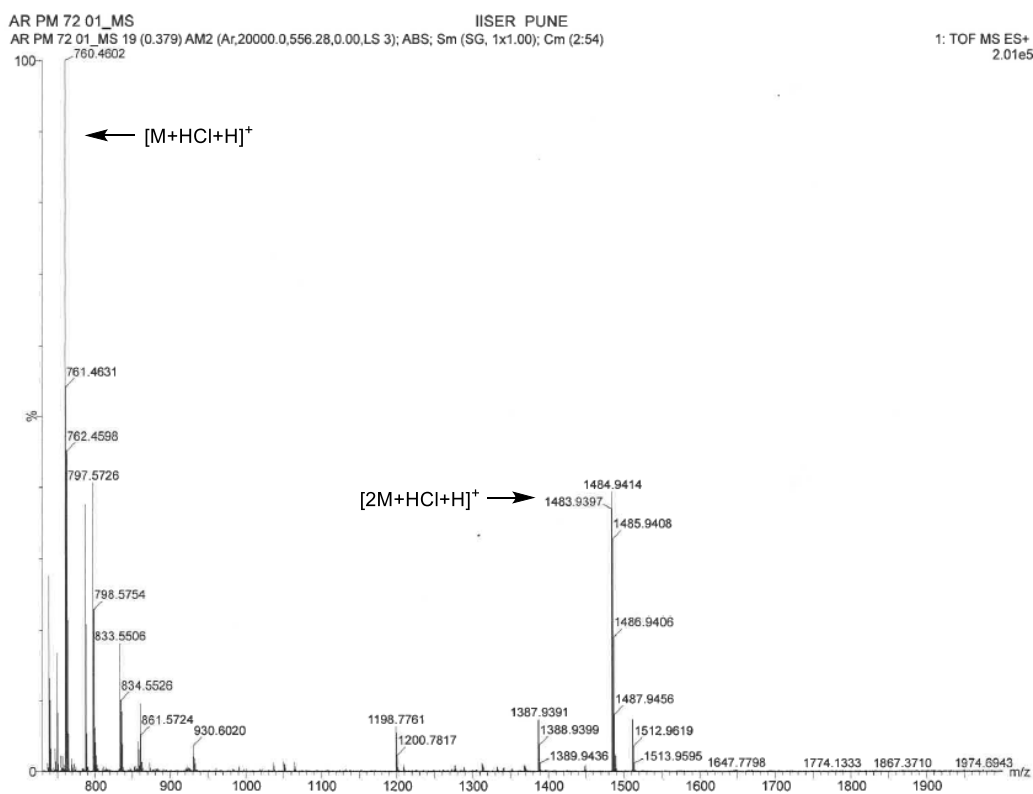


Figure 3A.13: ESI-MS spectrum of 1:1 molar mixture of **1** and Me_4NCl prepared in acetonitrile.

3A.2.5. Molecular Dynamics Simulation

To determine the structure of the tripodal molecule **1** with a bound Cl^- ions inside the bilayer system, we have carried out molecular dynamics (MD) simulation with **1** and one Cl^- ion embedded inside a pre-equilibrated 1,2-dipalmitoyl-*sn*-phosphocholine (DPPC)/water lipid bilayer system. The crystal structure of tripodal compound **1** was taken initially with one Cl^- kept in its cavity at the start of the simulation. The equilibrated structure of the overall system is shown in

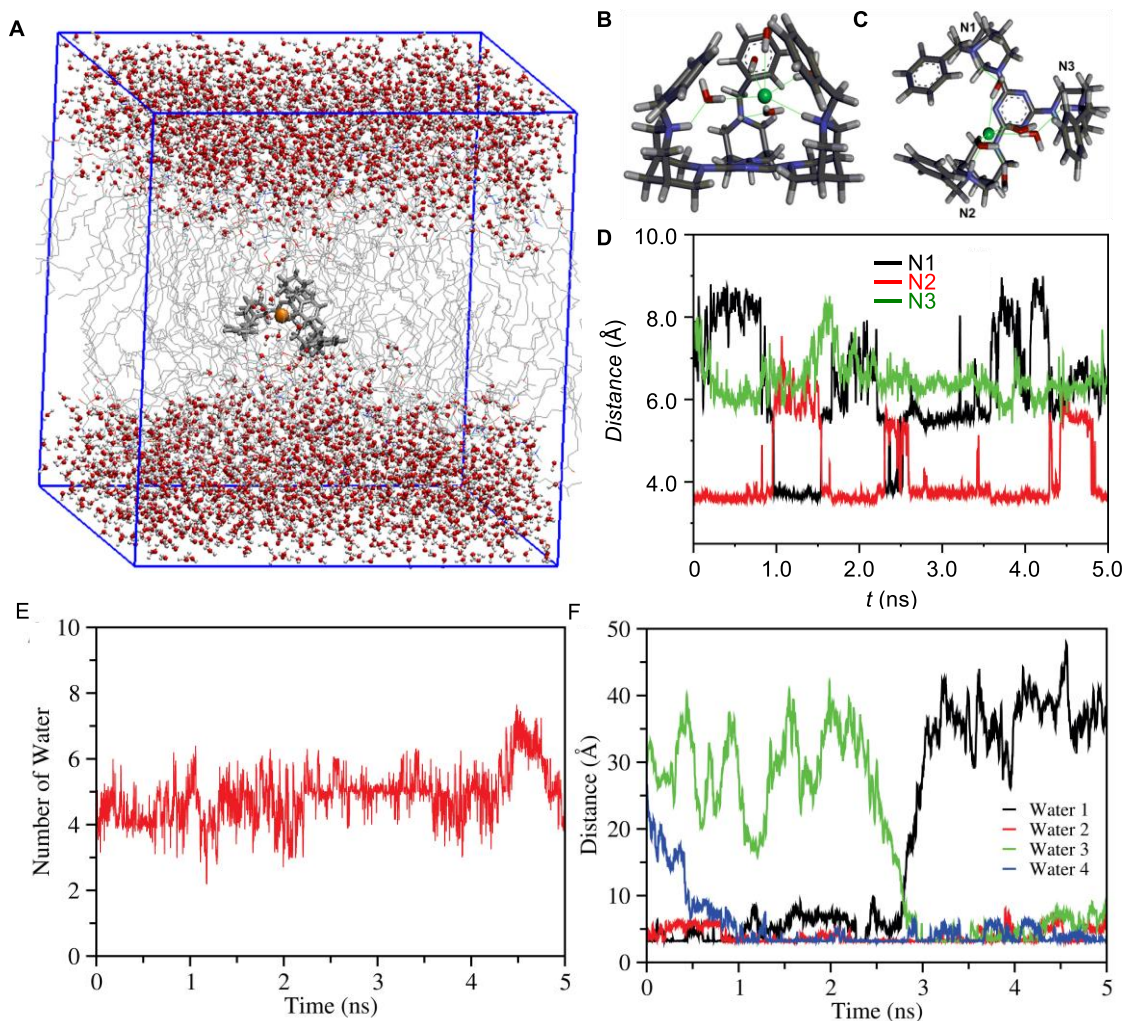


Figure 3A.14: **A)** The equilibrated system with **1** inserted in DPPC lipid layer along with the bound Cl^- . A representative structure of the complex formed during MD between chloride ion, **1** and water molecules inside its inner cavity with **B)** side view and **C)** top view, respectively. **D)** The distance between Cl^- and the three positively charged N-atoms marked as N1, N2 and N3 in **C)** for the duration of MD trajectory. **E)** The number of water molecules within 4 Å of Cl^- in the 5ns simulation. **F)** The distances between Cl^- and four different water molecules denoted as water 1, water 2, water 3 and water 4 during the simulation.

Figure 3A.14A. We find that during the 5 ns production simulation at constant temperature and volume, some mobile water molecules could form interaction with the Cl^- ion by passing through the pores of DPPC bilayer. Although the overall number of water around Cl^- is around 5 (Figure 3A.14E), the nature of water coordination is dynamic, reflected from Figure 3A.14F, where the distance between some specific water molecules to the Cl^- is plotted. These data indicated that while water 1 and water 3 remain close to Cl^- at different instances, the water 2 is found to be close to the anion for the entire trajectory. Overall, the Cl^- forms one direct H-bond with one of the N–H sites of the molecule, and two additional water-mediated H–bonds with other N–H sites as seen from the representative structure obtained through cluster analysis of the 5 ns trajectory (Figure 3A.14B and 3A.14C). Redundant water molecules are removed for clarity. This is further verified from the distances between the N–H sites and Cl^- . Figure 3A.14D shows that the distance between one N-atom and Cl^- remains similar during the whole trajectory (due to a direct H-bond formation) while the distance with other two N-atoms vary with one N-atom being closer than the other at different stages of the simulation. The larger distance is due to the formation of water-mediated H–bond. All calculations were carried out by our collaborator Arnab Mukherjee and co-workers.

3A.3. Conclusion

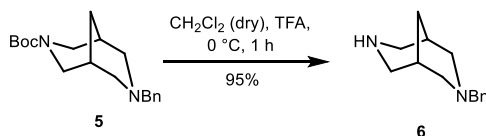
In conclusion, we have designed a new class of tripodal anion transporters based on triazine core by connecting it to 3,7-diazabicyclo[3.3.1]nonane arms. The bicyclic arm was selected to ensure better preorganization for anion recognition and hydrophobic outer surface for membrane permeation. Each bicyclic scaffold was further connected to arylmethylene moiety for controlling the protonated state of the connecting nitrogen atom, and also the amphiphilicity of the transporter which primarily controls the basicity of the connecting nitrogen atom. Ion transport activity across LUVs confirmed the highest activity for the benzyl followed by the pentafluorofluorobenzyl and then the unsubstituted receptor. First two receptors were selective Cl^- transporters with antiport exchange as the primary transport mechanism. Molecular dynamics simulation suggested that the cavity of the molecule enabled H-bonding of Cl^- ion via a direct H-bond with one protonated nitrogen atom while water mediated H-bond formation with two other protonated nitrogen atoms.

3A.4. Experimental Section

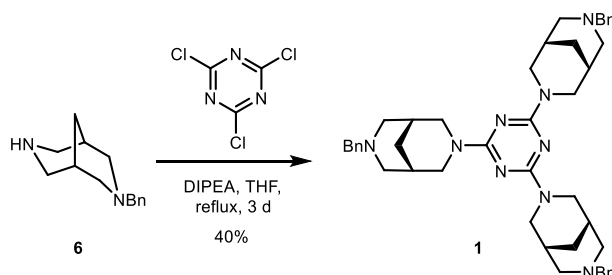
General Methods: All reagents for synthesis were purchased from commercial suppliers and used as received unless stated otherwise. All solvents were distilled to dry by standard protocol prior to use or purchased as dry and all reactions were performed under the nitrogen atmosphere. TLC was carried out with E. Merck silica gel 60-F₂₅₄ plates and column chromatography was carried out over silica gel (100-200 mesh). Egg yolk phosphatidylcholine (EYPC) was purchased from Avanti Polar Lipids as a solution in chloroform (25 mg/mL). HEPES buffer, HPTS, Lucigenin, carboxyfluorescein (CF), Triton X-100, NaOH and all inorganic salts of molecular biology grade were purchased from Sigma. Gel-permeation chromatography was performed on a column of Sephadex G-50 in buffer or salt solution as per requirement. Large unilamellar vesicles (LUV) were prepared by using mini extruder, equipped with a polycarbonate membrane of 100 nm (for HPTS assay) or 200 nm (for Lucigenin Assay) pore size, purchased from Avanti Polar Lipids.

Physical Measurements: The ¹H and ¹³C NMR spectra were recorded using 400 MHz Jeol or 400 MHz Bruker (or 100 MHz for ¹³C) spectrometers using either residual solvent signals as an internal reference or from internal tetramethylsilane on the δ scale relative to chloroform (δ 7.26), dimethyl sulfoxide (δ 2.50) or methanol (δ 3.31) for ¹H NMR and chloroform (δ 77.2 ppm), dimethyl sulfoxide (δ 39.5 ppm) or methanol (δ 49.0 ppm) for ¹³C NMR at 293 K. The chemical shifts (δ) are reported in ppm and coupling constants (J) in Hz. The following abbreviations are used: s (singlet), d (doublet) m (multiplet), dd (doublet of doublet). High-resolution mass spectra (HRMS) were obtained from MicroMass ESI-TOF MS spectrometer. Fluorescence spectra were recorded by using Fluoromax-4 from Jobin Yvon Edison equipped with an injector port and a magnetic stirrer. The pH of the buffer was adjusted to 7.0 by NaOH using Helmer pH meter. All FT-IR spectra were obtained using NICOLET 6700 FT-IR spectrophotometer as KBr disc and are reported in cm⁻¹. Melting points were measured using a VEEGO Melting point apparatus. All melting points were measured in open glass capillary and values are uncorrected. All data of fluorescence studies were normalised and processed either by Origin 8.5 or KaleidaGraph. Chloride efflux was monitored by Accumet Chloride Ion Selective Electrode (ISE) equipped with Accumet AB250 meter.

Synthesis:

Synthesis of (1*R*,5*S*)-3-benzyl-3,7-diazabicyclo[3.3.1]nonane **6**:Scheme 3A.2: Synthesis of compound **6**.

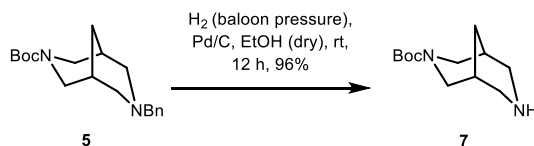
Compound **5** (0.15 g, 0.47 mmol) was taken in a round bottom flask and placed in an ice bath. To it dry CH₂Cl₂ (2 mL) was added followed by 1 mL TFA (trifluoroacetic acid). The reaction was kept to stir for 1 h. After completion of the reaction, the solvent was evaporated in vacuo to obtain a residue, followed by extraction with CH₂Cl₂ and washings with NaHCO₃ gives compound **6** as a yellow liquid in 95% yield (97 mg); **IR (KBr)**: ν/cm^{-1} : 3390, 2924, 2853, 1673, 1536, 1458, 1359, 1258, 1195, 1130; **¹H NMR (400 MHz, CDCl₃)**: δ 7.29-7.38 (m, 3H), 7.23-7.26 (m, 2H), 3.43-3.49 (m, 4H), 3.33 (d, $J = 13.2$ Hz, 2H), 3.13 (d, $J = 12.0$ Hz, 2H), 2.5 (d, $J = 11.6$ Hz, 2H), 2.13 (s, 2H), 1.89 (d, $J = 13.2$ Hz, 1H), 1.78 (d, $J = 12.8$ Hz, 1H); **¹³C NMR (100 MHz, CDCl₃)**: δ 136.28 (Ar-C), 129.31 (Ar-CH), 128.92 (Ar-CH), 127.99 (Ar-CH), 63.28 (Ar-CH₂-N), 58.25 (CH₂-N), 49.50 (CH₂-N), 30.81 (CH), 27.17 (CH); **HRMS (ESI)**: Calc. for C₁₄H₂₀N₂ [M+H]⁺: 217.1704; Found: 217.1708.

Synthesis of 2,4-bis((1*R*,5*S*)-7-benzyl-3,7-diazabicyclo[3.3.1]nonan-3-yl)-6-(7-benzyl-3,7-diazabicyclo[3.3.1]nonan-3-yl)-1,3,5-triazine **1**:Scheme 3A.3: Synthesis of compound **1**.

In a 50 mL round bottom flask cyanuric chloride (0.05 g, 0.27 mmol) and **6** (0.20 g, 0.95 mmol) were taken in 25 mL of dry THF and stirred at room temperature. White precipitate formed at this stage. After 1 h, DIPEA (400 μ L, 2.70 mmol) was added and reaction mixture was stirred for another 1 h at room temperature and then refluxed for 3 d. After completion of reaction, solvent was evaporated under vacuo. The residue obtained was extracted with CH₂Cl₂ (3 \times 100 mL) and

washed with brine solution. Organic layer was dried over Na_2SO_4 and column chromatography over silica gel was performed (*Eluent*: 4% MeOH in CHCl_3) to obtain pure **1** (78 mg) as a white solid with 40% yield; **M.p.**: 166 – 167 °C; **IR (KBr)**: ν/cm^{-1} : 3049, 2909, 2786, 1626, 1446, 1535, 1352, 1302, 1237, 1161; **$^1\text{H NMR}$ (400 MHz, $\text{DMSO-}d_6$)**: δ 7.03-7.19 (m, 15H), 4.82 (d, $J = 9.2$ Hz, 2H), 4.58 (d, $J = 10.0$ Hz, 2H), 4.48 (d, $J = 10.0$ Hz, 2H), 3.38-3.41 (m, 2H), 3.04-3.25 (m, 10H), 2.74-2.86 (m, 6H), 2.14-2.30 (m, 6H), 1.88-1.99 (m, 6H), 1.61-1.78 (m, 6H); **$^{13}\text{C NMR}$ (100 MHz, $\text{DMSO-}d_6$)**: δ 164.56 (triazene-C), 138.57 (Ar-C), 128.85 (Ar-CH), 128.37 (Ar-CH), 127.59 (Ar-CH), 127.09 (Ar-CH), 125.62 (Ar-CH), 63.53 (Ar- $\text{CH}_2\text{-N}$), 62.49 ($\text{CH}_2\text{-N}$), 58.49 ($\text{CH}_2\text{-N}$), 48.38 (CH_2), 47.27 (CH_2), 46.15 (CH_2), 29.18 ($-\text{CH}$), 28.14 ($-\text{CH}$); **HRMS(ESI)**: Calculated for $\text{C}_{45}\text{H}_{57}\text{N}_9$ $[\text{M}+\text{H}]^+$: 724.4810; Found: 724.4827.

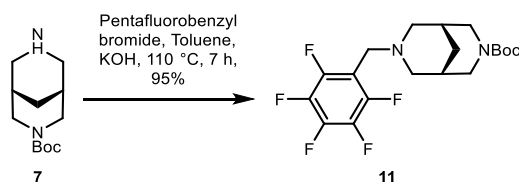
Synthesis of *tert*-butyl (1*R*,5*S*)-3,7-diazabicyclo[3.3.1]nonane-3-carboxylate **7**:



Scheme 3A.4: Synthesis of compound **7**.

In a 100 mL round bottom flask a solution of compound **5** (1.00 g, 3.00 mmol) in ethanol (40 mL) was kept for degassing with nitrogen for 2-3 h. Then Pd/C was added in equivalent ratio and a hydrogen balloon was attached using a two way joint to the round bottom flask. The reaction was kept to stir at room temperature overnight. After completion of the reaction it was filtered through celite bed using ethyl acetate. The filtrate was concentrated in vacuo to yield 96% compound **7** (0.69 g) as a blackish viscous liquid. The $^1\text{H NMR}$ and HRMS data was matching with that of the reported compound.¹²

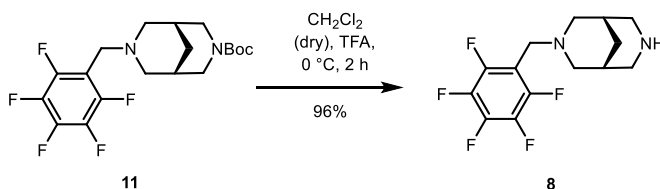
Synthesis of *tert*-butyl (1*R*,5*S*)-7-((perfluorophenyl)methyl)-3,7-diazabicyclo[3.3.1]nonane-3-carboxylate **11**:



Scheme 3A.5: Synthesis of compound **11**.

In a 50 mL round bottom flask compound **7** (0.70 g, 3.10 mmol) was dissolved in dry toluene (15 mL) and to this KOH (0.35 g, 6.20 mmol) was added. In another round bottom flask a solution of pentafluorobenzylbromide (0.89 g, 3.40 mmol) dissolved in dry toluene (10 mL) was added dropwise to the above solution. The resultant suspension was refluxed for 7 h at 110 °C. Completion of the reaction was checked using TLC plates. After completion of the reaction, solvent was evaporated under reduced pressure and the residue obtained was subjected to column chromatography using silica gel, to obtain 95% of compound **11** (1.2 g) as a yellowish liquid which upon cooling solidified. (*Eluent*: 8% EtOAc in petroleum ether). **M.p.**: 91 – 93 °C; **IR (KBr)**: ν/cm^{-1} : 2925, 2848, 1681, 1506, 1454, 1396, 1327, 1251, 1184, 1115; **¹H NMR(400 MHz, CDCl₃)**: δ 4.16 (d, $J = 12.4$ Hz, 1H), 4.02 (d, $J = 13.6$ Hz, 1H), 3.66-3.76 (m, 2H), 2.86-3.09 (m, 4H), 2.29 (t, $J = 12.0$ Hz, 2H), 1.80 (d, $J = 20.4$ Hz, 2H), 1.63 (d, $J = 12.8$ Hz, 1H), 1.49 (s, 1H) 1.46 (s, 9H); **¹³C NMR (100 MHz, CDCl₃)**: δ 155.04 (C=O), 146.53 (Ar-C), 143.85 (Ar-C), 138.28 (Ar-C), 109.33 (Ar-C), 78.55 (C-(CH₃)₃), 56.86 (CH₂-N), 56.56 (CH₂-N), 48.62 (CH₂-N), 48.49 (CH₂-N), 47.50 (Ar-CH₂-N), 30.71 (CH₂), 28.88 (CH₃), 28.69 (CH), 28.40 (CH); **HRMS (ESI)**: Calc. for C₁₉H₂₃F₅N₂O₂ [M+H]⁺: 407.1758; Found: 407.1759.

Synthesis of (1*R*,5*S*)-3-((perfluorophenyl)methyl)-3,7-diazabicyclo[3.3.1]nonane **8**:

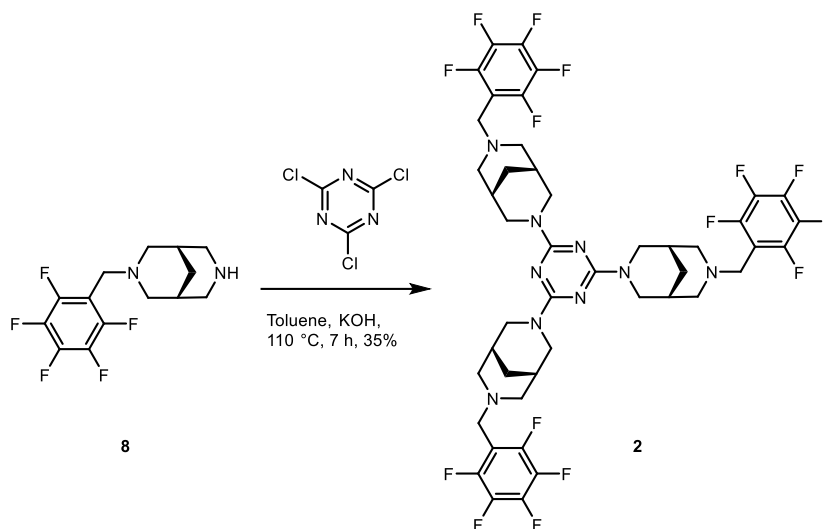


Scheme 3A.6: Synthesis of compound **8**.

Compound **11** (0.77 g, 1.90 mmol) was taken in a round bottom flask and placed in an ice bath. To it dry CH₂Cl₂ (2.5 mL) was added followed by TFA (2 mL). The reaction was kept to stir for 2 h. After completion of the reaction the reaction mixture was diluted with water (20 mL), saturated NaHCO₃ (3 mL) and CH₂Cl₂ (50 mL). Organic layer was separated and aqueous layer was extracted with CH₂Cl₂ (3 × 100 mL). The combined organic layer was dried over Na₂SO₄ and solvent was evaporated under reduced pressure to obtain the product compound **8** (0.556 g) in 96% yield; **M.p.**: 152 – 154 °C; **IR (KBr)**: ν/cm^{-1} : 3444, 2958, 1887, 1693, 1502, 1409, 1291, 1203, 1114, 1021; **¹H NMR(400 MHz, MeOH-*d*₄)**: δ 3.85 (s, 2H), 3.45 (d, $J = 12.4$ Hz, 2H), 3.22 (d, $J = 12.8$ Hz, 2H), 3.14 (d, $J = 11.2$ Hz, 2H), 2.54 (d, $J = 11.2$ Hz, 2H), 2.07 (s, 2H), 1.90 (d, $J = 13.2$

Hz, 1H), 1.70 (d, $J = 14.8$ Hz, 1H); ^{13}C NMR (100 MHz, MeOH- d_4): δ 119.71 (Ar-C), 116.82 (Ar-C), 113.95 (Ar-C), 110.41 (Ar-C), 57.80 (CH₂-N), 50.27 (Ar-CH₂-N), 30.47 (CH₂), 28.50 (CH); HRMS (ESI): Calc. for C₁₄H₁₅F₅N₅ [M+H]⁺: 307.1233; Found: 307.1232.

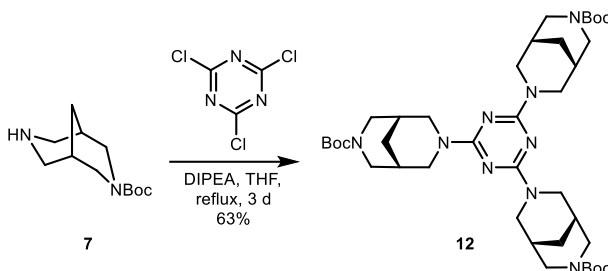
Synthesis of 2,4,6-tris((1R,5S)-7-((perfluorophenyl)methyl)-3,7-diazabicyclo[3.3.1]nonan-3-yl)-1,3,5-triazine 2:



Scheme 3A.7: Synthesis of compound 2.

In a 25 mL round bottom flask cyanuric chloride (0.013 g, 0.07 mmol) and amine **8** (0.10 g, 0.32 mmol) were dissolved in toluene (10 mL). KOH (0.08 g, 1.4 mmol) was added to above reaction mixture and refluxed for 7 h. After completion of reaction, solvent was removed under *vacuo* and then obtained residue was extracted with CH₂Cl₂ (3 × 50 mL) and washed with brine solution (3 × 50 mL). Organic layer was collected and dried over Na₂SO₄ and concentrated to give light brown residue. Column chromatography was performed over silica gel with that brown residue (*Eluent*: 100% chloroform) and compound **2** (35 mg) was obtained as off-white solid with 35% yield; **M.p.**: 142 – 144 °C; **IR (KBr)**: ν/cm^{-1} : 2909, 2850, 1652, 1531, 1443, 1335, 1298, 1239, 1117, 1033; **^1H NMR(400 MHz, CDCl₃)**: δ 4.54 (s, 6H), 3.51 (s, 6H), 3.40 (s, 6H), 2.89 (d, $J = 11.6$ Hz, 6H), 2.35 (d, $J = 11.2$ Hz, 6H), 1.89 (s, 6H), 1.70 (d, $J = 12.4$ Hz, 3H), 1.52 (d, $J = 13.6$ Hz, 3H); **^{13}C NMR (100 MHz, CDCl₃)**: δ 164.98 (triazene-C), 146.22 (Ar-C), 143.74 (Ar-C), 141.18 (Ar-C), 110.39 (Ar-C), 57.15 (CH₂-N), 48.45 (Ar-CH₂-N), 47.22 (CH₂), 29.28 (CH); **HRMS (ESI)**: Calc. for C₄₅H₄₂F₁₅N₉ [M+H]⁺: 994.3398; Found: 994.3390.

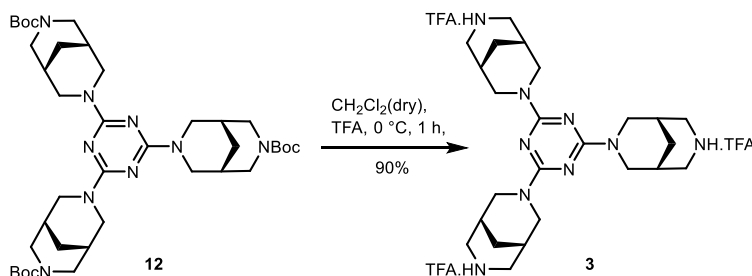
Synthesis of tri-*tert*-butyl 7,7',7''-(1,3,5-triazine-2,4,6-triyl)(1*R*,1'*R*,1''*R*,5*S*,5'*S*,5''*S*)-tris(3,7-diazabicyclo[3.3.1]nonane-3-carboxylate) 12:



Scheme 3A.8: Synthesis of compound 12.

In a round bottom flask cyanuric chloride (0.13 g, 0.70 mmol) and Boc-protected amine **7** (0.55g, 2.45 mmol) in THF (25 mL) was stirred for 1 h at room temperature. Di-isopropylethylamine (DIPEA) was added to the above solution. The reaction mixture was kept for stirring for 1 h followed by refluxing for 72 h. After reaction is complete no workup is required. The solvent is evaporated in vacuo to obtain a residue which is subjected to column chromatography to yield 63% compound **12** (0.40 g) as an off-white solid after pentane washings. (*Eluent*: 1% MeOH in Chloroform); **M.p.:** 199 – 201 °C; **IR (KBr):** ν/cm^{-1} : 2979, 2917, 2846, 1691, 1538, 1477, 1358, 1440, 1358, 1319, 1239, 1170; **¹H NMR(400 MHz, MeOH-*d*₄):** δ 3.96 (d, $J = 11.2$ Hz, 6H), 3.09 (d, $J = 12.0$ Hz, 15H), 1.95 (s, br, 6H), 1.81 (s, br, 9H), 1.28 (s, 27H); **¹³C NMR (100 MHz, MeOH-*d*₄):** δ 167.06 (triazene-C), 159.78 (C=O), 102.08 (C(CH₃)₃), 80.42 (CH₂-N), 29.61 (CH₂), 28.72 (CH₃), 23.39 (CH); **HRMS (ESI):** Calc. for C₃₉H₆₃N₉O₆ [M+H]⁺: 754.4979; Found: 754.4967.

Synthesis of 2,4,6-tri((1*R*,5*S*)-3,7-diazabicyclo[3.3.1]nonan-3-yl)-1,3,5-triazine 3:



Scheme 3A.9: Synthesis of compound 3.

Compound **12** (0.075 g, 0.10 mmol) was taken in a round bottom flask and placed in an ice bath. To it dry CH₂Cl₂ (2 mL) was added followed by TFA (2 mL). The reaction was kept to stir for 1 h. After completion of the reaction, the solvent was evaporated in vacuo to obtain a residue which on pentane washing followed by washings with diethyl ether yields compound **3** as TFA salt in 90% (66 mg) as an off-white solid; **M.p.:** 182 – 183 °C; **IR (KBr):** ν/cm^{-1} : 3434, 2868, 2370, 1798, 1689, 1593, 1543, 1496, 1444, 1343, 1283; **¹H NMR(400 MHz, MeOH-*d*₄):** δ 4.84 (d, *J* = 13.2 Hz, 6H) 3.52 (d, *J* = 12.8 Hz, 6H), 3.26 (s, 6H), 3.09 (d, *J* = 13.6 Hz, 6H), 2.25 (s, br, 6H), 2.09-1.95 (m, 9H); **¹³C NMR (100 MHz, MeOH-*d*₄):** δ 166.25 (triazene-C), 99.99 (CH₂-N), 29.78 (CH₂), 26.32 (CH); **HRMS (ESI):** Calc. for C₂₄H₃₉N₉ [M+H]⁺: 454.3398; Found: 454.3439.

Ion Transport Activity Study^{14b, 14c}

HEPES buffer, HPTS and Stock Solution Preparation: Solid HEPES and NaCl were dissolved in autoclaved water to prepare HEPES buffer (10 mM) with NaCl (100 mM) pH of the solution was adjusted to 7.0 by adding NaOH solution. Solid HPTS was dissolved in above buffer solution to give 1 mM solution of 100 mM HEPES containing NaCl (100 mM) of pH = 7.0. Stock solutions of all tripodal molecules were prepared by dissolving in HPLC grade DMSO/THF (9:1) (for HPTS assay) or THF/MeOH (2:4) (for Lucigenin assay).

Preparation of EYPC-LUVs \supset HPTS: 1 mL of egg yolk phosphatidylcholine (EYPC) (25 mg/mL) dissolved in chloroform was taken in a clean and dry small round bottomed flask. A thin transparent film of lipid was prepared by evaporating chloroform by purging with nitrogen and continuous rotation. The obtained film was dried in high vacuum for 5 h to remove all trace of CHCl₃. After 5 h that transparent film was hydrated with 1 mL of aforementioned HEPES buffer (1 mM HPTS, 10 mM HEPES, 100 mM NaCl, pH = 7.0) for 1 h with intermittent vortexing of atleast 5 times and then subjected to freeze-thaw cycle for \geq 15 times. Extrusions were done 19 times (must be an odd number) by a Mini-extruder equipped with a polycarbonate membrane having pore diameter of 100 nm. All extravesicular HPTS dyes were removed by gel filtration with Sephadex G-50 with 10 mM HEPES buffer (100 mM NaCl, pH = 7.0) and obtained vesicles were diluted to 6 mL with same buffer (10 mM HEPES, 100 mM NaCl, pH = 7.0) solution to give EYPC-LUVs \supset HPTS: \sim 5.0 mM EYPC, inside: 1 mM HPTS, 10 mM HEPES, 100 mM NaCl, pH = 7.0 and outside: 10 mM HEPES, 100 mM NaCl, pH = 7.0.

Ion Transport Activity Assay: In a clean and dry fluorescence cuvette, 1975 μL of HEPES buffer (10 mM HEPES, 100 mM NaCl, pH = 7.0) was taken followed by addition of 25 μL of EYPC-LUVs \supset HPTS vesicle in the same cuvette and was placed on fluorescence instrument equipped with magnetic stirrer (at $t = 0$ s). Fluorescence emission intensity of pH sensitive dye HPTS, F_t was monitored at $\lambda_{\text{em}} = 510$ nm ($\lambda_{\text{ex}} = 450$ nm) with time. After that a pH gradient between the intra and extra vesicular system was created by adding 20 μL of 0.5 M NaOH to the same cuvette at $t = 20$ s (Figure S1). Tripodal molecules were added at $t = 100$ s and finally at $t = 300$ s, vesicles were lysed with 25 μL of 10% Triton X-100 and this resulted in destruction of pH gradient (Figure 3A.3A) and saturation in fluorescence emission intensity was observed.

The time axis was normalized according to Equation 1:

$$t = t - 100 \quad \text{Equation (1)}$$

Fluorescence time courses (F_t) were normalized to fractional emission intensity I_F using Equation 2.

$$\% \text{ Fl Intensity } (I_F) = [(F_t - F_0) / (F_\infty - F_0)] \times 100 \quad \text{Equation (2)}$$

Where F_0 = Fluorescence intensity just before the tripodal molecule addition (at $t = 0$ s). F_∞ = Fluorescence intensity at saturation after complete leakage (at $t = 330$ s). F_t = Fluorescence intensity at time t . Concentration dependent experiment was carried out by increasing concentration of tripodal molecules (1–3). Change of HPTS fluorescence emission intensity of HPTS dye was monitored with time and addition of tripodal molecules resulted in destruction of pH gradient via either Na^+/OH^- symport or Na^+/H^+ antiport mechanism.

The concentration profile data were further analyzed by Hill Equation to get the Effective concentration (EC_{50}) and Hill Coefficient (n), (Equation 3).

$$Y = Y_\infty + (Y_0 - Y_\infty) / [1 + (c / EC_{50})^n] \quad \text{Equation (3)}$$

Where, Y_0 = Fluorescence intensity just before the tripodal molecule addition (at $t = 0$ s). Y_∞ = Fluorescence intensity with excess molecule concentration, c = Concentration of molecule.

Preparation of EYPC-LUVs \supset HPTS: Same vesicles of previous assay were used for this assay.

Cation Selectivity Assay: Same EYPC-LUVs \supset HPTS vesicles were used in this assay. 1975 μL of different HEPES buffer solutions (10 mM HEPES, 100 mM MCl, pH = 7.0; where, $\text{M}^+ = \text{Li}^+$,

Na^+ , K^+ , Rb^+ and Cs^+) were taken in a clean and dry fluorescence cuvette followed by addition of 25 μL of EYPC-LUVs \supset HPTS vesicle in slowly stirring condition by a magnetic stirrer equipped with the fluorescence instrument (at $t = 0$ s). The fluorescence emission intensity was monitored with time at $\lambda_{\text{em}} = 510$ nm ($\lambda_{\text{ex}} = 450$ nm). At $t = 20$ s, 20 μL of 0.5 M NaOH was added to the cuvette to make the pH gradient between the intra and extra vesicular pool. Tripodal transporters were added at $t = 100$ s and 10% Triton X-100 (25 μL) was added at $t = 300$ s, to lyse all vesicles for complete destruction of pH gradient. For data analysis and comparison, time (X-axis) was normalized according to equation 1 and fluorescence intensities (F_t) were normalized to fractional emission intensity I_F by using Equation 2.

Anion Selectivity Assay: Same EYPC-LUVs \supset HPTS vesicles were used in this assay. In a clean and dry fluorescence cuvette 1975 μL of HEPES buffer (10 mM HEPES, 100 mM NaX, at pH = 7.0; where, $\text{X}^- = \text{F}^-$, Cl^- , Br^- , I^- , OAc^- , NO_3^- , SCN^- and ClO_4^-) was added followed by addition of 25 μL of EYPC-LUVs \supset HPTS vesicle in slowly stirring condition by a magnetic stirrer equipped with the fluorescence instrument (at $t = 0$ s). HPTS fluorescence emission intensity (F_t) was monitored with time at $\lambda_{\text{em}} = 510$ nm ($\lambda_{\text{ex}} = 450$ nm). 20 μL of 0.5 M NaOH was added to the cuvette at $t = 20$ s to make the pH gradient between the intra and extra vesicular system. Tripodal transporters were added at $t = 100$ s and followed by addition of 10% Triton X-100 (25 μL) at $t = 300$ s to lyse all vesicles for complete destruction of pH gradient. For data analysis and comparison, time (X-axis) was normalized according to equation 1 and fluorescence intensities (F_t) were normalized to fractional emission intensity I_F by using Equation 2.

Determination of Ion Selectivity by FCCP Assay:^{14d} In a clean and dry fluorescence cuvette 1975 μL of HEPES buffer (10 mM HEPES, 100 mM NaCl, pH = 7.0) was taken followed by addition of 25 μL of EYPC-LUVs \supset HPTS in stirring condition by a magnetic stirrer equipped with the fluorescence instrument (at $t = 0$ s). HPTS fluorescence intensity was monitored with time and F_t was observed at $\lambda_{\text{em}} = 510$ nm ($\lambda_{\text{ex}} = 450$ nm). At $t = 20$ s, 20 μL of 0.5 M NaOH was added to the cuvette to make the pH gradient between the intra and extra vesicular solution. FCCP (2.5 μM) was added at $t = 50$ s (whenever necessary) and tripodal transporters were added at $t = 100$ s (whenever necessary) and finally at $t = 300$ s, 25 μL of 10% Triton X-100 was added to that cuvette resulting destruction of pH gradient. Fluorescence intensities (F_t) were normalized to fractional emission intensity I_F using Equation 2 and time scale was normalized according to Equation 1.

Preparation of EYPC-LUVs \supset HPTS: Same vesicles of previous assay were used for this assay.

Determination of Ion Selectivity by Valinomycin assay:^{14d} In a clean and dry fluorescence cuvette 1975 μL of HEPES buffer (10 mM HEPES, 100 mM NaCl, pH = 7.0) was added followed by addition of 25 μL of EYPC-LUVs \supset HPTS in slowly stirring condition by a magnetic stirrer equipped with the fluorescence instrument (at $t = 0$ s). The time course of HPTS fluorescence emission intensity, F_t was observed at $\lambda_{\text{em}} = 510$ nm ($\lambda_{\text{ex}} = 450$ nm). 20 μL of 0.5 M NaOH was added to the cuvette at $t = 20$ s to make the pH gradient between the intra and extra vesicular system. Valinomycin (2.5 pM) was added at $t = 50$ s (whenever necessary) and tripodal molecule was added at $t = 100$ s (whenever necessary) and finally at $t = 300$ s, 25 μL of 10% Triton X-100 was added to lyse those vesicles resulting destruction of pH gradient. Fluorescence intensities (F_t) were normalized to fractional emission intensity I_F using Equation 2.

HEPES buffer, HPTS Solution Preparation for Direct Selectivity Assay: Solid HEPES was dissolved in autoclaved water to prepare HEPES buffer (10 mM) and pH of the solution was adjusted to 7.0. Solid HPTS was dissolved in above buffer solution to give 1 mM solution.

Preparation of EYPC-LUVs \supset HPTS for Direct Cation Selectivity Assay: 1 mL of egg yolk phosphatidylcholine (EYPC) (25 mg/mL) dissolved in chloroform was taken in a clean and dry small round bottomed flask. A thin transparent film of lipid was prepared by evaporating chloroform by purging with nitrogen and continuous rotation. The obtained film was dried in high vacuum for 5 h to remove all trace of CHCl_3 . After 5 h that transparent film was hydrated with 1 mL of aforementioned HEPES buffer (1 mM HPTS, 10 mM HEPES, pH = 7.0) for 1 h with intermittent vortexing of at least 5 times and then subjected to freeze-thaw cycle for ≥ 15 times. Extrusions were done 19 times (must be an odd number) by a Mini-extruder equipped with a polycarbonate membrane having pore diameter of 100 nm. All extravesicular HPTS dyes were removed by gel filtration with Sephadex G-50 with 10 mM HEPES buffer (pH = 7.0) and obtained vesicles were diluted to 6 mL with same buffer (10 mM HEPES, pH = 7.0) solution to give EYPC-LUVs \supset HPTS: ~ 5.0 mM EYPC, inside: 1 mM HPTS, 10 mM HEPES, pH = 7.0 and outside: 10 mM HEPES, pH = 7.0.

Ion Transport Activity Assay for Direct Cation Selectivity Assay: In a clean and dry fluorescence cuvette, 1975 μL of HEPES buffer (10 mM HEPES, pH = 7.0) was taken followed by addition of 25 μL of EYPC-LUVs \supset HPTS vesicle in the same cuvette and was placed on fluorescence instrument equipped with magnetic stirrer (at $t = 0$ s). Fluorescence emission intensity

of pH sensitive dye HPTS, F_t was monitored at $\lambda_{em} = 510$ nm ($\lambda_{ex} = 450$ nm) with time. After that a pH gradient between the intra and extra vesicular system was created by adding 20 μ L of 0.5 M MOH ($M^+ = Li^+, Na^+, K^+, Rb^+, Cs^+$) to the same cuvette at $t = 20$ s. Tripodal molecule **1** (0.25 μ M) were added at $t = 100$ s and finally at $t = 300$ s, vesicles were lysed with 25 μ L of 10% Triton X-100 and this resulted in destruction of pH gradient and saturation in fluorescence emission intensity was observed. The time axis was normalized according to Equation 1 and fluorescence time courses (F_t) were normalized to fractional emission intensity I_F using Equation 2.

Determination of Chloride Ion Selectivity by Lucigenin assay:¹⁸

Preparation of EYPC-LUVs \Rightarrow Lucigenin for Concentration Dependent Assay and Symport

Assay: A solution of EYPC (25 mg/mL) dissolved in $CHCl_3$ was taken in a clean and dry small round bottom flask. The solvents were evaporated slowly by a stream of nitrogen, followed by drying under vacuum for at least 4 h. After that 1 mL of 1 mM *N,N'*-Dimethyl-9,9'-biacridinium dinitrate (Lucigenin dye) in 225 mM $NaNO_3$ (dissolved in water) was added, and the suspension was hydrated for 1 h with occasional vortexing of 4-5 times and then subjected to freeze-thaw cycle (≥ 20 times). The vesicle solution was extruded through a polycarbonate membrane with 200 nm pores 19 times (has to be an odd number), to give vesicles with a mean diameter of ~ 200 nm. The extracellular Lucigenin was removed from the vesicles by size exclusion column chromatography by gel filtration (Sephadex G-50) using 225 mM $NaNO_3$ (pH = 6.4) as eluent. The vesicles were diluted to 4 mL with 225 mM $NaNO_3$.

Determination of Chloride Ion Selectivity by Lucigenin assay: In a clean and dry fluorescence cuvette 50 μ L of above lipid solution and 1950 μ L of 225 mM $NaNO_3$ was taken and kept in slowly stirring condition by a magnetic stirrer equipped with fluorescence instrument (at $t = 0$ s). Lucigenin fluorescence emission intensity, F_t was monitored at $\lambda_{em} = 535$ nm ($\lambda_{ex} = 450$ nm) with time. 25 μ L of 2 N NaCl was added to the cuvette at $t = 50$ s to make the NaCl salt gradient between the intra and extra vesicular system. Tripodal molecule was added at $t = 100$ s and finally at $t = 300$ s, 25 μ L of 10% Triton X-100 was added to lyse those vesicles for 100% chloride influx. Fluorescence intensities (F_t) were normalized to fractional emission intensity I_F using Equation 4.

$$\text{Normalized Fl Intensity } (I_F) = [(F_t - F_0) / (F_{\infty} - F_0)] \times (-100) \quad (\text{Equation 4})$$

For symport assay only instead of NaCl, different salt pulses of MCl ($M^+ = \text{Li}^+, \text{Na}^+, \text{K}^+, \text{Rb}^+, \text{and Cs}^+$) were applied to the cuvette at $t = 50$ s and Tripodal molecule **1** was added at $t = 100$ s and all other experimental assay condition is same. Fluorescence intensities (F_t) were normalized to fractional emission intensity I_F using Equation 4.

To quantify transport abilities of both tripodal compounds **1** and **2**, half-lives ($t_{1/2}$) and initial rates (I_R) were calculated. Half-lives ($t_{1/2}$) of transport activities were obtained by fitting fluorescence quenching curve of both compounds (at 20 μM) to a single exponential decay function with Equation 5 and followed by calculation of half-life by Equation 6.

$$I/I_0 = a + b.e^{-ct} \quad \text{(Equation 5)}$$

$$t_{1/2} = 0.693/c \quad \text{(Equation 6)}$$

Initial rate, I_R for the transport process was obtained by fitting fluorescence quenching curve with the double exponential decay equation,

$$I/I_0 = y_0 + a.e^{(-bt)} + c.e^{(-dt)} \quad \text{(Equation 7)}$$

Now, differentiating with respect to t gives:

$$\partial y/\partial t = a.b.e^{(-bt)} + c.d.e^{(-dt)} \quad \text{(Equation 8)}$$

Initial rate I_R was calculated by putting $t = 0$ s in the above equation:

$$I_R = \partial y/\partial t_{t=0} = a.b + c.d \quad \text{(Equation 9)}$$

Preparation of EYPC-LUVs \supset Lucigenin for Antiport Study: A solution of EYPC (25 mg) dissolved in CHCl_3 was taken in a clean and dry small round bottom flask. The solvents were evaporated slowly by a stream of nitrogen, followed by drying under vacuum for at least 4 h. After vortexing 1 mL of 1 mM Lucigenin in 225 mM NaCl (dissolved in water) was added, and the suspension was hydrated for 1 h with occasional vortexing of 5 times and then subjected to freeze-thaw cycle (≥ 20 times). The vesicle solution was extruded through a polycarbonate membrane with 200 nm pores 19 times (must be an odd number), to give vesicles with a mean diameter of ~ 200 nm. The extracellular Lucigenin dye was removed from the vesicles by size exclusion gel chromatography (Sephadex G-50) using 225 mM NaCl as eluent. The vesicles were diluted to 4 mL with 225 mM NaCl.

Effect of Extravesicular Anion in Chloride Efflux: In a clean and dry fluorescence cuvette 50 μL of above lipid solution and 1950 μL of isoosmolar solutions of different salts of NaX ($\text{X}^- = \text{F}^-$, NO_3^- , SO_4^{2-} , HCO_3^- and ClO_4^-) were taken and kept in slowly stirring condition by a magnetic stirrer equipped with the fluorescence instrument (at $t = 0$ s). Kinetic experiment was carried out by monitoring Lucigenin fluorescence emission intensity, F_t at $\lambda_{\text{em}} = 535$ nm ($\lambda_{\text{ex}} = 450$ nm). Tripodal molecule **1** was added at $t = 100$ s and finally at $t = 300$ s, 25 μL of 10% Triton X-100 was added to lyse those vesicles for 100% chloride influx. Fluorescence intensities (F_t) were normalized to fractional emission intensity I_F using Equation 2.

Preparation of POPC-LUVs \Rightarrow Lucigenin: A solution of 0.65 mL of 1-palmitoyl-2-oleoyl-*sn*-glycero-3-phosphocholine (POPC, 16.45 mg) dissolved in CHCl_3 was taken in a clean and dry small round bottom flask. After this, same protocol was followed as discussed earlier for lucigenin symport assay.

Preparation of Cholesterol: POPC-LUVs \Rightarrow Lucigenin:¹⁸ A solution of 0.5 mL of 1-palmitoyl-2-oleoyl-*sn*-glycero-3-phosphocholine (POPC, 13.14 mg) dissolved in CHCl_3 was taken in a clean and dry small round bottom flask. Then cholesterol (3.2 mg) was taken in same round bottom flask. After this, same protocol was followed as discussed earlier for lucigenin symport assay.

Determination of Cl^- Selectivity by Lucigenin assay: Same as symport assay.

Determination of Cl^- Selectivity by Cholesterol: Same as discussed before.

Determination of Chloride Ion Efflux by Ion Selective Electrode:

Preparation of EYPC-LUVs \Rightarrow for Chloride Efflux Assay at Different pH Solutions: A series of phosphate buffers (pH = 5.3, 6, 6, 8, 8.8) was prepared with NaNO_3 (500 mM). A solution of EYPC (25 mg/mL) dissolved in CHCl_3 was taken in a clean and dry small round bottom flask. The solvents were evaporated slowly by a stream of nitrogen, followed by drying under vacuum for at least 4 h. After that 1 mL in 500 mM NaCl (dissolved in buffer of corresponding pH) was added, and the suspension was hydrated for 1 h with occasional vortexing of 4-5 times and then subjected to freeze-thaw cycle (≥ 20 times). The vesicle solution was extruded through a polycarbonate membrane with 200 nm pores 19 times (has to be an odd number), to give vesicles with a mean diameter of ~ 200 nm. The extracellular chloride was removed from the vesicles by dialysis. The vesicles were diluted to 1.5 mL with 500 mM NaNO_3 . In same way five sets of vesicle were prepared with five different buffers solutions of pH.

Determination of Chloride Ion Selectivity by ISE: In a clean and dry glass vial, 50 μL of above lipid solution and 1950 μL of 500 mM NaNO_3 of respective pH buffer solutions was taken and kept in slowly stirring condition by a magnetic stirrer (at $t = 0$ s) and chloride efflux was monitored with time. Tripodal molecule was added at $t = 60$ s and finally at $t = 300$ s, 25 μL of 10% Triton X-100 was added to lyse those vesicles for 100% chloride influx. Chloride efflux were normalized using Equation 4.

Preparation of EYPC-LUVs \supset CF: A thin lipid film was prepared by evaporating a solution of 12.5 mg EYPC in 0.5 ml CHCl_3 in vacuo for 4 h. After that lipid film was hydrated with 0.5 mL buffer (10 mM HEPES, 10 mM NaCl, 50 mM CF, pH 7.0) for 1 h with occasional vortexing of 4-5 times and then subjected to freeze-thaw cycle (≥ 20 times). The vesicle solution was extruded through a polycarbonate membrane with 100 nm pores 19 times (has to be an odd number), to give vesicles with a mean diameter of ~ 100 nm. The extracellular dye was removed size exclusion chromatography (Sephadex G-50) with 10 mM HEPES buffer (100 mM NaCl, pH 7.0. Final) Final concentration: ~ 2.5 mM EYPC lipid; intravesicular solution: 10 mM HEPES, 10 mM NaCl, 50 mM CF, pH 7.0; extraventricular solution: 10 mM HEPES, 100 mM NaCl, pH 7.0.

Determination of Ion Leakage by CF Assay: In a clean and dry fluorescence cuvette 25 μL of above lipid solution and 1975 μL of 10 mM HEPES buffer (100 mM NaCl, pH 7.0) was taken and kept in slowly stirring condition by a magnetic stirrer equipped with the fluorescence instrument (at $t = 0$ s). The time course of CF fluorescence emission intensity, F_t was observed at $\lambda_{\text{em}} = 517$ nm ($\lambda_{\text{ex}} = 492$ nm). Tripodal molecules were added at $t = 100$ s and finally at $t = 300$ s, 25 μL of 10% Triton X-100 was added to lyse those vesicles for 100% chloride influx. Fluorescence intensities (F_t) were normalized to fractional emission intensity I_F using Equation 4.

Crystal Structure Parameters:¹⁹ All tripodal compounds were crystallized from chloroform/MeOH mixture at room temperature. Single-crystal X-ray data of all tripodal receptors **1–3** were collected at 200 K on a Bruker KAPPA APEX II CCD Duo diffractometer (operated at 1500 W power: 50 kV, 30 mA) using graphite-monochromated Mo $\text{K}\alpha$ radiation ($\lambda = 0.71073$ Å). The data integration and reduction were further processed with SAINT software. A multi-scan absorption correction was applied to the collected reflections. The structures were solved by the direct method using SHELXTL and were refined on F^2 by full-matrix least-squares technique using the SHELXL-97 program package within the WINGX programme. All non-hydrogen atoms

were refined anisotropically and all hydrogen atoms were located in successive difference Fourier maps and were treated as riding atoms using SHELXL default parameters. The structures were examined by using the *Adsym* subroutine of PLATON to confirm that no additional symmetry could be applied to the models. CCDC numbers for tripodal receptors (**1-3**) are 1494040, 1494041 and 1494042 respectively which contain the supplementary crystallographic data for this paper. These data are provided free of charge by The Cambridge Crystallographic Data Centre.

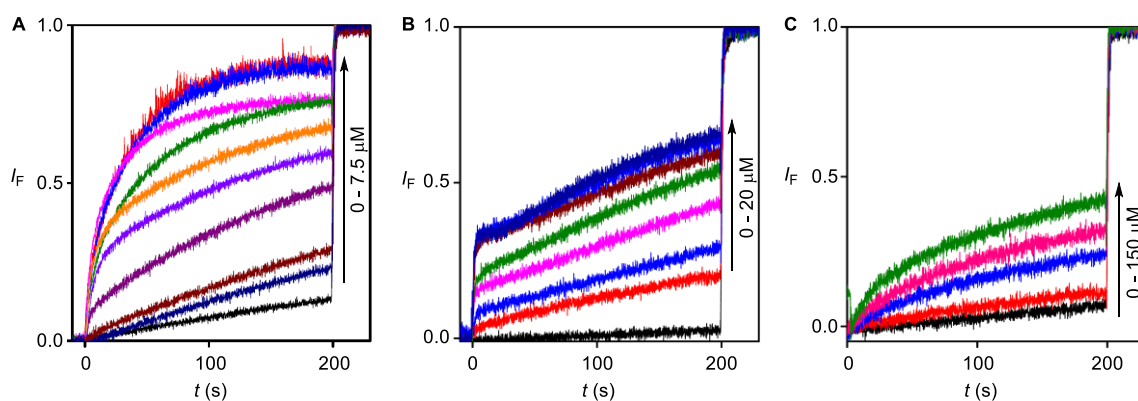
Mass Spectrometric Studies for Anion Recognition: Tripodal compound **1** and tetramethylammoniumchloride (TMACl) were prepared separately in acetonitrile and were mixed in 1:1 ratio and formation of complex was monitored by Electrospray Ionization Mass Spectrometric (ESI-MS) studies. The samples were electrosprayed as 10 μM solutions of compound **1** and (TMACl) in acetonitrile at flow rate of 0.4 mL/min. A constant spray and highest intensities were achieved with a capillary voltage of 3000 V at a source temperature of 80 $^{\circ}\text{C}$. The parameters for sample cone (40 V) and extractor cone voltage (5 V) were set for maximum intensities of the desired complexes. From the ESI-MS spectrum data, signals corresponding to $[\text{M}+\text{HCl}+\text{H}]^{+}$ and $[2\text{M}+\text{HCl}+\text{H}]^{+}$ were observed (where, M = exact molecular weight of **1**).

Simulation Details: We have taken a total of 95 DPPC molecules and 3313 water molecules in the system. Additional two Cl^{-} ions were added in addition to the Cl^{-} ion embedded along with the tripodal molecule **1** inside DPPC bilayer. SPC model²⁰ was taken for water and GROMOS-53a6 united atom force field²¹ was used for DPPC molecules. The parameters for all the atoms of the molecule with GROMOS-53a6 force field were generated using the automated topology builder created by Malde, *et al.*²² Initially the system was energy minimized using steepest descent method²³ for 10000 steps. This was followed by equilibration for 5ns at constant 300K temperature and 1 bar pressure using Nosé-Hoover thermostat²⁴⁻²⁵ and Parrinello-Rahman barostat²⁶ with a coupling constant of 0.4 ps for each. Electrostatic interactions were treated using PME electrostatics²⁷ with 10 Å cut-off with the Van der Waals cut-off was set at 10 Å. The simulation box was found to be $5.95 \times 5.95 \times 6.33 \text{ nm}^3$ in size after the equilibration step. A final 5ns molecular dynamics simulation at constant 300K temperature and volume was carried out with similar treatment of temperature, electrostatics and vdW as in equilibration process.

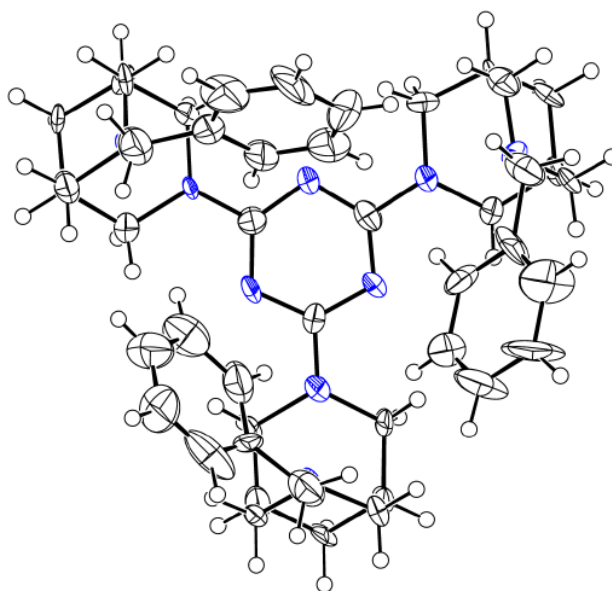
Evidence for mobile water molecules: We have calculated the number of water molecules within 4 Å of radius from the Cl^{-} ion. The numbers are shown in Figure 3A.14E. We have checked the distance between Cl^{-} ion and three water molecules close to it at different simulation time. The

first water (water 1) is taken to be the water that made H-bond at the initial configuration with the Cl^- . Similarly the second water (water 2), third water (water 3) and fourth water (water 4) were taken from frames at 2.5 ns, 3 ns and 5 ns respectively, where they were found to make H-bond with Cl^- at those instances. We can see that while water 1 leaves around 3 ns, water 3 replaces it. Therefore, the water molecules around Cl^- are dynamic where only the overall number and not the specific identity of water are preserved.

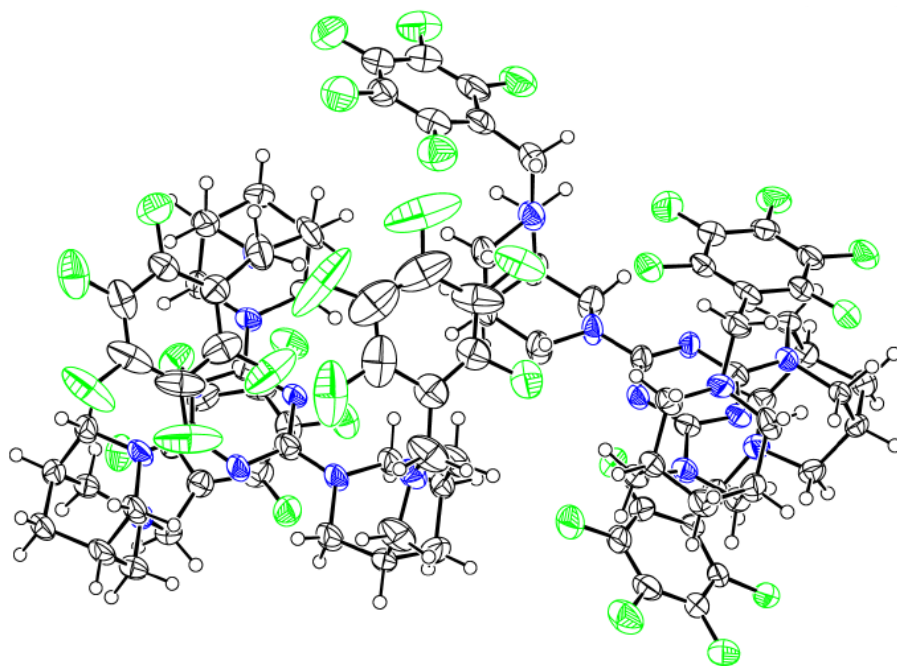
3A.5. Appendix Section



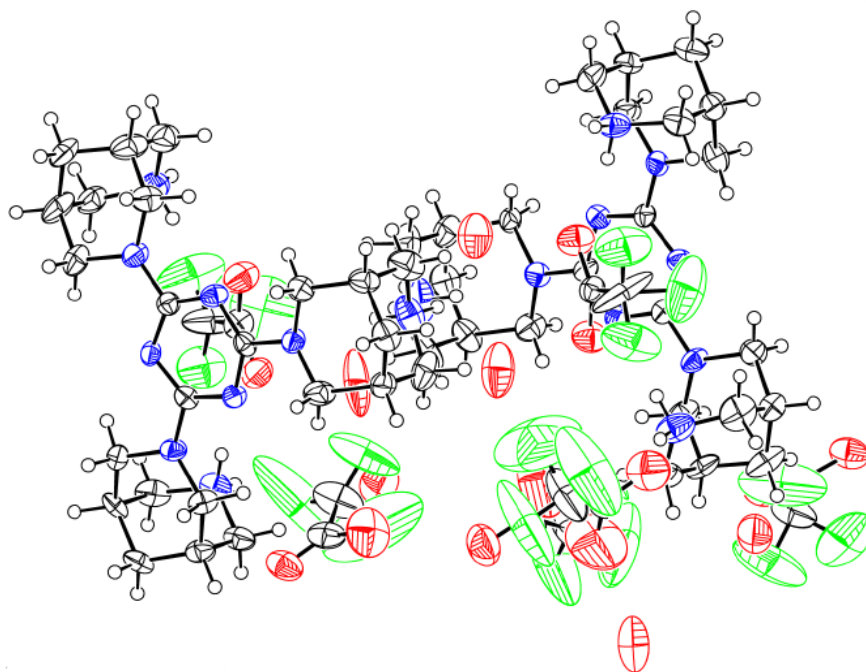
Appendix 3A.1: Ion transport assay of **A)** tripodal transporter **1**, **B)** tripodal transporter **2** and **C)** transporter **3** using EYPC-LUVs \supset HPTS.



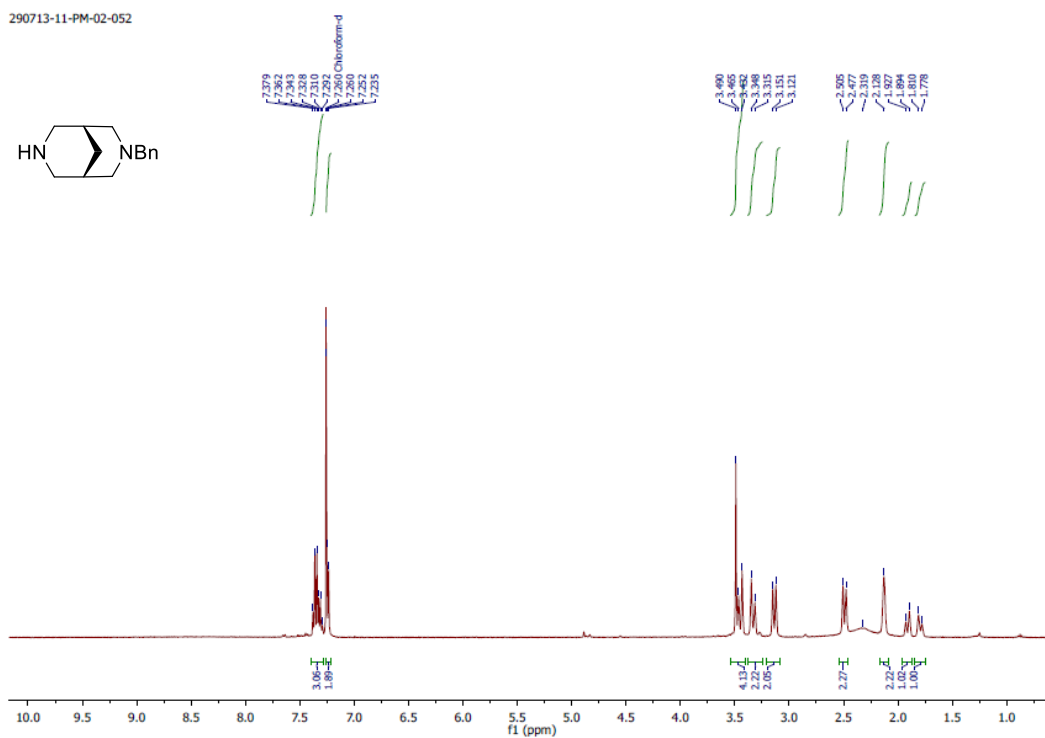
Appendix 3A.2: ORTEP diagram of tripodal compound **1**.



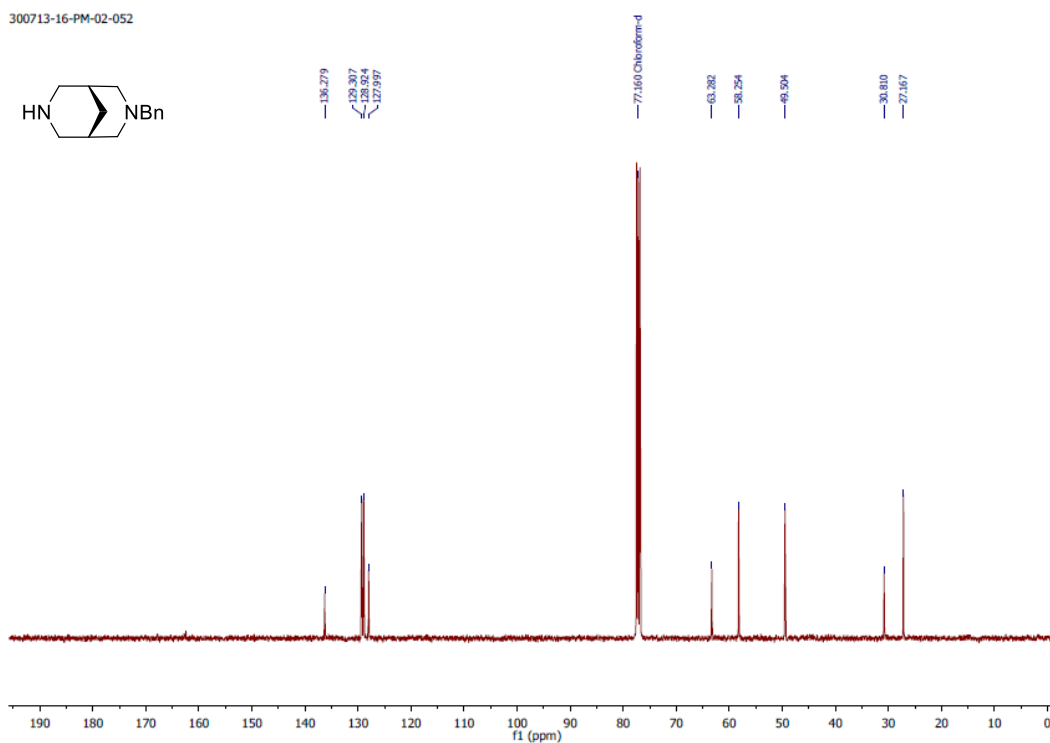
Appendix 3A.3: ORTEP diagram of tripodal compound 2.



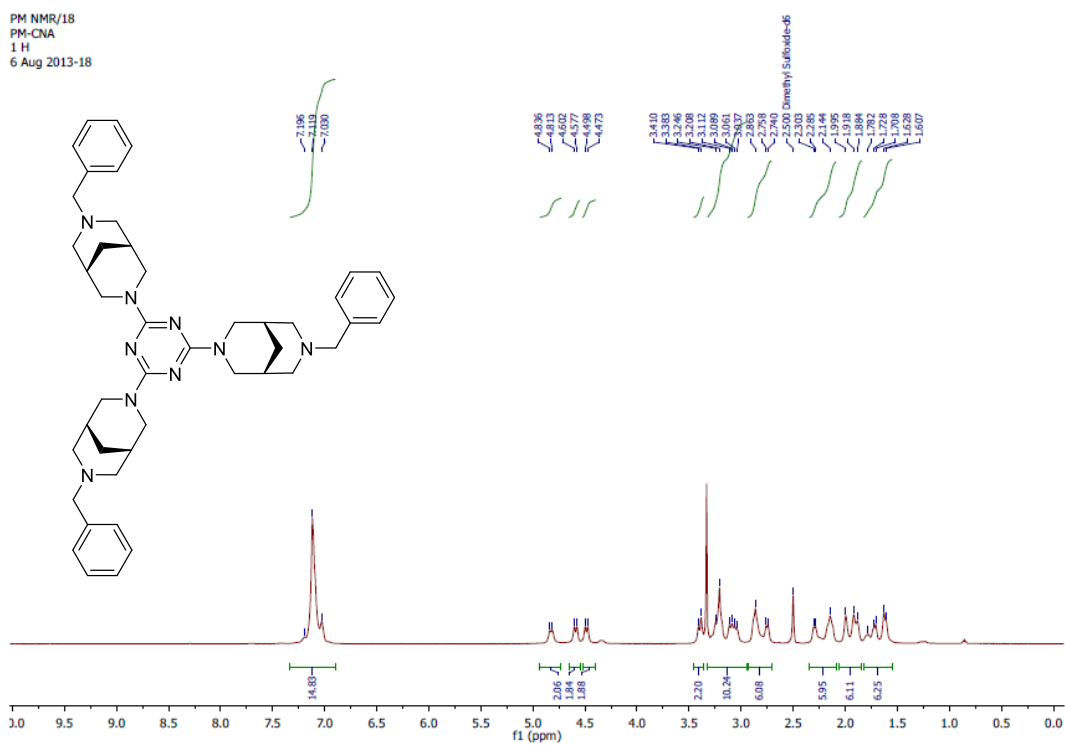
Appendix 3A.4: ORTEP diagram of tripodal compound 3.



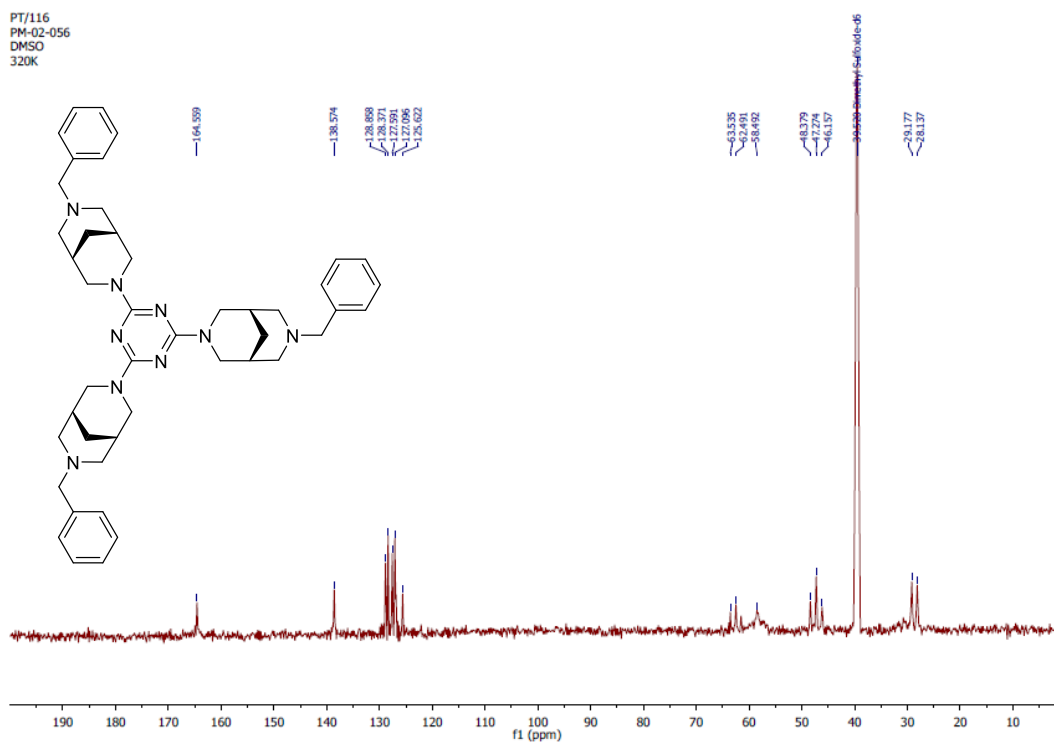
Appendix 3A.5: ¹H NMR spectrum of **6** in CDCl₃.



Appendix 3A.6: ¹³C NMR spectrum of **6** in CDCl₃.

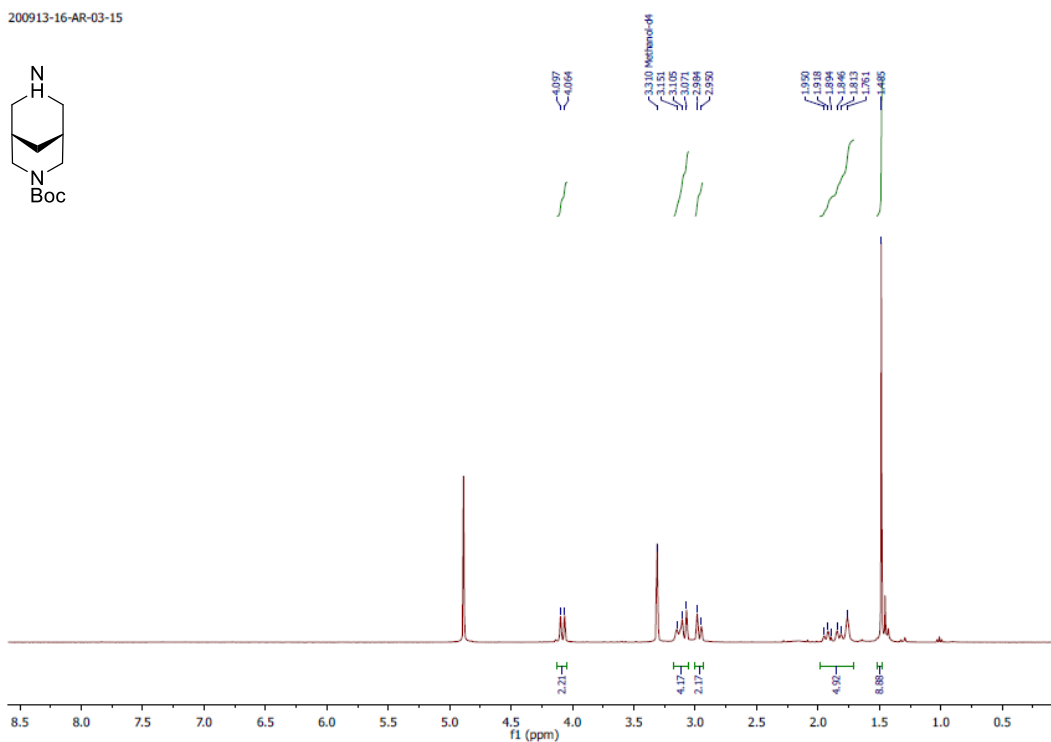
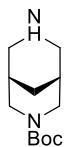


Appendix 3A.7: ^1H NMR spectrum of **1** in $\text{DMSO-}d_6$.



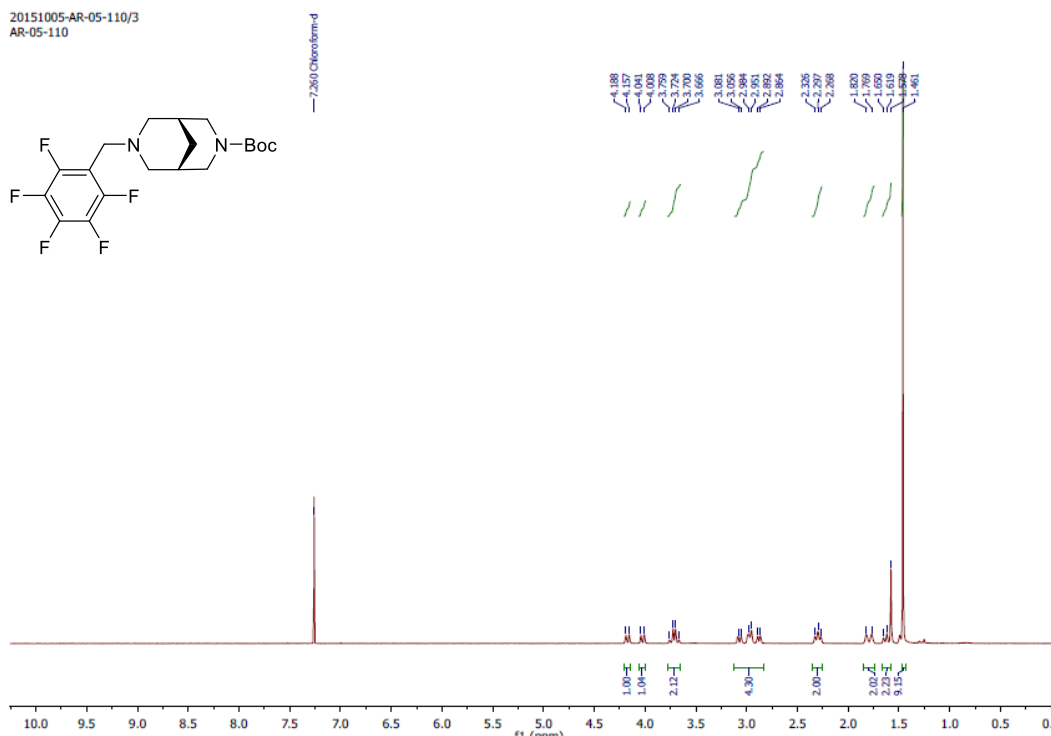
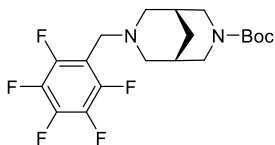
Appendix 3A.8: ^{13}C NMR spectrum of **1** in $\text{DMSO-}d_6$.

200913-16-AR-03-15

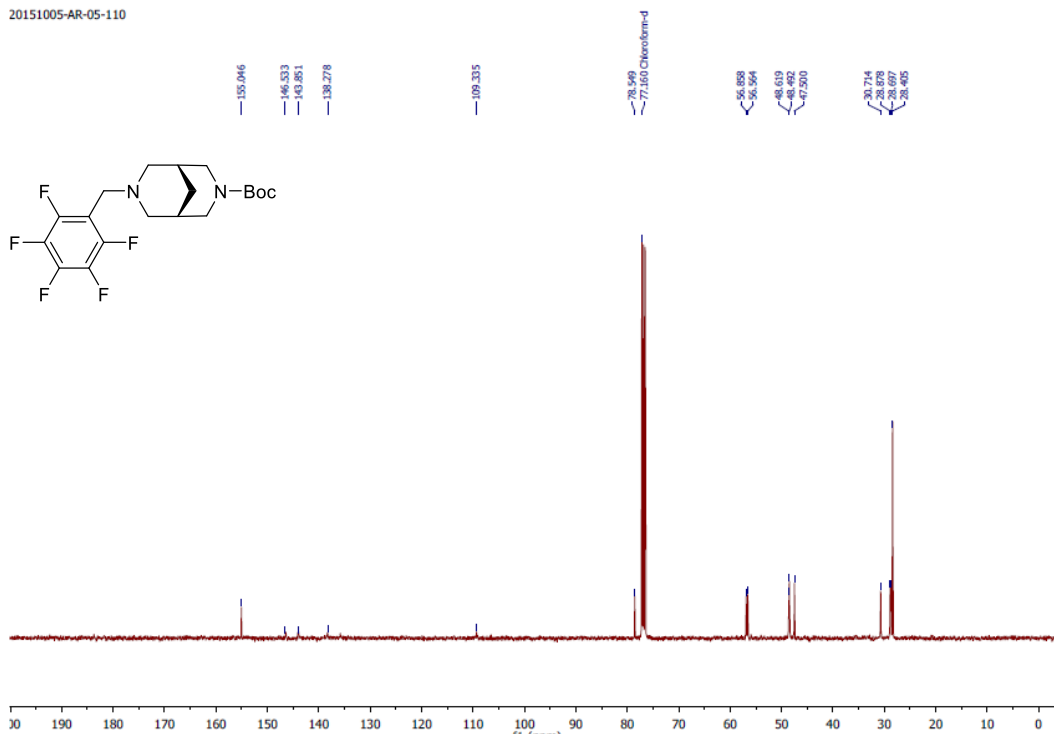


Appendix 3A.9: ^1H NMR spectrum of **7** in $\text{MeOH-}d_4$.

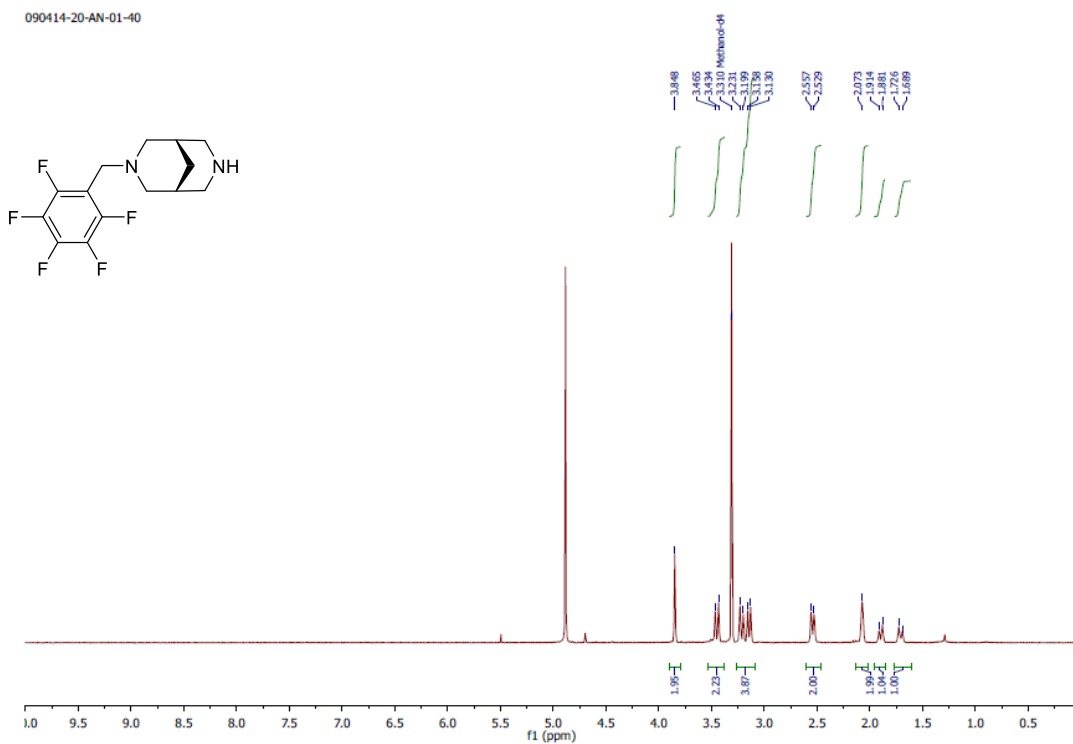
20151005-AR-05-110/3
AR-05-110



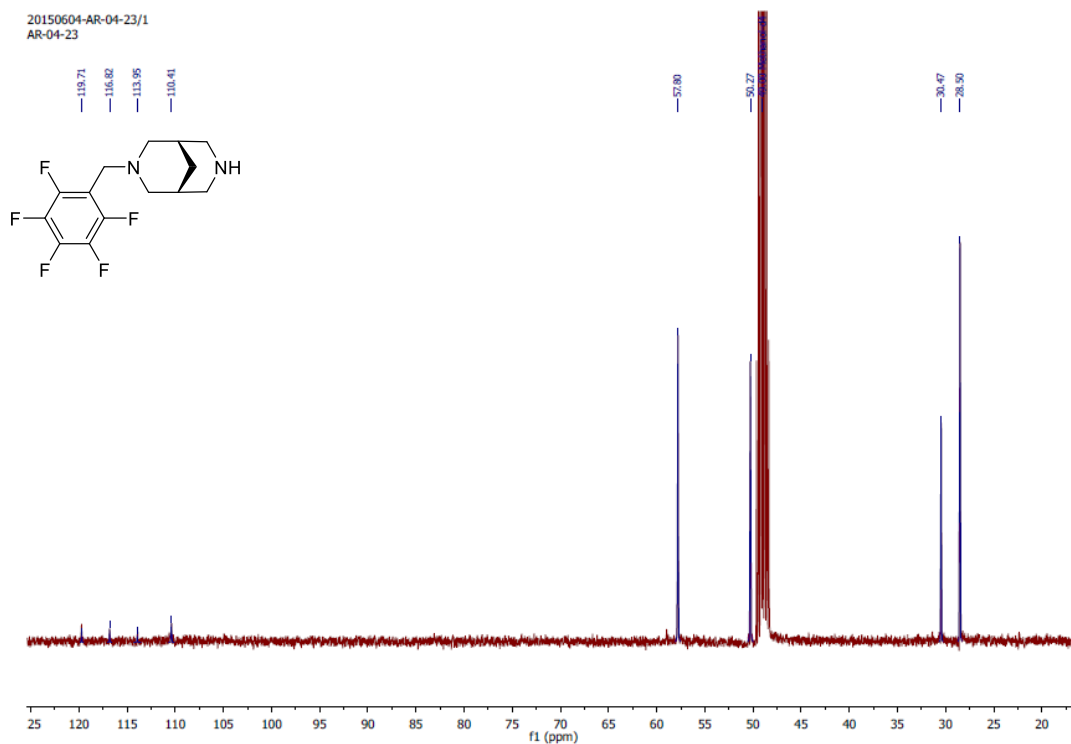
Appendix 3A.10: ^1H NMR spectrum of **11** in CDCl_3 .



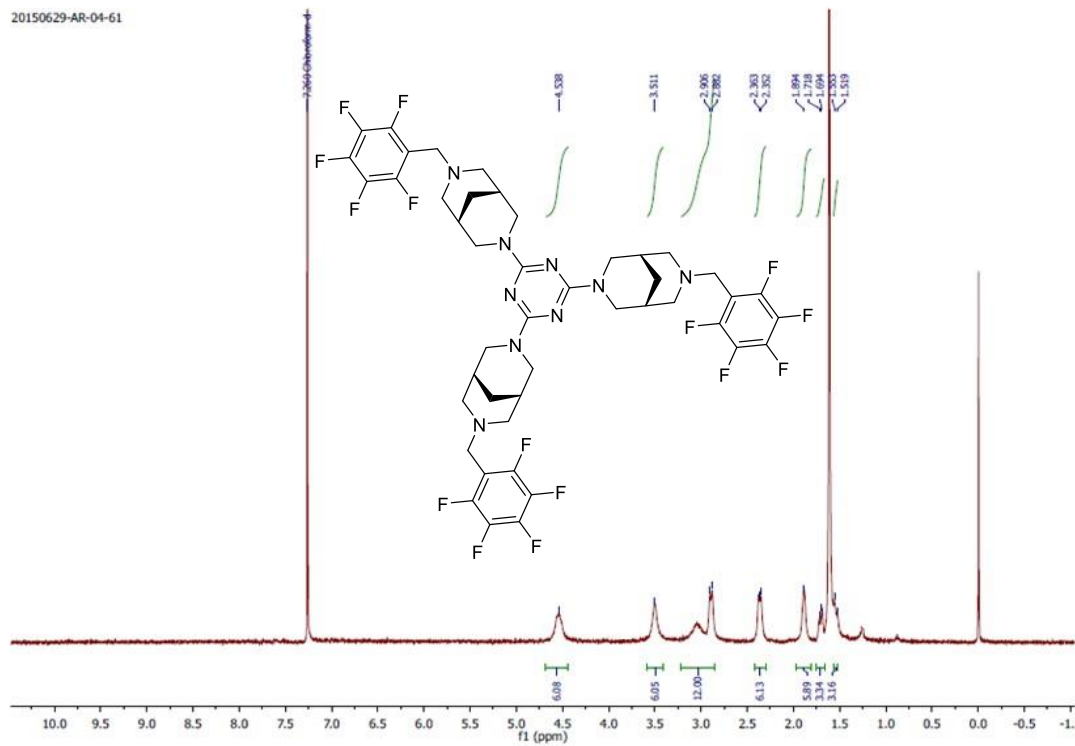
Appendix 3A.11: ¹³C NMR spectrum of **11** in CDCl₃.



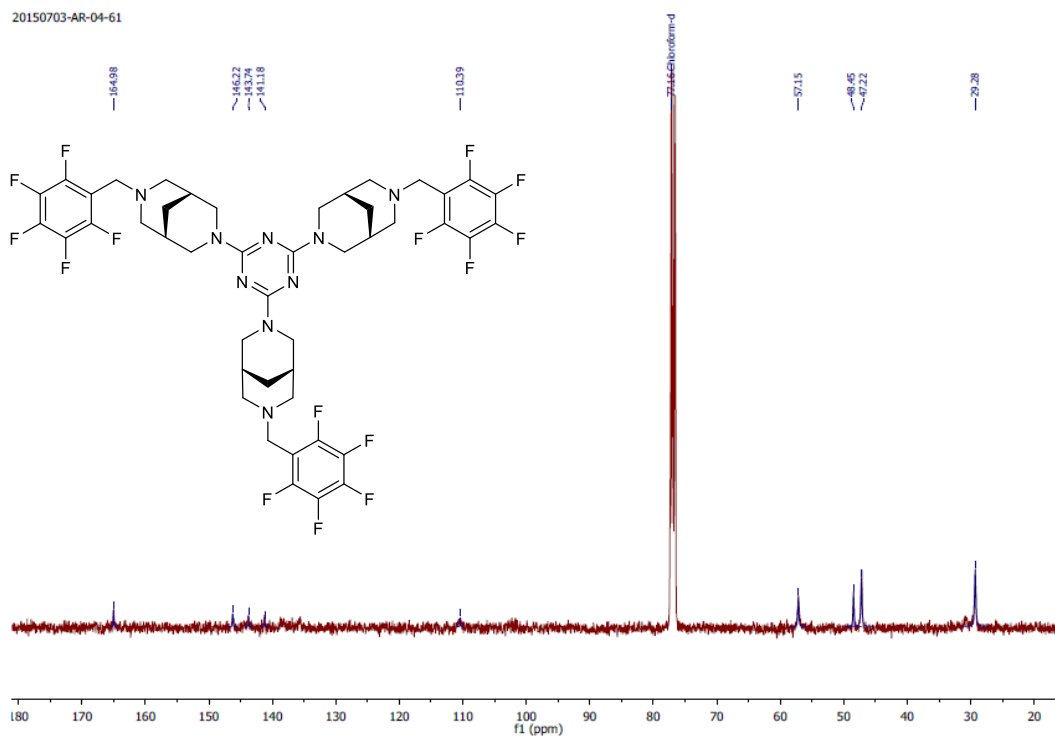
Appendix 3A.12: ¹H NMR spectrum of **8** in MeOH-*d*₄.



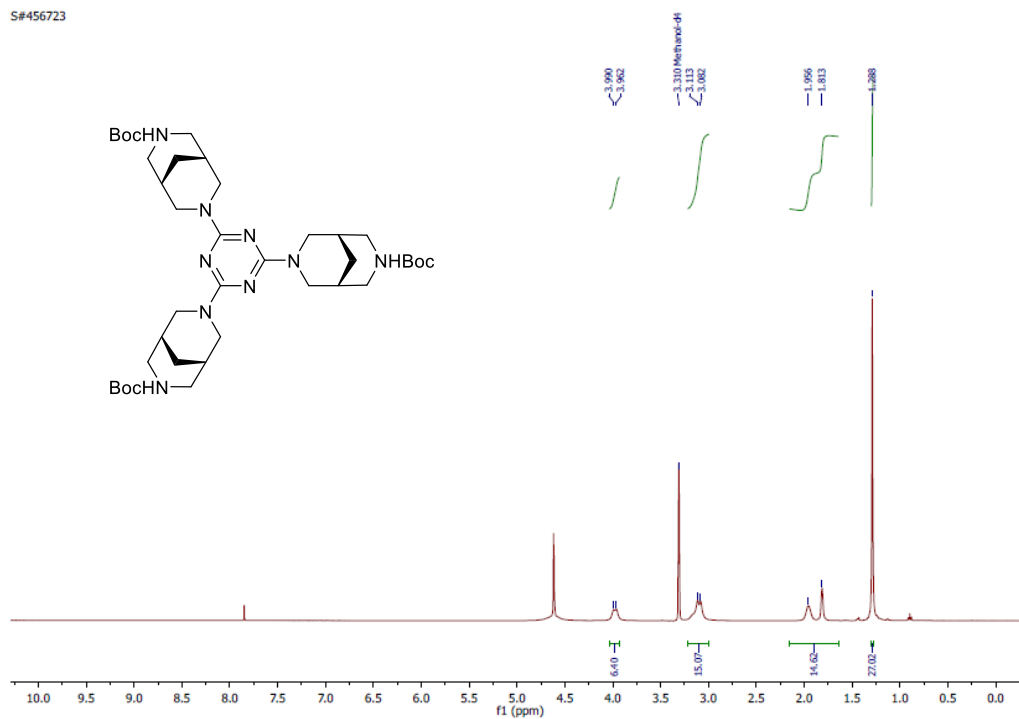
Appendix 3A.13: ^{13}C NMR spectrum of **8** in $\text{MeOH-}d_4$.



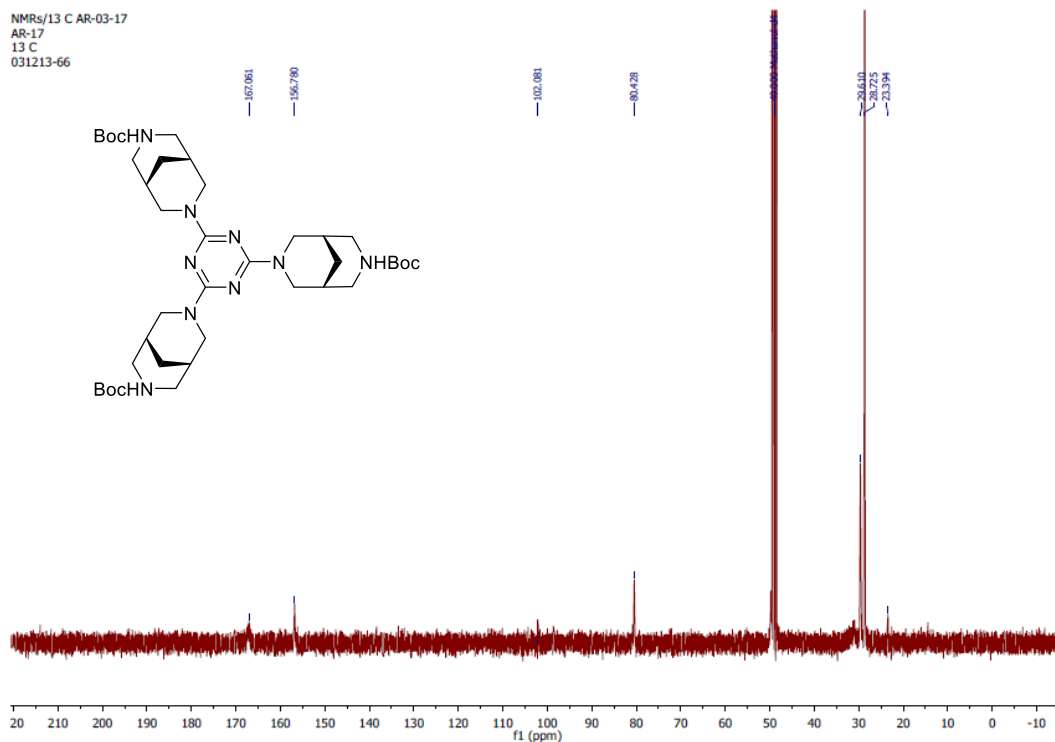
Appendix 3A.14: ^1H NMR spectrum of **2** in CDCl_3 .



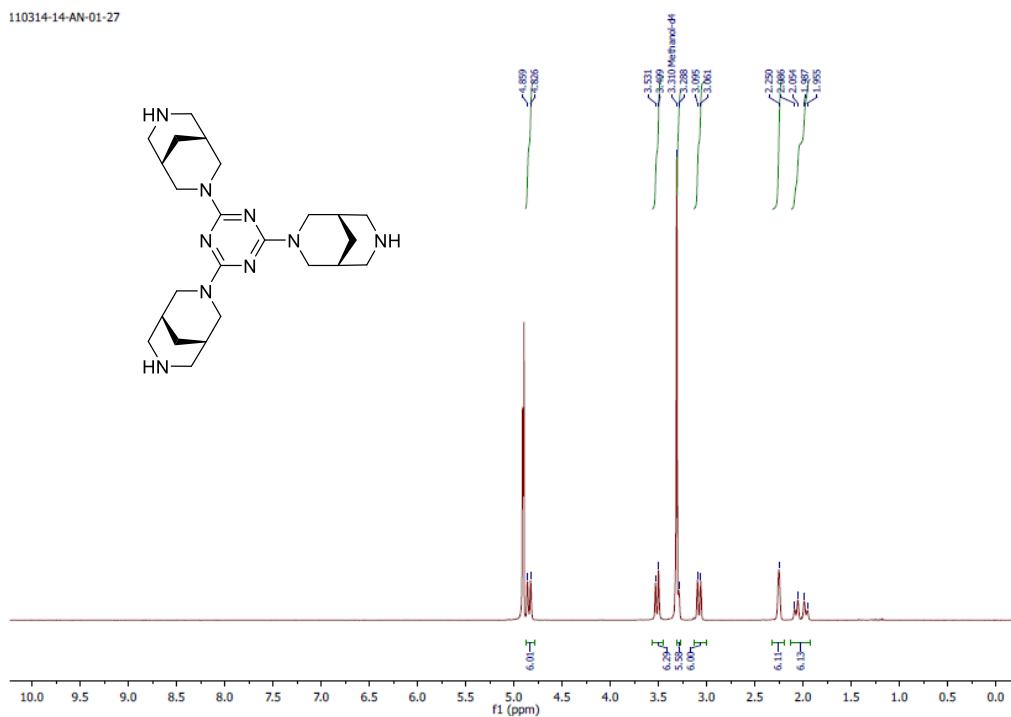
Appendix 3A.15: ^{13}C NMR spectrum of **2** in CDCl₃.



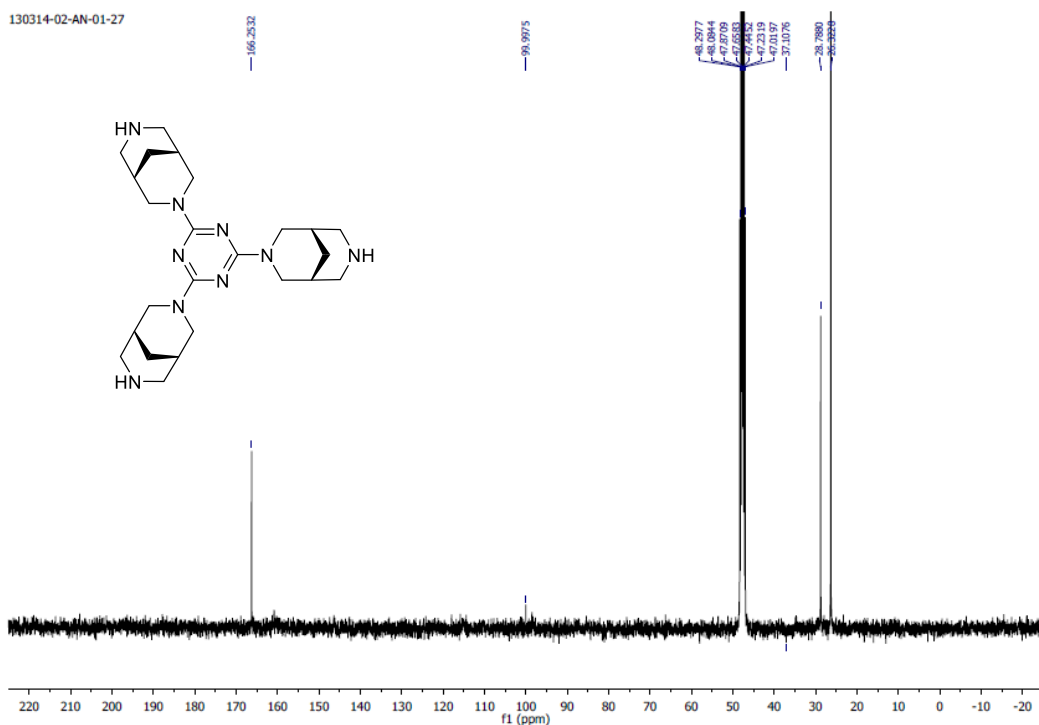
Appendix 3A.16: ^1H NMR spectrum of **12** in MeOH-*d*₄.



Appendix 3A.17: ^{13}C NMR spectrum of **12** in $\text{MeOH-}d_4$.



Appendix 3A.18: ^1H NMR spectrum of **3** in $\text{MeOH-}d_4$.



Appendix 3A.19: ^{13}C NMR spectrum of **3** in $\text{MeOH-}d_4$.

3A.6. References

- (a) Gale, P. A.; Busschaert, N.; Haynes, C. J. E.; Karagiannidis, L. E.; Kirby, I. L. *Chem. Soc. Rev.* **2014**, *43*, 205-241; (b) Kim, S. K.; Sessler, J. L. *Chem. Soc. Rev.* **2010**, *39*, 3784-3809; (c) Gale, P. A. *Chem. Commun.* **2011**, *47*, 82-86; (d) Haynes, C. J. E.; Gale, P. A. *Chem. Commun.* **2011**, *47*, 8203-8209; (e) Robertson, J. W. F.; Kasianowicz, J. J.; Banerjee, S. *Chem. Rev.* **2012**, *112*, 6227-6249; (f) Matile, S.; Vargas Jentsch, A.; Montenegro, J.; Fin, A. *Chem. Soc. Rev.* **2011**, *40*, 2453-2474.
- Jentsch, T. J.; Stein, V.; Weinreich, F.; Zdebik, A. A., *Molecular Structure and Physiological Function of Chloride Channels.* **2002**, *82*, 503-568.
- (a) Duran, C.; Thompson, C. H.; Xiao, Q.; Hartzell, C. *Annu. Rev. physiol.* **2010**, *72*, 95-121; (b) Benz, R.; Hancock, R. E. W. *J. Gen. Physiol.* **1987**, *89*, 275-95.
- Bukovnik, U.; Sala-Rabanal, M.; Francis, S.; Frazier, S. J.; Schultz, B. D.; Nichols, C. G.; Tomich, J. M. *Mol. Pharm.* **2013**, *10*, 3959-3966.
- (a) Sessler, J. L.; Eller, L. R.; Cho, W.-S.; Nicolaou, S.; Aguilar, A.; Lee, J. T.; Lynch, V. M.; Magda, D. J. *Angew. Chem., Int. Ed.* **2005**, *44*, 5989-5992; (b) Sato, T.; Konno, H.; Tanaka, Y.; Kataoka, T.; Nagai, K.; Wasserman, H. H.; Ohkuma, S. *J. Biol. Chem.* **1998**, *273*, 21455-21462; (c) Ohkuma, S.; Sato, T.; Okamoto, M.; Matsuya, H.; Arai, K.; Kataoka, T.; Nagai, K.; Wasserman, H. H. *Biochem. J.* **1998**, *334*, 731-741; (d) Matsuyama, S.; Llopis, J.; Deveraux, Q. L.; Tsien, R. Y.; Reed, J. C. *Nat. Cell Biol.* **2000**, *2*, 318-325; (e) Seganish, J. L.; Davis, J. T. *Chem. Commun.* **2005**, 5781-5783; (f) Saha, T.; Hossain, M. S.; Saha, D.; Lahiri, M.; Talukdar, P. *J. Am. Chem. Soc.* **2016**, *138*, 7558-7567;

- (g) Moore, S. J.; Haynes, C. J. E.; Gonzalez, J.; Sutton, J. L.; Brooks, S. J.; Light, M. E.; Herniman, J.; Langley, G. J.; Soto-Cerrato, V.; Perez-Tomas, R.; Marques, I.; Costa, P. J.; Felix, V.; Gale, P. A. *Chem. Sci.* **2013**, *4*, 103-117; (h) Moore, S. J.; Wenzel, M.; Light, M. E.; Morley, R.; Bradberry, S. J.; Gomez-Iglesias, P.; Soto-Cerrato, V.; Perez-Tomas, R.; Gale, P. A. *Chem. Sci.* **2012**, *3*, 2501-2509.
6. (a) Gorteau, V.; Bollot, G.; Mareda, J.; Perez-Velasco, A.; Matile, S. *J. Am. Chem. Soc.* **2006**, *128*, 14788-14789; (b) Gorteau, V.; Bollot, G.; Mareda, J.; Matile, S. *Org. Biomol. Chem.* **2007**, *5*, 3000-3012; (c) Perez-Velasco, A.; Gorteau, V.; Matile, S. *Angew. Chem., Int. Ed.* **2008**, *47*, 921-923; (d) Vargas Jentzsch, A.; Emery, D.; Mareda, J.; Metrangolo, P.; Resnati, G.; Matile, S. *Angew. Chem., Int. Ed.* **2011**, *50*, 11675-11678; (e) Jentzsch, A. V.; Emery, D.; Mareda, J.; Nayak, S. K.; Metrangolo, P.; Resnati, G.; Sakai, N.; Matile, S. *Nat. Commun.* **2012**, *3*, 905; (f) Gale, P. A.; Light, M. E.; McNally, B.; Navakhun, K.; Sliwinski, K. E.; Smith, B. D. *Chem. Commun.* **2005**, 3773-3775; (g) McNally, B. A.; Koulov, A. V.; Smith, B. D.; Joos, J.-B.; Davis, A. P. *Chem. Commun.* **2005**, 1087-1089; (h) Xin, P.; Zhu, P.; Su, P.; Hou, J.-L.; Li, Z.-T. *J. Am. Chem. Soc.* **2014**, *136*, 13078-13081; (i) Lee, J. H.; Lee, J. H.; Choi, Y. R.; Kang, P.; Choi, M.-G.; Jeong, K.-S. *J. Org. Chem.* **2014**, *79*, 6403-6409; (j) Choi, Y. R.; Kim, G. C.; Jeon, H.-G.; Park, J.; Namkung, W.; Jeong, K.-S. *Chem. Commun.* **2014**, *50*, 15305-15308; (k) Lee, E.-B.; Ryu, H.; Lee, I.; Choi, S.; Hong, J.-H.; Kim, S. M.; Jeon, T.-J.; Cho, D.-G. *Chem. Commun.* **2015**, *51*, 9339-9342; (l) Elmes, R. B. P.; Busschaert, N.; Czech, D. D.; Gale, P. A.; Jolliffe, K. A. *Chem. Commun.* **2015**, *51*, 10107-10110; (m) Madhavan, N.; Robert, E. C.; Gin, M. S. *Angew. Chem., Int. Ed.* **2005**, *44*, 7584-7587; (n) Le Duc, Y.; Michau, M.; Gilles, A.; Gence, V.; Legrand, Y.-M.; van der Lee, A.; Tingry, S.; Barboiu, M. *Angew. Chem., Int. Ed.* **2011**, *50*, 11366-11372; (o) Benz, S.; Macchione, M.; Verolet, Q.; Mareda, J.; Sakai, N.; Matile, S. *J. Am. Chem. Soc.* **2016**, *138*, 9093-9096.
7. Kuswandi, B.; Nuriman ; Verboom, W.; Reinhoudt, D. *Sensors* **2006**, *6*, 978-1017.
8. Caltagirone, C.; Mulas, A.; Isaia, F.; Lippolis, V.; Gale, P. A.; Light, M. E. *Chem. Commun.* **2009**, 6279-6281.
9. Lee, S.; Hua, Y.; Park, H.; Flood, A. H. *Org. Lett.* **2010**, *12*, 2100-2102.
10. (a) Frontera, A.; Gamez, P.; Mascal, M.; Mooibroek, T. J.; Reedijk, J. *Angew. Chem., Int. Ed.* **2011**, *50*, 9564-9583; (b) Cotelle, Y.; Benz, S.; Avestro, A.-J.; Ward, T. R.; Sakai, N.; Matile, S. *Angew. Chem., Int. Ed.* **2016**, *55*, 4275-4279; (c) Wang, D.-X.; Wang, M.-X. *J. Am. Chem. Soc.* **2013**, *135*, 892-897; (d) Wang, D.-X.; Zheng, Q.-Y.; Wang, Q.-Q.; Wang, M.-X. *Angew. Chem., Int. Ed.* **2008**, *47*, 7485-7488; (e) Wang, X.-D.; Li, S.; Ao, Y.-F.; Wang, Q.-Q.; Huang, Z.-T.; Wang, D.-X. *Org. Biomol. Chem.* **2016**, *14*, 330-334.
11. Marvin 5.8.0, **2012**, ChemAxon (<http://www.chemaxon.com>).
12. Haridas, V.; Sadanandan, S.; Sharma, Y. K.; Chinthalapalli, S.; Shandilya, A. *Tetrahedron Lett.* **2012**, *53*, 623-626.
13. Eibl, C.; Munoz, L.; Tomassoli, I.; Stokes, C.; Papke, R. L.; Gündisch, D. *Bioorg. Med. Chem.* **2013**, *21*, 7309-7329.
14. (a) Sakai, N.; Matile, S. *J. Am. Chem. Soc.* **2003**, *125*, 14348-14356; (b) Talukdar, P.; Bollot, G.; Mareda, J.; Sakai, N.; Matile, S. *J. Am. Chem. Soc.* **2005**, *127*, 6528-6529; (c) Saha, T.; Roy, A.; Gening, M. L.; Titov, D. V.; Gerbst, A. G.; Tsvetkov, Y. E.; Nifantiev, N. E.; Talukdar, P. *Chem. Commun.* **2014**, *50*, 5514-5516; (d) Saha, T.; Dasari, S.; Tewari, D.; Prathap, A.; Sureshan, K. M.; Bera, A. K.; Mukherjee, A.; Talukdar, P. *J. Am. Chem. Soc.* **2014**, *136*, 14128-14135; (e) Roy, A.;

- Saha, T.; Gening, M. L.; Titov, D. V.; Gerbst, A. G.; Tsvetkov, Y. E.; Nifantiev, N. E.; Talukdar, P. *Chem. Eur. J.* **2015**, *21*, 17445-17452.
15. (a) Benz, R.; McLaughlin, S. *Biophys. J.* **1983**, *41*, 381-398; (b) Sakai, N.; Brennan, K. C.; Weiss, L. A.; Matile, S. *J. Am. Chem. Soc.* **1997**, *119*, 8726-8727.
 16. Rose, L.; Jenkins, A. T. A. *Bioelectrochemistry* **2007**, *70*, 387-393.
 17. (a) Lisbjerg, M.; Valkenier, H.; Jessen, B. M.; Al-Kerdi, H.; Davis, A. P.; Pittelkow, M. *J. Am. Chem. Soc.* **2015**, *137*, 4948-4951; (b) Cooper, J. A.; Street, S. T. G.; Davis, A. P. *Angew. Chem., Int. Ed.* **2014**, *53*, 5609-5613; (c) Edwards, S. J.; Valkenier, H.; Busschaert, N.; Gale, P. A.; Davis, A. P. *Angew. Chem., Int. Ed.* **2015**, *54*, 4592-4596; (d) Judd, L. W.; Davis, A. P. *Chem. Commun.* **2010**, *46*, 2227-2229.
 18. Cranwell, P. B.; Hiscock, J. R.; Haynes, C. J. E.; Light, M. E.; Wells, N. J.; Gale, P. A. *Chem. Commun.* **2013**, *49*, 874-876.
 19. a) SAINT Plus, (Version 7.03); Bruker AXS Inc.: Madison, WI, **2004**; b) G. M. Sheldrick, SHELXTL, Reference Manual: version 5.1: Bruker AXS; Madison, WI, **1997**; c) G. M. Sheldrick, *Acta Crystallogr. Sect. A*, 2008, 112; d) WINGX version 1.80.05 Louis Farrugia, University of Glasgow; e) A. L. Spek, PLATON, A Multipurpose Crystallographic Tool, Utrecht University, Utrecht, The Netherlands, **2005**.
 20. H. J. C. Berendsen, J. P. M. Postma, W. F. van Gunsteren, J. Hermans, Interaction Models for Water in Relation to Protein Hydration. *In Intermolecular Forces*; Pullman, B., Ed.; Reidel: Dordrecht, **1981**, 331-342.
 21. C. Oostenbrink, A. Villa, A.E. Mark, W. F. van Gunsteren, *J. Comput. Chem.* **2004**, *25*, 1656-1676.
 22. A. K. Malde, L. Zuo, M. Breeze, M. Stroet, D. Poger, P.C. Nair, C. Oostenbrink, A. E. Mark, *J. Chem. Theory Comput.* **2011**, *7*, 4026-4037.
 23. T. Schlick, *Molecular Modeling and Simulation: An Interdisciplinary Guide*. 2nd ed.; Springer: New York, **2010**.
 24. S. Nosé, *Mol. Phys.* **1984**, *52*, 255 -268.
 25. W. G. Hoover, *Phys. Rev. A* **1985**, *31*, 1695-1697.
 26. M. Parrinello, A. Rahman, *J. Appl. Phys.* **1981**, *52*, 7182-7190.
 27. T. Darden, D. York, L. Pedersen, *J. Chem. Phys.* **1993**, *98*, 10089-10092.

Chapter 3B

One-pot Synthesis and Transmembrane Chloride
Transport Properties of C₃-Symmetric Benzoxazine
Urea

3B.1. Introduction

The transport of anions across cell membrane plays very crucial role in several biological processes such as signal transduction, control of intracellular pH, regulation of cell volume, stabilization of resting membrane potential, and fluid transport in epithelia.¹ Over the past decade, there has been an emerging interest in the design of small molecules that facilitate transmembrane anion transport, particularly chloride, bicarbonate and sulfate.² This interest in synthetic chloride transporters has encouraged, mainly by the realization that misregulated chloride transport across cell membranes can lead to potential diseases (*i.e.* “channelopathies”) including cystic fibrosis, Dent’s disease, myotonia, epilepsy, etc.³ Thus it is very important to recognize the actions of artificial transport systems to treat channelopathies, by overcoming the missing activities of natural transporters, and such a destined goal is still unfulfilled.⁴ Therefore designs of synthetic small molecules are progressively gaining pertinence as these small molecules can mimic the activity and mechanism of transport of natural ionophores. Some of the synthetic anionophores are already recognized to have intriguing pharmacological activities as some of them have potential immunosuppressive, antimalarial, antineoplastic and antimicrobial activities at concentrations below their cytotoxicity level to healthy cells.^{1b, 5}

A common approach to design small molecule anion transporters are based on hydrogen-bond donor groups such as amide, urea, thiourea etc., and often these groups allow multiple cooperative interactions with the anion.⁶ Therefore, we realized that affinity towards anion can be increased, and profoundly tuned by providing the receptor with several hydrogen-bond donor groups which can be systematically exploited to obtain transmembrane anion transport very effectively. Hydrogen bond-forming ability of amide and urea are very crucial in the supramolecular chemistry because these residues can be used either in self-assembly or ion recognition. Supramolecular assembly of these residues were applied for forming ion channels where the cavity allowed either cation or water transport.⁷ Urea derivatives are superior in comparison to an amide as anion recognizing residues owing to more acidic N–H groups. Therefore, these groups were used further in the designs of dipodal and tripodal anion carriers to take the advantage of cooperative H-bonding interactions.^{1c, 6c, 8} However, the designs of tripodal anion carriers with a high degree of preorganization are rare,⁹ and mostly constructed on a preexisting rigid core moiety, *e.g.* cholic acid.^{1c, 8c} We, on the other hand, aimed the design of new

tripodal anion transporters by the facile construction of the rigid core. This strategy was envisaged to allow efficient synthesis and manipulation of transport activity of anionophores based on the selection of recognizing arms. Herein we report the design, synthesis and ion transport behavior of new tripodal receptors **1-2** based on the C_3 -symmetric benzoxazine core, and anion recognizing arms composed of either amide or urea moieties (Figure 3B.1A). As stated above, the tris-urea based receptor **2** was predicted to be better anion receptor compared to the tris-amide based receptor **1** due to its more acidic N–H groups (Figure 3B.1A).

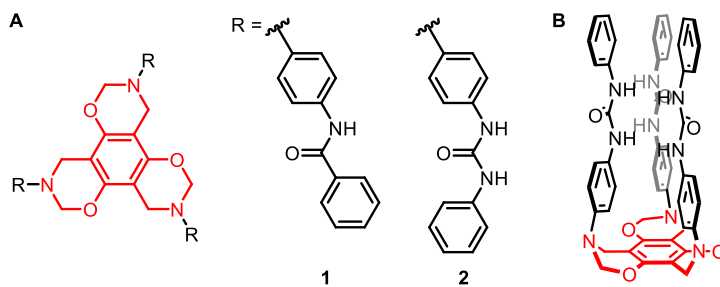
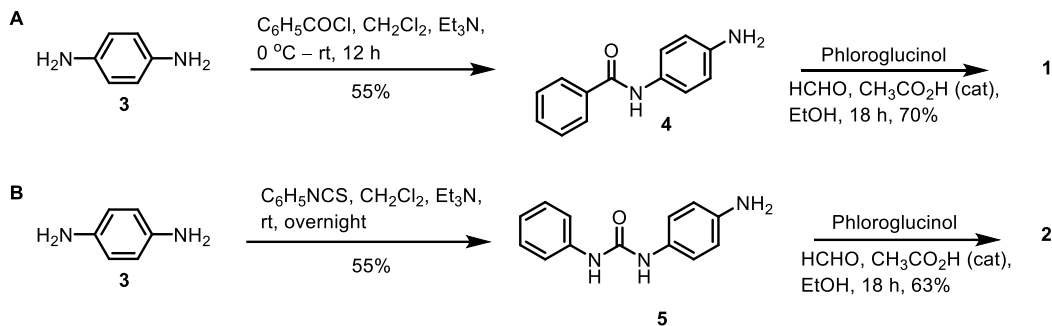


Figure 3B.1: A) Structures of C_3 -symmetric tripodal receptors **1-2** and B) representation of the anion binding cavity of **2**.

3B.2. Results and Discussions

3B.2.1. Synthesis

Syntheses of tripodal molecules **1** and **2** were initiated from *p*-phenylenediamine **3** (Scheme 3B.1). Compound **3** was converted to amide **4** upon reaction with benzoyl chloride with 55% yield.¹⁰ The amide **4** was then reacted with phloroglucinol in presence of formaldehyde and catalytic amount of acetic acid in EtOH following the protocol reported by Singh *et al*¹¹ to obtain the receptor **1** in 70% yield (for ^1H and ^{13}C -NMR spectrum, see Appendix 3B.6 and 3B.7 respectively). In this step, each arm was linked to the core through the Mannich aminomethylation and a sequential ring closure condensation. Synthesis of the urea arm **5** was carried by reaction of compound **3** and phenylisocyanate in CH_2Cl_2 with 55% yield.¹² Reaction of urea **5**, phloroglucinol, formaldehyde and catalytic amount of acetic acid in EtOH, following aforementioned protocol provided tripodal urea **2** in 63% yield (for ^1H and ^{13}C -NMR spectrum, see Appendix 3B.8 and 3B.9 respectively).



Scheme 3B.1: Synthesis of tripodal receptors **1–2**.

3B.2.2. Binding Study

The Cl^- binding with tripodal receptors **1–2** were evaluated by $^1\text{H-NMR}$ spectroscopy in $\text{DMSO-}d_6$.¹³ Upon addition of tetrabutylammonium chloride (TBACl), a significant downfield shift ($\Delta\delta \sim 0.8$ ppm) of N–H signals were observed for urea receptor **2** while corresponding change for amide receptor **1** was negligible (Figure 3B.5). Job plot analysis¹⁴ for compound **2** provided 1:1 (host : guest) stoichiometry (Figure 3B.3B) and subsequently the stability constant¹⁵ = 335 M^{-1} was determined (Figure 3B.2) by fitting in the 1:1 model of WineQNMR program (Appendix 3B.5).

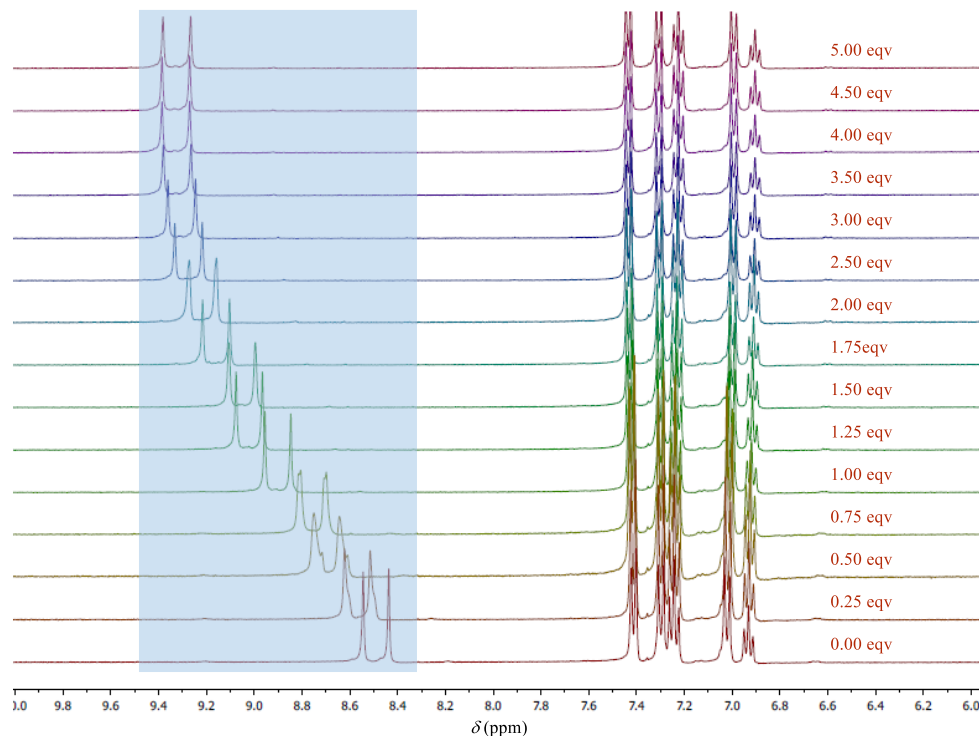


Figure 3B.2: Stack plot of $^1\text{H-NMR}$ ($\text{DMSO-}d_6$) of **2** upon addition of increasing amounts of TBACl.

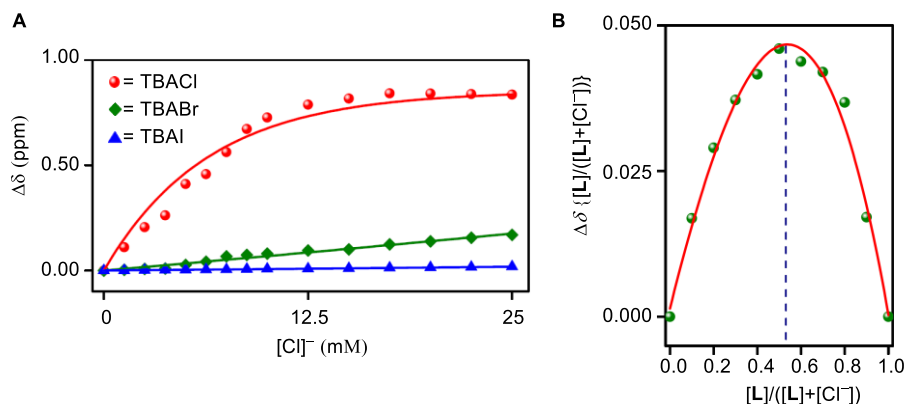


Figure 3B.3: A) Shift of the N–H protons of **2** upon addition of TBACl, TBABr and TBAI in DMSO- d_6 and B) Job plot of receptor **2** (**L**) with TBACl in DMSO- d_6 .

However, very weak and negligible binding were observed for **2** with TBABr (Appendix 3B.3) and TBAI (Appendix 3B.4), respectively (Figure 3B.3A). For receptor **1**, the binding constant with chloride could not be determined because of insignificant change observed for the N–H proton (Figure 3B.4). These results indicate much stronger bonding of tripodal compound **2** compared to **1** with Cl^- ion due to presence of higher number of hydrogen-bond donor groups in this system.

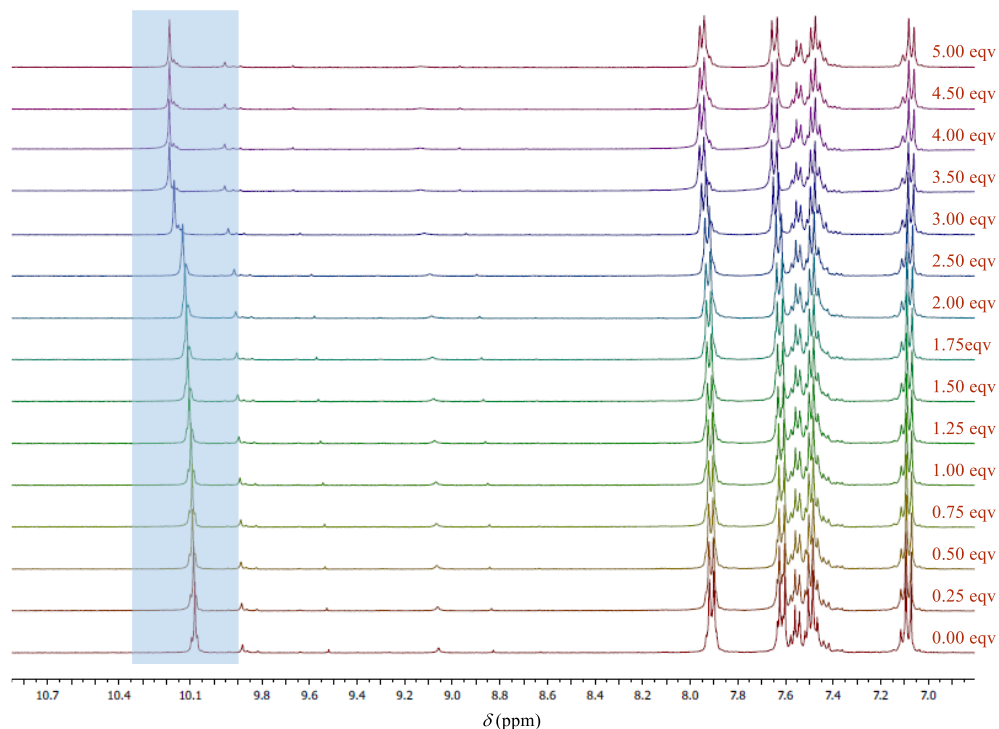


Figure 3B.4: Stack plot of 1H -NMR (DMSO- d_6) of **1** upon addition of increasing amounts of TBACl.

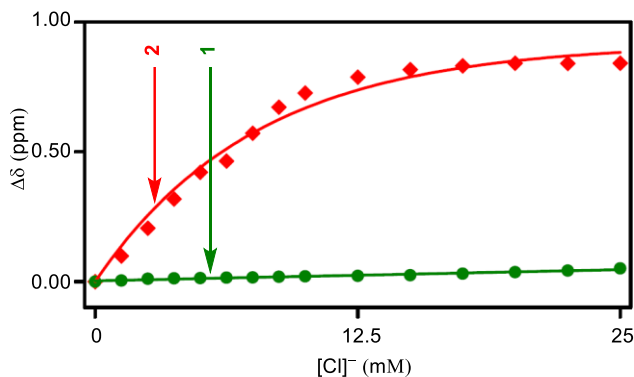


Figure 3B.5: Shift of the N–H protons of receptors **1** and **2** upon addition of TBACl in DMSO- d_6 .

3B.2.3. Ion Transport Activity Study

Ion transport properties of compounds **1** and **2** across large unilamellar vesicles (LUVs), prepared from egg yolk phosphatidylcholine (EYPC) lipid with encapsulated with pH sensitive fluorescent dye 8-hydroxypyrene-1,3,6-trisulfonate (HPTS),^{5a, 16} were determined by applying a pH gradient, $\Delta \text{pH} = 0.8$ ($\text{pH}_{\text{in}} = 7.0$ and $\text{pH}_{\text{out}} = 7.8$). Upon the addition of each compound, the transport activity was measured through the collapse of the applied pH gradient *i.e.* via either H^+ efflux or OH^- influx. Ion transport activity of receptor **2** was found to be superior compared to the receptor **1** (Figure 3B.6A). Concentration dependent ion transport ability of **2** (Figure 3B.6B) provided $EC_{50} = 8.2 \mu\text{M}$ and Hill coefficient $n = 1.4$ (Figure 3B.6C) when dose-response analysis was carried out from concentration dependent assay by taking normalized values at $t = 10$ s. These data indicated that one molecule of **2** is involved in the active structure formation. For receptor **1**, the Hill coefficient could not be obtained due to its low activity.

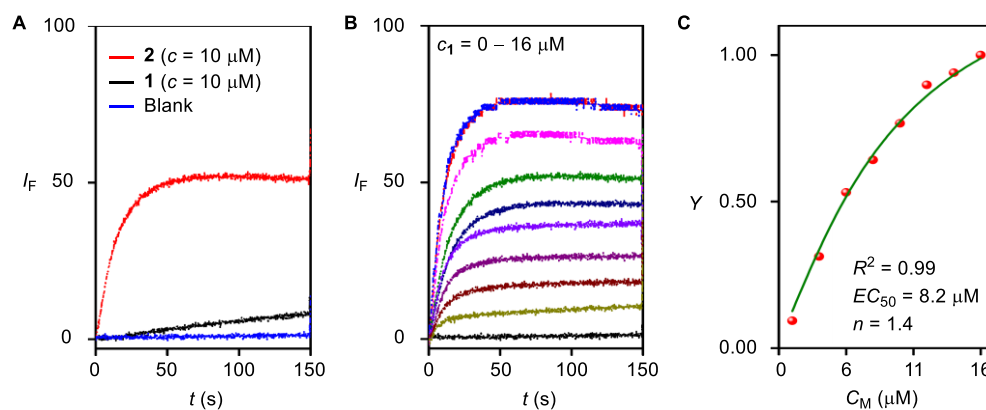


Figure 3B.6: **A)** Comparison of ion transport activity for receptors **1–2**, **B)** concentration profile of receptor **2**, presented as a function of time with their normalized emission intensity I_F and **C)** representation of Hill plot for tripodal receptor **2**.

Based on the aforementioned ion transport activity of receptor **2**, its ability to discriminate among different ions was evaluated across EYPC-LUVs with entrapped HPTS.¹⁷ Replacement of the extravesicular NaCl with iso-osmolar MCl ($M^+ = \text{Li}^+, \text{K}^+, \text{Rb}^+, \text{and Cs}^+$) did not cause any significant change in the transport activity of **2** (Figure 3B.7A). However, the changes provoked by different iso-osmolar extravesicular anions NaA ($A^- = \text{Cl}^-, \text{Br}^-, \text{I}^-, \text{NO}_3^-, \text{SCN}^-, \text{and ClO}_4^-$) exchange were clearly stronger (Figure 3B.7B) with the selectivity sequence, $\text{Cl}^- > \text{NO}_3^- > \text{Br}^- > \text{I}^- > \text{SCN}^- > \text{ClO}_4^-$. The observed selectivity sequence for anion could be outcome of several processes such as (1) either OH^-/Cl^- exchange or H^+/Cl^- co-transport due to pH gradient; (2) either Cl^-/A^- exchange induced by anion gradient, followed by OH^-/A^- exchange or H^+/A^- co-transport encouraged by pH gradient, and (3) either OH^-/A^- exchange or H^+/A^- co-transport against pH gradient. In order to determine the correct mechanism, ion transport studies were done with identical intravesicular and extravesicular buffer solution by varying only the anions (Figure 3B.7C). The observed data suggests same selectivity sequence ($\text{Cl}^- > \text{NO}_3^- > \text{Br}^- > \text{I}^- > \text{SCN}^- > \text{ClO}_4^-$) ruling out all other possibilities, and establishing OH^-/A^- exchange as the primary transport mechanism.

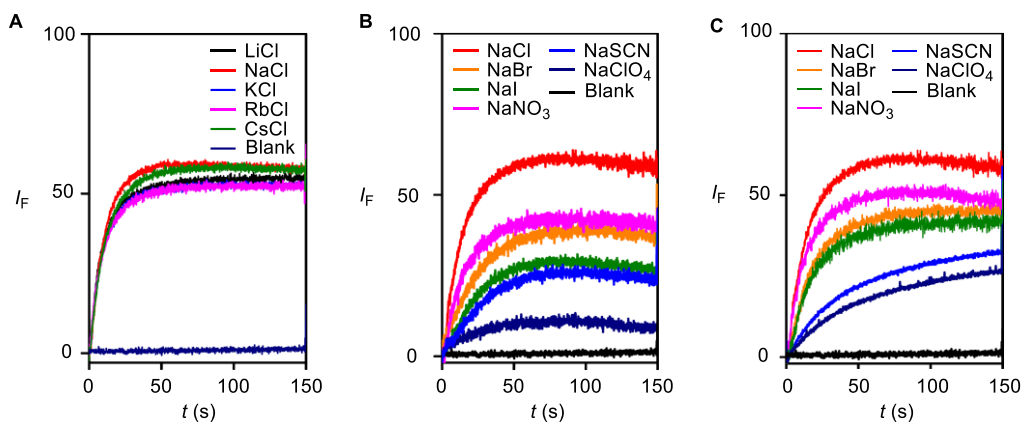


Figure 3B.7: Effect of extravesicular **A)** cations and **B)** anions on ion transport by **2** and **C)** anion selectivity of compound **2** was determined with identical intravesicular and extravesicular anions A^- across EYPC-LUVs with entrapped HPTS.

To gain additional evidence of Cl^- selectivity of tripodal transporter **2**, Cl^- leakage studies were performed across EYPC-LUVs with entrapped lucigenin dye.^{6c, 18} With iso-osmolar intravesicular and extravesicular NaNO_3 (200 mM), an external pulse of NaCl (25 mM) was applied. The influx of Cl^- upon addition of compound **2** was monitored through the decay in

lucigenin fluorescence. The concentration dependent activity profile of compound **2** (Figure 3B.8A) provided the initial rate $I_R = 0.026 \text{ s}^{-1}$ and half-life $t_{1/2} = 57 \text{ s}$ indicating fast Cl^- transport by compound **2** ($14 \mu\text{M}$). Replacement of extravesicular NaCl with MCl ($\text{M}^+ = \text{Li}^+, \text{Na}^+, \text{K}^+, \text{Rb}^+$ and Cs^+) resulted in no significant change in Cl^- influx rate (Figure 3B.8B) suggesting that the M^+/Cl^- symport mechanism is not operative during the ion transport by compound **2**. To understand the effect of anions, LUVs prepared with NaCl (200 mM) were dispersed in NaX (200 mM , $\text{X}^- = \text{NO}_3^-, \text{HCO}_3^-, \text{and } \text{SO}_4^{2-}$) and **2** was added. In this study, clear changes in the Cl^- rates were observed (Figure 3B.8C). The resulting trend of anion influx confirms the Cl^-/X^- antiport as the main transport mechanism working during the ion transport by compound **2**.

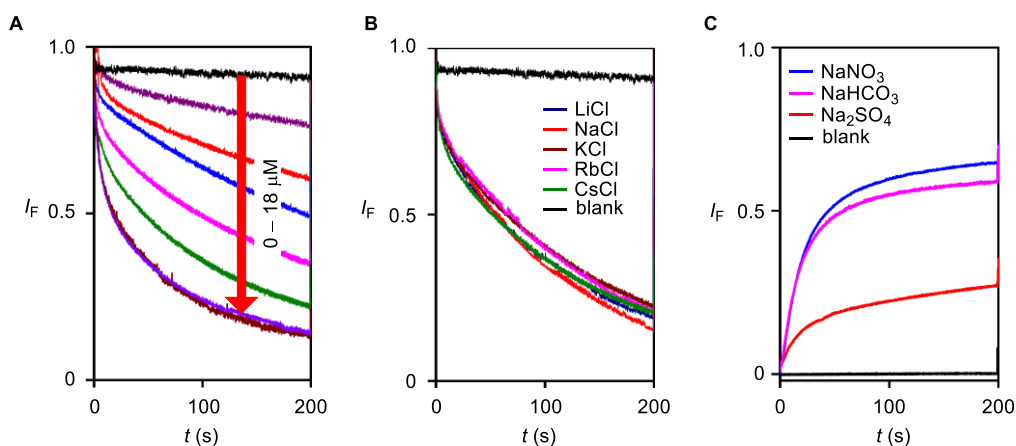


Figure 3B.8: A) Cl^- Influx by **2** across EYPC-LUVs with entrapped lucigenin, B) effect of extravesicular cations on Cl^- influx by **2** and C) effect of extravesicular anions on Cl^- efflux by **2**.

The Cl^- transport by tripodal compound **2** was further studied in presence of valinomycin, an efficient K^+ carrier.¹⁹ LUVs were prepared from EYPC with entrapped lucigenin (1 mM), iso-osmolar intra- and extravesicular NaNO_3 (200 mM). Subsequently, an extravesicular KCl (25 mM) pulse was applied prior to each experiment. Addition of valinomycin (100 nM) did not show any quenching of lucigenin fluorescence. However the receptor **2** ($10 \mu\text{M}$), in the presence of valinomycin (100 nM), exhibited significant quenching of lucigenin fluorescence as compared to quenching caused by **2** ($10 \mu\text{M}$) alone (Figure 3B.9A). These results further support that receptor **2** is an effective antiporter of anions. Evidence of the mobile carrier mechanism was derived from U-tube experiment using chloroform as an organic phase separating two aqueous phases, one containing the chloride salt and other with nitrate salt. Significant chloride transport through the

U-tube was monitored for 6 days with chloride selective electrode and obtained data indicated that **2** can operate via mobile carrier mechanism (Figure 3B.9B).

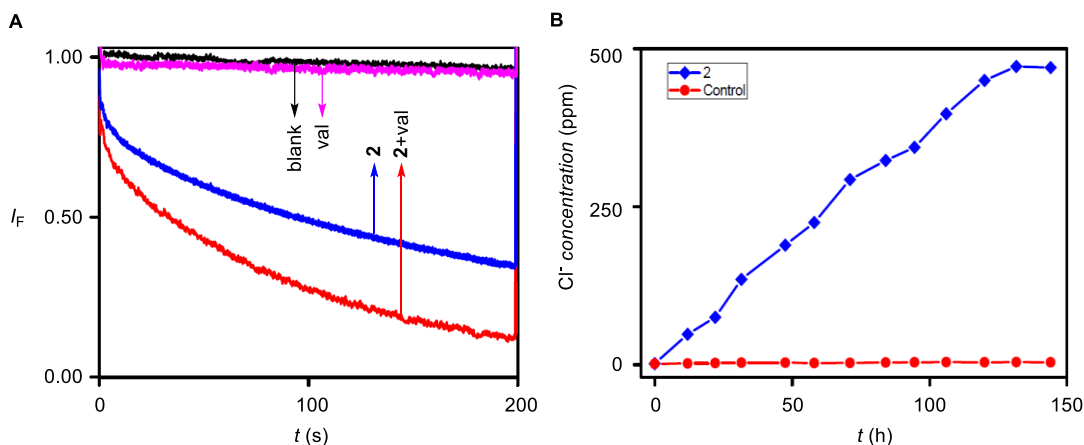


Figure 3B.9: A) Cl^- transport assay by lucigenin assay with valinomycin for **2** and B) Cl^- concentration in the aqueous receiving phase of U-tube experiments for **2** and without addition of compound and

3B.2.4. Mass Spectrometric Studies

The direct experimental evidence of affinity for Cl^- ion of compound **2** was established by Electrospray Ionization Mass Spectrometric (ESI-MS) studies in the negative mode. In this

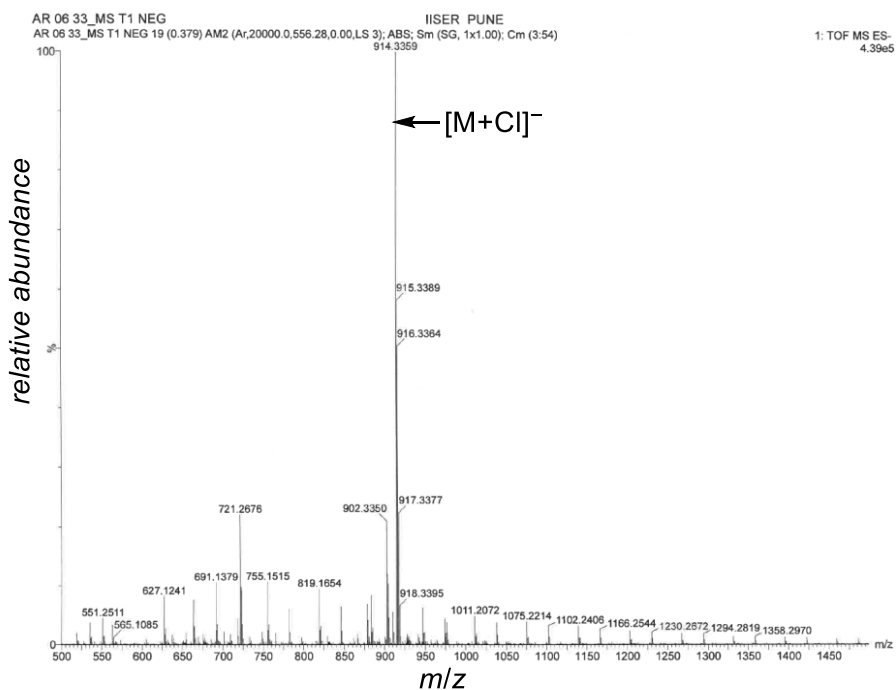


Figure 3B.10: ESI-MS spectrum recorded from of 1:1 molar mixture of receptor **2** and Me_4NCl prepared in acetonitrile.

experiment, solutions of **2** (10 μM) in acetonitrile, was mixed (in 1:3, 1:2, 1:1, 2:1, 3:1 molar ratios) and ESI-MS was recorded. Each set showed $m/z = 914.3359$ which corresponds to the adduct **2**+Cl⁻ confirming 1:1 Cl⁻ binding (Figure 3B.10).

3B.2.5. Molecular Dynamics Simulation Study

To determine the Cl⁻ bound structure of the molecule, the molecule was initially optimized along with a Cl⁻ ion using semi-empirical PM6 method²⁰ in Gaussian 09 program package.²¹ The optimized structure was then inserted inside a pre-equilibrated 1,2-dipalmitoyl-*sn*-phosphocholine (DPPC)/water lipid bilayer system. Initially position restraint was applied to the molecule and Cl⁻ ion, and the system was equilibrated for 1 ns at constant temperature and pressure. Then the restraint was removed and a 5 ns long simulation was carried out at same conditions. From analyzing the last 1 ns of the 5 ns trajectory we found that the Cl⁻ remained bound to the molecule with an average of five water molecules within 4 Å of the ion. The overall structure of the simulation box is shown in Figure 3B.11A. From cluster analysis of the 1 ns trajectory, the Cl⁻

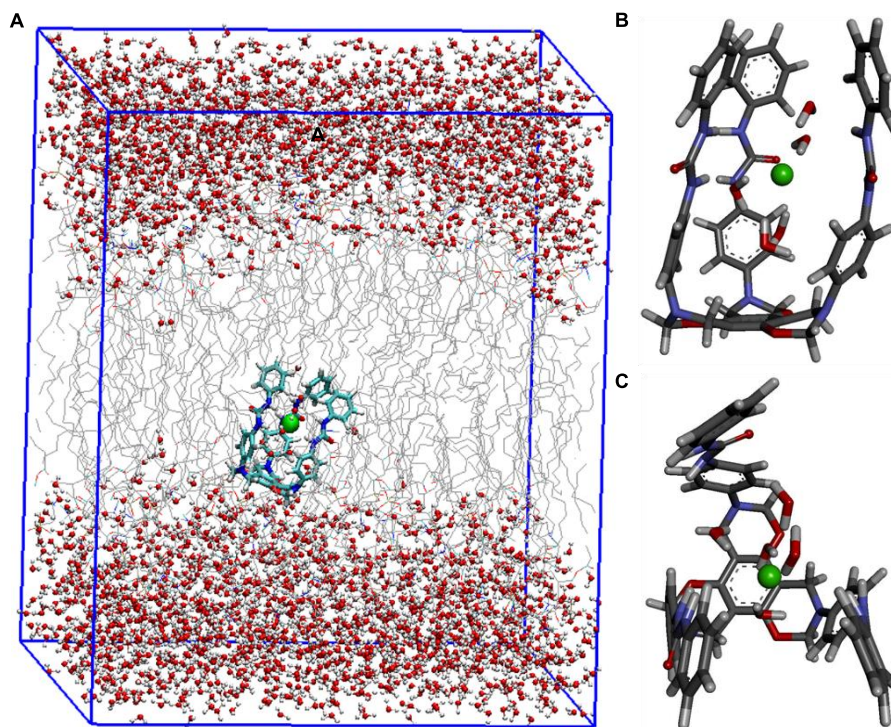


Figure 3B.11: **A)** The simulation box with the Cl⁻ (green sphere) bound molecule (shown in stick model) inserted inside DPPC lipid bilayer (gray lines). The water molecules are shown in ball and stick model with red and white. The Cl⁻ bound structure of **2** along with the H-bonded water molecules with **B)** side view and **C)** top view obtained from the MD simulation.

bound structure is obtained where water molecules were found to form H-bonds with the Cl^- ion. The water molecules also form H-bonded network, supported by the H-bonding with N-H, C=O, and aromatic ring of molecule (Figure 3B.11B and 3B.11C). All calculations were carried out by our collaborator Arnab Mukherjee and co-workers.

3B.3. Conclusion

In conclusion, we have developed new class of tripodal tris-amide and tris-urea based receptors which can mediate Cl^- transport across large unilamellar vesicles. These receptors were designed on a benzoxazine core, and synthesized in one-pot through the Mannich aminomethylation and a sequential ring closure condensation for connecting each arm. $^1\text{H-NMR}$ titrations in $\text{DMSO-}d_6$ revealed that the tris-urea is better as Cl^- ion binding receptor in comparison to the tris-amide derivative, and it also forms a 1:1 complex with the ion. Importantly, it was found that the tris-urea compound is also a more effective anion carrier with selectivity sequence: $\text{Cl}^- > \text{NO}_3^- > \text{Br}^- > \text{I}^- > \text{SCN}^- > \text{ClO}_4^-$, and the antiport mechanism during anion transport was also established. Molecular dynamics simulation suggests that the Cl^- ion binds to the polar cavity of the receptor assisted by hydrogen bonding from a few water molecules, which in turn forms hydrogen bonding to the polar groups of the receptor and among themselves.

3B.4. Experimental Section

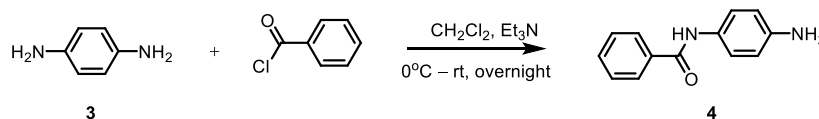
General Methods: All the reagents and fluorescent dyes including HPTS and lucigenin were purchased from commercial suppliers and used as received unless stated otherwise. All chemical reactions were performed under the nitrogen atmosphere. Solvents were dried by standard methods prior to use or purchased as dry grade solvents. Thin-layer chromatography (TLC) was carried out on aluminium sheets coated with E. Merck silica gel 60-F₂₅₄ and silica gel column chromatography was performed over silica gel (100-200 mesh) obtained from commercial suppliers. EYPC (Egg yolk phosphatidylcholine) was purchased from Avanti Polar Lipids as a solution in chloroform (25 mg/mL). HEPES buffer, Triton X-100, NaOH and all inorganic molecular biology grade salts were purchased from Sigma-Aldrich. Gel filtration chromatography was performed on a column of Sephadex G-50 with respective buffer solution or salt solution. Large unilamellar vesicles (LUV) were prepared by using mini extruder, equipped with a polycarbonate membrane of 100 nm (for

HPTS assay) or 200 nm (for lucigenin assay) pore size as per requirement, obtained from Avanti Polar Lipids.

Physical Measurements All ^1H - and ^{13}C -NMR spectra were recorded on 400 MHz Jeol ECS-400 or Bruker AMX-400 (or 100 MHz for ^{13}C) spectrometers using residual solvent signals as an internal reference on the δ scale relative to chloroform (δ 7.26), methanol (δ 3.31) and dimethylsulphoxide (δ 2.5 ppm) for ^1H -NMR and dimethylsulphoxide (δ 49.0 ppm) for ^{13}C -NMR. The chemical shifts (δ) are reported in ppm and coupling constants (J) are in Hz. The following abbreviations are used to explain the observed multiplicities: s (singlet), d (doublet) t (triplet) and m (multiplet). High-resolution mass spectra were obtained from by using a Bruker MicrOTOF-Q II XL spectrometer. Fluorescence spectra were recorded by using Fluoromax-4 from Jobin Yvon Edison equipped with a magnetic stirrer and an injector port. The pH of the buffer solution used for fluorescence experiment was adjusted by using NaOH with Helmer pH meter. FT-IR spectra were obtained using NICOLET 6700 FT-IR spectrophotometer as KBr disc and were reported in cm^{-1} . All melting points were measured in open glass capillary using a VEEGO Melting point and values are uncorrected. All data of fluorescence studies were normalised and processed by KaleidaGraph and Origin 8.5 softwares.

Synthesis Procedure:

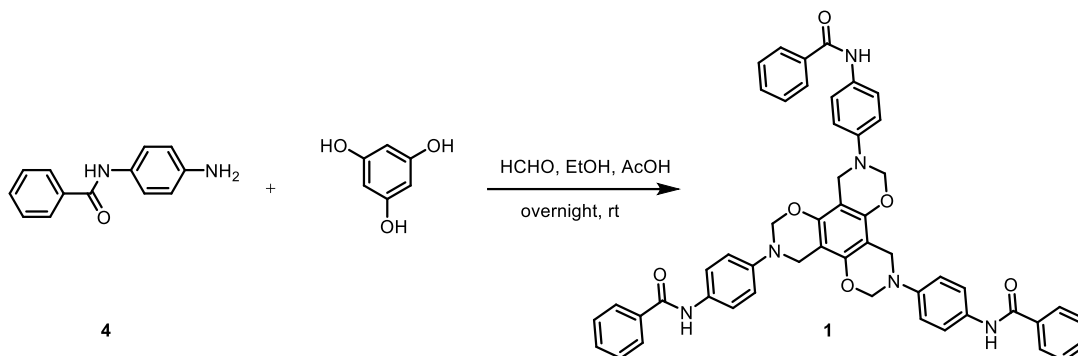
Synthesis of *N*-(4-aminophenyl)benzamide **4**:



Scheme 3B.2: Synthesis of compound **4**.

Compound **4** was prepared using reported procedure.²² In a 25 mL round bottom flask *p*-phenylenediamine **3** (200 mg, 1.85 mmol) was dissolved in dry CH_2Cl_2 (5 mL) and Et_3N (258 μL , 1.85 mmol) was added to it and then reaction mixture was cooled to 0°C . Benzoyl chloride (271 μL , 1.48 mmol) dissolved in dry CH_2Cl_2 (5 mL) was added to the reaction mixture dropwise and stirred overnight. Reaction was monitored by thin layer chromatography (TLC). After completion of reaction, solvent was evaporated from the reaction mixture and obtained brown crude solid was purified by flash column chromatography (2% $\text{MeOH}/\text{CHCl}_3$) to afford light brown solid compound **4**. Yield: 172 mg (55%). Obtained ^1H -NMR data is matching with reported data.

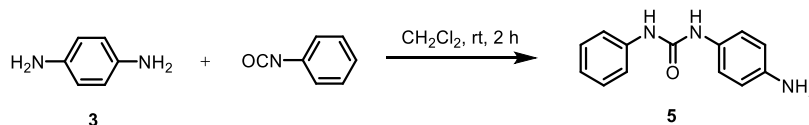
Synthesis of *N,N',N''*-((2*H*,6*H*,10*H*-benzo[1,2-*e*:3,4-*e'*:5,6-*e''*]tris([1,3]oxazine)-3,7,11(4*H*,8*H*,12*H*)-triyl)tris(benzene-4,1-diyl)tribenzamide **1**:



Scheme 3B.3: Synthesis of receptor **1**.

In a 25 mL round bottom flask, a mixture of phloroglucinol (14 mg, 0.12 mmol) and 37% aqueous formaldehyde solution (57 μ L, 0.72 mmol) was dissolved in EtOH (2 mL). Compound **4** (75 mg, 0.36 mmol) was dissolved in EtOH (2 mL) in another round bottom flask and was added to the reaction mixture slowly at room temperature and subsequently glacial acetic acid (70 μ L) was added. The reaction mixture was stirred for 12 h at room temperature. Reaction TLC was monitored with time with consumption of starting amine **4**. Precipitation was observed with due course of time in the reaction mixture. The solid precipitate was isolated by a simple filtration followed by washing with water, MeOH and finally with Et₂O. Obtained solid compound **1** was dried over vacuum (70 mg, 70%) as yellow solid. **M.p.:** 130 – 131 °C; **IR (KBr):** ν/cm^{-1} : 3328, 2908, 1655, 1601, 1533, 1457, 1408, 1316, 1254, 1083, 1001; **¹H-NMR (400 MHz, DMSO-*d*₆):** δ 10.08 (s, 1H), 7.90 (d, *J* = 7.2 Hz, 2H), 7.48 – 7.62 (m, 5H), 7.07 (d, *J* = 8.8 Hz, 2H), 5.41 (s, 2H), 4.38(s, 2H); **¹³C-NMR (100 MHz, DMSO-*d*₆):** δ 165.1, 149.6, 144.1, 134.9, 132.5, 131.3, 128.3, 128.5, 121.6, 117.7, 100.5, 79.1, 44.8; **HRMS (ESI):** Calcd. C₅₁H₄₂N₆O₆ [M+H]⁺: 835.3238; Found: 835.3248.

Synthesis of 1-(4-aminophenyl)-3-phenylurea **5:**

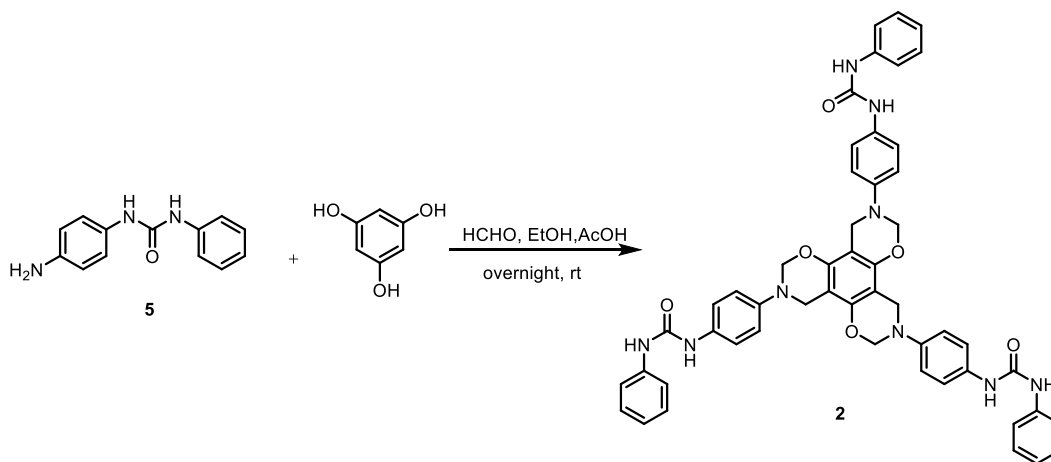


Scheme 3B.4: Synthesis of compound **5**.

Compound **5** was prepared using reported protocol.¹² In a 25 mL round bottom flask *p*-Phenylenediamine **3** (200 mg, 1.85 mmol) was dissolved in dry CH₂Cl₂ (5 mL) and

phenylisocyanate (222 μL , 2.03 mmol) dissolved in dry CH_2Cl_2 (5 mL) was added to the reaction mixture dropwise and stirred for 2 h at room temperature. After completion of reaction, solid compound was isolated through simple filtration and washed with CH_2Cl_2 and finally with pentane to afford white solid compound **5**. Yield: 210 mg (55%). Obtained $^1\text{H-NMR}$ data is matching with reported data.

Synthesis of 1,1',1''-((2*H*,6*H*,10*H*-benzo[1,2-*e*:3,4-*e'*:5,6-*e''*]tris([1,3]oxazine)-3,7,11(4*H*,8*H*,12*H*)-triyl)tris(benzene-4,1-diyl)tris(3-phenylurea) **2:**



Scheme 3B.5: Synthesis of compound **2**.

In a 25 mL round bottom flask, a mixture of phloroglucinol (6.8 mg, 0.05 mmol) and 37% aqueous formaldehyde solution (26.4 μL , 0.32 mmol) was dissolved in EtOH (2 mL). Compound **5** (37 mg, 0.16 mmol) was dissolved in EtOH (2 mL) in another round bottom flask and was added to the reaction mixture slowly at room temperature and subsequently glacial acetic acid (40 μL) was added. The reaction mixture was stirred for 12 h at room temperature. Reaction TLC was monitored with time with consumption of starting amine **5**. Precipitation was observed with due course of time in the reaction mixture. The solid precipitation was isolated by a simple filtration followed by washing with water, MeOH and finally with Et_2O . Obtained solid compound **2** was dried over vacuum (30 mg, 63%) as light yellow solid. **M.p.:** > 300 $^\circ\text{C}$; **IR (KBr):** ν/cm^{-1} : 3320, 2850, 1667, 1602, 1552, 1504, 1441, 1377, 1309, 1219, 1070; **$^1\text{H-NMR}$ (400 MHz, $\text{DMSO-}d_6$):** δ 8.54 (s, 1H), 8.44 (s, 1H), 7.40 (d, $J = 7.6$ Hz, 2H), 7.28 (d, $J = 9.2$ Hz, 2H), 7.22 (t, $J = 8.4$ Hz, 2H), 7.01 (d, $J = 9.2$ Hz, 2H), 6.90 (t, $J = 7.2$ Hz, 1H), 5.35 (s, 2H), 4.33 (s, 2H); **$^{13}\text{C-NMR}$ (100 MHz, $\text{DMSO-}d_6$):** δ 152.6, 149.6, 142.9, 139.8, 133.22, 128.7, 121.6, 119.6, 118.3, 118.0, 100.4, 79.3, 45.0; **HRMS (ESI):** Calcd. $\text{C}_{51}\text{H}_{45}\text{N}_9\text{O}_6$ $[\text{M}+\text{H}]^+$: 880.3568; Found: 880.3564.

Anion Binding by ¹H-NMR Titrations

¹H-NMR titrations for receptor 1: ¹H-NMR titration was carried out by successive addition of TBACl (from 300 mM stock) directly to the NMR tube containing receptor **1** (5 mM) in DMSO-*d*₆. The amide N-H of receptor **1** at $\delta = 10.08$ ppm was monitored and no significant change was observed with increasing concentration of TBACl (Figure 3B.4), TBABr (Appendix 3B.1), TBAI (Appendix 3B.2).

¹H-NMR titrations for receptor 2: ¹H-NMR titration was carried out by successive addition of TBACl (from 300 mM stock) directly to the NMR tube containing receptor **2** (5 mM) in DMSO-*d*₆. The ¹H-NMR signal of urea N-H for receptor **2** at $\delta = 8.54$ ppm and 8.44 ppm were monitored and significant change of urea N-H was observed with increasing concentration of TBACl (Figure 3B.2). A very minor change in urea N-H signal was observed for TBABr (Appendix 3B.3) and no significant change was observed for TBAI (Appendix 3B.4).

Job plot from continuous variation method: In order to determine the binding stoichiometry of the complex, a Job plot experiment was performed by the ¹H-NMR studies of the receptor with varying amount of chloride anion.¹⁴ Each stock solution of receptor (5 mM) and TBA⁺Cl⁻ (5 mM) was prepared in DMSO-*d*₆ at 25 °C. Ten NMR samples (500 μ L) were prepared with different proportions of the receptor (**L**) and chloride solution so that the total concentration of for each sample should be 2.5 mM. The change in the NMR signals of one of urea N-H at $\delta = 8.436$ ppm with the mole fraction of chloride is listed in Table 3B.1. The Job plot, shown in Figure 3B.3B, was obtained plotting $\Delta\delta([L]/([L] + [Cl^-]))$ with $([L]/([L] + [Cl^-]))$, indicating a 1:1 complex stoichiometry.

Table 3B.1: Data for the Job plot performed by continuous variation method in DMSO-*d*₆.

	TBACl (μ L)	L (μ L)	TBACl (mM)	L (mM)	$[L]/([Cl^-]+[L])$	δ (ppm)	$\Delta\delta$ (ppm)	Y Axis
1	450	50	2.025	0.225	0.1	8.605	0.169	0.0169
2	400	100	1.8	0.45	0.2	8.581	0.145	0.029
3	350	150	1.575	0.675	0.3	8.56	0.124	0.0372
4	300	200	1.35	0.9	0.4	8.54	0.104	0.0416
5	250	250	1.125	1.125	0.5	8.528	0.092	0.046
6	200	300	0.9	1.35	0.6	8.509	0.073	0.0438
7	150	350	0.675	1.575	0.7	8.497	0.061	0.0427
8	100	400	0.45	1.8	0.8	8.482	0.046	0.0368

9	50	450	0.225	2.025	0.9	8.455	0.019	0.0171
10	0	500	0	2.25	1	8.436	0	0

Determination of ion transport activity by HPTS Assay:²³

HEPES buffer, HPTS and stock solution preparation: Same protocol as discussed in Chapter 3A. Stock solutions of all molecules were prepared either by dissolving in HPLC grade DMSO (for HPTS assay) or DMF (for lucigenin Assay).

Preparation of EYPC-LUVs \Rightarrow HPTS: Same protocol as discussed in Chapter 3A.

Description of the ion transport activity assay: Same protocol as discussed in Chapter 3A.

The time axis was normalized according to Equation 1:

$$t = t - 100 \quad \text{(Equation 1)}$$

The time of tripodal receptor addition can be normalized to $t = 0$ s and time of Triton-X 100 addition was normalized to $t = 150$ s.

Time courses (F_t) were normalized to fractional emission intensity I_F using Equation 2.

$$\% \text{ Fl Intensity } (I_F) = [(F_t - F_0) / (F_\infty - F_0)] \times 100 \quad \text{(Equation 2)}$$

Where F_0 = Fluorescence intensity just before the tripodal molecule addition (at 0 s). F_∞ = Fluorescence intensity at saturation after complete leakage (at 275 s). F_t = Fluorescence intensity at time t . Concentration dependent experiment was carried out by increasing concentration of receptors. Addition of receptor 1 (30 μ M) did not show any significant increment in HPTS fluorescence however receptor 2 displayed strong ion transport activity in a concentration dependent manner.

The concentration profile data were further analyzed by Hill equation to get the Effective concentration (EC_{50}) and Hill coefficient (n) discussed in Chapter 3A.

Determination of ion Selectivity by HPTS assay:

Preparation of EYPC-LUVs \Rightarrow HPTS for cation selectivity: As described in Chapter 3A.

Preparation of EYPC-LUVs \Rightarrow HPTS for Anion Selectivity: As described in Chapter 3A.

Anion Selectivity Assay with Varied Extravesicular Buffer Solutions: Same as Chapter 3A.

Preparation of EYPC-LUVs \Rightarrow HPTS for Anion Selectivity with Identical Intravesicular and Extravesicular Buffer Solutions: Six different vesicles with six different buffers 10 mM HEPES, 100 mM NaX, at pH = 7.0; where, $X^- = Cl^-, Br^-, I^-, NO_3^-, SCN^-,$ and ClO_4^-) were prepared following same protocol as described in Chapter 3A.

Anion Selectivity Assay with Identical Intravesicular and Extravesicular Buffer Solutions:

In a clean and dry fluorescence cuvette 1975 μL of HEPES buffer (10 mM HEPES, 100 mM NaX, at pH = 7.0; where, $\text{X}^- = \text{Cl}^- \text{Br}^- , \text{I}^- , \text{NO}_3^- , \text{SCN}^-$ and ClO_4^-) was added followed by addition of 25 μL of EYPC-LUVs \supset HPTS vesicle containing same salt in slowly stirring condition by a magnetic stirrer equipped with the fluorescence instrument (at $t = 0$ s). HPTS fluorescence emission intensity (F_t) was monitored with time at $\lambda_{\text{em}} = 510$ nm ($\lambda_{\text{ex}} = 450$ nm). 20 μL of 0.5 M NaOH was added to the cuvette at $t = 20$ s to make the pH gradient between the intra and extra vesicular system. The transporter **2** was added at $t = 100$ s and at $t = 250$ s, of 10% Triton X-100 (25 μL) was added to lyse all vesicles for complete destruction of pH gradient (Figure 3B.7C).

For data analysis and comparison, time (X-axis) was normalized between the point of transporter addition (*i.e.* $t = 100$ s was normalized to $t = 0$ s) and end point of experiment (*i.e.* $t = 250$ s was normalized to $t = 150$ s).

Determination of chloride ion selectivity by lucigenin assay: ^{18b,13a}

Preparation of EYPC-LUVs \supset Lucigenin for concentration dependent assay and symport assay and preparation of EYPC-LUVs \supset Lucigenin for antiport study: Same as Chapter 3A.

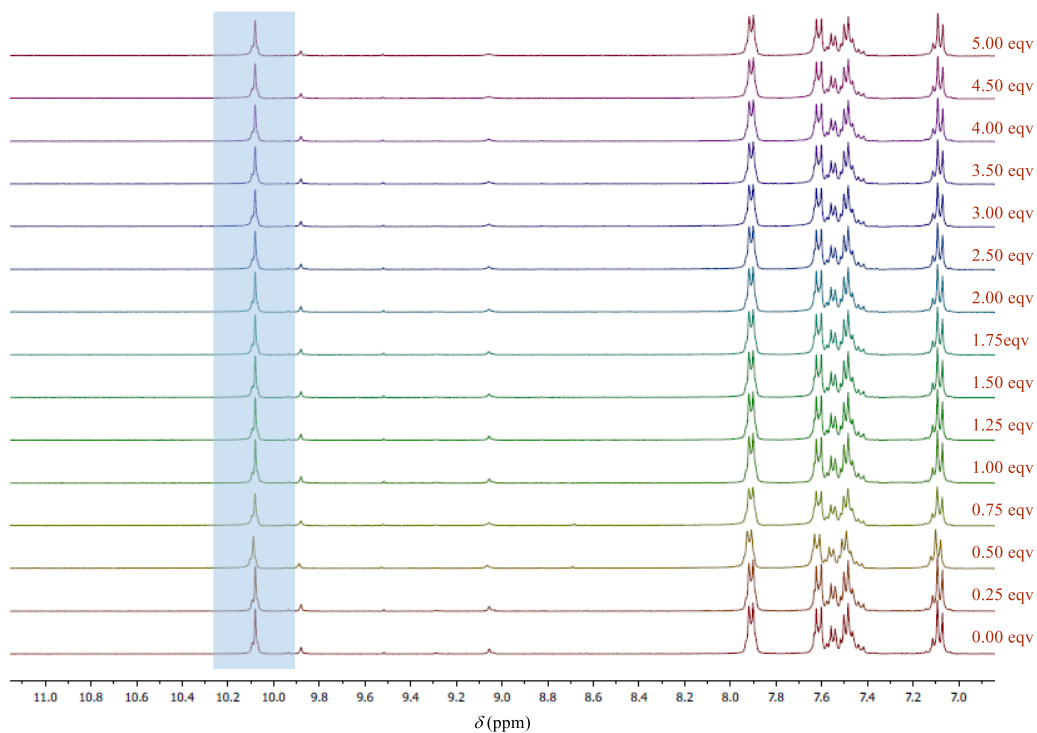
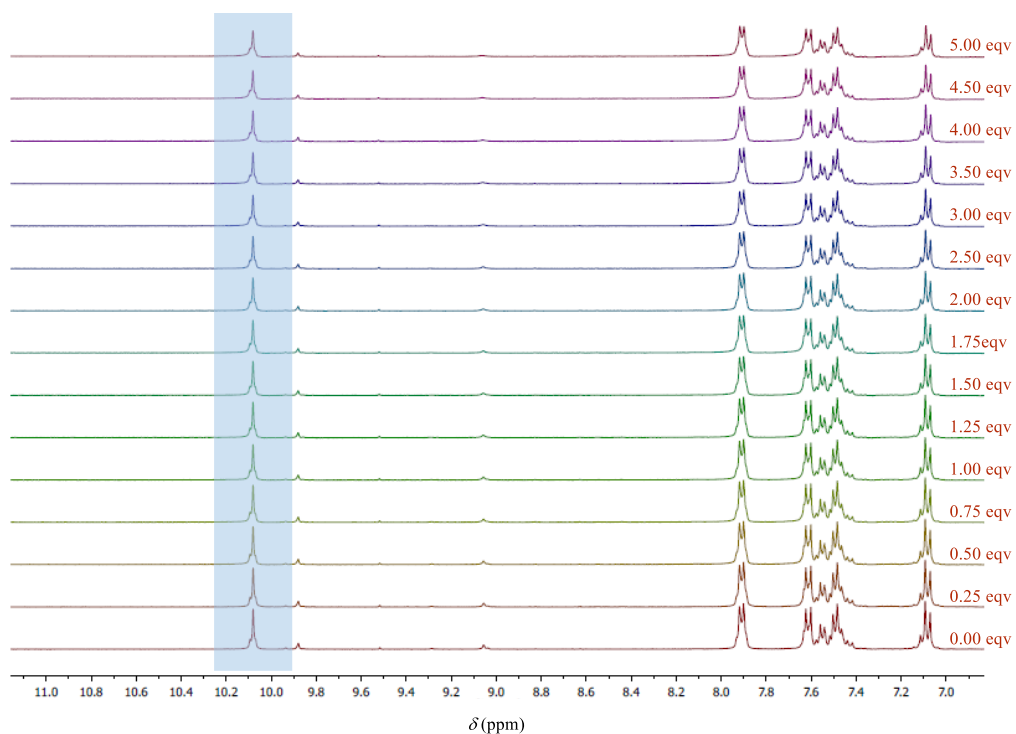
U-tube Experiment: U-tube experiment was carried out to discriminate the mechanism of chloride transport via channel or mobile carrier. In this experiment bulk organic phase behaves as a substitution of lipid bilayer and under such assay condition transport via channel is impossible. Tripodal receptor **2** was dissolved in chloroform (1 mM) with few drops of DMSO (due to solubility issue) and 1 mM $\text{TBA}^+\text{PF}_6^-$ to provide the counterions during transport and this organic solution (15 mL) was placed between two aqueous phases (7.5 mL each) as a membrane model mimicking a vesicle assay. The source aqueous phase was loaded with sodium chloride (500 mM, pH 7.0 with 5 mM sodium phosphate salts) and the receiving aqueous phase was loaded with sodium nitrate (500 mM, pH 7.0 with 5 mM sodium phosphate salts). Chloride transport at the receiving end was monitored for 6 days using a chloride selective electrode and obtained data showed an increase in chloride concentration in the receiving phase over time. A control experiment was carried out with neat chloroform containing $\text{TBA}^+\text{PF}_6^-$ (1 mM) and no change of chloride concentration was observed with time. These results support that mobile carrier mechanism is the mode of chloride transport.

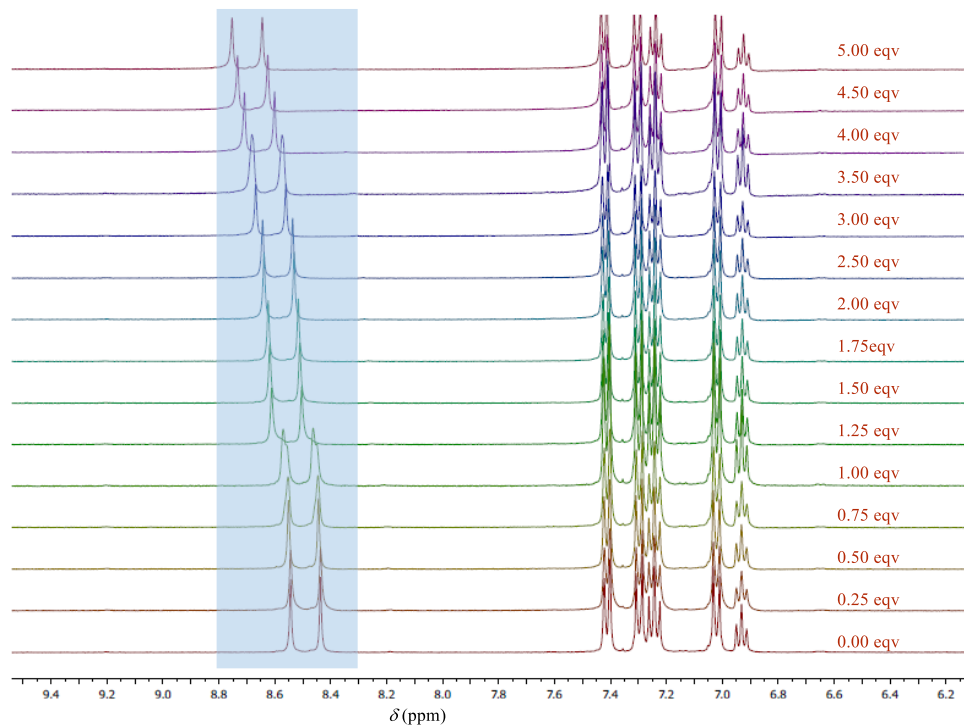
Mass Spectrometric Studies for Anion Recognition: In this experiment, both compound **2** and tetramethylammoniumchloride (TMACl) were prepared in acetonitrile and mixed in 1:3, 1:2, 1:1,

2:1, 3:1 molar ratio and formation of complex was monitored by Electrospray Ionization Mass Spectrometric (ESI-MS) studies in negative mode. The samples were electrosprayed as 10 μM solutions of compound **2** and (TMACl) in acetonitrile at flow rate of 0.4 mL/min. A constant spray and highest intensities were achieved with a capillary voltage of 3000 V at a source temperature of 80 $^{\circ}\text{C}$. The parameters for sample cone (40 V) and extractor cone voltage (5 V) were set for maximum intensities of the desired complexes. From the all ESI-MS spectrum data, only one intense signal corresponding to $[\text{M}+\text{Cl}]^{-}$ was observed (where, M = exact molecular weight of **2**) which further supports 1:1 chloride binding with compound **2**. Here only one data has been included as all of them showed same mass value.

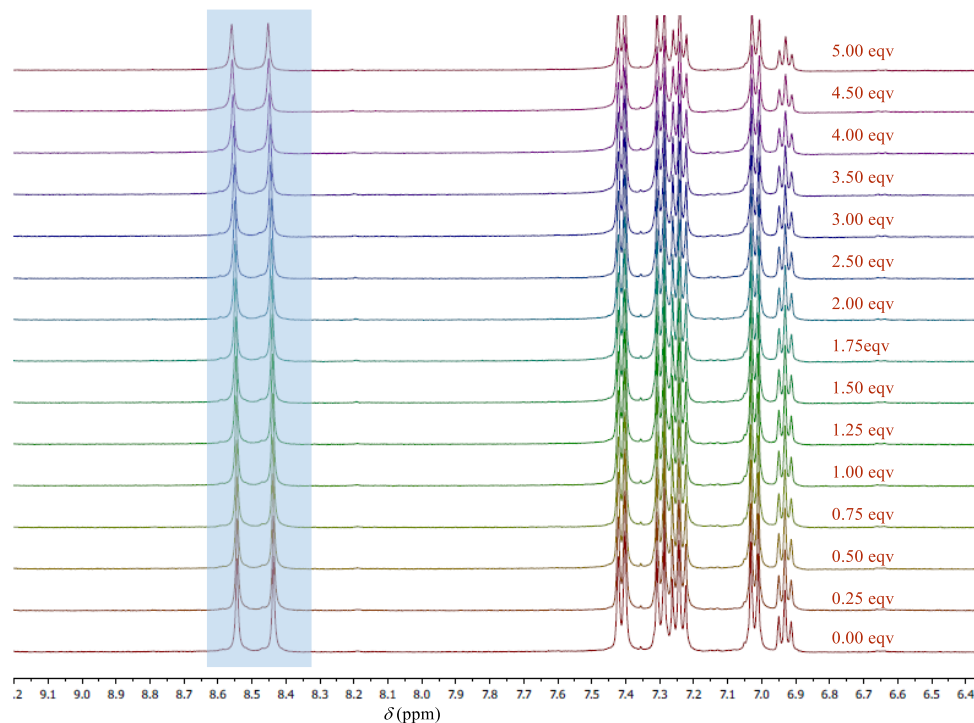
Simulation Details: To determine the Cl^{-} bound structure of the molecule, the molecule was initially optimized along with a Cl^{-} ion using semi-empirical PM6 method²⁰ in Gaussian 09 program package.²¹ The optimized structure was inserted in a box of 95 DPPC molecules. 2972 water molecules were added to solvate the system along with an additional Na^{+} ion to neutralization. SPC model²⁴ was taken for water and GROMOS-53a6 united atom force field²⁵ was used for DPPC molecules. The automated topology builder created by Malde, *et al.*²⁶ has been used to create the all atom topology parameters of the molecule with GROMOS-53a6 force field. Initially the system was energy minimized using steepest descent method²⁷ for 10000 steps with position restraint on the heavy atoms of the molecule and the Cl^{-} ion. This was followed by equilibration for 1 ns at constant 300 K temperature and 1 bar pressure using Nosé-Hoover thermostat²⁸⁻²⁹ and Parrinello-Rahman barostat³⁰ with a coupling constant of 0.4 ps for each. PME electrostatics³¹ was used for electrostatic interactions using a 10 \AA cut-off and the Van der Waals cut-off was set at 10 \AA . The simulation box was found to be $5.63 \times 5.63 \times 6.87 \text{ nm}^3$ in size after the equilibration step. A final 5 ns molecular dynamics simulation at constant 300 K temperature and 1 bar pressure was carried out with similar treatment of temperature, electrostatics and vdW as in equilibration process. The last 1 ns of this 5 ns trajectory has been used to generate the Cl^{-} bound structure. The overall structure of the system is shown in Figure 3B.10.

3B.5. Appendix Section

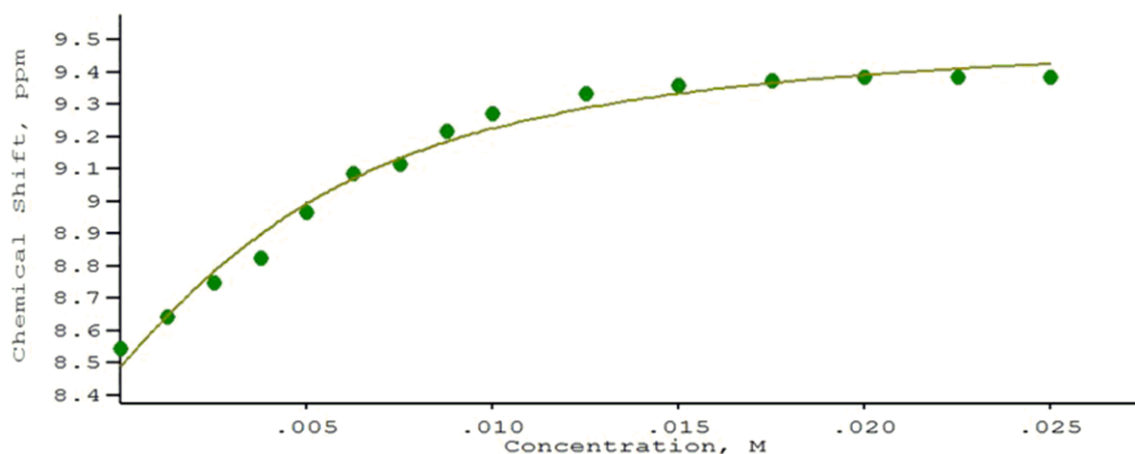
Appendix 3B.1: Stack plot of ¹H-NMR (DMSO-*d*₆) of **1** upon addition of increasing amounts of TBABr.Appendix 3B.2: Stack plot of ¹H-NMR (DMSO-*d*₆) of **1** upon addition of increasing amounts of TBAl.



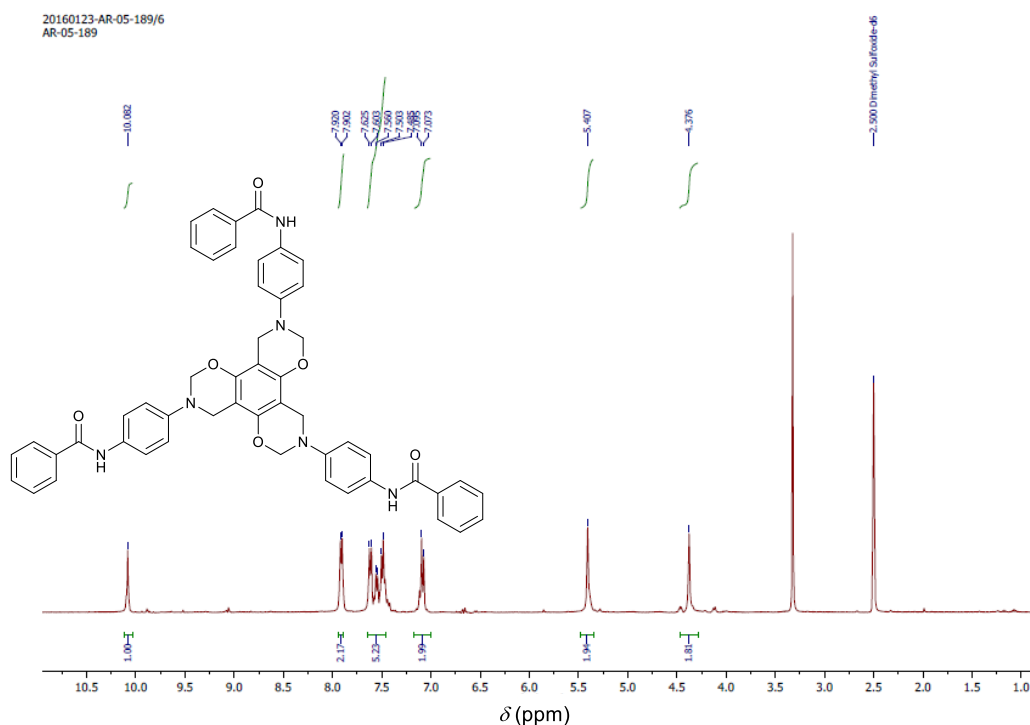
Appendix 3B.3: Stack plot of $^1\text{H-NMR}$ ($\text{DMSO-}d_6$) of **2** upon addition of increasing amounts of TBABr.



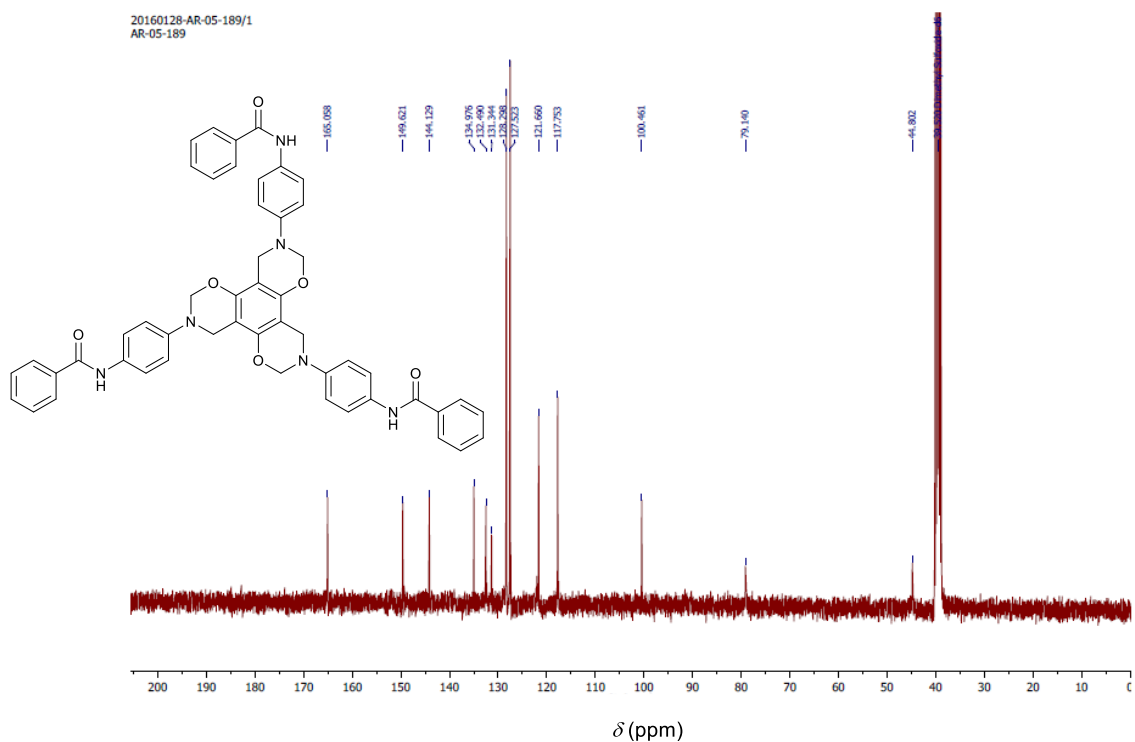
Appendix 3B.4: Stack plot of $^1\text{H-NMR}$ ($\text{DMSO-}d_6$) of **2** upon addition of increasing amounts of TBAI.



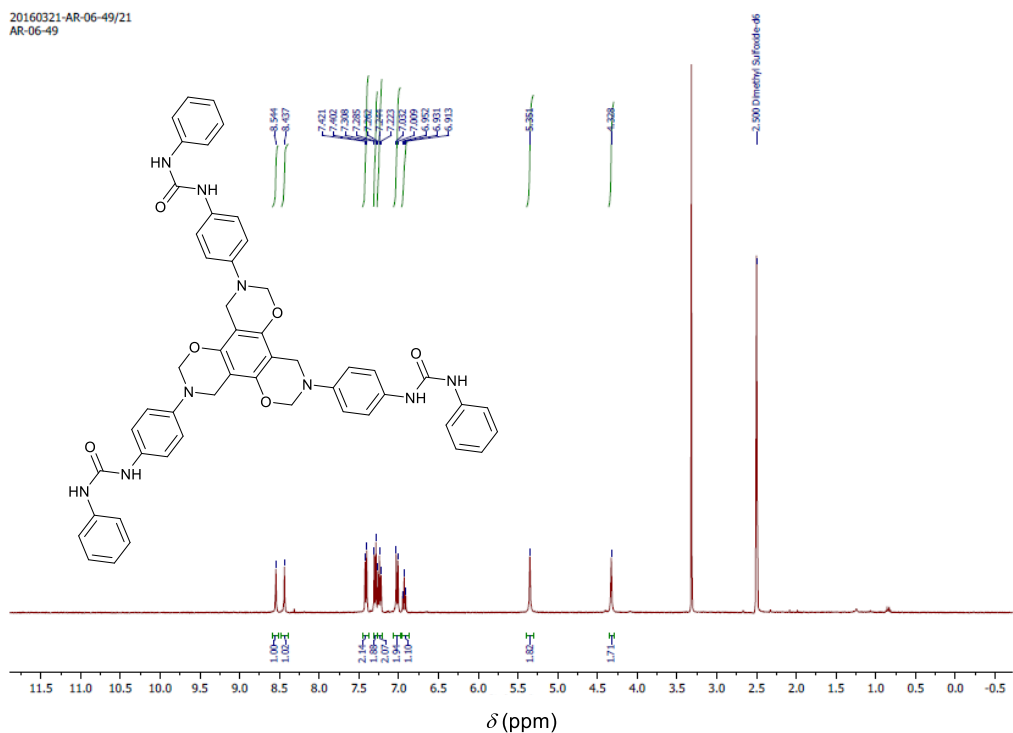
Appendix 3B.5: Plot of concentration of TBACl versus δ fitted to 1:1 binding model of WinEQNMR2 program for receptor 2.



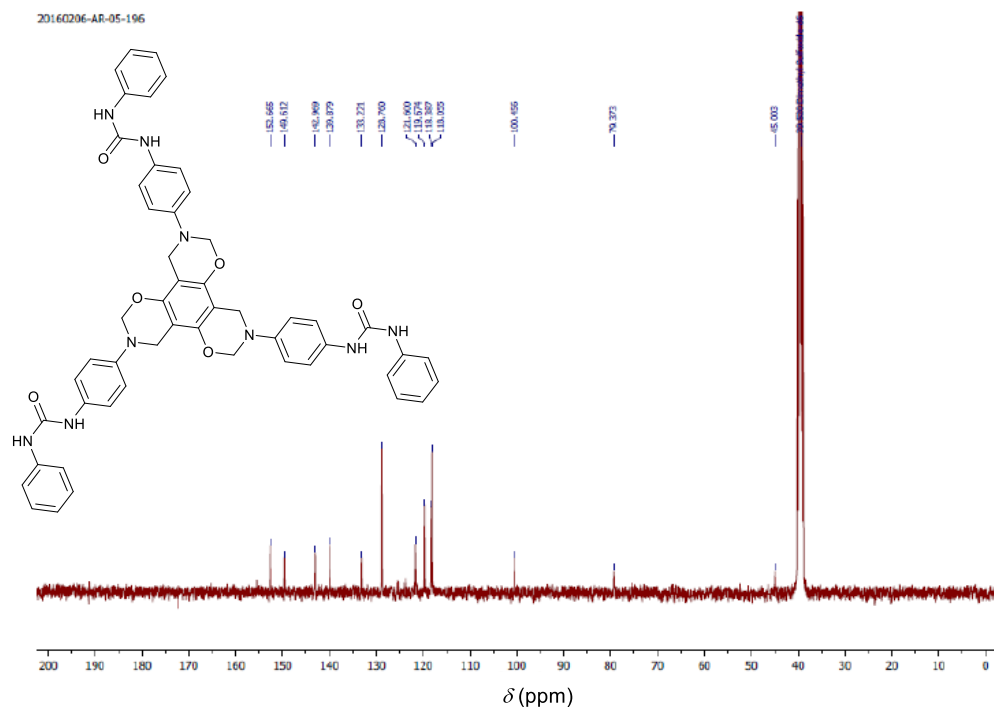
Appendix 3B.6: $^1\text{H-NMR}$ spectrum of receptor 1 in $\text{DMSO-}d_6$.



Appendix 3B.7: ^{13}C -NMR spectrum of receptor 1 in $\text{DMSO-}d_6$.



Appendix 3B.8: ^1H -NMR spectrum of receptor 2 in $\text{DMSO-}d_6$.



Appendix 3B.9: ^{13}C -NMR spectrum of receptor 2 in $\text{DMSO-}d_6$.

3B.6. References

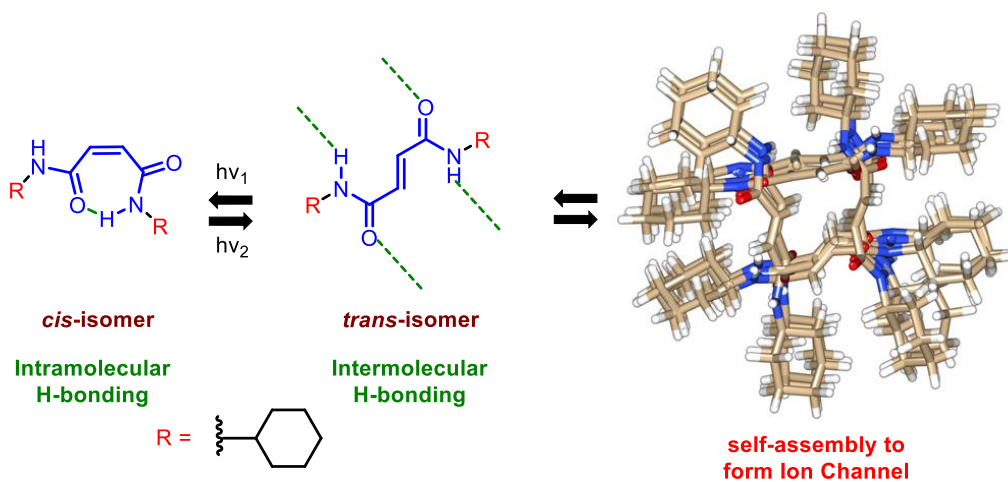
- (a) Jentsch, T. J.; Stein, V.; Weinreich, F.; Zdebik, A. A. *Physiol. Rev.* **2002**, *82*, 503-568; (b) Ko, S.-K.; Kim, S. K.; Share, A.; Lynch, V. M.; Park, J.; Namkung, W.; Van Rossom, W.; Busschaert, N.; Gale, P. A.; Sessler, J. L.; Shin, I. *Nat. Chem.* **2014**, *6*, 885-892; (c) DeCoursey, T. E.; Chandy, K. G.; Gupta, S.; Cahalan, M. D. *Nature* **1984**, *307*, 465-468.
- (a) Matile, S.; Vargas Jentsch, A.; Montenegro, J.; Fin, A. *Chem. Soc. Rev.* **2011**, *40*, 2453-2474; (b) Davis, J. T.; Okunola, O.; Quesada, R. *Chem. Soc. Rev.* **2010**, *39*, 3843-3862; (c) Gale, P. A. *Acc. Chem. Res.* **2011**, *44*, 216-226; (d) Elie, C.-R.; Noujeim, N.; Pardin, C.; Schmitzer, A. R. *Chem. Commun.* **2011**, *47*, 1788-1790.
- Ohkuma, S.; Sato, T.; Okamoto, M.; Matsuya, H.; Arai, K.; Kataoka, T.; Nagai, K.; Wasserman, H. *Biochem. J.* **1998**, *334*, 731-741;
- Jentsch, T. J.; Hubner, C. A.; Fuhrmann, J. C. *Nat. Cell. Biol.* **2004**, *6*, 1039-1047.
- (a) Saha, T.; Hossain, M. S.; Saha, D.; Lahiri, M.; Talukdar, P. *J. Am. Chem. Soc.* **2016**, *138*, 7558-7567; (b) Soto-Cerrato, V.; Manuel-Manresa, P.; Hernando, E.; Calabuig-Fariñas, S.; Martínez-Romero, A.; Fernández-Dueñas, V.; Sahlholm, K.; Knöpfel, T.; García-Valverde, M.; Rodilla, A. M.; Jantus-Lewintre, E.; Farràs, R.; Ciruela, F.; Pérez-Tomás, R.; Quesada, R. *J. Am. Chem. Soc.* **2015**, *137*, 15892-15898.
- (a) Davis, J. T.; Gale, P. A.; Okunola, O. A.; Prados, P.; Iglesias-Sánchez, J. C.; Torroba, T.; Quesada, R. *Nat. Chem.* **2009**, *1*, 138-144; (b) Wenzel, M.; Light, M. E.; Davis, A. P.; Gale, P. A. *Chem. Commun.* **2011**, *47*, 7641-7643; (c) Busschaert, N.; Wenzel, M.; Light, M. E.; Iglesias-Hernández,

- P.; Pérez-Tomás, R.; Gale, P. A. *J. Am. Chem. Soc.* **2011**, *133*, 14136-14148; (d) Hussain, S.; Brotherhood, P. R.; Judd, L. W.; Davis, A. P. *J. Am. Chem. Soc.* **2011**, *133*, 1614-1617; (e) Judd, L. W.; Davis, A. P. *Chem. Commun.* **2010**, *46*, 2227-2229; (f) Andrews, N. J.; Haynes, C. J. E.; Light, M. E.; Moore, S. J.; Tong, C. C.; Davis, J. T.; Harrell Jr, W. A.; Gale, P. A. *Chem. Sci.* **2011**, *2*, 256-260.
7. (a) Gilles, A.; Barboiu, M. *J. Am. Chem. Soc.* **2016**, *138*, 426-432; (b) Licsandru, E.; Kocsis, I.; Shen, Y.-x.; Murail, S.; Legrand, Y.-M.; van der Lee, A.; Tsai, D.; Baaden, M.; Kumar, M.; Barboiu, M., *J. Am. Chem. Soc.* **2016**, *138*, 5403-5409; (c) Le Duc, Y.; Michau, M.; Gilles, A.; Gence, V.; Legrand, Y.-M.; van der Lee, A.; Tingry, S.; Barboiu, M. *Angew. Chem., Int. Ed.* **2011**, *50*, 11366-11372.
 8. (a) Busschaert, N.; Gale, P. A.; Haynes, C. J. E.; Light, M. E.; Moore, S. J.; Tong, C. C.; Davis, J. T.; Harrell, J. W. A. *Chem. Commun.* **2010**, *46*, 6252-6254; (b) Gorteau, V.; Bollot, G.; Mareda, J.; Matile, S. *Org. Biomol. Chem.* **2007**, *5*, 3000-3012; (c) Clare, J. P.; Ayling, A. J.; Joos, J.-B.; Sisson, A. L.; Magro, G.; Pérez-Payán, M. N.; Lambert, T. N.; Shukla, R.; Smith, B. D.; Davis, A. P. *J. Am. Chem. Soc.* **2005**, *127*, 10739-10746; (d) Valkenier, H.; López Mora, N.; Kros, A.; Davis, A. P. *Angew. Chem., Int. Ed.* **2015**, *54*, 2137-2141.
 9. Busschaert, N.; Karagiannidis, L. E.; Wenzel, M.; Haynes, C. J. E.; Wells, N. J.; Young, P. G.; Makuc, D.; Plavec, J.; Jolliffe, K. A.; Gale, P. A. *Chem. Sci.* **2014**, *5*, 1118-1127.
 10. Hie, L.; Fine Nathel, N. F.; Shah, T. K.; Baker, E. L.; Hong, X.; Yang, Y.-F.; Liu, P.; Houk, K. N.; Garg, N. K. *Nature* **2015**, *524*, 79-83.
 11. Singh, R.; Schober, M.; Hou, X.; Seay, A.; Chu, Q. *Tetrahedron Lett.* **2012**, *53*, 173-175.
 12. Rodríguez, F.; Rozas, I.; Kaiser, M.; Brun, R.; Nguyen, B.; Wilson, W. D.; García, R. N.; Dardonville, C. *J. Med. Chem.* **2008**, *51*, 909-923.
 13. (a) Cranwell, P. B.; Hiscock, J. R.; Haynes, C. J. E.; Light, M. E.; Wells, N. J.; Gale, P. A. *Chem. Commun.* **2013**, *49*, 874-876; (b) Haynes, C. J. E.; Berry, S. N.; Garric, J.; Herniman, J.; Hiscock, J. R.; Kirby, I. L.; Light, M. E.; Perkes, G.; Gale, P. A. *Chem. Commun.* **2013**, *49*, 246-248; (c) Busschaert, N.; Elmes, R. B. P.; Czech, D. D.; Wu, X.; Kirby, I. L.; Peck, E. M.; Hendzel, K. D.; Shaw, S. K.; Chan, B.; Smith, B. D.; Jolliffe, K. A.; Gale, P. A. *Chem. Sci.* **2014**, *5*, 3617-3626.
 14. Saeed, M. A.; Fronczek, F. R.; Hossain, M. A. *Chem. Commun.* **2009**, 6409-6411.
 15. Hynes, M. J. *J. Chem. Soc., Dalton Trans.* **1993**, 311-312.
 16. (a) Vargas Jentzsch, A.; Emery, D.; Mareda, J.; Metrangolo, P.; Resnati, G.; Matile, S. *Angew. Chem., Int. Ed.* **2011**, *50*, 11675-11678; (b) Sakai, N.; Matile, S. *J. Am. Chem. Soc.* **2003**, *125*, 14348-14356.
 17. (a) Gorteau, V.; Bollot, G.; Mareda, J.; Perez-Velasco, A.; Matile, S. *J. Am. Chem. Soc.* **2006**, *128*, 14788-14789; (b) Talukdar, P.; Bollot, G.; Mareda, J.; Sakai, N.; Matile, S. *J. Am. Chem. Soc.* **2005**, *127*, 6528-6529.
 18. (a) Choi, Y. R.; Chae, M. K.; Kim, D.; Lah, M. S.; Jeong, K.-S. *Chem. Commun.* **2012**, *48*, 10346-10348; (b) Lisbjerg, M.; Valkenier, H.; Jessen, B. M.; Al-Kerdi, H.; Davis, A. P.; Pittelkow, M. *J. Am. Chem. Soc.* **2015**, *137*, 4948-4951.
 19. Shang, J.; Si, W.; Zhao, W.; Che, Y.; Hou, J.-L.; Jiang, H. *Org. Lett.* **2014**, *16*, 4008-4011.
 20. Stewart, J. J. P. *J. Mol. Model.* **2007**, *13*, 1173-1213.
 21. Frisch, M. J.; Trucks, G. W.; Schlegel, H. B.; Scuseria, G. E.; Robb, M. A.; Cheeseman, J. R.; Scalmani, G.; Barone, V.; Mennucci, B.; Petersson, G. A.; Nakatsuji, H.; Caricato, M.; Li, X.; Hratchian, H. P.; Izmaylov, A. F.; Bloino, J.; Zheng, G.; Sonnenberg, J. L.; Hada, M.; Ehara, M.; Toyota, K.; Fukuda, R.; Hasegawa, J.; Ishida, M.; Nakajima, T.; Honda, Y.; Kitao, O.; Nakai, H.; Vreven, T.; Montgomery Jr., J. A.; Peralta, J. E.; Ogliaro, F.; Bearpark, M. J.; Heyd, J.; Brothers, E.

- N.; Kudin, K. N.; Staroverov, V. N.; Kobayashi, R.; Normand, J.; Raghavachari, K.; Rendell, A. P.; Burant, J. C.; Iyengar, S. S.; Tomasi, J.; Cossi, M.; Rega, N.; Millam, N. J.; Klene, M.; Knox, J. E.; Cross, J. B.; Bakken, V.; Adamo, C.; Jaramillo, J.; Gomperts, R.; Stratmann, R. E.; Yazyev, O.; Austin, A. J.; Cammi, R.; Pomelli, C.; Ochterski, J. W.; Martin, R. L.; Morokuma, K.; Zakrzewski, V. G.; Voth, G. A.; Salvador, P.; Dannenberg, J. J.; Dapprich, S.; Daniels, A. D.; Farkas, Ö.; Foresman, J. B.; Ortiz, J. V.; Cioslowski, J.; Fox, D. J. *Gaussian 09*, Gaussian, Inc.: Wallingford, CT, USA, **2009**.
22. Hie L., Fine Nathel N. F., Shah T. K., Baker E. L., Hong X., Yang Y.-F., Liu P., Houk K. N., Garg N. K. *Nature* **2015**, *524*, 79-83.
 23. Roy A., Saha T., Gening M. L., Titov D. V., Gerbst A. G., Tsvetkov Y. E., Nifantiev N. E., Talukdar P. *Chem. Eur. J.* **2015**, *21*, 17445-17452.
 24. Berendsen H. J. C., Postma J. P. M., Gunsteren van W. F., Hermans J., Interaction Models for Water in Relation to Protein Hydration. In *Intermolecular Forces*; Pullman, B., Ed.; Reidel: Dordrecht, **1981**; pp 331-342.
 25. Oostenbrink C., Villa A., Mark A. E., Gunsteren van W. F. *J. Comput. Chem.* **2004**, *25*, 1656-1676.
 26. Malde A. K., Zuo L., Breeze M., Stroet M., Poger D., Nair P. C. Oostenbrink C., Mark A. E., *J. Chem. Theory Comput.* **2011**, *7*, 4026-4037.
 27. Schlick T. *Molecular Modeling and Simulation: An Interdisciplinary Guide*. 2nd ed.; Springer: New York, **2010**.
 28. Nosé S. *Mol. Phys.* **1984**, *52*, 255-268.
 29. Hoover W. G. *Phys. Rev. A* **1985**, *31*, 1695-1697.
 30. Parrinello M., Rahman A. *J. Appl. Phys.* **1981**, *52*, 7182-7190.
 31. Darden T., York D., Pedersen L. *J. Chem. Phys.* **1993**, *98*, 10089-10092.

Chapter 4

Synthesis of Maleimide and Fumaramide Derivatives and Evaluation of Their Ion Transport Activity



4.1. Introduction

Natural ion channel and pore proteins are key components of cells due to their potential ability to regulate the flow of charged species and molecules across the cell membranes. They have crucial role for numerous fundamental physiological processes in human body such as controlling membrane excitability, maintaining intracellular pH, cell proliferation, hormone secretion, transepithelial transport, signal transduction, osmolyte homeostasis and waste removal.¹ The complicated molecular structures and ion transport mechanism of natural ion channel proteins have compelled chemist to develop synthetic ion channel for the permeation of charged species and small organic molecule across lipid bilayer. Thus, mimicking the action of natural ion channels using synthetic ion transport system may enhance the understanding of mechanism of transporting biological ion channels but also open potential applications in channelopathies. Among various anions, chloride is one of the essential anion in biological systems. Misregulation of chloride transport is responsible for many severe human diseases, including cystic fibrosis, nephrolithiasis, myotonia, and Dravet syndrome. There is considerable interest in designing and developing ion transport machinery for selective transport of chloride that operate efficiently in lipid bilayer membranes to understand the fundamental mechanism of action of biological ion channels but most of them have relatively complex molecular structure, high molecular weight, lower water solubility which limit their application in drug discovery. Therefore, it remains an intriguing challenge to develop synthetic systems that can mimic biological functions of natural chloride channels.

There has been enduring interest in the development of smart transport mechanisms to achieve controlled ion transport across lipid membranes.² The design of synthetic ion channels which respond towards specific external stimuli, such as pH gradients, ligand, voltage, light has gained significant attention recently.³ The advantages of these reversible ion channels are to achieve controlled and selective ion transport through bilayer membrane. Indeed, among all these gated ion channel, light-responsive ion channels are fascinating due to their high degree of reproducibility and temporal control with potential applications in environmental monitoring, nanomedicines and biosensing devices. Many synthetic ion channels, reported so far are constructed by forming active structure either with single molecule or self-assembly of repeating units. Typical supramolecular architectures of the synthetic ion channels are based on crown

ethers, cyclodextrins, cyclic peptides, aromatic macrocycles etc. scaffolds. Talukdar *et al.* reported a ligand-gated synthetic based on dialkoxynaphthalene (DAN) donors and naphthalenediimide (NDI) acceptors.⁴ Anion transport activity across lipid bilayer could be improved as compared to cation transport activity by opening of the ion channel when *trans*-isomer was converted to *cis*-isomer in presence of light. Liu *et al.* described one more example of light-controlled self-assembled ion channels based on structurally simple azobenzene-based amphiphilic small molecules, where both the isomers form active ion channels with individual conduction properties.^{3g} Also few light-stimulated chloride ion carriers have been reported recently.⁵ Such artificial ion transporters of simple structure with gating activity offers a new open up to comprehend the complex transport phenomena and complex fabrication of natural ion channels.

In this study, design and syntheses of quite a few pairs of maleimide (*cis*-isomer) derivatives (**1a-5a**) and fumaramide (*trans*-isomer) derivatives (**1b-5b**) comprising of photo-sensitive alkene core, amide moiety and different short aliphatic chains (*n*-butyl, *n*-hexyl and cyclohexyl group) to maintain amphiphilicity in the bilayer membrane structure have been described. P. Talukdar and co-workers reported better channel formation in case of cyclohexyl protected mannitol due to the network of strong hydrogen bonding interactions and van der Waals interactions of cyclohexyl rings.⁶ However, isopropyl protected mannitol has very weak ion transport activity due to its less hydrophobic nature and missing van der Waals interactions of the cyclohexyl rings. With this idea, we introduced two pairs of maleimide and fumaramide derivatives with two amines *i.e.* **4c** and **5c**. It was anticipated that the *trans*-derivatives would get stacked together to form an extended sheet type structures by self-assembly through intramolecular hydrogen bonding of amide N-H of one molecule to carbonyl group of another molecule of next layer and alkyl groups provide hydrophobic interactions with the membrane. The formation of sheet-like assembly was indicated earlier by Zerbetto and co-workers.⁷ In bilayer membrane, these supramolecular sheets (either three or four) would arrange to form active supramolecular barrel rosette ion channel structure with hydrophilic interior and hydrophobic exterior. However, it is known from literature that *cis*-derivatives form seven membered ring through intramolecular hydrogen bonding and hence would not give any self-assembled structure.⁸ Thus, only *trans*-derivatives will exhibit potential ion channel activity and *cis*-derivatives will be inactive or less active due to lack of formation of self-

assembled structure. All *cis*-derivatives can be converted to *trans*-derivatives upon irradiation of visible light and so these *trans*-derivatives can display photo-switchable ion transport activity and light-gated ion channel activity could be observed.

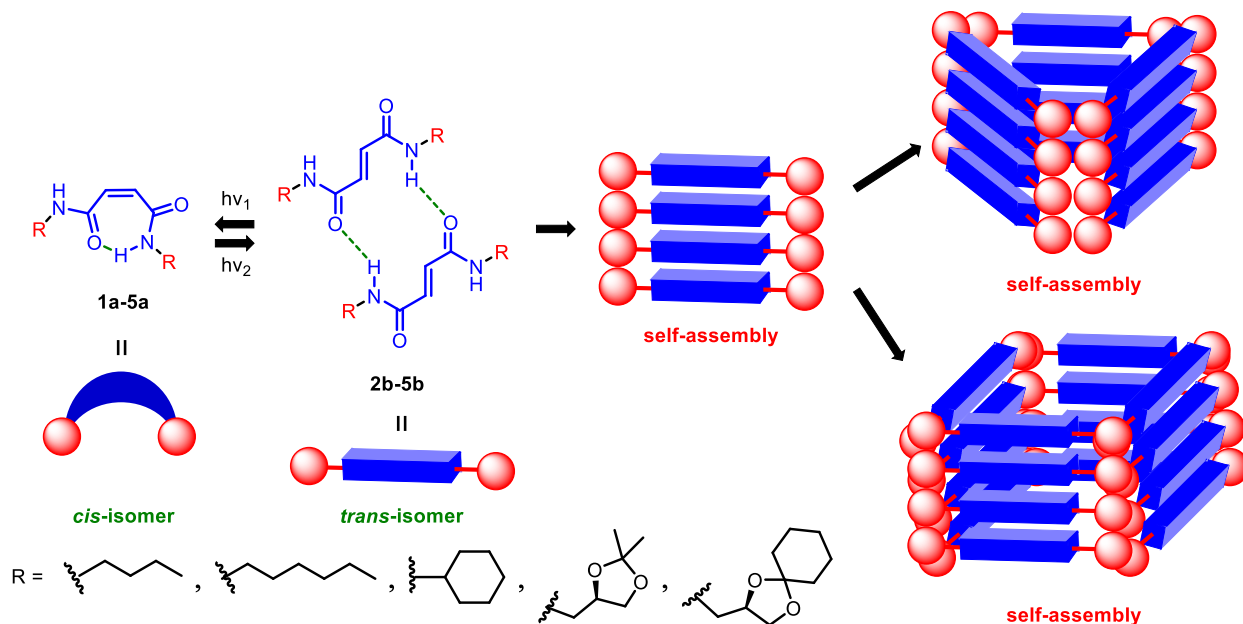


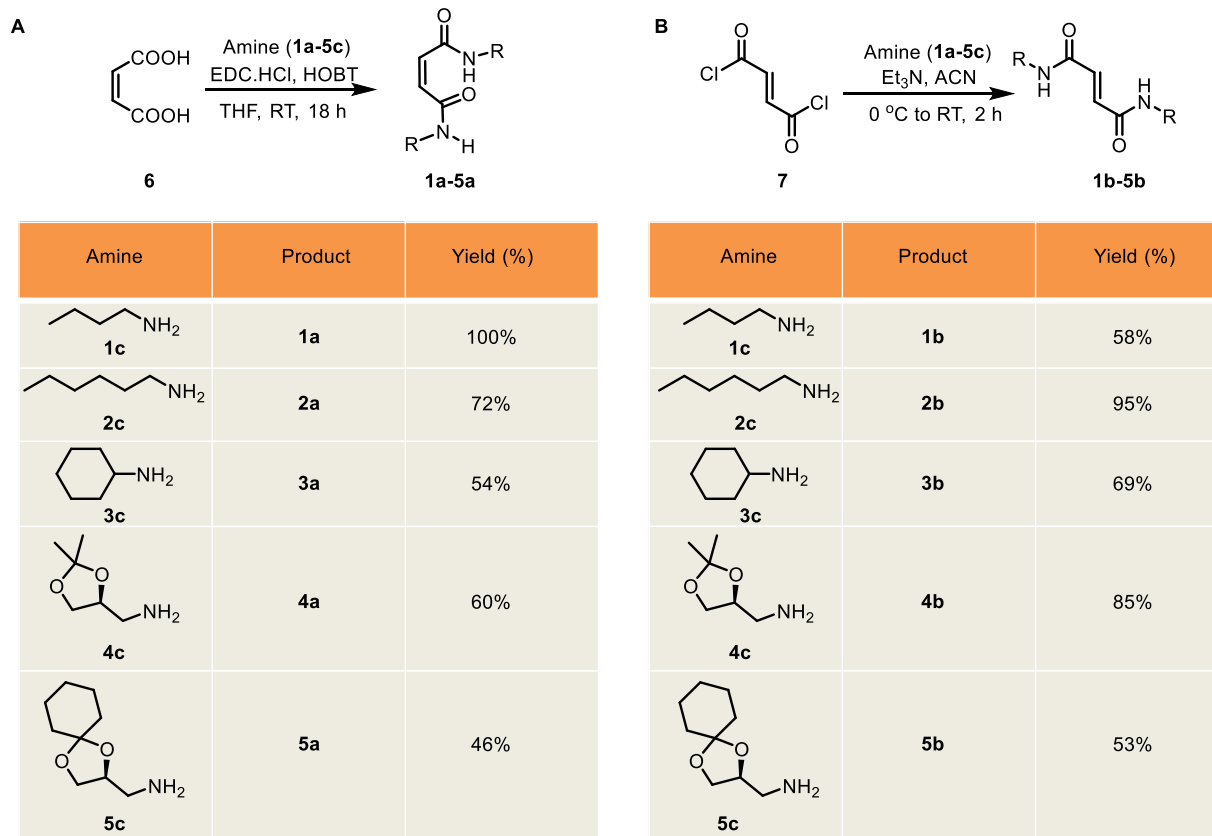
Figure 4.1: Structure of designed maleimide derivatives (**1a-5a**) and fumaramide derivatives (**2b-5b**) and probable mode of self-assembly for the channel formation.

4.2. Results and Discussions

4.2.1. Synthesis

All maleimide derivatives (**1a-5a**) commenced with the coupling reaction of maleic acid **6** and appropriate amines (**1c-5c**) in presence of EDC.HCl and HOBT in THF solvent to afford product with 46% to 100% yield. The syntheses of all fumaramide derivatives (**1b-5b**) were carried out with fumaryl chloride **7** and appropriate amines (**1c-5c**) in presence of triethylamine and acetonitrile solvent. All *trans*-products were obtained as white solid with yield ranging from 53% to 95 % yield. All compounds were characterized by $^1\text{H-NMR}$, $^{13}\text{C-NMR}$, HRMS, IR and melting points. Crystal structures of compounds **2b**, **3a** and **3b** were obtained from mixture of MeOH/ CHCl_3 (1:1) solvent system. Crystal structure of compound **2b** indicated that they stack together to form a flat ribbon type structure (Appendix 4.2). Crystal structure of compound **3a** indicated formation of seven membered ring through intramolecular hydrogen bonding (Appendix 4.3). On the other hand, crystal structure of compound **3b** showed one molecule interacts with

another molecule through intermolecular hydrogen bonding in a zigzag pattern (Appendix 4.4). Due to steric effect of cyclohexyl moiety (in chair conformation), the possibility of flat ribbon type self-assembly among them was less which was further evident from crystal structure.



Scheme 4.1: Synthesis of **A**) maleimide derivatives (**1a-5a**) and **B**) fumaramide derivatives (**1b-5b**).

4.2.2. Ion Transport Activity

The ability of transport ions across lipid bilayer membranes was evaluated by fluorescence leakage assay by using large unilamellar vesicles (LUVs) prepared from egg yolk phosphatidylcholine (EYPC) liposomes by entrapping pH-sensitive fluorescent dye, 8-hydroxy-1,3,6-pyrenetrisulfonate (HPTS).⁹ In this assay, a pH gradient of 0.8 unit was introduced across the vesicles ($\text{pH}_{\text{in}} = 7.0$ and $\text{pH}_{\text{out}} = 7.8$) by applying NaOH in the extravesicular solution. Upon addition of active transporter molecules, a destruction of the applied pH gradient occurred via H^+ ion efflux or OH^- ion influx leading to the increase of pH inside the vesicle. The activity was monitored by enhancement in the fluorescence intensity of HPTS ($\lambda_{\text{ex}} = 450 \text{ nm}$, $\lambda_{\text{em}} = 510 \text{ nm}$) of intravesicular pool. Finally, Triton-X was added to destruct the pH gradient for lysing all

vesicles. Activity of compounds were evaluated at varied concentrations indicating concentration dependent responses during the transport process. The fractional activities (Y) at $t = 200$ s were plotted against respective concentrations and obtained dose-response curves were then subjected to Hill Analysis to obtain effective concentration to reach 50% maximum activity (EC_{50}). Among all compounds, **3b** displayed the highest activity compared to all other compounds with lowest

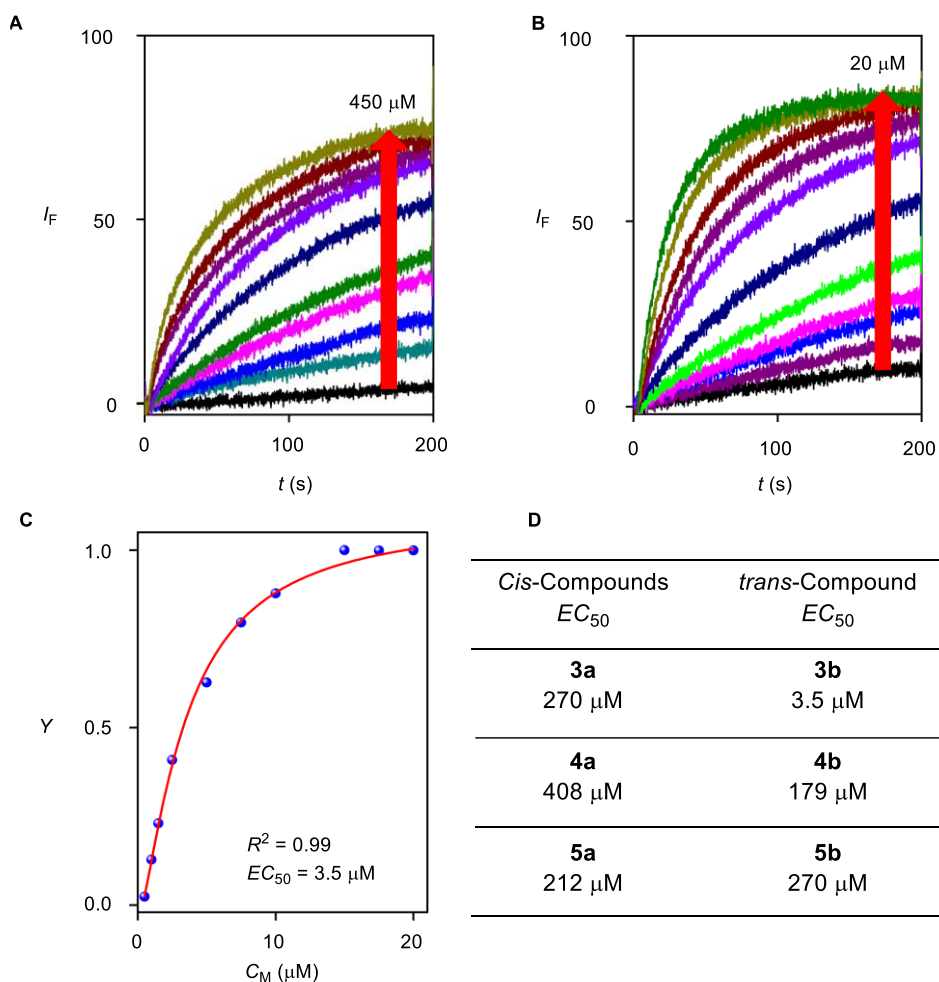


Figure 4.2: Concentration profiles of **A)** compound **3a** and **B)** compound **3b** by varying concentration with EYPC-LUVs \rightarrow HPTS vesicles, **C)** representation of Hill plot for compound **3b** from HPTS assay and **D)** EC_{50} values of three pairs of compounds.

$EC_{50} = 3.5 \mu\text{M}$ (Figure 4.2C). Ion transport activity for compounds **1a**, **1b** and **2a** could not be determined due to formation of precipitate under assay condition at very low concentration. In case of all pairs, *trans*-isomer displayed better ion transport activity as compared to its *cis*-isomer as anticipated *i.e.* **3b** (3.5 μM) > **3a** (270 μM), **4b** (179 μM) > **4a** (408 μM) and **5b** (44 μM) > **5a**

(212 μM). These data indicates that trans-isomer with cyclohexyl moiety **3b** has much better ion transport activity (77 fold) (Figure 4.2B) as compared to its cis-isomer **3a** (Figure 4.2A) which consequently corroborates with our prediction. Therefore further studies were carried out with this pair of compounds.

Ion transport activity of compound **3b** stimulated us to study its ion selectivity and the mechanism of ion transport. At first, carbonyl cyanide 4-(trifluoromethoxy)phenylhydrazone (FCCP), a proton transporter was used to evaluate which antiport mechanism H^+/M^+ (M^+ = alkali metal cation) or OH^-/X^- (X^- = monovalent anion) is predominating in the ion transport process.¹⁰ In this assay, after application of pH gradient by NaOH, FCCP transport H^+ ion selectively from the intravesicular solution to extravesicular solution. Concentration of FCCP was chosen to be 2.5 μM so that only FCCP exhibits negligible ion transport. On the contrary, the ion transport activity of compound **3b** improved significantly in presence of FCCP (2.5 μM) as compared to ion transport activity of compound **3b** (3.5 μM) alone, indicating the cooperative effect of FCCP and compound **3b**. This data indicated that compound **3b** does not transport H^+ consequently, supporting to the X^-/OH^- antiport as the operating mechanism (Figure 4.3A). In the next stage, to compare preferential selectivity among OH^- and Cl^- ; valinomycin was applied during HPTS assay.¹¹ Valinomycin is a K^+ selective carrier which transport K^+ from extravesicular water pool to the interior of vesicles and simultaneous OH^- and/or Cl^- influx is expected to maintain the charge equality by compound. Valinomycin (2.5 pM) alone showed very insignificant ion transport activity. Fluorescence intensity enhancement was monitored in presence and absence of valinomycin with compound **3b** (3.5 μM) and obtained data displayed similar ion transport rate in both cases indicating preferential transport of Cl^- over OH^- (*i.e.* a $\text{Cl}^- > \text{OH}^-$ selectivity) (Figure 4.3B). Therefore from FCCP and valinomycin assay, it can be concluded that compound **3b** acts as an OH^-/Cl^- exchanger with a faster rate of transport of Cl^- compared to OH^- .

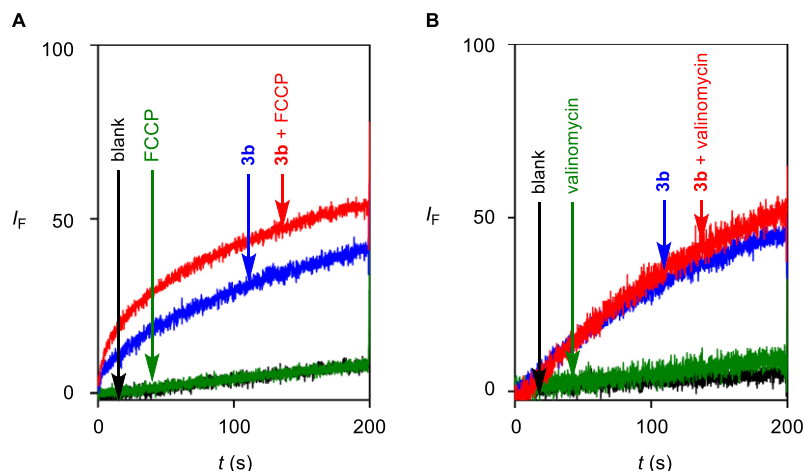


Figure 4.3: **A)** Ion transport activity of compound **3b** (3.5 μM) determined in the absence and in the presence of FCCP. **B)** Ion transport activity of compound **3b** (3.5 μM) determined in the absence and in the presence of valinomycin.

In the next stage, ion selectivity of ion channel formed by compound **3b** was evaluated across EYPC-LUVs with entrapped HPTS in the presence of intravesicular NaCl salt. All experiments were performed with the concentration at EC_{50} of a compound **3b**. In case of cation selectivity assay (Figure 4.4A), extravesicular NaCl solution was replaced by iso-osmolar MCl ($M^+ = \text{Li}^+, \text{K}^+, \text{Rb}^+, \text{and } \text{Cs}^+$) and variation of the external cations did not cause any significant differences in transport activity by compound **3b** (3.5 μM). However, substantial changes were observed when extravesicular anions NaX ($X^- = \text{Cl}^-, \text{Br}^-, \text{I}^-, \text{NO}_3^-, \text{SCN}^-, \text{ClO}_4^-$) were varied. A selectivity topology, $\text{Cl}^- > \text{Br}^- > \text{SCN}^- > > \text{ClO}_4^- > \text{NO}_3^- > \text{I}^-$ was observed after addition of compound **3b** (3.5 μM) which clearly demonstrated the involvement of anions in the transport process (Figure 4.4B). Among all anions, **3b** displayed highest selectivity toward Cl^- ion.

Further Cl^- selectivity was evaluated by lucigenin assay (Figure 4.4C). In this assay, transport of Cl^- across LUVs (EYPC-LUVs \supset Lucigenin) can be monitored by quenching of lucigenin fluorescence ($\lambda_{\text{ex}} = 455 \text{ nm}$, $\lambda_{\text{em}} = 535 \text{ nm}$). The LUVs were encapsulated with NaNO_3 (225 mM) and lucigenin (1 mM) and were suspended in NaNO_3 (225 mM) solution. During assay, NaCl (25 mM) was added to the extravesicular water pool, and quenching of fluorescence was observed after addition of transporters. Triton X was added at the end of experiment to destroy all the vesicles. Ion channel formed by compound **3b** showed quenching of lucigenin fluorescence emission in a concentration dependent manner by promoting transport of Cl^- into the vesicle and

NO_3^- out of the vesicle which consequently provides direct proof of Cl^- transport. Further, to quantify transport efficiency, half-life ($t_{1/2}$) and initial rate (I_R) of compound **3b** ($40 \mu\text{M}$) was calculated and $t_{1/2} = 121 \text{ s}$ and $I_R = 0.67 \text{ s}^{-1}$ was obtained from lucigenin quenching plot. The Cl^- transport activity was further studied by using same lucigenin vesicles in presence of valinomycin, an efficient K^+ carrier (Figure 5B). In this assay, KCl (25 mM) pulse was applied at $t = 20 \text{ s}$ followed by addition of valinomycin ($t = 50 \text{ s}$) and channel forming molecule **3b** ($t = 100 \text{ s}$) (Appendix 4.7). Valinomycin (100 nM) alone did not cause any quenching of lucigenin fluorescence. However, combination of compound **3b** ($70 \mu\text{M}$) and valinomycin (100 nM) resulted significant quenching of lucigenin fluorescence. All these results further reconfirmed that receptor **3b** is an effective chloride transporter.

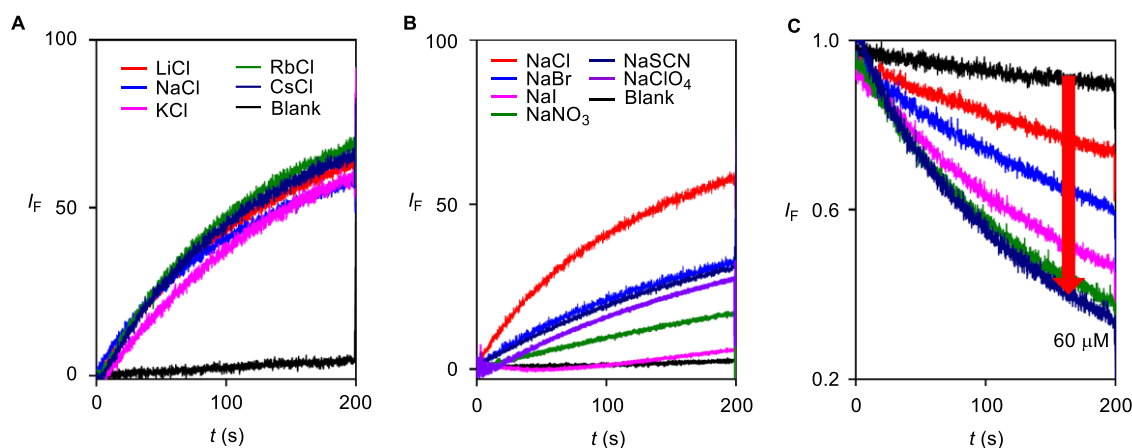


Figure 4.4: A) Cation selectivity of **3b** ($3.5 \mu\text{M}$) determined from HPTS assay with varied extravesicular cations M^+ , B) Anion selectivity of **3b** ($3.5 \mu\text{M}$) determined with varied extravesicular anions X^- with intravesicular Cl^- ion and C) Chloride transport by compound **3b** ($0 - 60 \mu\text{M}$) by nitrate/chloride exchange.

4.2.3. Light-induced Transport Activity

Next, in order to investigate light-responsive ion channel formation and chloride transport, transport ability was examined before and after application of light of compound **3a** using EYPC-LUVs. In this experiment, ion transport activity for *cis*-isomer **3a** ($10 \mu\text{M}$) was checked and as expected, no substantial transport activity was observed at this concentration of compound **1c**. Then compound **3a** in $\text{CH}_3\text{CN}/\text{CH}_3\text{OH}$ (1:1) solvent system was irradiated with 365 nm light for 15 min at room temperature in presence of catalytic amount of bromine and ion transport activity across lipid bilayer was checked by HPTS assay. The presence of catalytic amount of bromine

initiates radical reaction which leads to isomerization of double bonds. As anticipated the converted *trans*-isomer, which was denoted by *trans*-1 in the figure 4.5, was found to transport ions almost equal proficiently as pure *trans*-isomer **3b**. Therefore, light-responsive ion channel formation and ability to transport ion was established. Then, this converted *trans*-1 was irradiated with 290 nm light for 30 min at room temperature to obtain *cis*-isomer (*cis*-1) back in CH₃CN/CH₃OH (1:1) solvent system and ion transport activity was evaluated. The transport ability was significantly absent as a result of conversion of all *trans*-1 to *cis*-1. In similar way, we carried out three consecutive cycles and obtained data indicated switching *on/off* ion transport activity and about 95 % ion transport ability retained for *trans*-isomer after three cycles.

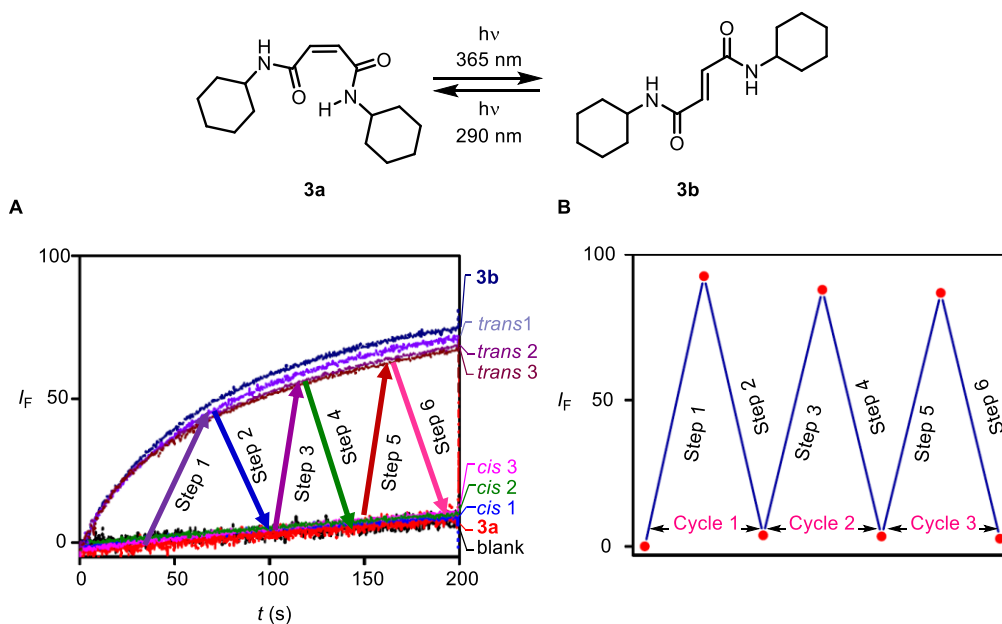


Figure 4.5: A) Representation of light gated activity of compound **3a** (10 μ M) based on HPTS assay and B) representation of data for three complete cycles.

4.2.4. Bilayer Lipid Membrane

In the next stage, the incorporation of compound **3b** in the lipid bilayer to form ion channel was investigated by bilayer lipid membrane (BLM) experiment.^{6, 12} In this experiment, two compartments (*cis* and *trans* chambers) containing KCl solution (1 M) were separated by a planar lipid bilayer composed of diphytanoylphosphatidylcholine (diPhyPC). When compound **3b** (20 μ M) was added to *cis*-chamber, distinct single channel opening and closing was realized at different holding potential, indicating formation of channel in the lipid bilayer. The single channel

conductance of this pore was determined to be 60.8 ± 1 pS in 1 M KCl solution. Current–time traces are shown in Figure 4.6 for compound **3b** at applied positive potential +100 mV (Figure 4.6A) and as well as in negative potential –100 mV (Figure 4.6A). The diameter of the pore formed by compound **3b** was also determined as 3.84 \AA by same BLM experiment by +

$$1/g = (l + \pi d/4)(4\rho/\pi d^2)$$

Where, g = corrected conductance (obtained by multiplying measured conductance with the Sansom's correction factor), l = length of the ion channel (37 \AA), and ρ = resistivity of the 1 M KCl solution ($\rho = 9.47 \text{ \Omega}\cdot\text{cm}$).

The diameter of unsolvated Cl^- is 3.6 \AA which is close to the calculated pore size which consequently validating with the observed Cl^- selectivity of the artificial ion channel formed by compound **3b**.

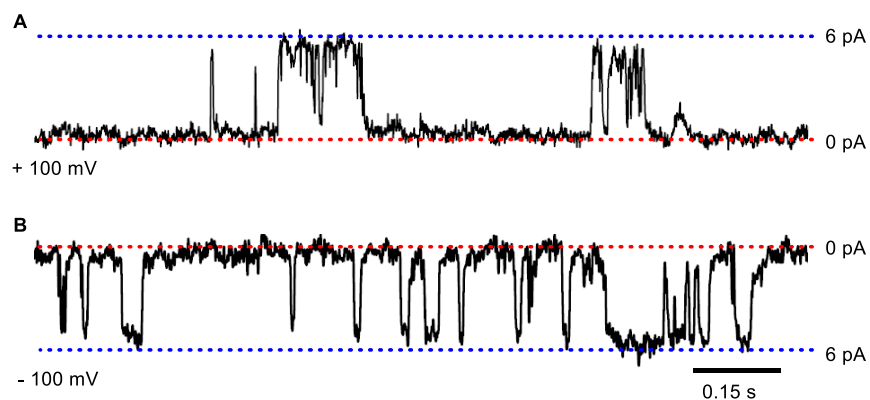


Figure 4.6: Single-channel current traces recorded **A)** at +100 mV and **B)** at –100 mV holding potentials in 1 M symmetrical KCl solution. 0 pA at the right-hand side indicates the baseline current. The main conductance state is indicated by two dotted lines.

4.2.5. Molecular Modelling of Ion Channel

In the next stage, to investigate the molecular image, formation of ion channel and origin of ion selectivity of the ion channel, we have proposed a model based on 8 layers of 4 molecules of compound **3b**. Crystal structure of compound **3b** indicated one molecule interacts with another molecule through intermolecular hydrogen bonding in a zigzag pattern (Appendix 4.4). Due to steric effect of cyclohexyl moiety (in chair conformation), the formation of flat ribbon type self-assembly among them was less possible. Therefore, we proposed that 4 molecules will interact with each other by H-bonding to form a layer and about 8 layers (all layers are interconnected through H-bonding) are required to form a full channel across lipid bilayer. We have performed

semi-empirical quantum calculations to understand the molecular level insight of the structure. We have optimized the presumed structure with MPOAC2012 software with PM6-DH+ method. We have taken the middle two layers to calculate the cavity size. The cavity is found to be 3.1 Å. We observed that the cavity is not exactly circular. Hence, we also calculated the major and the minor axes which turned out to be 3.6 Å and 1.8 Å, respectively. However, the conductance experiment resulted radius value to be 3.84 Å which is clearly close to the calculated minor axis value. These calculations also indicated that one of alkene C-H bonds are oriented towards inner core of channel which is the genesis of chloride selectivity through H-bonding.

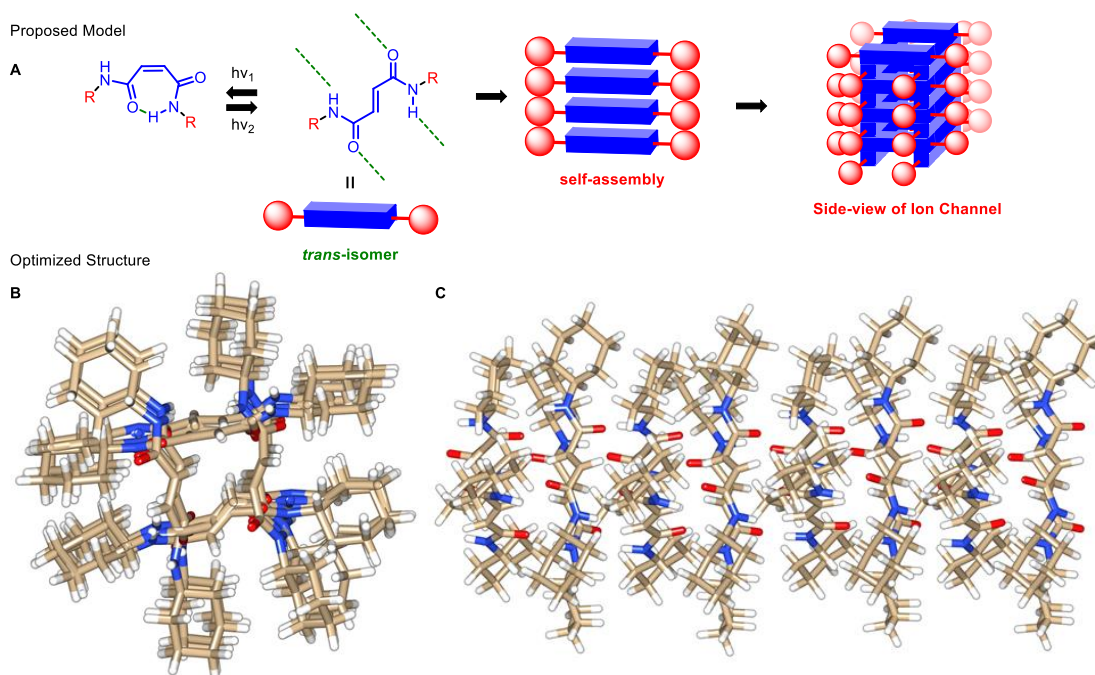


Figure 4.7: A) Proposed model of ion channel formation, B) Top view and C) side view of the optimized structures of ion channel formed by **3b**.

4.3. Conclusion

In conclusion, we have designed a new series of *cis*-isomers based on light sensitive double bond core. We postulated that upon irradiation of light, these *cis*-isomers convert into *trans*-isomers which can self-assemble to form a rosette-type ion channel. Therefore, five pairs of maleimide (*cis*-isomer) derivatives and fumaramide (*trans*-isomer) derivatives were synthesised and their ion transport ability was evaluated by fluorescence based vesicle leakage assay with EYPC liposomes. As expected higher activity was observed for *trans*-isomer in comparison with *cis*-isomer and highest activity was observed in case of *trans*-isomer with cyclohexyl side arm

($EC_{50} = 3.5 \mu\text{M}$) and this compound is almost 77 fold more active as compared to its *cis*-isomer. Further experiment based on chloride sensitive lucigenin dye showed that compound can transport anions particularly chloride across EYPC liposome which was proved by EYPC and Lucigenin assay. Light-gated ion transport activity was assessed with EYPC liposomes and observed data suggested nearly 95 % activity retained after three consecutive cycles. Additionally, formation of ion channel was demonstrated by bilayer lipid membrane experiment and from single-channel conductance measurements, diameter of channel was found to be 3.84 Å which is close to diameter of unsolvated chloride ion.

4.4. Experimental Section

General Methods: All reactions were performed under the nitrogen atmosphere. All the reagents for synthesis were purchased from commercial sources and used without further purification. Solvents were purchased as dry or dried by standard methods prior to use. Thin layer chromatography (TLC) was carried out with E. Merck silica gel 60-F₂₅₄ plates and column chromatography was performed over silica gel (100-200 mesh) obtained from commercial suppliers and accompanied with UV-detector ($\lambda = 365 \text{ nm}, 254 \text{ nm}$). Egg yolk phosphatidylcholine (EYPC) lipid was procured from Avanti Polar Lipids as a solution in chloroform (25 mg/mL). HEPES buffer, HPTS dye, lucigenin dye, Triton X, NaOH and inorganic salts of molecular biology grade were obtained from Sigma-Aldrich. Gel-permeation chromatography was performed on a column of Sephadex G-50 in buffer containing salt solution or only salt solution, as per requirement. Large unilamellar vesicles (LUV) were prepared by using mini extruder, equipped with a polycarbonate membrane of 100 nm (in case of HPTS Assay) or 200 nm (in case of Lucigenin Assay) pore size, obtained from Avanti Polar Lipids

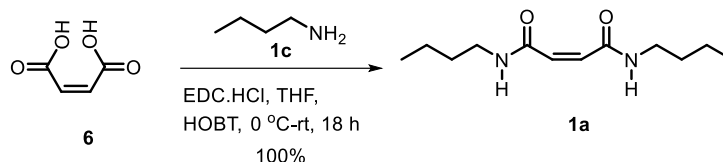
Physical Measurements: The ^1H and ^{13}C NMR spectra were recorded on 400 MHz Jeol ECS-400 (or 100 MHz for ^{13}C) spectrometers using either residual solvent signals as an internal reference or from internal tetramethylsilane on the δ scale (DMSO- d_6 δ_{H} 2.50 ppm, MeOH- d_4 δ_{H} 3.31 ppm, CDCl_3 δ_{H} 7.26 ppm and DMSO- d_6 δ_{C} 39.52 ppm, MeOH- d_4 δ_{C} 49.00 ppm, CDCl_3 δ_{C} 77.16 ppm). The chemical shifts (δ) are reported in ppm and coupling constants (J) in Hz. The following abbreviations are used: s (singlet), d (doublet) m (multiplet), dd (doublet of doublet), td (triplet of doublet). High-resolution mass spectra were obtained from MicroMass ESI-TOF MS

spectrometer. Steady State fluorescence experiments were carried out in a micro fluorescence cuvette (Hellma, path length 1.0 cm) on a Fluoromax 4 instrument (Horiba Jobin Yvon) equipped with an injector port and a magnetic stirrer. (FT-IR) spectra were obtained using NICOLET 6700 FT-IR spectrophotometer as KBr disc and reported in cm^{-1} . Melting points were measured using a VEEGO Melting point apparatus. All melting points were measured in open glass capillary and values are uncorrected. The pH of the buffer solution used for fluorescence experiment was adjusted as per requirement by NaOH using Helmer pH meter. All data of fluorescence studies were processed either by Origin 8.5 or KaleidaGraph.

General Procedure for synthesizing Maleimide Derivatives (1a – 5a): In a 25 mL round bottom flask, maleic acid (200 mg, 1.72 mmol), amine (4.13 mmol) and HOBt (632 mg, 4.13 mmol) were dissolved in THF (12 mL) and cooled to 0 °C. Then EDC.HCl (989 mg, 5.16 mmol) was added to the above reaction portionwise. The reaction was stirred at room temperature for 18 h. After completion of reaction, THF was removed under reduced pressure and obtained residue was extracted with ethyl acetate (2×100 mL) and water (2×100 mL). Organic layer was washed with brine solution (2×50 mL). Organic layer was then evaporated under vacuo to give light brown residue and column chromatography over silica gel was performed to get the expected compounds as semi-solid or solid (colorless to white solid) with 46% to 100 % yield.

General Procedure for synthesizing Fumaryl Derivatives (1b – 5b): In a 25 mL round bottom flask, a solution of amine (3.92 mmol) and Et_3N (364 μL , 2.61 mmol) in CH_3CN (4 mL) were taken and cooled to 0 °C. A solution of fumaryl chloride (200 mg, 133 μL , 1.30 mmol) in CH_3CN (2 mL) was added drop wise during a period of 1 h at same temperature. The reaction was stirred for additional 1 h at room temperature. White precipitate was observed in the reaction mixture. After completion of reaction, solvent was removed under reduced pressure. Residue obtained was extracted with EtOAc (2×100 mL) and water (2×100 mL). Organic layer was washed with brine (2×50 mL) solution and was evaporated under reduced pressure to obtain light brown to white solid which was further purified by silica gel column chromatography. Expected products were obtained as white solid with yield ranging from 53% to 95%.

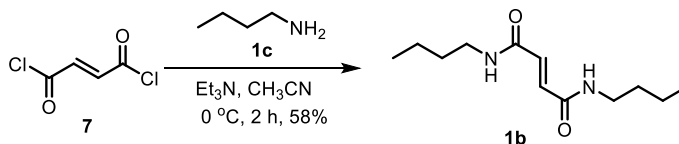
Synthesis of *N*¹, *N*⁴-dibutylmaleamide (**1a**):



Scheme 4.2: Synthesis of compound **1a**.

Synthesis of compound **1a**: Compound **1a** (173 mg) was obtained as colorless yellow semi-solid product with yield (100%). **IR (KBr)**: ν/cm^{-1} : 3270, 3061, 2958, 2930, 2868, 1666, 1614, 1548, 1462, 1372; **¹H NMR (400 MHz, DMSO-*d*₆)**: δ 9.2 (t, *J* = 5.6 Hz, 2H), 6.0 (s, 2H), 3.1 (m, 4H), 1.4 (m, 4H), 1.2 (m, 4H), 0.9 (t, *J* = 7.2 Hz, 6H); **¹³C NMR (100 MHz, DMSO-*d*₆)**: δ 164.4, 131.8, 38.3, 30.8, 19.6, 13.6; **HRMS (ESI)**: Calc. for C₁₂H₂₂N₂O₂ [M+H]⁺: 227.1759; Found: 227.1769.

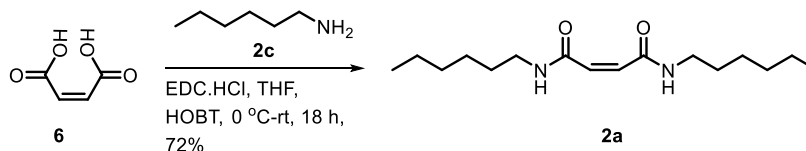
Synthesis of *N*¹, *N*⁴-dibutylfumaramide (**1b**):



Scheme 4.3: Synthesis of compound **1b**.

Synthesis of compound **1b**: Product with 58% yield (170 mg) was obtained as white solid. **M.p.**: 270 – 271 °C; **IR (KBr)**: ν/cm^{-1} : 3286, 3070, 2947, 2857, 1632, 1545, 1457, 1343, 1192, 991; **¹H NMR (400 MHz, DMSO-*d*₆)**: δ 8.3 (s, 2H), 6.7 (s, 2H), 3.1 (dd, *J* = 6.8 Hz, 6 Hz, 4H), 1.4 (m, 4H), 1.2 (m, 4H), 0.8 (t, *J* = 7.2 Hz, 6H); **¹³C NMR (100 MHz, DMSO-*d*₆)**: δ 163.4, 132.1, 38.0, 30.5, 19.0, 12.9; **HRMS (ESI)**: Calc. for C₁₂H₂₂N₂O₂ [M+H]⁺: 227.1759; Found: 227.1765.

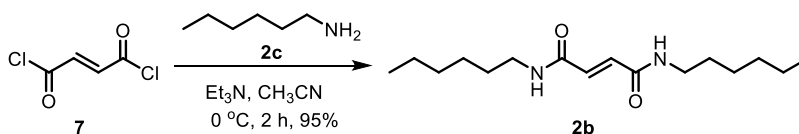
Synthesis of *N*¹, *N*⁴-dihexanoylmaleamide (**2a**):



Scheme 4.4: Synthesis of compound **2a**.

Synthesis of compound **2a**: Yield 72% (350 mg) was obtained as colorless semi-solid product. **IR (KBr)**: ν/cm^{-1} : 1265, 1371, 1461, 1549, 1615, 1666, 2860, 2926, 3063, 3281; **$^1\text{H NMR}$ (400 MHz, DMSO- d_6)**: δ 9.2 (t, $J = 5.2$ Hz, 2H), 6.0 (s, 2H), 3.0 (m, 4H), 1.4 (m, 4H), 1.2 (m, 12H), 0.8 (m, 6H); **$^{13}\text{C NMR}$ (100 MHz, DMSO- d_6)**: δ 164.4, 131.9, 38.7, 30.9, 28.7, 26.1, 22.0, 13.8; **HRMS (ESI)**: Calc. for $\text{C}_{16}\text{H}_{30}\text{N}_2\text{O}_2$ $[\text{M}+\text{H}]^+$: 283.2385; Found: 283.2390.

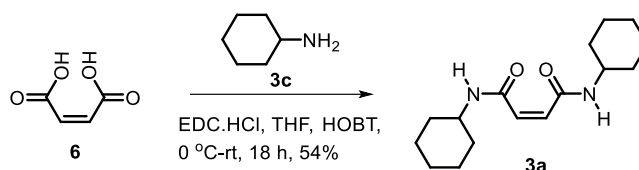
Synthesis of N^1, N^4 -dihexylfumaramide (**2b**):



Scheme 4.5: Synthesis of compound **2b**.

Synthesis of compound **2b**: Product with yield of 95% (350 mg) was obtained as white solid. **M.p.**: $210 - 211\text{ }^\circ\text{C}$; **IR (KBr)**: ν/cm^{-1} : 3290, 3067, 2944, 2850, 2746, 1631, 1543, 1458, 1327, 1190; **$^1\text{H NMR}$ (400 MHz, MeOH- d_4)**: δ 6.8 (s, 2H), 3.2 (t, $J = 7.2$ Hz, 4H), 1.5 (m, 4H), 1.3 (m, 12H), 0.9 (m, 6H); **$^{13}\text{C NMR}$ (100 MHz, DMSO- d_6)**: δ 163.2, 131.8, 38.1, 30.1, 28.1, 25.3, 21.1, 12.9; **HRMS (ESI)**: Calc. for $\text{C}_{16}\text{H}_{30}\text{N}_2\text{O}_2$ $[\text{M}+\text{H}]^+$: 283.2385; Found: 283.2380.

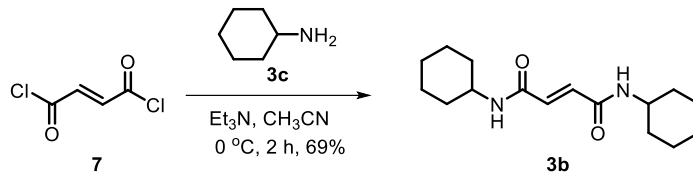
Synthesis of N^1, N^4 -dicyclohexylmaleamide (**3a**):



Scheme 4.6: Synthesis of compound **3a**.

Synthesis of compound **3a**: Product was obtained as white solid product with yield 54% (260 mg); **M.p.**: $132 - 133\text{ }^\circ\text{C}$; **IR (KBr)**: ν/cm^{-1} : 3270, 3070, 2932, 2843, 1613, 1531, 1444, 1337, 1245, 1093; **$^1\text{H NMR}$ (400 MHz, MeOH- d_4)**: δ 6.1 (s, 2H), 3.6 (m, 2H), 1.9 (dd, $J = 2.8, 12.4$ Hz, 4H), 1.7 (td, $J = 3.6, 13.2$ Hz, 4H), 1.6 (m, 2H), 1.2 - 1.4 (m, 10H); **$^{13}\text{C NMR}$ (100 MHz, MeOH- d_4)**: δ 166.1, 133.1, 49.8, 33.4, 26.6, 25.9; **HRMS (ESI)**: Calc. for $\text{C}_{16}\text{H}_{26}\text{N}_2\text{O}_2$ $[\text{M}+\text{H}]^+$: 279.2072; Found: 279.2069.

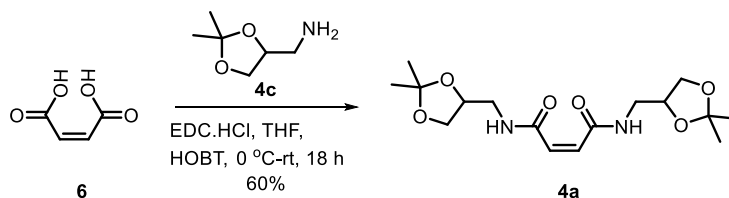
Synthesis of *N*¹, *N*⁴-dicyclohexylfumaramide (**3b**):



Scheme 4.7: Synthesis of compound **3b**.

Synthesis of compound **3b**: Product was obtained as white solid product with yield 69% (250 mg); **M.p.**: $> 300\text{ }^\circ\text{C}$; **IR (KBr)**: ν/cm^{-1} : 3286, 3078, 2926, 1636, 1545, 1445, 1345, 1181, 994; **¹H NMR (400 MHz, DMSO-*d*₆)**: δ 7.9 (s, 2H), 6.8 (s, 2H), 3.6 (m, 2H), 1.5 – 1.7 (m, 10H), 1.1 – 1.3 (m, 10H); **¹³C NMR (100 MHz, MeOH-*d*₄)**: δ 162.6, 132.3, 47.3, 31.7, 24.7, 23.8; **HRMS (ESI)**: Calc. for $\text{C}_{16}\text{H}_{26}\text{N}_2\text{O}_2$ $[\text{M}+\text{H}]^+$: 279.2072; Found: 279.2064.

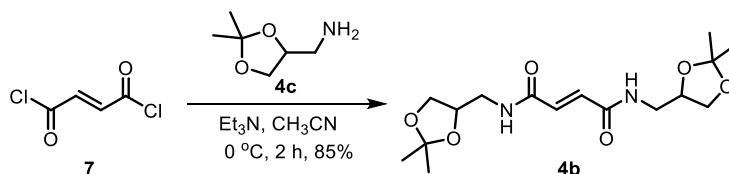
Synthesis of *N*¹, *N*⁴-bis((2,2-dimethyl-1,3-dioxolan-4-yl)methyl)maleamide (**4a**):



Scheme 4.8: Synthesis of compound **4a**.

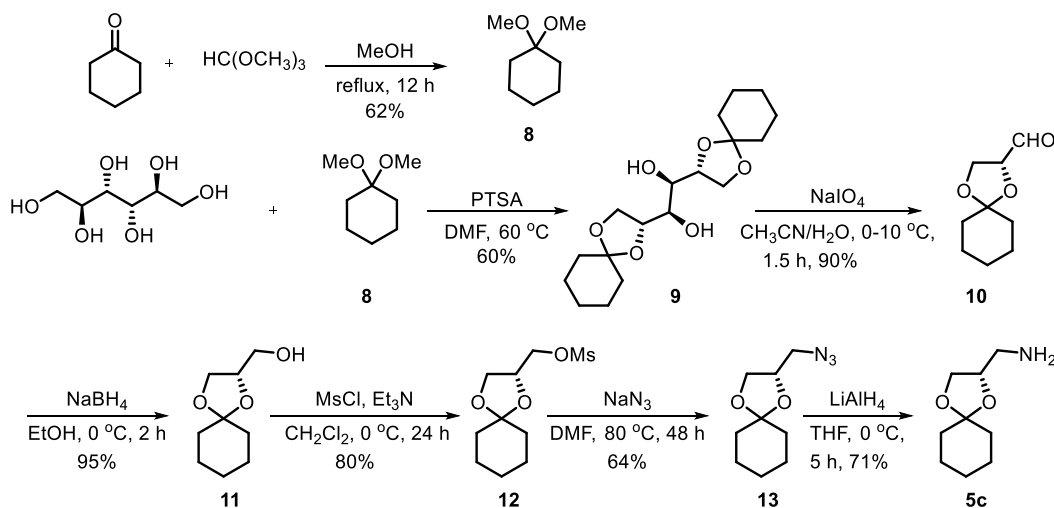
Synthesis of compound **4a**: Amine was synthesized according to reported protocol.¹³ Product (349 mg) was obtained as colorless semi-solid product with 60% yield. **IR (KBr)**: ν/cm^{-1} : 3217, 3059, 2985, 2935, 2882, 1668, 1618, 1547, 1451, 1375; **¹H NMR (400 MHz, CDCl₃)**: δ 8.1 (s, 2H), 6.1 (s, 2H), 4.3 (m, 2H), 4.0 (m, 2H), 3.7 (m, 2H), 3.6 (m, 2H), 3.4 (m, 2H), 1.4 (s, 6H), 1.3 (m, 6H); **¹³C NMR (100 MHz, CDCl₃)**: δ 164.7, 132.3, 109.3, 74.0, 66.6, 41.7, 26.5, 25.0; **HRMS (ESI)**: Calc. for $\text{C}_{16}\text{H}_{26}\text{N}_2\text{O}_6$ $[\text{M}+\text{H}]^+$: Calc. for 343.1864; Found: 343.1871.

Synthesis of *N*¹, *N*⁴-bis((2,2-dimethyl-1,3-dioxolan-4-yl)methyl)fumaramide (**4b**):



Scheme 4.9: Synthesis of compound 4b.

Synthesis of compound **4b**: Product (380 mg) was obtained as colorless semi-solid product with 85% yield. **M.p.**: 195 – 196 °C; **IR (KBr)**: ν/cm^{-1} : 3250, 3093, 2931, 1634, 1582, 1376, 1337, 1245, 1213, 1156; **¹H NMR (400 MHz, MeOH-*d*₄)**: δ 6.9 (s, 2H), 4.2 (m, 2H), 4.0 (m, 2H), 3.6 (m, 2H), 3.4 (m, 4H), 1.4 (s, 6H), 1.3 (s, 6H); **¹³C NMR (100 MHz, DMSO-*d*₆)**: δ 163.9, 132.6, 108.4, 74.1, 66.5, 41.4, 26.7, 25.3; **HRMS (ESI)**: Calc. for C₁₆H₂₆N₂O₆ [M+Na]⁺: 365.1688; Found: 365.1694.



Scheme 4.10: Synthesis of compound 5c.

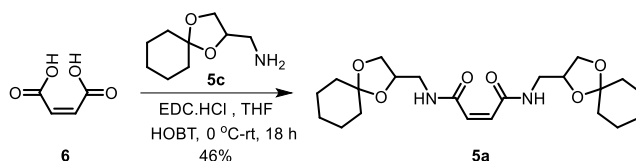
Synthesis of compound **5c**: compound **10** was prepared following reported protocol.¹⁴ Compound **11** prepared from **10** according to reported procedure¹⁵ and compound **12** was synthesized by reported protocol.¹⁶

Synthesis of compound **13**: In a 50 mL round bottom flask, NaN₃ (850 mg) was added to a solution of **12** (2.7 g) in dry dimethylformamide (DMF) (15 mL) at room temperature and the reaction was stirred at 80 °C for 48 h. After that the resultant mixture was extracted with ethyl acetate and purified using flash column chromatography. Yield (64%). Obtained compound was directly used for next step to prepare compound **5c**.

Synthesis of compound **5c**: In a 50 mL round bottom flask, compound **13** (500 mg) was taken in dry THF (15 mL) under nitrogen atmosphere and cooled down to at 0 °C. Then LiAlH₄ (144 mg) was added portionwise. Ice bath was removed and the resultant mixture was stirred at room temperature for 5h. After that the reaction was cooled to 0 °C and ethyl acetate was added slowly

followed by the addition of saturated Na_2SO_4 to quench LiAlH_4 . White precipitate was formed which was filtered off and filtrate was extracted with ethyl acetate and dried over Na_2SO_4 and concentrated under reduced pressure to obtain compound **5c** (410 mg) as transparent liquid. (71%). Obtained data was matching with reported product.¹⁷

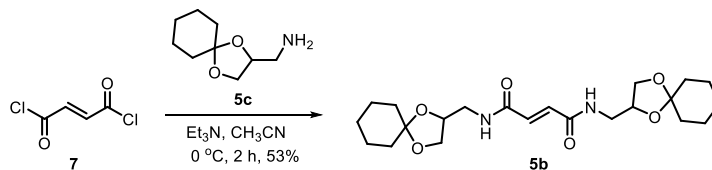
Synthesis of N^1, N^4 -bis((1,4-dioxaspiro[4.5]decan-2-yl)methyl)maleamide (**5a**):



Scheme 4.11: Synthesis of compound **5a**.

Synthesis of compound **5a**: Product (333 mg) was obtained as semi-solid product with yield 46%; **IR (KBr)**: ν/cm^{-1} : 3279, 2933, 2858, 1669, 1618, 1548, 1441, 1366, 1222, 1163; **$^1\text{H NMR}$ (400 MHz, $\text{DMSO-}d_6/\text{CDCl}_3(1:1)$)**: δ 9.1 (t, $J = 5.6$ Hz, 2H), 6.1 (s, 2H), 4.1 (t, $J = 5.6$ Hz, 2H), 3.9 (t, $J = 6$ Hz, 2H), 3.6 (t, $J = 6$ Hz, 2H), 3.2 (t, $J = 5.6$ Hz, 4H), 1.5 (d, $J = 17.6$ Hz, 20H); **$^{13}\text{C NMR}$ (100 MHz, $\text{DMSO-}d_6/\text{CDCl}_3(1:1)$)**: δ 164.8, 131.5, 108.8, 73.6, 66.3, 41.4, 36.0, 34.5, 24.6, 23.5, 23.3; **HRMS (ESI)**: Calc. for $\text{C}_{22}\text{H}_{34}\text{N}_2\text{O}_6$ $[\text{M}+\text{H}]^+$: 423.2488; Found: 423.2495.

Synthesis of N^1, N^4 -bis((1,4-dioxaspiro[4.5]decan-2-yl)methyl)fumaramide (**5b**):



Scheme 4.12: Synthesis of compound **5b**.

Synthesis of compound **5b**: Product (290 mg) was obtained as white powdered solid product with yield 53%. **M.p.**: 290 – 291 °C; **IR (KBr)**: ν/cm^{-1} : 3532, 3295, 3083, 2941, 2854, 1644, 1548, 1446, 1348, 1263; **$^1\text{H NMR}$ (400 MHz, $\text{DMSO-}d_6$)**: δ 8.5 (t, $J = 6$ Hz, 2H), 6.8 (s, 2H), 4.0 (p, $J = 6.0$ Hz, 2H), 3.9 (d, $J = 6.0$ Hz, 1H), 3.8 (d, $J = 6.4$ Hz, 1H), 3.6 (d, $J = 6.0$ Hz, 1H), 3.5 (d, $J = 6.0$ Hz, 1H), 3.2 (t, $J = 5.6$ Hz, 4H), 1.5 – 1.3 (m, 20H); **$^{13}\text{C NMR}$ (100 MHz, $\text{DMSO-}d_6$)**: δ 163.9, 132.6, 108.8, 73.7, 66.2, 41.5, 36.1, 34.5, 24.6, 23.5, 23.4; **HRMS (ESI)**: Calc. for $\text{C}_{22}\text{H}_{34}\text{N}_2\text{O}_6$ $[\text{M}+\text{Na}]^+$: 445.2314; Found: 445.2319.

Determination of ion transport activity by HPTS LUVs: Same as discussed in Chapter 3A.

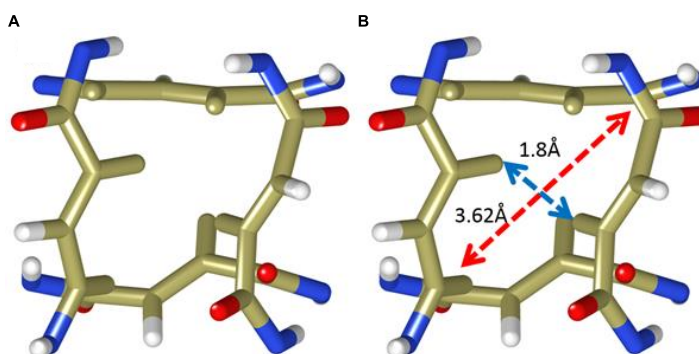
Determination of ion selectivity, FCCP and Valinomycin Assay by HPTS LUVs: Same as discussed in Chapter 3A.

Determination of chloride ion selectivity experiment by Lucigenin Assay: Same protocol as discussed in Chapter 3A.

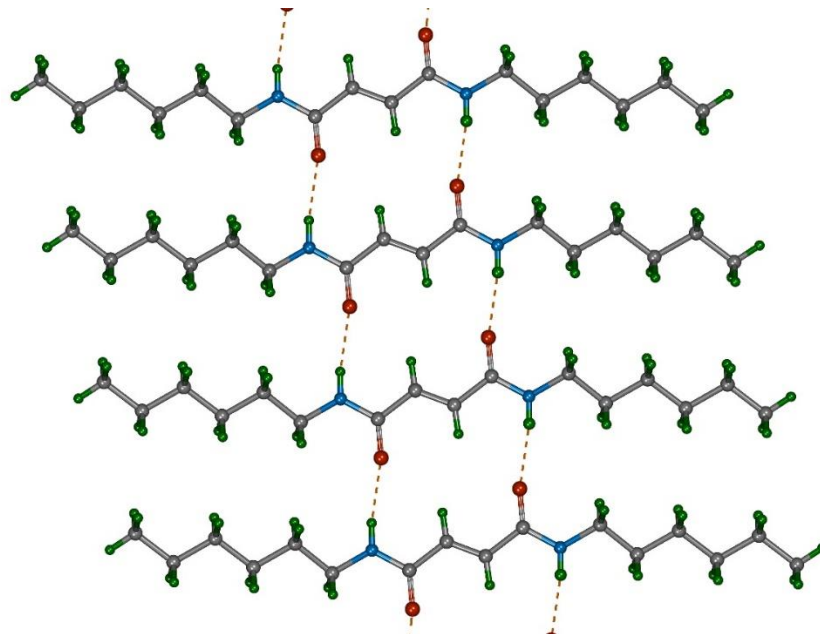
Planar Bilayer Conductance Measurements: Bilayer membrane (BLM) was formed across an aperture of 150 μM diameter in a polystyrene cup (Warner Instrument, USA) with lipid diphytanoylphosphatidylcholine (Avanti Polar Lipids), dissolved in *n*-decane (18mg/mL). Both chambers (*cis* and *trans*) were filled with symmetrical solution, containing 1 M KCl. The *cis* compartment was held at virtual ground and the *trans* chamber was connected to the BC 535 headstage (Warner Instrument, USA) via matched Ag-AgCl electrodes. Compound **3b** (20 μM) was added to the *cis* chamber and the solution was stirred with magnetic stirrer for 10 min. Channel formation was confirmed by the distinctive channel opening and closing events after applying voltages. Currents were low pass filtered at 1 kHz using pClamp9 software (Molecular probes, USA) and analog-to-digital converter (Digidata 1440, Molecular probes). All data were analyzed by the software pClamp 9.

Average Diameter: We have calculated the average diameter from the radius of gyration method on the middle two layers of the optimized structure. We have considered only the inner atoms of the layers to calculate the average diameter as shown in Appendix 4.1A. The average diameter is found to be 3.10 \AA . We have also calculated the major and the minor axis for the cavity in a similar way as we calculated the average diameter which came out to be 3.62 \AA and 1.80 \AA respectively. Major and minor axes are shown in Appendix 4.1B.

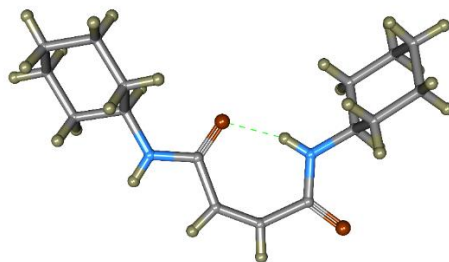
4.5. Appendix Section



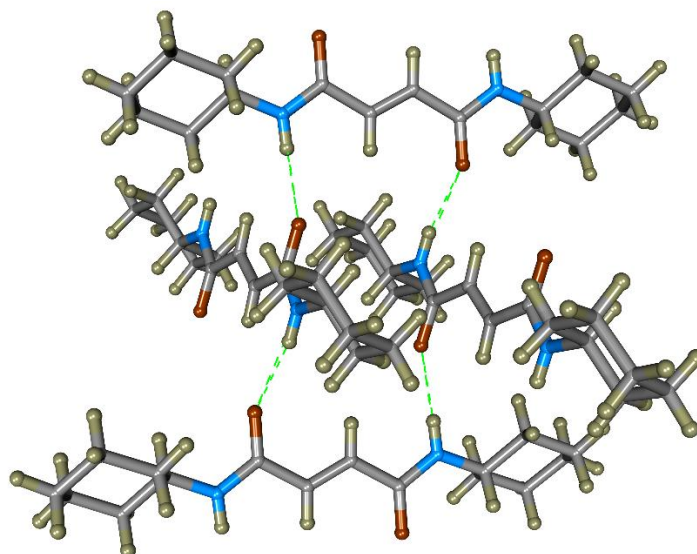
Appendix 4.1: **A)** Represents the middle layers of the optimized structure. Inner atoms which are shown in Khaki color are used for average diameter calculation and **B)** representation of the major and the minor axes.



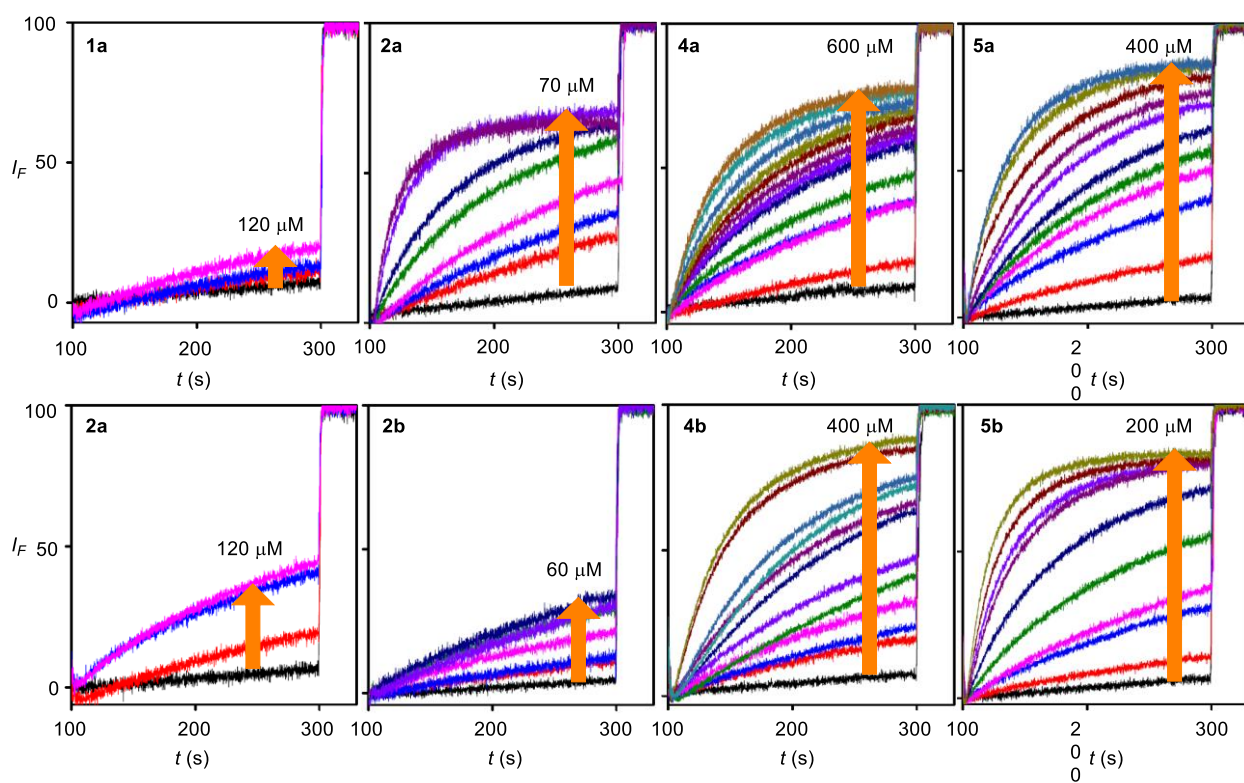
Appendix 4.2: Crystal structure of **1b**.



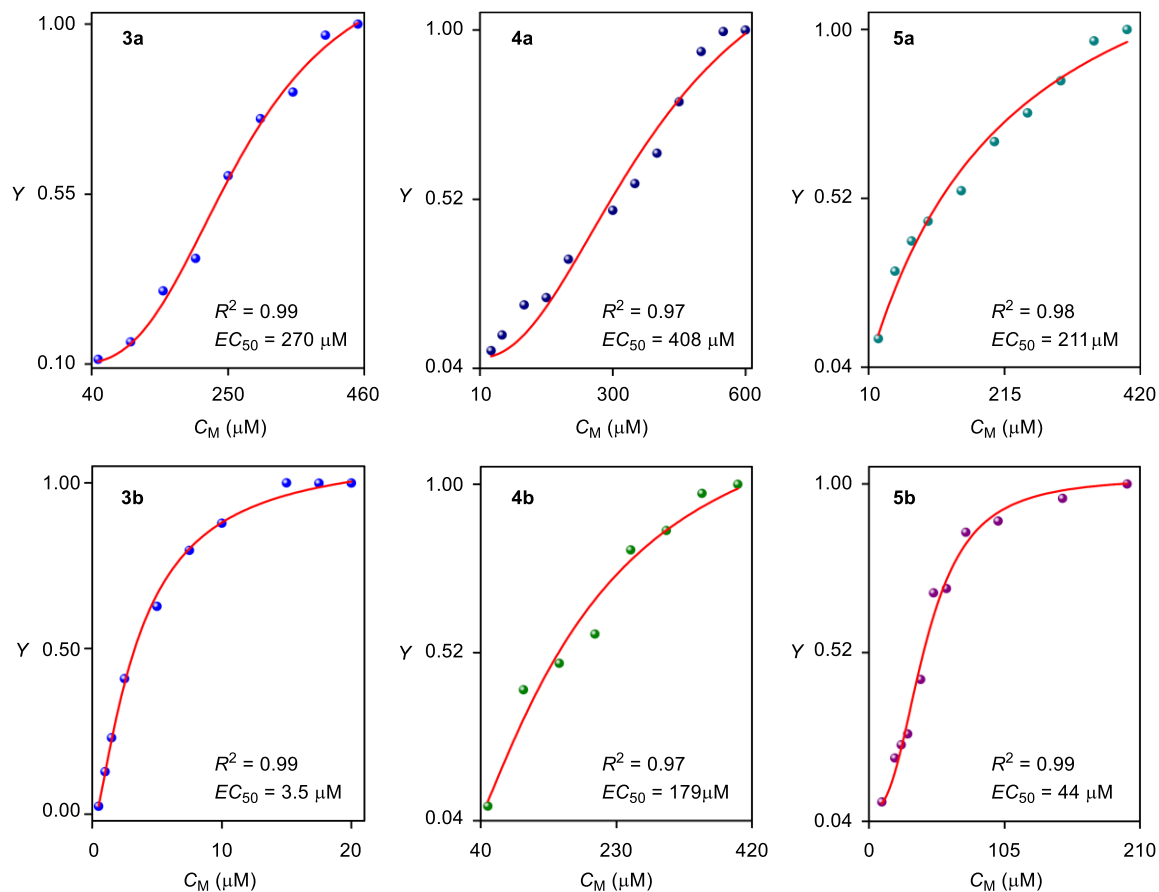
Appendix 4.3: Crystal structure of **3a**.



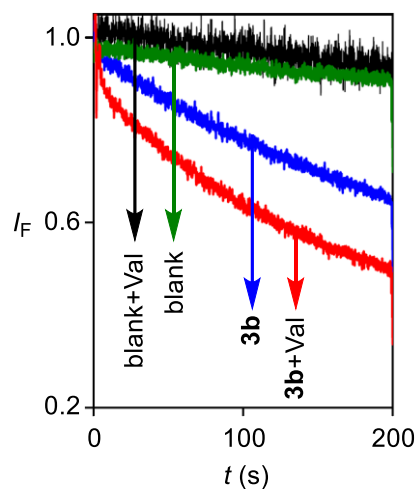
Appendix 4.4: Crystal structure of **3b**.



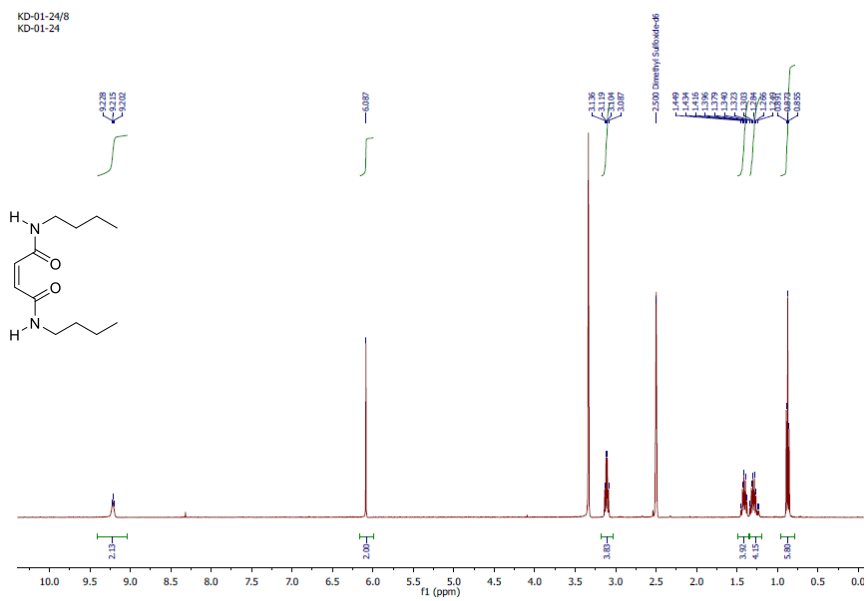
Appendix 4.5: Concentration profile of maleimide derivatives (**1a**, **2a**, **4a**, and **5a**) and fumaramide derivatives (**1b**, **2b**, **4b**, and **5b**) by varying concentration with EYPC-LUVs \Rightarrow HPTS vesicles.



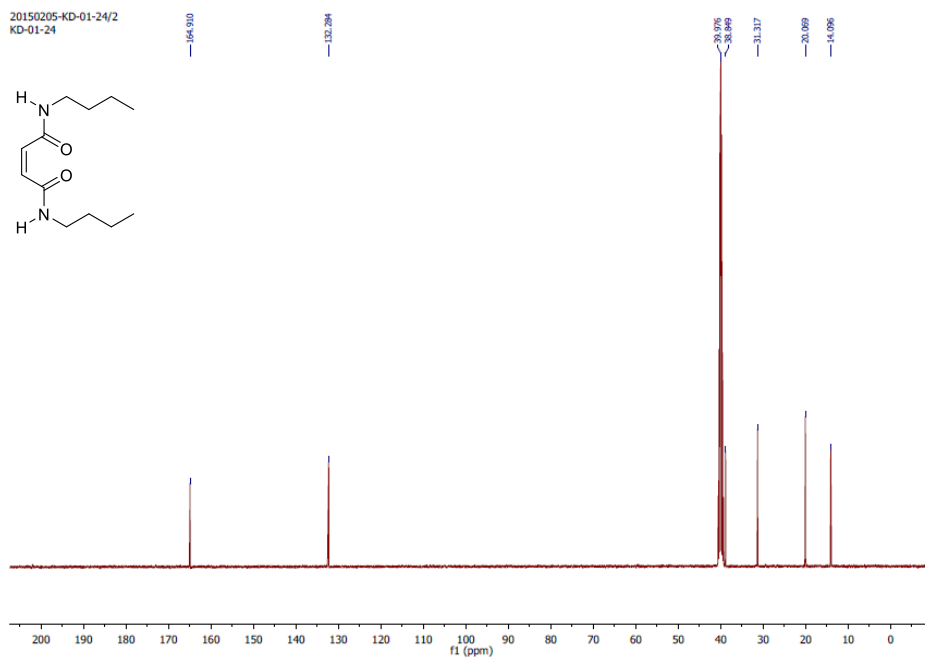
Appendix 4.6. Representation of Hill plots for all active compounds.



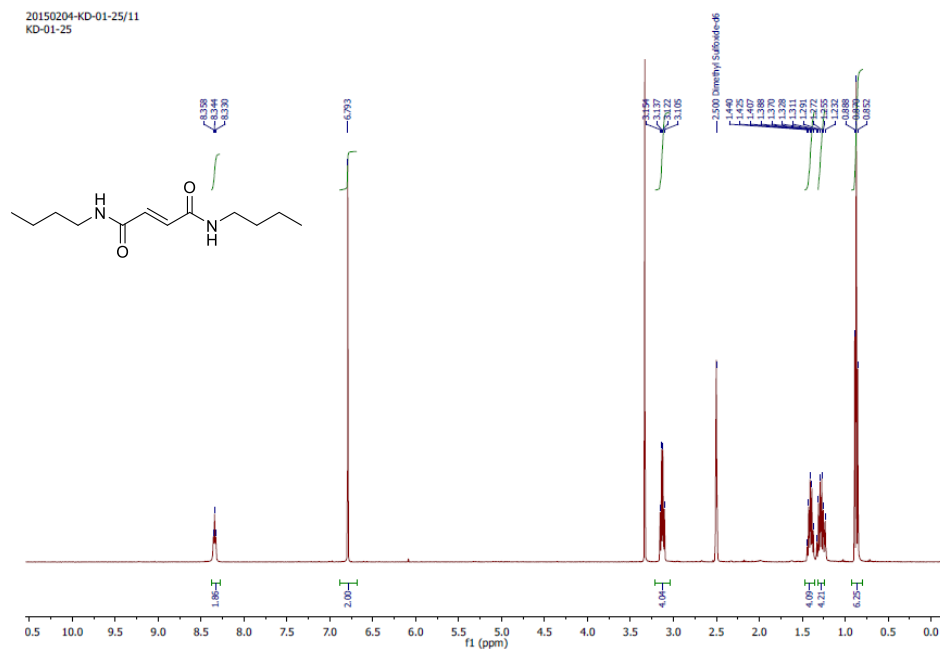
Appendix 4.7: Chloride transport assay by monitoring quenching of lucigenin fluorescence with valinomycin and compound **3b** ($30 \mu\text{M}$).



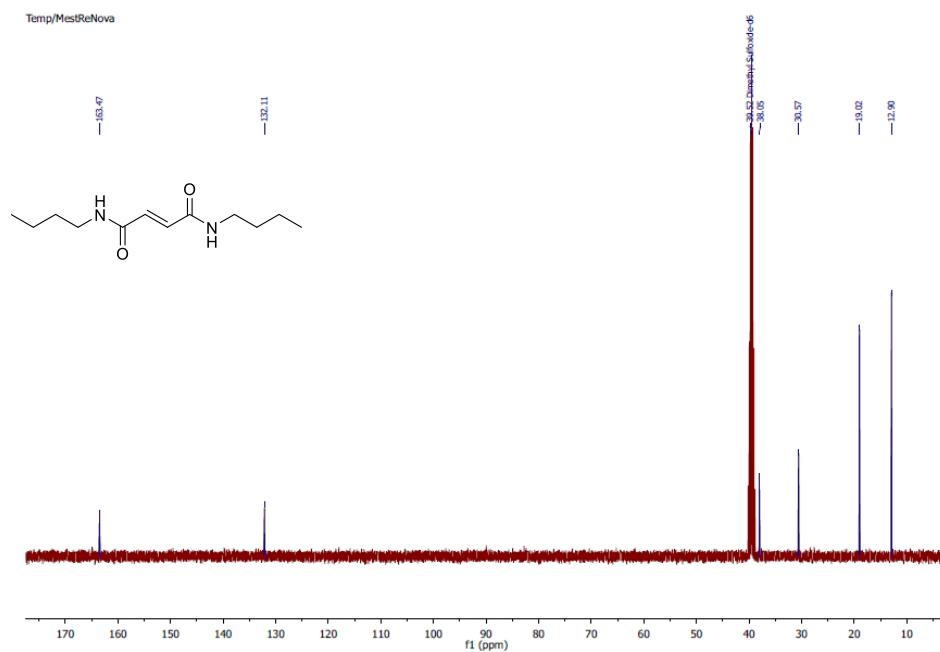
Appendix 4.8: ^1H NMR spectra of **1a** in $\text{DMSO-}d_6$.



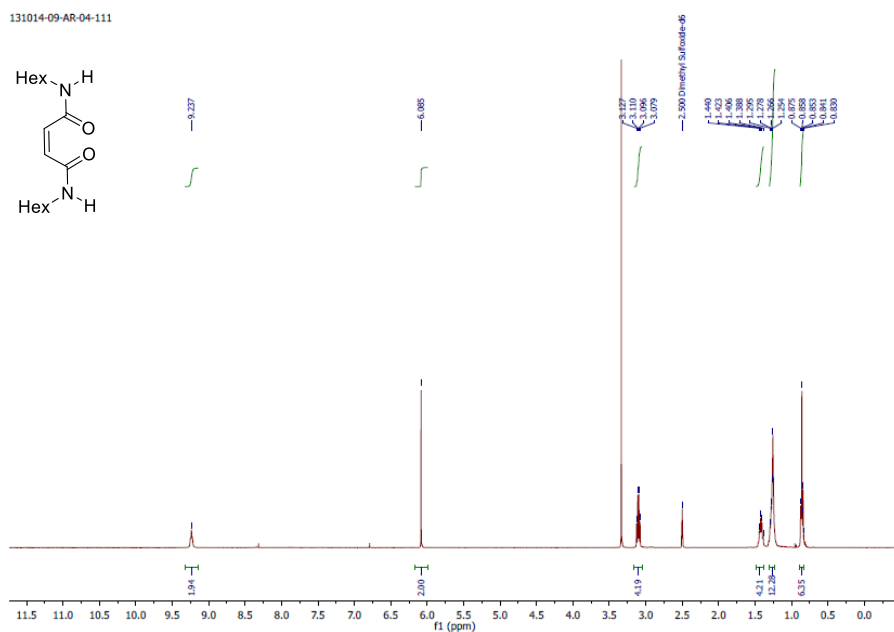
Appendix 4.9: ^{13}C NMR spectra of **1a** in $\text{DMSO-}d_6$.



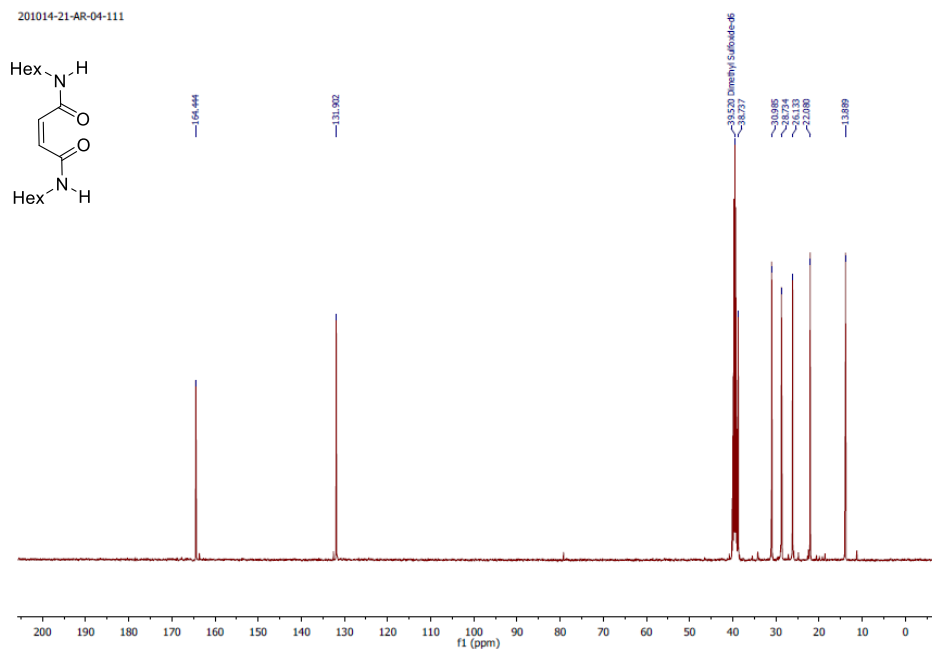
Appendix 4.10: ^1H NMR spectra of **1b** in $\text{DMSO-}d_6$.



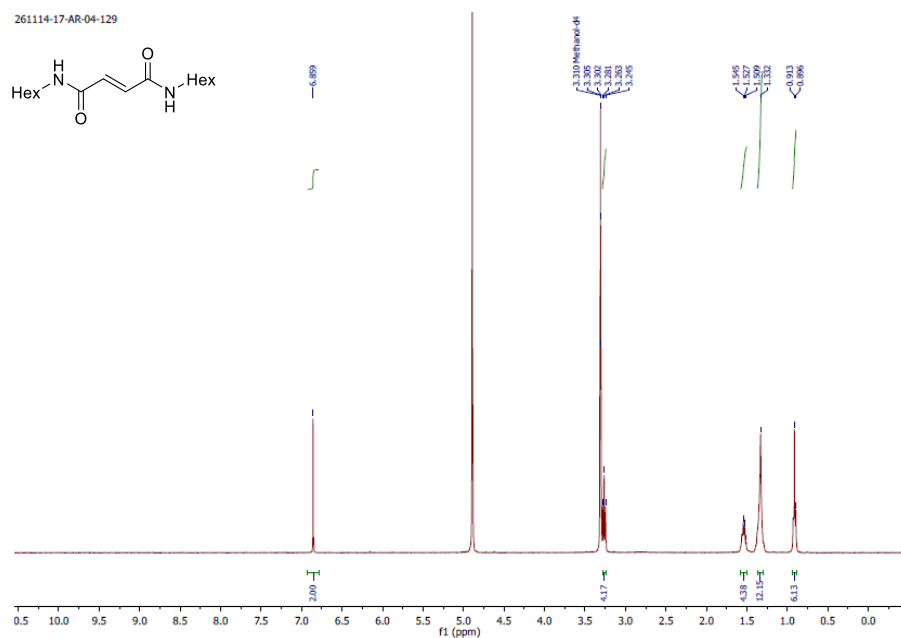
Appendix 4.11: ^{13}C NMR spectra of **1b** in $\text{DMSO-}d_6$.



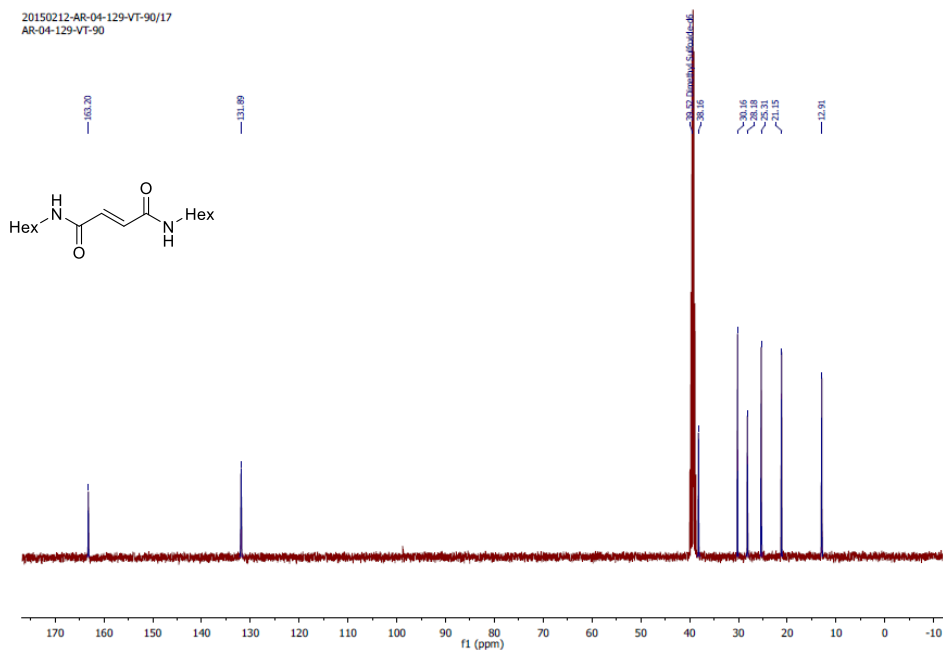
Appendix 4.12: ^1H NMR spectra of **2a** in $\text{DMSO-}d_6$.



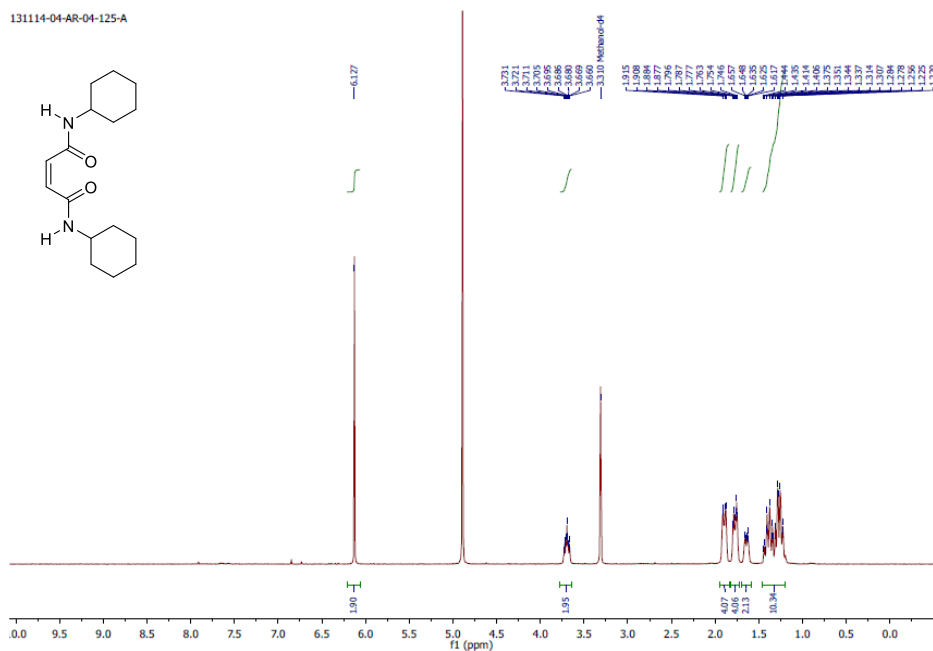
Appendix 4.13: ^{13}C NMR data of **2a** in $\text{DMSO-}d_6$.



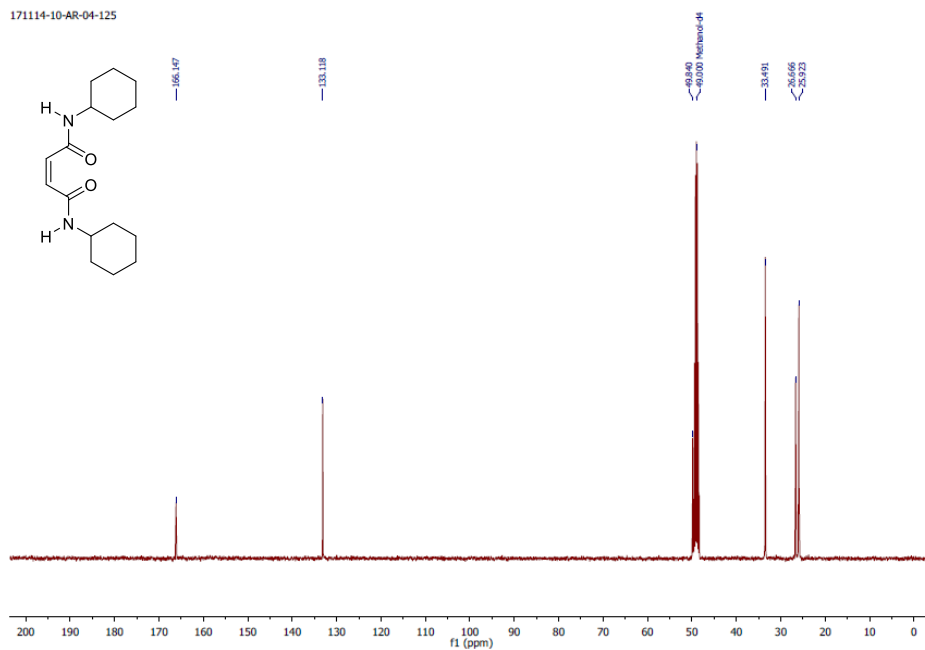
Appendix 4.14: ^1H NMR spectra of probe **2b** in $\text{MeOH-}d_4$.



Appendix 4.15: ^{13}C NMR spectra of probe **2b** in $\text{DMSO-}d_6$.

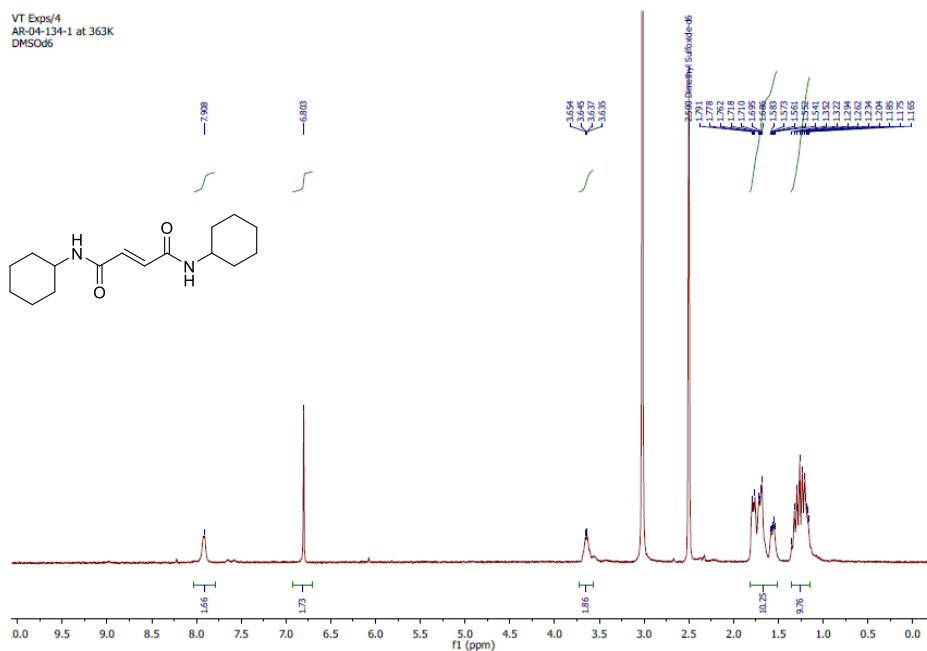


Appendix 4.16: ^1H NMR spectra of probe **3a** in MeOH- d_4 .

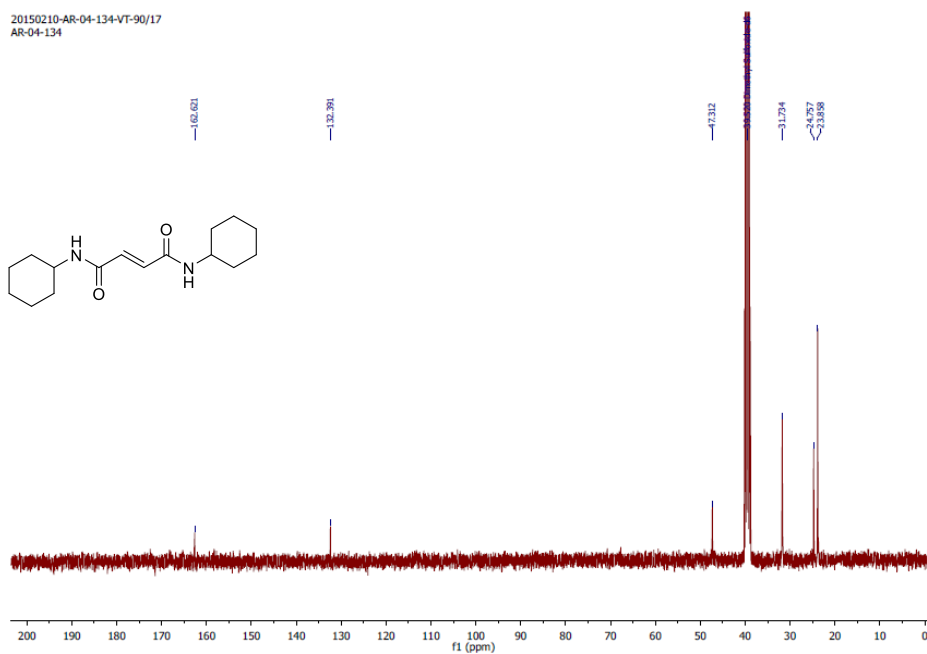


Appendix 4.17: ^{13}C NMR spectra of probe **3a** in MeOH- d_4 .

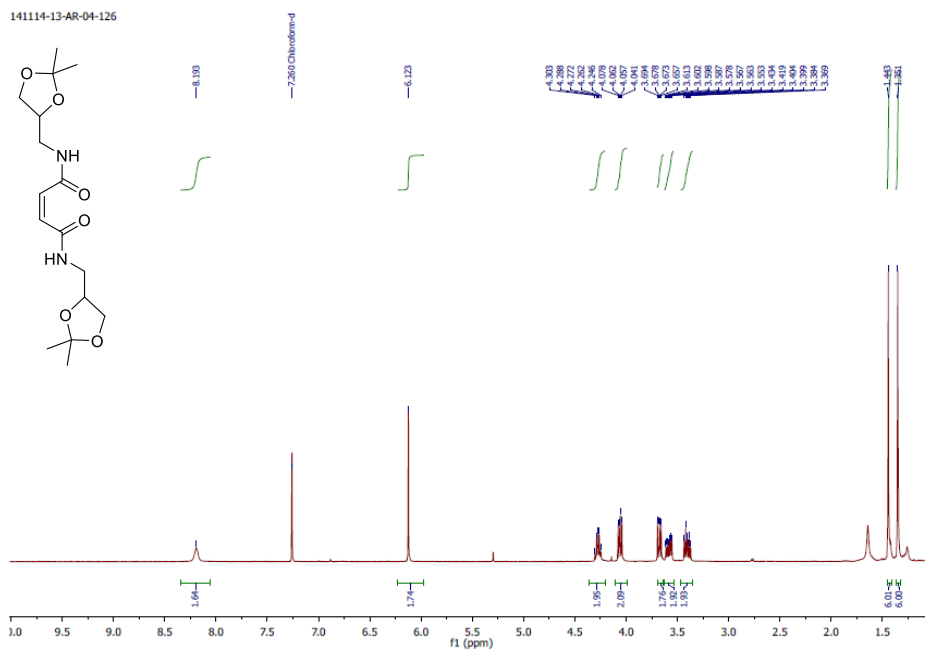
Chapter 4



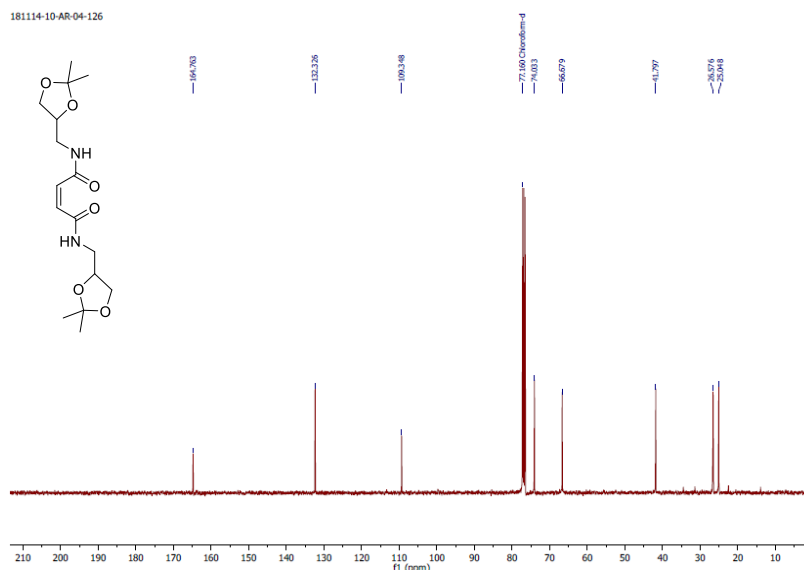
Appendix 4.18: ^1H NMR spectra of probe **3b** in $\text{DMSO-}d_6$.



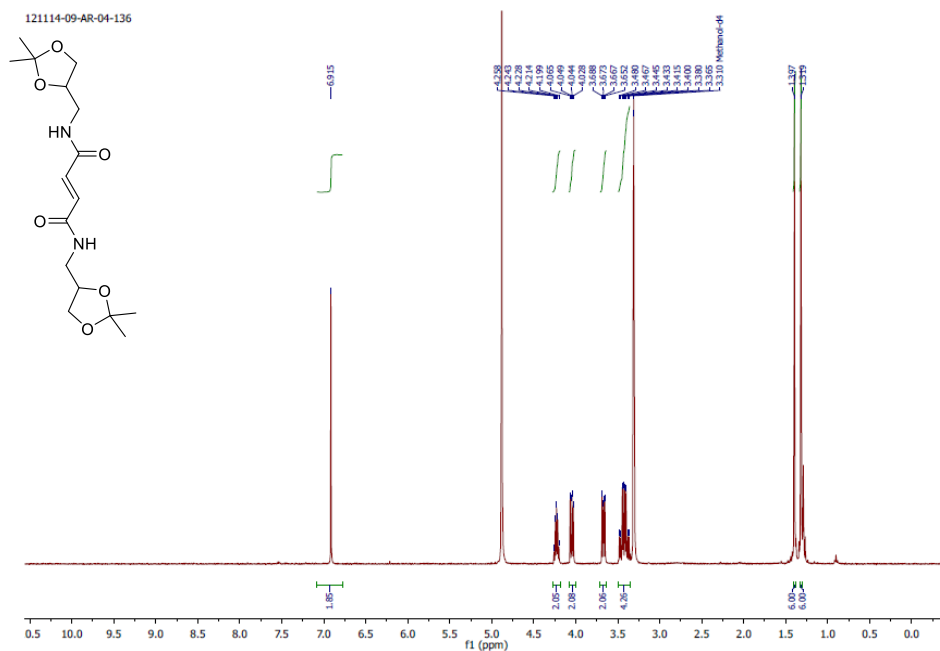
Appendix 4.19: ^{13}C NMR spectra of probe **3b** in $\text{DMSO-}d_6$.



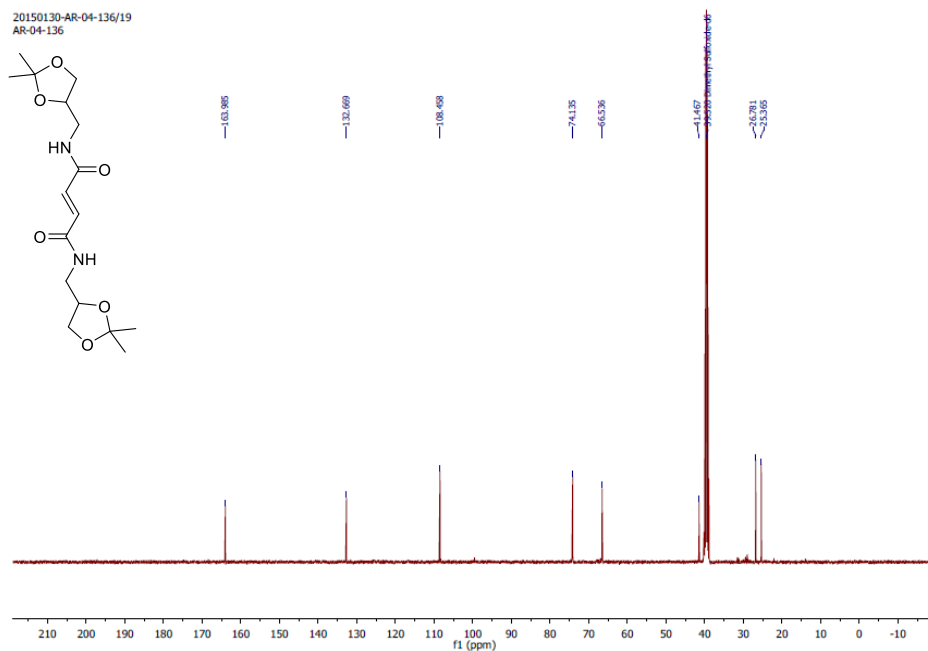
Appendix 4.20: ^1H NMR spectra of probe **4a** in CDCl₃.



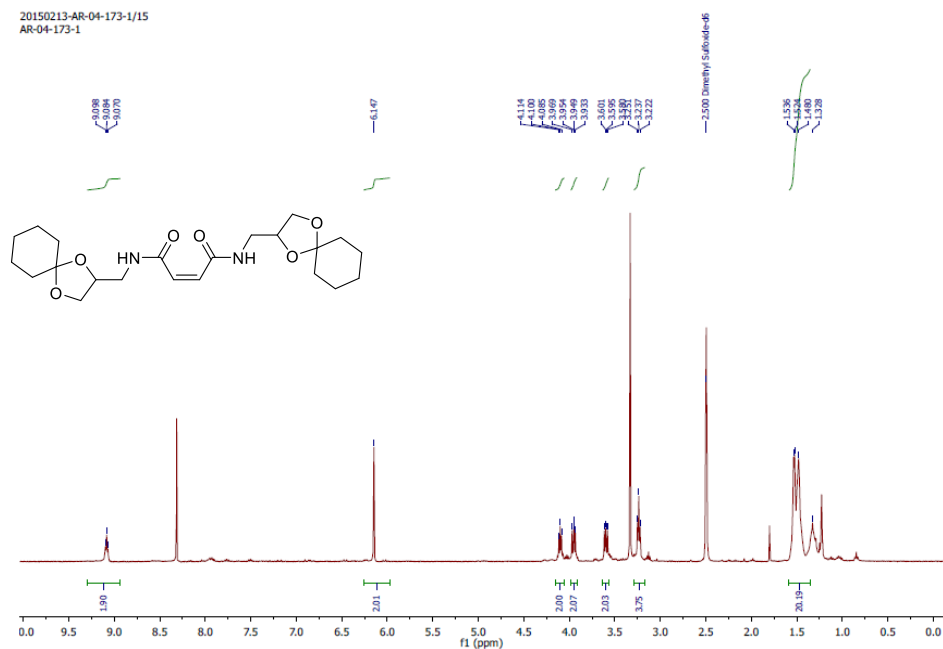
Appendix 4.21: ^{13}C NMR spectra of probe **4a** in CDCl₃.



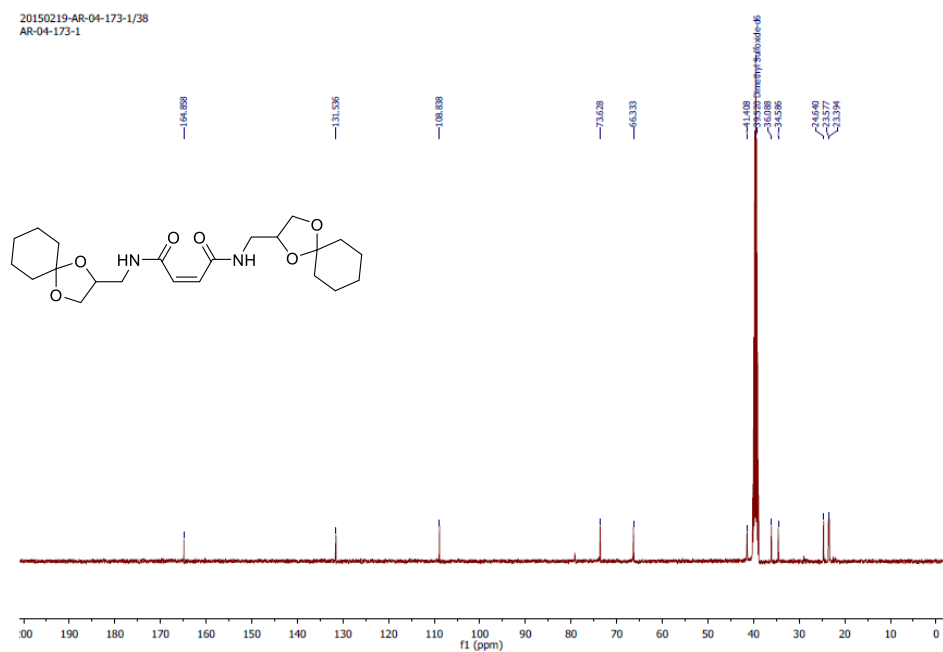
Appendix 4.22: ^1H NMR spectra of probe **4b** in MeOH- d_4 .



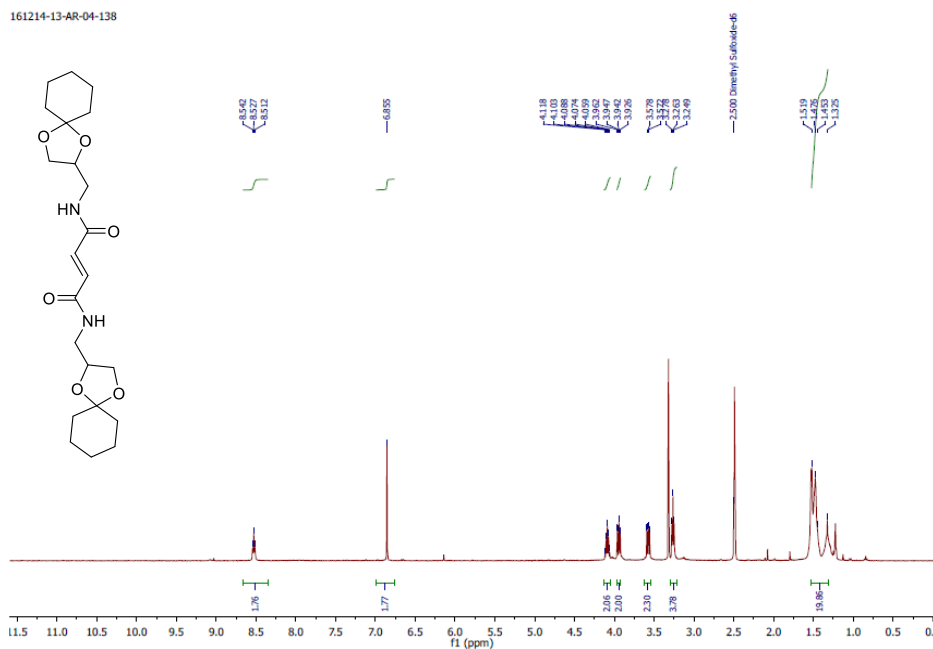
Appendix 4.23: ^{13}C NMR spectra of probe **4b** in DMSO- d_6 .



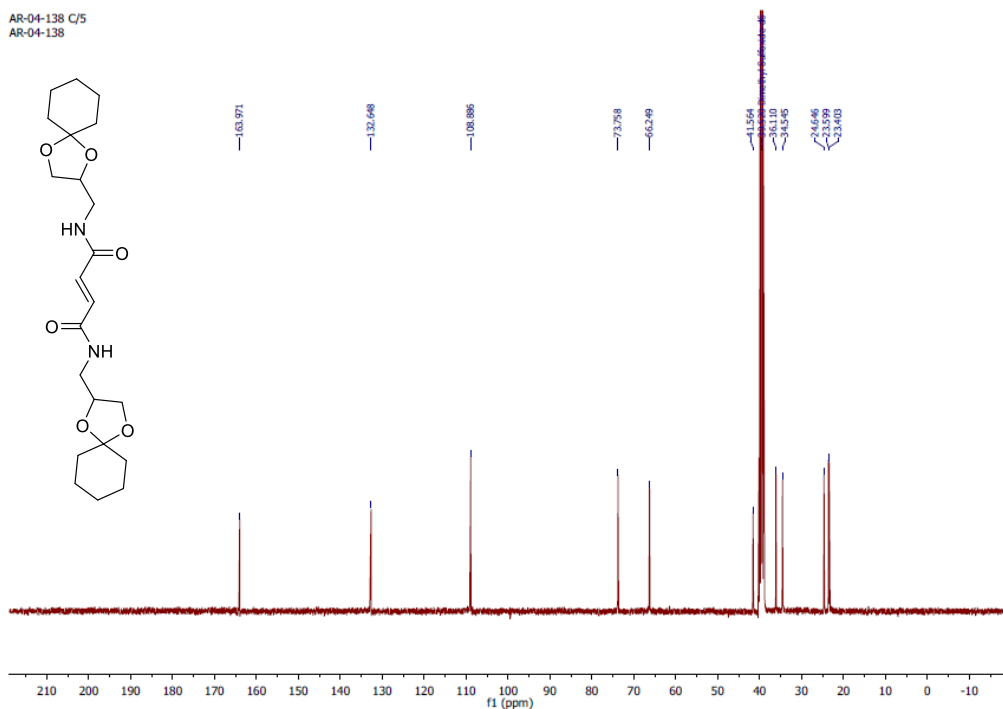
Appendix 4.24: ^1H NMR spectra of probe **5a** in $\text{DMSO-}d_6$.



Appendix 4.25: ^{13}C NMR spectra of probe **5a** in $\text{DMSO-}d_6$.



Appendix 4.26: ^1H NMR spectra of probe **5b** in DMSO- d_6 .



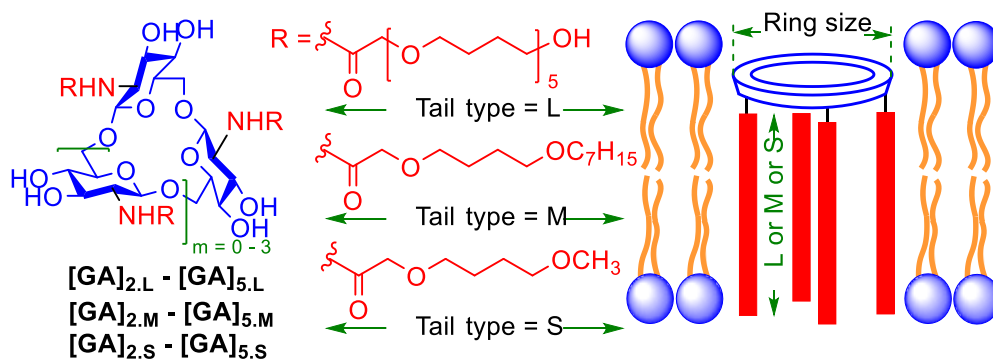
Appendix 4.27: ^{13}C NMR spectra of probe **5b** in DMSO- d_6 .

4.6. References

1. (a) De Riccardis, F.; Izzo, I.; Montesarchio, D.; Tecilla, P. *Acc. Chem. Res.* **2013**, *46*, 2781-2790; (b) Matile, S.; Vargas Jentsch, A.; Montenegro, J.; Fin, A. *Chem. Soc. Rev.* **2011**, *40*, 2453-2474; (c) Gale, P. A.; Pérez-Tomás, R.; Quesada, R. *Acc. Chem. Res.* **2013**, *46*, 2801-2813.
2. (a) Davis, J. T.; Okunola, O.; Quesada, R. *Chem. Soc. Rev.* **2010**, *39*, 3843-3862; (b) Davis, A. P.; Sheppard, D. N.; Smith, B. D. *Chem. Soc. Rev.* **2007**, *36*, 348-357.
3. (a) Borisenko, V.; Zhang, Z.; Woolley, G. A., *Biochim. Biophys. Acta.* **2002**, *1558*, 26-33; (b) Sakai, N.; Houdebert, D.; Matile, S. *Chem. Eur. J.* **2003**, *9*, 223-232; (c) Gorteau, V.; Perret, F.; Bollot, G.; Mareda, J.; Lazar, A. N.; Coleman, A. W.; Tran, D.-H.; Sakai, N.; Matile, S. *J. Am. Chem. Soc.* **2004**, *126*, 13592-13593; (d) Goto, C.; Yamamura, M.; Satake, A.; Kobuke, Y. *J. Am. Chem. Soc.* **2001**, *123*, 12152-12159; (e) Lien, L.; Jaikaran, D. C. J.; Zhang, Z.; Woolley, G. A. *J. Am. Chem. Soc.* **1996**, *118*, 12222-12223; (f) Chang, C.-y.; Niblack, B.; Walker, B.; Bayley, H. *Chem. Biol.* **1995**, *2*, 391-400; (g) Liu, T.; Bao, C.; Wang, H.; Lin, Y.; Jia, H.; Zhu, L. *Chem. Commun.* **2013**, *49*, 10311-10313; (h) Jog, P. V.; Gin, M. S. *Org. Lett.* **2008**, *10*, 3693-3696.
4. Talukdar, P.; Bollot, G.; Mareda, J.; Sakai, N.; Matile, S. *J. Am. Chem. Soc.* **2005**, *127*, 6528-6529.
5. Choi, Y. R.; Kim, G. C.; Jeon, H.-G.; Park, J.; Namkung, W.; Jeong, K.-S. *Chem. Commun.* **2014**, *50*, 15305-15308.
6. Saha, T.; Dasari, S.; Tewari, D.; Prathap, A.; Sureshan, K. M.; Bera, A. K.; Mukherjee, A.; Talukdar, P. *J. Am. Chem. Soc.* **2014**, *136*, 14128-14135.
7. Biscarini, F.; Cavallini, M.; Leigh, D. A.; León, S.; Teat, S. J.; Wong, J. K. Y.; Zerbetto, F. *J. Am. Chem. Soc.* **2002**, *124*, 225-233.
8. Shakuntala, K.; Foro, S.; Gowda, B. T. *Acta Cryst. E* **2011**, *67*, 1415.
9. (a) Roy, A.; Saha, D.; Mukherjee, A.; Talukdar, P. *Org. Lett.* **2016**, *18*, 5864-5867; (b) Roy, A.; Saha, T.; Gening, M. L.; Titov, D. V.; Gerbst, A. G.; Tsvetkov, Y. E.; Nifantiev, N. E.; Talukdar, P. *Chem. Eur. J.* **2015**, *21*, 17445-17452.
10. Sakai, N.; Brennan, K. C.; Weiss, L. A.; Matile, S. *J. Am. Chem. Soc.* **1997**, *119*, 8726-8727.
11. Rose, L.; Jenkins, A. T. A. *Bioelectrochemistry* **2007**, *70*, 387-393.
12. Si, W.; Li, Z.-T.; Hou, J.-L. *Angew. Chem. Int. Ed.* **2014**, *53*, 4578-4581.
13. Lohray, B. B.; Sekar Reddy, A.; Bhushan, V. *Tetrahedron Asym.* **1996**, *7*, 2411-2416.
14. Chattopadhyay, A.; Mamdapur, V. R. *J. Org. Chem.* **1995**, *60*, 585-587.
15. Rouf, A.; Aga, M. A.; Kumar, B.; Taneja, S. C. *Tetrahedron Lett.* **2013**, *54*, 6420-6422.
16. Chattopadhyay, S. K.; Biswas, T.; Biswas, T. *Tetrahedron Lett.* **2008**, *49*, 1365-1369.
17. Baker, T. J.; Goodman, M. *Synthesis* **1999**, *1999*, 1423-1426.

Chapter 5

Trimodal Control of Ion Transport Activity of Cyclo-Oligo-(1→6)-β-D-Glucosamine Based Artificial Ion Transport Systems



5.1. Introduction

Naturally occurring ion channel proteins are essential for living organisms due to their crucial role in regulating the flow of ions and molecules through the cell membrane.¹ Most of the naturally occurring ion channels are made up of complex protein structure, is very difficult to modulate the activity and they are also pretty much unstable for handling. So development of new synthetic ion channels as a mimic of natural channels is an important area of research. Carbohydrates have played a crucial role in designing artificial ion transporters and channels in recent years. Over the last several years, cyclodextrins (CDs) have been used as a rigid scaffold to construct several artificial ion transport systems.² Scientists have reported formation of ion channel by CDs when attached with membrane spanning linkers. For example, Tabushi and coworkers have reported cation selective A,C,D,F,-tetra-6-(6-n-butyrylamino-n-hexylsulfenyl)- β -cyclodextrin as a half-channel dimer.^{2a} Later on, Fyles and coworkers have reported cation selective triazole-linked another β -CD derivatives as half-channel dimers.^{2d, 2f} The per-(2,3-di-O-heptyl)-6-methoxyPEG-6-(1,2,3-triazole)- β -CDs displayed pH-dependent aggregation characteristics in the lipid membranes.^{2e} Gin and coworkers reported a unimolecular ion channel (full-channel monomer) based on aminocyclodextrin derivative (Figure 5.1A),^{2b, 2c} and the ion channel formed by β -CD derivative exhibited anion transport with a selectivity topology of $I^- > Br^- > Cl^-$. The dehydration energy dependent sequence (Hofmeister series or Eisenman halide sequence I) is very common. However, Cl^- selective channels have been proved to have potential channel replacement therapy. We have realised that the design of a Cl^- selective ion channel based on CDs (α -, β - and γ -CD) is challenging because of large and hydrophobic interior (Figure 5.1C). The inner diameters of CDs ($d_{\alpha-CD} = 0.45-0.57$ nm, $d_{\beta-CD} = 0.62-0.78$ nm and $d_{\gamma-CD} = 0.79-0.95$ nm) are very large compared to the diameter of Cl^- ion ($d_{Cl^-} = 0.36$ nm) (Figure 5.1B). Unfortunately, literature indicates that smaller analogs of CDs are synthetically inaccessible.³ Molecular recognition studies and theoretical calculation revealed that the cavity present in β -CD is mostly hydrophobic. As a result, hydrophobic interior and inaccessibility of smaller analogs of CDs limit the probability of forming Cl^- selective ion channel.⁴

There are few reports by Hindsgaul *et. al.*, Gin *et. al.*, and Montesarchio *et. al.* of synthesizing glucose-based macrocycles of different oligomericity containing surrogate linkages instead of the natural O-glycosidic bonds.⁵ Ion transport activity of few cyclic phosphate-based

cyclooligosaccharides were investigated by attaching hydrophobic tail of different length, and sometimes by modifying on oligosaccharides macrocycles.⁶ Yet, study for Cl⁻ selectivity of these macrocycles was not widely explored. To overcome the aforesaid limitations, new cyclic functionalized agents were required with smaller and more hydrophilic cavities. A series of homologous cyclic oligo-(1→6)-β-D-glucosamine (GA) macrocycles [GA]₂ – [GA]₇ consisting of two to seven glucosamine units were reported recently by Nifantiev and coworkers.^{4, 7} The molecular dynamics (MD) simulation studies indicate an interesting correlation between oligomericity and rigidity of these macrocycles (Figure 5.1E).^{4, 8} Pore diameter of the macrocycles follows an increasing order from dimeric to tetrameric cyclo-(1→6)-β-D-glucosamines [GA]_{2,Ac} – [GA]_{4,Ac} (0.35 to 0.58 nm) (Figure 5.1F). However, in case of larger macrocycles [GA]_{5,Ac} – [GA]_{7,Ac}, the effective pore diameter fluctuates because of the complicated shape and conformational flexibility of these macrocycles. Therefore, diameter of GA macrocycles offers a rigid platform upto four membered ring to construct artificial ion transport systems and beyond that ion transport activity should be less. The presence of free amino groups in the macrocycle facilitates attachment of hydrophobic tails required to produce an active transmembrane pore.⁸ Additionally, the presence of defined hydrophilic cavity within the tetrameric macrocycle was also revealed by theoretical calculations (Figure 5.1G)⁴ and this can be considered as an essential criteria for constructing the polar pore for recognizing hydrophilic anions. This characteristic helps migration of ions through the GA cavities with lower free energy loss as compared to CD cavities.

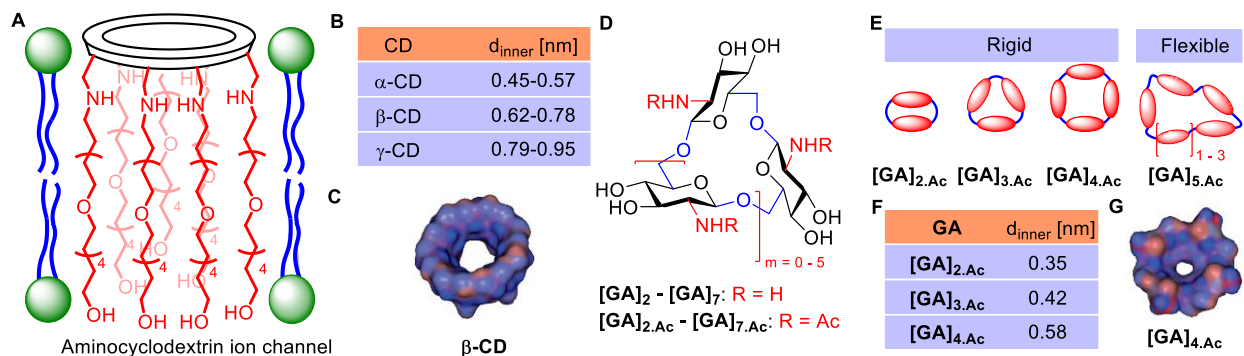


Figure 5.1: **A)** Structure of the aminocyclodextrin channel, **B)** Inner diameter of α-, β-, and γ-CD, **C)** Representation of hydrophilic (red) and hydrophobic (blue) areas in β-CD, **D)** Structures of oligo-(1→6)-β-D-glucosamine macrocycles [GA]₂ – [GA]₇, **E)** Representation of oligomericity *versus* rigidity for [GA]_{2,Ac} – [GA]_{5,Ac}, **F)** Inner diameters of [GA]_{2,Ac} – [GA]_{4,Ac}, **G)** Representation of hydrophilic (red) and hydrophobic (blue) areas in [GA]_{4,Ac}.

Therefore, new synthetic ion transport system was designed based on macrocycles $[GA]_2 - [GA]_5$. To replicate both the full-channel monomer (reported by Gin and coworkers) and half-channel dimer (reported by Fyles and coworkers) models in the GA system, primarily three types of tails were selected. A pentabutylene glycol-based chain was selected^{2b} as a long tail for constructing the full-channel monomer (Figure 5.2A) in the egg yolk phosphatidylcholine (EYPC) lipid membranes (thickness = 0.35 – 0.40 nm). Based on this idea, the glycoconjugates $[GA]_{2,L} - [GA]_{5,L}$ can act as full-channel monomers⁸ (Figure 5.2A). All experiment of $[GA]$ derivatives with long (L) tails were already carried out in our laboratory by Tanmoy Saha. A medium sized 4-(heptyloxy)butan-1-ol tail was selected to construct the half-channel monomer and related structures were described as $[GA]_{2,M} - [GA]_{5,M}$ (Figure 5.2B). In this case, the active channel structure was proposed based on the self-assembly of two half-channel monomer units. Such a

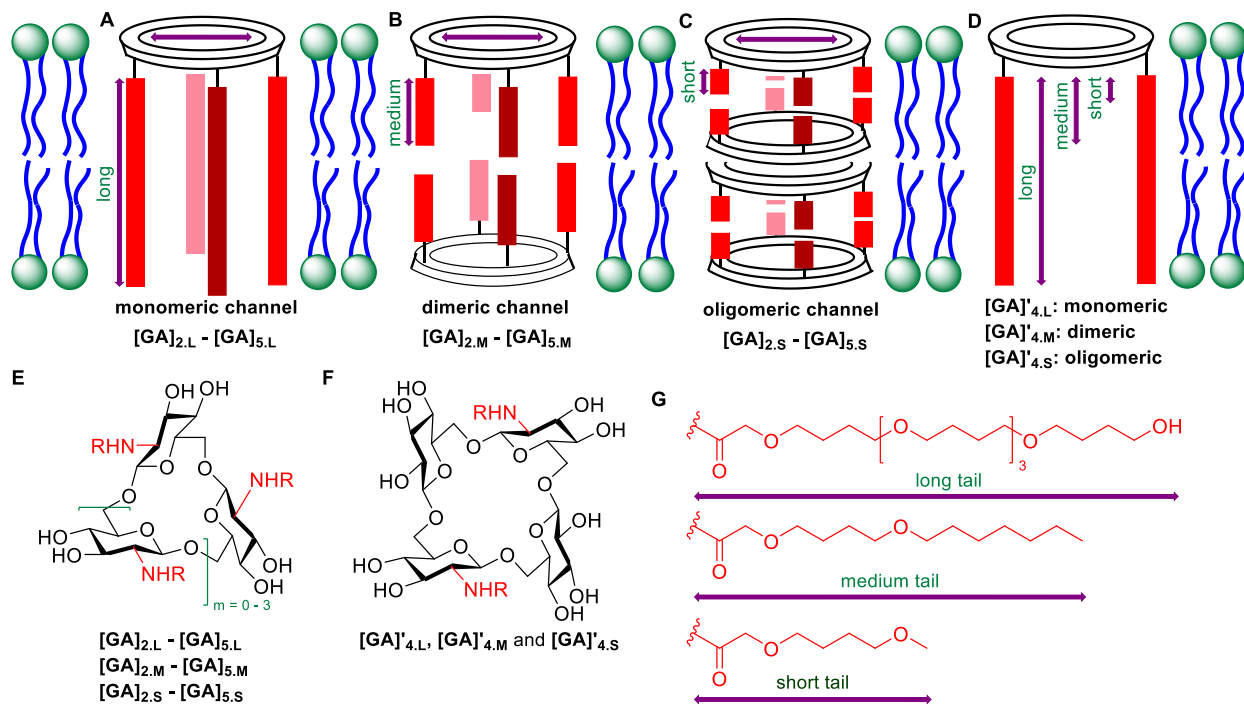


Figure 5.2: (A – C) Proposed models of ion transport systems with tunable pore diameter and varied tail length. (D) Model of “hybrid” cyclic tetrasaccharide based transport system with fewer numbers of tails. (E) Structures of the oligo-(1→6)-β-D-glucosamine based ion transporting molecules $[GA]_{2,L} - [GA]_{5,L}$, $[GA]_{2,M} - [GA]_{5,M}$, and $[GA]_{2,s} - [GA]_{5,s}$, (F) Structures of “hybrid” cyclic tetrasaccharide based ion transporting molecules $[GA]'_{4,L}$, $[GA]'_{4,M}$, and $[GA]'_{4,s}$. (G) Description of hydrophobic tails linked to designed macrocycles.

self-assembled system was expected to exhibit lower activity compared to the corresponding full-channel monomer. A third type of tail, based on 4-methoxybutan-1-ol was also selected to design the derivatives [GA]_{2,s}–[GA]_{5,s} (Figure 5.2C). The stacked self-assembly of these molecules was proposed as the active structure in the lipid membranes and, therefore, expected to display lesser activity compared to corresponding medium and long linker connected molecules. A “hybrid” tetrasaccharide-based macrocycle [GA]’₄ (Figure 5.2D) was also introduced to evaluate the effect of the number of tails on the ion transporting activity. This class of macrocycle was accessible for covalent linking of only two tails and thereby, molecules [GA]’_{4,L}, [GA]’_{4,M}, and [GA]’_{4,S} were designed based on linking of long, medium and short tails (Figure 5.2F). Such a design was important to examine the significance of hydrophobic tails in the membrane permeation of transporting molecules.

5.2. Results and Discussions

5.2.1. Synthesis

All compounds were synthesized by our collaborator Marina L. Gening and co-workers.

5.2.2. Ion Transport Activity

Ion transporting activity of all glucosamine derivatives were evaluated by fluorescence assay using large unilamellar vesicles (LUVs). The LUVs with entrapped 8-hydroxypyrene-1,3,6-trisulfonate (HPTS) were prepared from EYPC lipid.⁹ A pH gradient across the vesicles ($\text{pH}_{\text{in}} = 7.0$ and $\text{pH}_{\text{out}} = 7.8$) was applied by the addition of NaOH in the extraventricular solution followed by addition of a GA derivative. Upon addition of such molecule, a destruction of the applied pH gradient occurred via H^+ ion efflux or OH^- ion influx leading to the increase of pH inside the vesicles. This process resulted in the fluorescence enhancement of HPTS ($\lambda_{\text{ex}} = 450$ nm, $\lambda_{\text{em}} = 510$ nm). Finally, the complete destruction of the pH gradient was achieved by addition of Triton-X at $t = 300$ s. Figure 5.3A represents the comparison of ion transport activities of all compounds at an identical monomer concentration of 1.5 μM . For medium tail connected glucosamines, the activity sequence of $[\text{GA}]_{2,\text{M}} < [\text{GA}]_{3,\text{M}} < [\text{GA}]_{4,\text{M}} > [\text{GA}]_{5,\text{M}}$ was observed. Similar activity sequences were observed for short tail ($[\text{GA}]_{2,\text{S}} < [\text{GA}]_{3,\text{S}} < [\text{GA}]_{4,\text{S}} > [\text{GA}]_{5,\text{S}}$) connected glucosamines, which further supported our design (Figure 5.3B). Five membered macrocycles imposes greater

extent of loss of rigidity because of the lateral pressure of the lipid membrane.^{8, 10} This outcome confirmed that the ion transport activity increased with the increase in oligomericity of glucosamines (*i.e.* increase in the pore size) if the macrocycle is rigid (for di-, tri- and tetrameric systems). For a fixed oligomericity, the transporting activity increased with the length of the tail *i.e.* $[GA]_{2,S} < [GA]_{2,M} < [GA]_{2,L}$, $[GA]_{3,S} < [GA]_{3,M} < [GA]_{3,L}$, $[GA]_{4,S} < [GA]_{4,M} < [GA]_{4,L}$, and $[GA]_{5,S} < [GA]_{5,M} < [GA]_{5,L}$. The comparison diagram also suggests the importance of the number of membrane-spanning tails connected to a glucosamine macrocycle. For example, the observed trends of activities $[GA]_{4,M} > [GA]'_{4,M}$ indicate the better membrane permeability whenever a more number of tails are connected. The slight deviation of the trend observed for $[GA]_{4,S}$ and $[GA]'_{4,S}$ may be ignored because activities of both compounds were low.

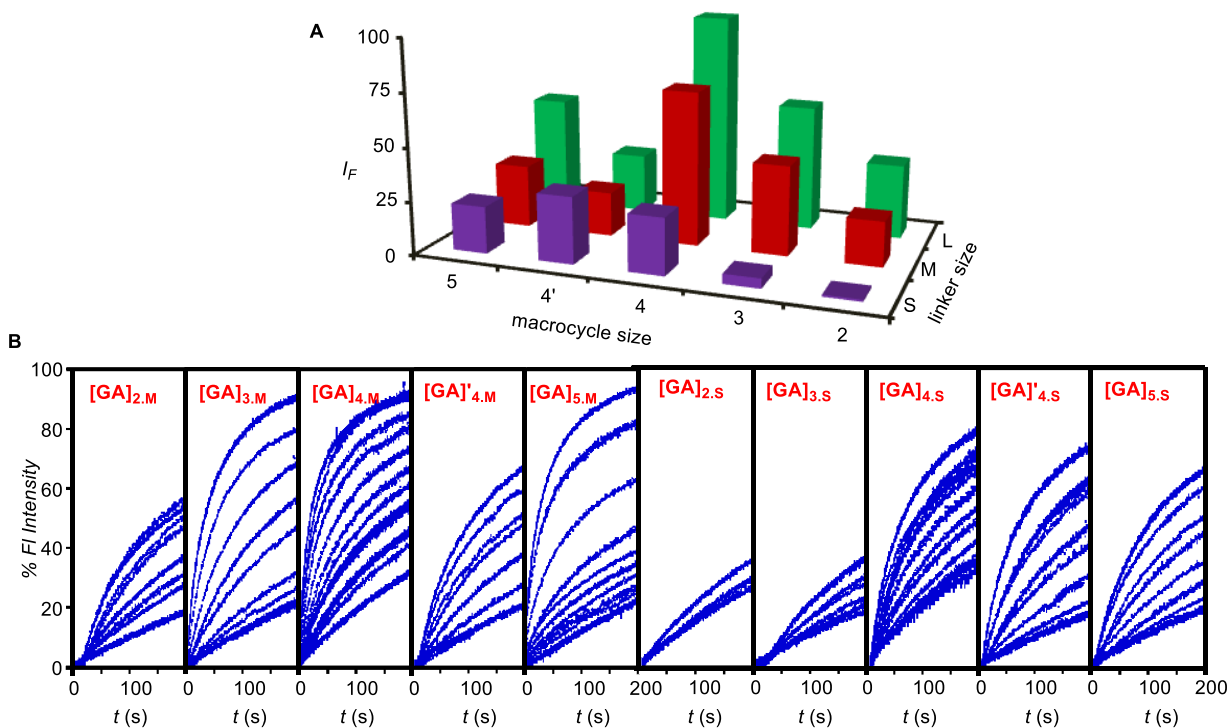


Figure 5.3: A) Comparison of ion transporting activity of glycoconjugates $[GA]_{2,L} - [GA]_{5,L}$, $[GA]_{2,M} - [GA]_{5,M}$, $[GA]_{2,S} - [GA]_{5,S}$, $[GA]'_{4,L} - [GA]'_{4,S}$ at 1.5 μ M concentrations and B) ion transport activity of medium tail and short tail compounds using EYPC-LUVs \supset HPTS.

In the next stage, ion transporting activities of all synthesized compounds were recorded at varied monomer concentrations and fractional activities (Y) at $t = 100$ s were plotted against respective concentrations. Among all compounds, $[GA]_{4,L}$ displayed the highest activity compared to all glucosamine derivatives with lowest effective concentration at the half-maximal response,

$EC_{50} = 0.75 \mu\text{M}$ with Hill coefficient $n = 1.2$ which signified the single monomer as the active structure (as $n \sim 1$). Medium tail connected glucosamine derivatives $[\text{GA}]_{4,\text{M}} (1.7 \mu\text{M}) < [\text{GA}]_{3,\text{M}} (2.7 \mu\text{M}) < [\text{GA}]'_{4,\text{M}} (3.8 \mu\text{M}) < [\text{GA}]_{2,\text{M}} (4.5 \mu\text{M}) < [\text{GA}]_{5,\text{M}} (4.77 \mu\text{M})$ (Figure 4). For the medium tail connected tetrasaccharide $[\text{GA}]_{4,\text{M}}$, the Hill coefficient $n = 2.0$ indicates the dimeric structure as an active supramolecule in the lipid membranes. Hill coefficient values for other medium tail connected derivatives ($n = 1.5$ for $[\text{GA}]_{3,\text{M}}$, $n = 3.0$ for $[\text{GA}]_{5,\text{M}}$, $n = 1.7$ for $[\text{GA}]_{2,\text{M}}$) shifted from their ideal values, possibly due to the deviation from the typical sigmoidal dose-response curve. Among short tail connected derivatives, EC_{50} values of $[\text{GA}]_{2,\text{S}}$ and $[\text{GA}]_{3,\text{S}}$ could not be determined due to low activity. The hill analysis for short linker connected glucosamines were not performed because of very low activity. Other thermodynamic factors such as higher water solubility and poor membrane permeability could also contribute to the poor activities of these molecules. For a specific size of the macrocycle, activity increased with the increase in tails length.

5.2.3. Ion Selectivity Assay

Cation selectivity of all oligo-(1→6)- β -D-glucosamine derivatives attached with medium and small tail across the EYPC-LUVs were measured in the presence of intravesicular NaCl, isoosmolar extravesicular monovalent metal chlorides (MCl , $\text{M}^+ = \text{Li}^+, \text{Na}^+, \text{K}^+, \text{Rb}^+, \text{and Cs}^+$) after applying a pH gradient.⁸⁻⁹ Each experiment was carried out with the respective concentration at EC_{50} of a glucosamine derivative. Upon varying the external cation with isoosmolar intravesicular NaCl, no definite differences in transport activity were observed (Figure 5.4A). Therefore, similar studies were carried out in the presence of intravesicular NaCl, isoosmolar extravesicular sodium halides (NaX , $\text{X}^- = \text{Cl}^-, \text{Br}^-, \text{and I}^-$) after applying a pH gradient. Strongly basic F^- ion was excluded for this purpose. Upon variation of the extravesicular anion, a uniform $\text{Cl}^- > \text{Br}^- > \text{I}^-$ selectivity sequence (*i.e.* reverse of common Hofmeister halide sequence) was observed for each glucosamine derivative (Figure 5.4B). Therefore, proposed Cl^- selectivity during ion transport was achieved based on designed oligo-(1→6)- β -D-glucosamine derivatives attached with medium and small tail.

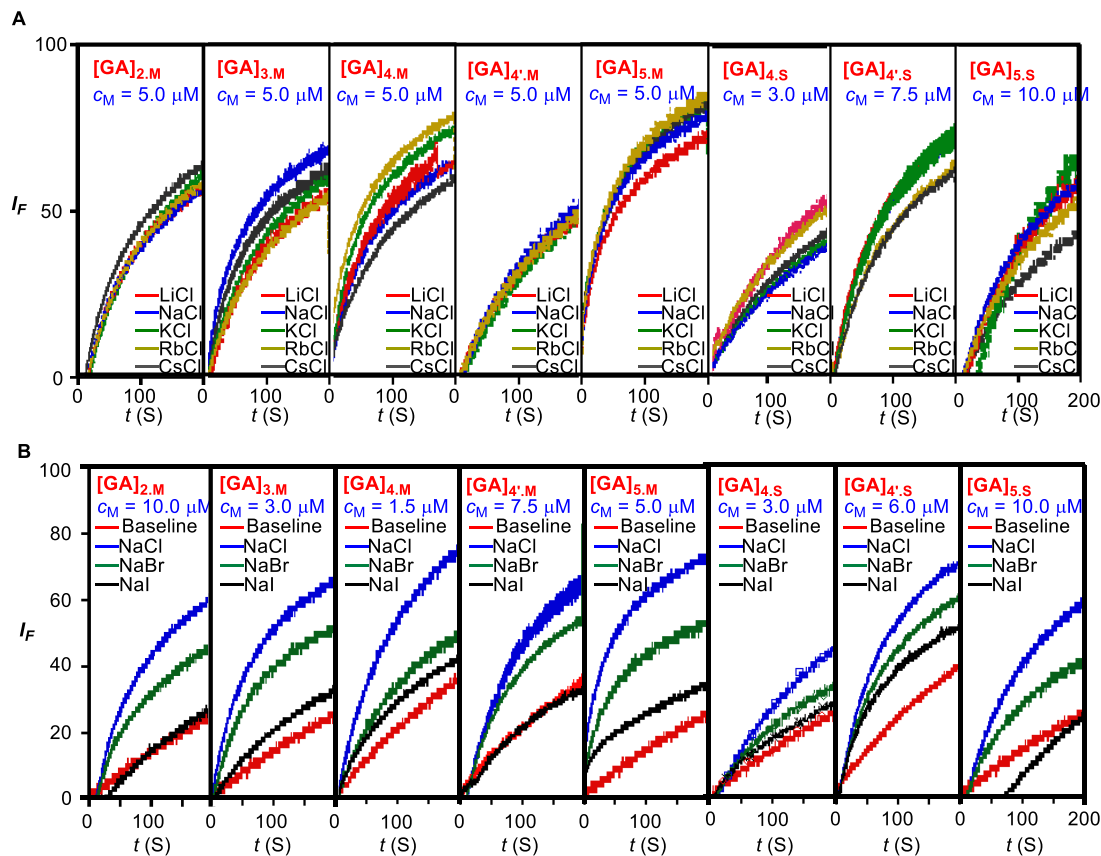


Figure 5.4: A) Cation and B) anion selectivity of [GA]_{2.M}, [GA]_{3.M}, [GA]_{4.M}, [GA]_{4'.M}, [GA]_{5.M}, [GA]_{4.S}, [GA]_{4'.S} and [GA]_{5.S} using EYPC-LUVs \supset HPTS.

5.3. Conclusion

In summary, artificial ion channels were designed on the basis of a new type of functionalized cyclic oligosaccharide scaffolds, namely cyclo-oligo-(1 \rightarrow 6)- β -D-glucosamines. They were rationally designed for Cl⁻ selectivity due to presence of smaller and hydrophilic cavity in comparison with cyclodextrins. Additionally, amenability of ring-size alteration and its associated correlation with the ring rigidity made it possible to control the ion transporting activity. Importance of number of membrane spanning tails was established by varying tail length and number of tails. Half-channel dimers as the active structures were formed with a medium sized tail. Short tail connected derivatives that displayed poor ion transport activity worked as negative controls for ion transport studies. All molecules displayed a uniform Cl⁻ > Br⁻ > I⁻ selectivity sequence.

5.4. Experimental Section

General Methods: Egg yolk phosphatidylcholine (EYPC) was purchased from Avanti Polar Lipids as a solution in chloroform (25 mg/mL). HEPES buffer, HPTS, Triton X, NaOH and inorganic salts of molecular biology grade were purchased from Sigma. Gel-permeation chromatography was performed on a column of Sephadex LH-20 gel (25×300 mm, $V_0 = 25$ mL) in $\text{CHCl}_3/\text{MeOH}$ (1:1, v/v). Large unilamellar vesicles (LUVs) were prepared by using mini extruder, equipped with a polycarbonate membrane of 100 nm pore size, obtained from Avanti Polar Lipids.

Physical Measurements: Fluorescence spectra were recorded by using Fluoromax-4 from Jobin Yvon Edison equipped with an injector port and a magnetic stirrer. 10 mM HEPES (with 100 mM NaCl) buffer solution used for fluorescence experiment and the pH of the buffer was adjusted to 7.0 by NaOH using Helmer pH meter. All data of fluorescence studies were processed either by Origin 8.5 or KaleidaGraph.

Determination of ion transport activity by HPTS LUVs: Same protocol as discussed in Chapter 3A.

Determination of ion selectivity Assay by HPTS LUVs: Same protocol as discussed in Chapter 3A.

5.5. References

- (a) Song, L.; Hobaugh, M. R.; Shustak, C.; Cheley, S.; Bayley, H.; Gouaux, J. E. *Science* **1996**, *274*, 1859-1866; (b) Mosgaard, L. D.; Heimburg, T. *Acc. Chem. Res.* **2013**, *46*, 2966-2976; (c) Zhang, J.; Liu, Q.; Liu, X.; Zhang, S.; Jiang, P.; Wang, Y.; Luo, S.; Li, Y.; Wang, Q. *Chem. Commun.* **2015**, *51*, 1297-1300; (d) Cai, Y.; Jiao, J.; Bin, Z.; Zhang, Y.; Yang, P.; Lu, H. *Chem. Commun.* **2015**, *51*, 772-775; (e) Barbier-Brygoo, H.; De Angeli, A.; Filleur, S.; Frachisse, J.-M.; Gambale, F.; Thomine, S.; Wege, S. *Annu. Rev. Plant Biol.* **2011**, *62*, 25-51.
- (a) Tabushi, I.; Kuroda, Y.; Yokota, K. *Tetrahedron Lett.* **1982**, *23*, 4601-4604; (b) Madhavan, N.; Robert, E. C.; Gin, M. S. *Angew. Chem., Int. Ed.* **2005**, *44*, 7584-7587; (c) Madhavan, N.; Gin, M. S. *ChemBioChem* **2007**, *8*, 1834-1840; (d) Chui, J. K. W.; Fyles, T. M. *Chem. Commun.* **2010**, *46*, 4169-4171; (e) El Ghouli, Y.; Renia, R.; Faye, I.; Rassou, S.; Badi, N.; Bennevault-Celton, V.; Huin, C.; Guegan, P., *Chem. Commun.* **2013**, *49*, 11647-11649; (f) Chui, J. K. W.; Fyles, T. M. *Org. Biomol. Chem.* **2014**, *12*, 3622-3634.
- Immel, S.; Brickmann, J.; Lichtenthaler, F. W. *Liebigs Ann.* **1995**, 929-42.
- Gening, M. L.; Titov, D. V.; Grachev, A. A.; Gerbst, A. G.; Yudina, O. N.; Shashkov, A. S.; Chizhov, A. O.; Tsvetkov, Y. E.; Nifantiev, N. E. *Eur. J. Org. Chem.* **2010**, *2010*, 2465-2475.

5. (a) Hoffmann, B.; Bernet, B.; Vasella, A. *Helv. Chim. Acta.* **2002**, *85*, 265-287; (b) Bodine, K. D.; Gin, D. Y.; Gin, M. S. *J. Am. Chem. Soc.* **2004**, *126*, 1638-1639; (c) Bodine, K. D.; Gin, D. Y.; Gin, M. S. *Org. Lett.* **2005**, *7*, 4479-4482; (d) Di Fabio, G.; Randazzo, A.; D'Onofrio, J.; Ausín, C.; Pedroso, E.; Grandas, A.; De Napoli, L.; Montesarchio, D. *J. Org. Chem.* **2006**, *71*, 3395-3408.
6. (a) Coppola, C.; Saggiomo, V.; Di Fabio, G.; De Napoli, L.; Montesarchio, D. *J. Org. Chem.* **2007**, *72*, 9679-9689; (b) Licen, S.; Coppola, C.; D'Onofrio, J.; Montesarchio, D.; Tecilla, P. *Org. Biomol. Chem.* **2009**, *7*, 1060-1063; (c) Coppola, C.; Paciello, A.; Mangiapia, G.; Licen, S.; Boccalon, M.; De Napoli, L.; Paduano, L.; Tecilla, P.; Montesarchio, D. *Chem. Eur. J.* **2010**, *16*, 13757-13772.
7. Titov, D. V.; Gening, M. L.; Gerbst, A. G.; Chizhov, A. O.; Tsvetkov, Y. E.; Nifantiev, N. E. *Carbohydrate Res.* **2013**, *381*, 161-178.
8. Saha, T.; Roy, A.; Gening, M. L.; Titov, D. V.; Gerbst, A. G.; Tsvetkov, Y. E.; Nifantiev, N. E.; Talukdar, P. *Chem. Commun.* **2014**, *50*, 5514-5516.
9. (a) Saha, T.; Dasari, S.; Tewari, D.; Prathap, A.; Sureshan, K. M.; Bera, A. K.; Mukherjee, A.; Talukdar, P. *J. Am. Chem. Soc.* **2014**, *136*, 14128-14135; (b) Vargas Jentzsch, A.; Emery, D.; Mareda, J.; Metrangolo, P.; Resnati, G.; Matile, S. *Angew. Chem., Int. Ed.* **2011**, *50*, 11675-11678; (c) Hennig, A.; Gabriel, G. J.; Tew, G. N.; Matile, S. *J. Am. Chem. Soc.* **2008**, *130*, 10338-10344; (d) Sakai, N.; Brennan, K. C.; Weiss, L. A.; Matile, S. *J. Am. Chem. Soc.* **1997**, *119*, 8726-8727; (e) Gorteau, V.; Bollot, G.; Mareda, J.; Perez-Velasco, A.; Matile, S. *J. Am. Chem. Soc.* **2006**, *128*, 14788-14789.
10. Cantor, R. S. *J. Phys. Chem. B* **1997**, *101*, 1723-1725.